Supporting Information

Construction of modular Pd/Cu multimetallic chains via ligand- and anion-controlled metal-metal interactions

Orestes Rivada-Wheelaghan,[a,†,§] Shubham Deolka,[a,§] Ramadoss Govindarajan,[a] Eugene Khaskin,[a] Robert R. Fayzullin,[b] Shrinwantu Pal[c] and Julia R. Khusnutdinova *[a]

[a]Coordination Chemistry and Catalysis Unit, Okinawa Institute of Science and Technology Graduate University 1919–1 Tancha, Onna–son, 904–0495, Okinawa, Japan. Email: juliak@oist.jp

[b]Arbuzov Institute of Organic and Physical Chemistry, Kazan Scientific Center, Russian Academy of Sciences, 8 Arbuzov Street, Kazan 420088, Russian Federation.

[c]Department of Chemistry and Biotechnology, Graduate School of Engineering, The University of Tokyo, 7-3-1 Hongo, Bunkyo-ku, Tokyo 113-8656, Japan.

§ These authors made equal contributions.

† Current address: Université de Paris, Laboratoire d'Electrochimie Moléculaire, UMR 7591 CNRS, 15 rue Jean-Antoine de Baïf, F-75205 Paris Cedex 13, France.

Table of Contents

I. Experimental Procedures

General specifications

All reactions were performed using standard Schlenk or glovebox techniques under dry nitrogen or argon atmosphere if not indicated otherwise. All chemicals unless noted otherwise were purchased from major commercial suppliers (TCI, Sigma-Aldrich and Nacalai Tesque) and used without purification. Anhydrous solvents were dispensed from an MBRAUN solvent purification system and degassed prior to use. Anhydrous deuterated solvents were purchased from Eurisotop and stored over 4 Å molecular sieves. $[Cu(MeCN)_4]BAr^F{}_4$,[1] palladium dimer $Pd_2(Bzhq)_2(AcO)_2$[2] were prepared according to literature procedures. The ligand precursor, $\mathbf{L_PH}$ was previously reported in the literature[3] and was prepared according to the published procedure. All the metal complexes were prepared under nitrogen atmosphere in a glovebox.

Instrumentation: NMR spectra were measured on JEOL ECZ600R 600MHz and JEOL ECZ400S 400 MHz spectrometers. The following abbreviations are used for describing NMR spectra: s (singlet), d (doublet), t (triplet), td (triplet of doublets), ddd (doublet of doublets of doublets), vd (virtual doublet), vt (virtual triplet), br (broad). Electrospray Ionization Mass Spectrometry (ESI-MS) measurements were performed on a Thermo Scientific ETD apparatus. Elemental analyses were performed using an Exeter Analytical CE440 instrument. FT-IR spectra were measured using Agilent Cary 630 with ATR module in an argon-filled glovebox. The following abbreviations are used for describing FT-IR spectra: s (strong), m (medium), w (weak), br (broad). Absorbance UV/vis spectra were collected using an Agilent Cary 60 instrument.

Synthesis of 1-$BAr^F{}_4$

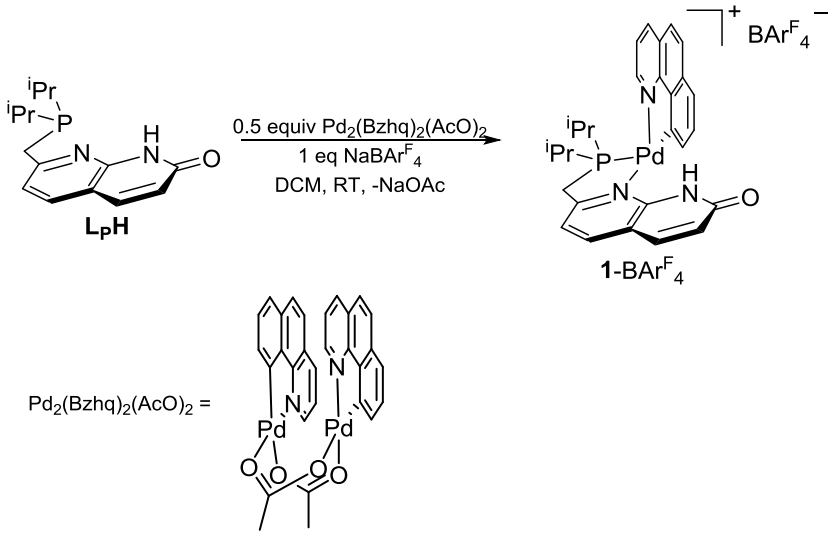

Scheme S1. Synthesis of **1**-$BAr^F{}_4$.

Ligand $\mathbf{L_PH}$ (554 mg, 2 mmol), palladium precursor $Pd_2(Bzhq)_2(AcO)_2$ (686 mg, 1 mmol) and $NaBAr^F{}_4$ (887 mg, 1 mmol) where placed in a 20 mL vial inside the glovebox. To the solid mixture 10 mL of dichloromethane were added and the mixture was left to stir for 1 h at room temperature (RT). Then the solvent was removed under vacuum and the product was extracted from the remaining solid with diethyl ether (3 x 5 mL), yielding 1.34 g of complex **1**-$BAr^F{}_4$, 93% yield. Crystals of complex **1**-$BAr^F{}_4$ were obtained by dissolving **1**-$BAr^F{}_4$ in CH_2Cl_2 (DCM) and layering the solution with hexane.

^{1}H NMR (600 MHz, -15 ºC, CD_2Cl_2) δ: 10.62 (br s, 1H, N-H), 8.29 (d,1H, $^3J_{HH}$ = 7.6 Hz, CH_{ar}), 8.04 (d, 2H, $^3J_{HH}$ = 7.5 Hz, CH_{ar}), 7.84 (d,2H, $^3J_{HH}$ = 8.4 Hz, 1H, CH_{ar}), 7.76 (m, 1H, CH_{ar}), 7.70 (s, 8H, *ortho*-

CH_{BARF}), 7.63 (d, $^{3}J_{HH}$ = 8.6 Hz, 1H, CH_{ar}), 7.59 (m, 1H, CH_{ar}), 7.50 (m, 2H, 4 *para*-CH_{BARF} + 2 CH_{ar}), 7.39 (d, $^{3}J_{HH}$ = 7.7 Hz, 2H, CH_{ar}), 6.07 (s, 1H, CH_{ar}), 4.03 (dd, $^{2}J_{HH}$ = 17.3, $^{2}J_{HP}$ = 7.3 Hz, 1H, CH_2), 3.40 (dd, $^{2}J_{HH}$ = 17.3, $^{2}J_{HP}$ = 13.8 Hz, 1H, CH_2), 2.86 (m, 1H, C*H*$(CH_3)_2$), 2.27 (m, 1H, C*H*$(CH_3)_2$), 1.42 (dd, $^{3}J_{HP}$ = 18.0, $^{3}J_{HH}$ = 7.0 Hz, 3H, CH(C*H*$_3)_3$), 1.34 (dd, $^{3}J_{HP}$ = 13.5, $^{3}J_{HH}$ = 6.8 Hz, 3H, CH(C*H*$_3)_3$), 1.21 (dd, $^{3}J_{HP}$ = 19.7, $^{3}J_{HH}$ = 7.2 Hz, 3H, CH(C*H*$_3)_3$), 0.68 (dd, $^{3}J_{HP}$ = 17.3, $^{3}J_{HH}$ = 6.8 Hz, 3H, CH(C*H*$_3)_3$).

$^{13}C\{^{1}H\}$ NMR (151 MHz, - 15 ºC, CD_2Cl_2) δ: 161.77 (m, C_q, C_{BARF}), 161.5 (C_q), 159.68 (C_q), 153.61 (C_q), 151.41 (C_q), 148.44 (C_q), 147.92 (C_{ar}), 141.79 (C_q), 140.63 (C_{ar}), 139.38 (C_{ar}), 138.78 (C_{ar}), 136.46 (d, $^{3}J_{CP}$ = 9.3 Hz, C_{ar}), 134.78 (*orto*-CH_{BARF}), 130.15 (d, $^{3}J_{CP}$ = 5.2 Hz, C_{ar}), 129.89 (C_{ar}), 128.78 (m, Cq, C_{BARF}), 127.0 (C_q), 127.27, 125.46, 124.94 (C_{ar}), 124.13 (C_q, $^{1}J_{FC}$ = 272 Hz, C_{BARF}), 123.80(C_{ar}), 123.66 (C_{ar}), 122.12 (C_{ar}), 121.85, 118.84 (d, $^{2}J_{CP}$ = 7.1 Hz, C_q), 117.57 (C_q, C_{BARF}), 115.49 (C_q), 33.89 (d, $^{1}J_{CP}$ = 25.7 Hz CH_2), 26.42 (d), 21.56 (d, $^{1}J_{CP}$ = 27.5 Hz, *C*H$(CH_3)_2$), 19.59 (CH(*C*H$_3)_2$), 19.14 (CH(*C*H$_3)_2$), 18.71 (CH(*C*H$_3)_2$), 15.98 (d, $^{2}J_{CP}$ = 6.8 Hz, (CH(*C*H$_3)_2$).

$^{31}P\{^{1}H\}$ NMR (262 MHz, CD_2Cl_2, -15 °C) δ: 76.14.

Elemental Analysis: Expt (Calc): $C_{60}H_{41}NBF_{24}N_3OPd$: C 50.25(50.60) H 2.87(2.90) N 2.99(2.95).

ESI-HRMS (m/z pos): Found (Calcd): $C_{28}H_{29}ON_3PPd^{+}$ 560.1079 (560.1078).

FT-IR (ATR, solid): 2979 (br, w), 2867 (br, w), 1664 (s), 1353 (s), 1274 (s), 1276 (s), 1123 (br, s), 1066 (s), 886 (m) cm^{-1}.

UV-vis (MeCN), λ, nm (ε, $M^{-1}\cdot cm^{-1}$) : 399 (2195), 380 (3079), 349 (4135), 335 (4651), 286 (8125), 214 (34170).

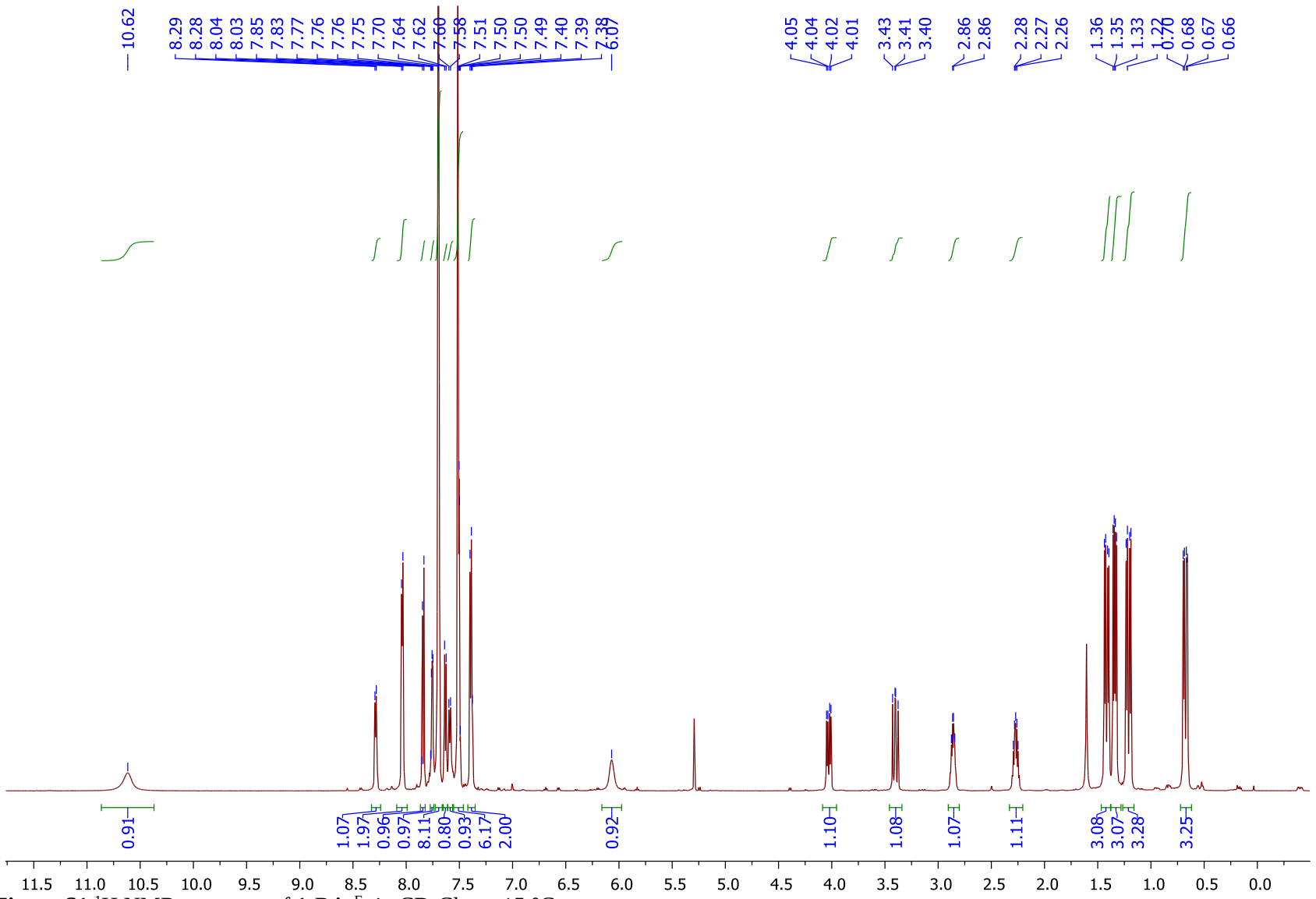

Figure S1.[1]H NMR spectrum of **1**-BAr^F_4 in CD_2Cl_2 at -15 °C.

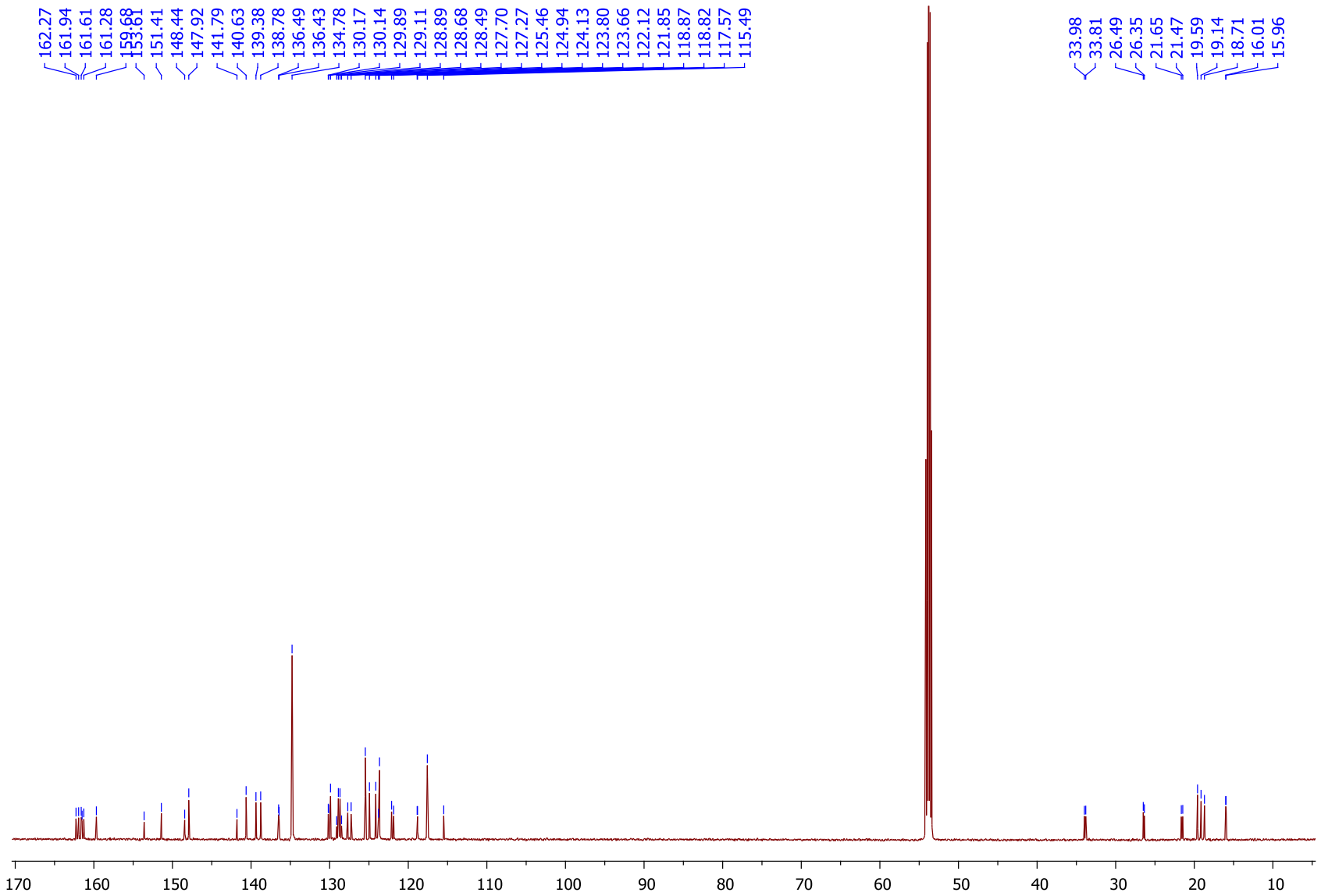

Figure S2.[13]C NMR spectrum of **1**-BAr^F_4 in CD_2Cl_2 at -15 °C.

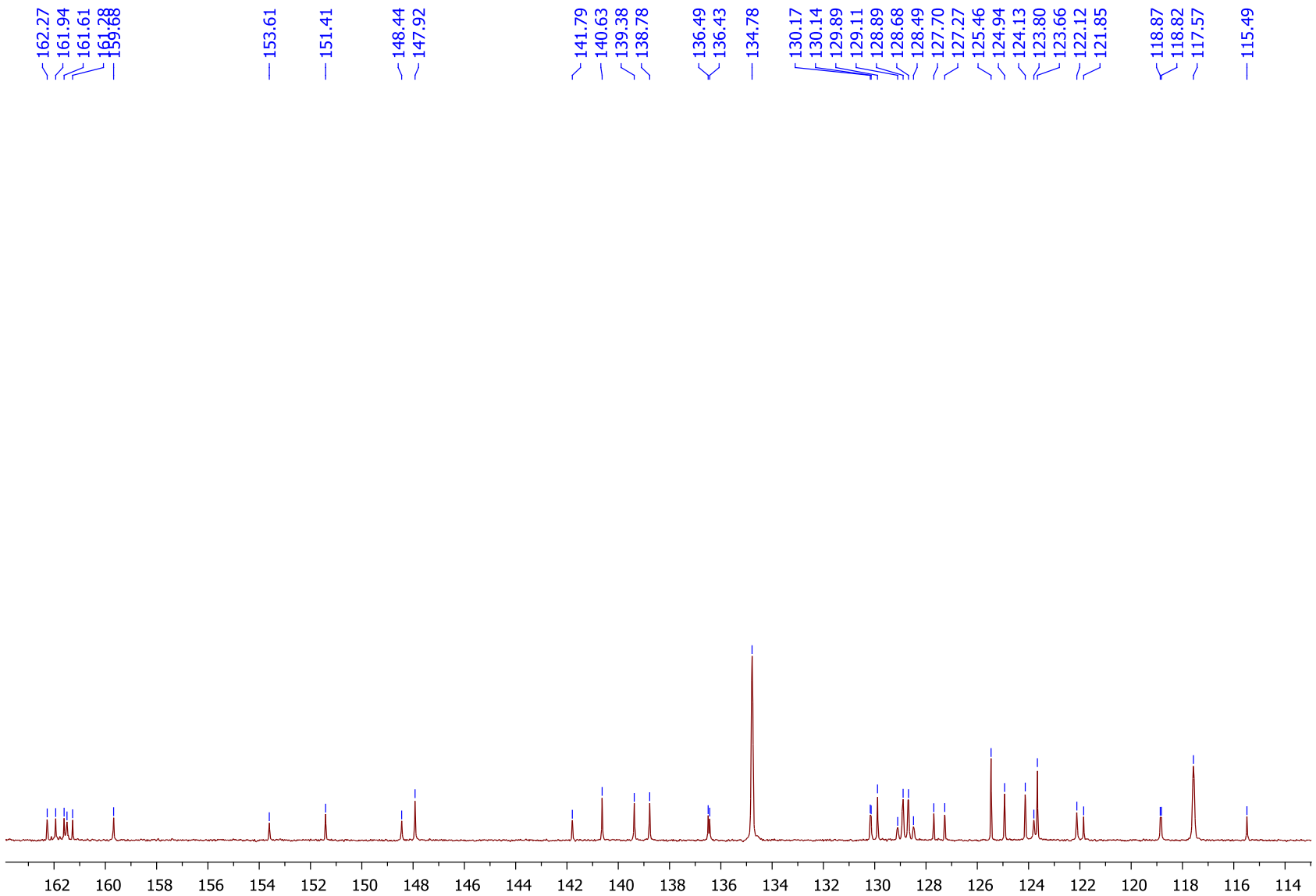

Figure S3. Expanded ^{13}C NMR spectrum of **1**-BAr^{F}_{4} in CD_2Cl_2 at -15 °C.

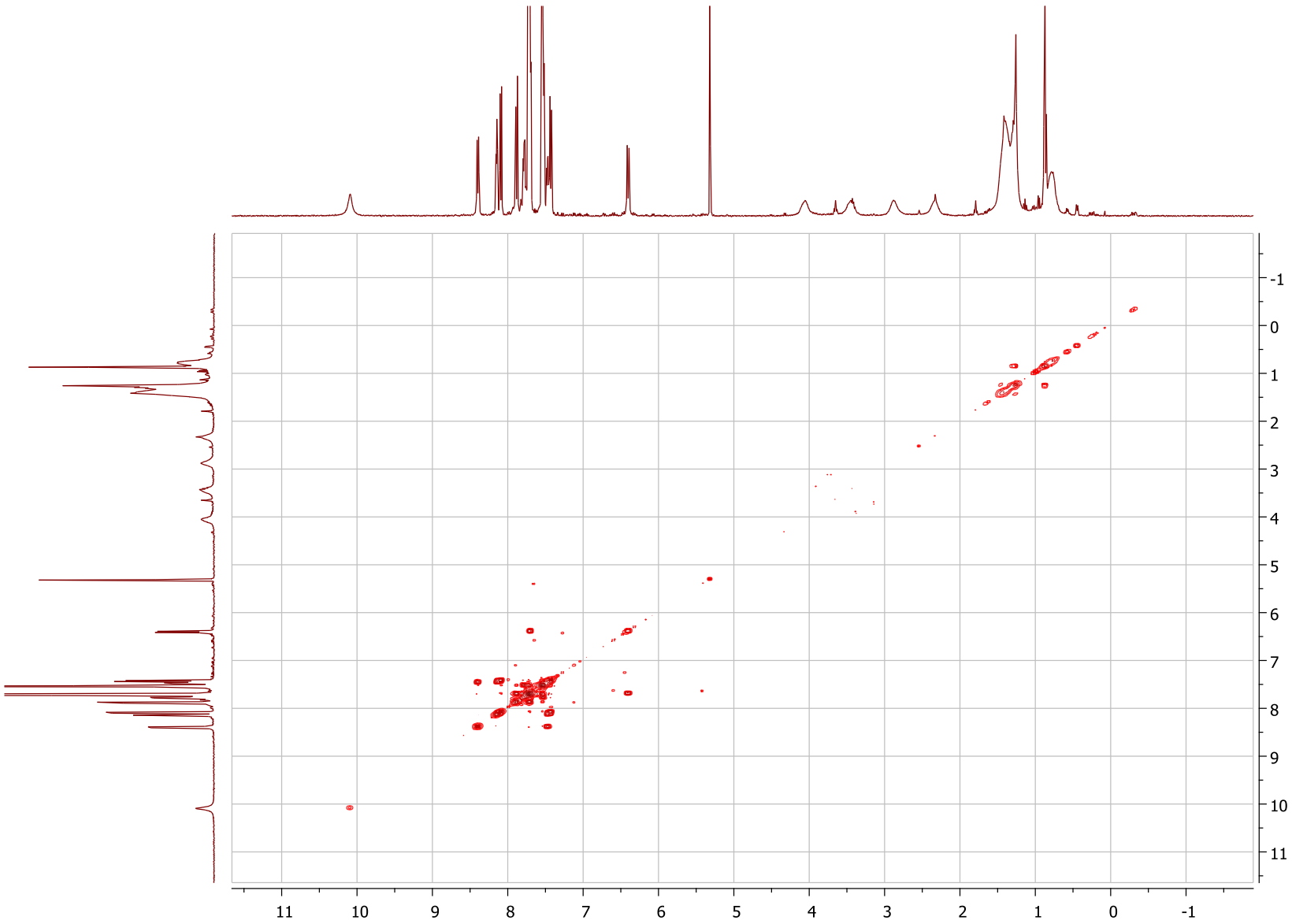

Figure S4. ^{1}H-^{1}H COSY spectrum of **1**-BAr$^{F}_{4}$ in CD_2Cl_2 at 22 °C.

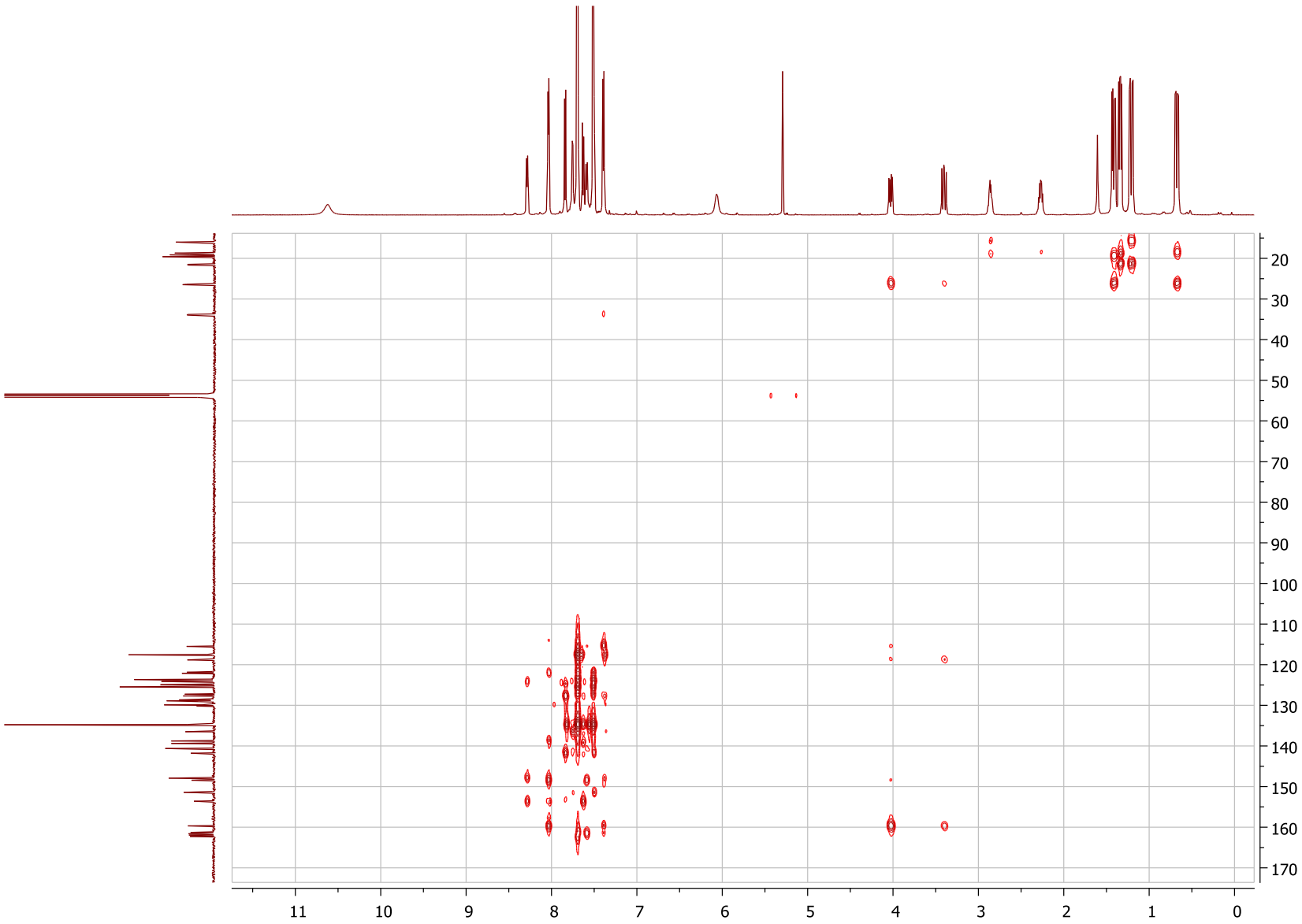

Figure S5. ^{1}H-^{13}C HMBC spectrum of **1**-BAr^{F}_{4} in CD_2Cl_2 at -15 °C.

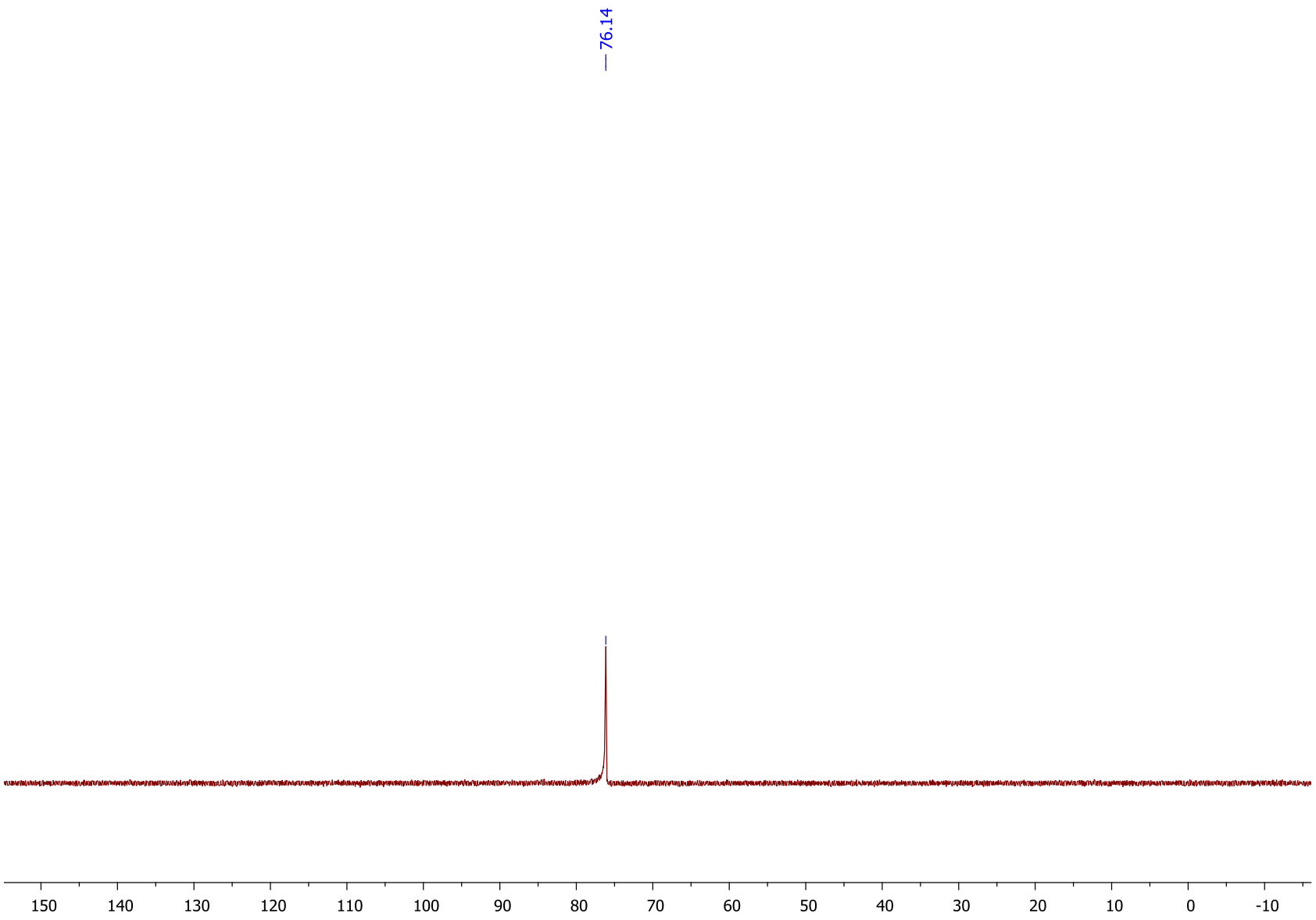

Figure S6. ^{31}P NMR spectrum of **1**-BAr^{F}_{4} in CD_2Cl_2 at -15°C.

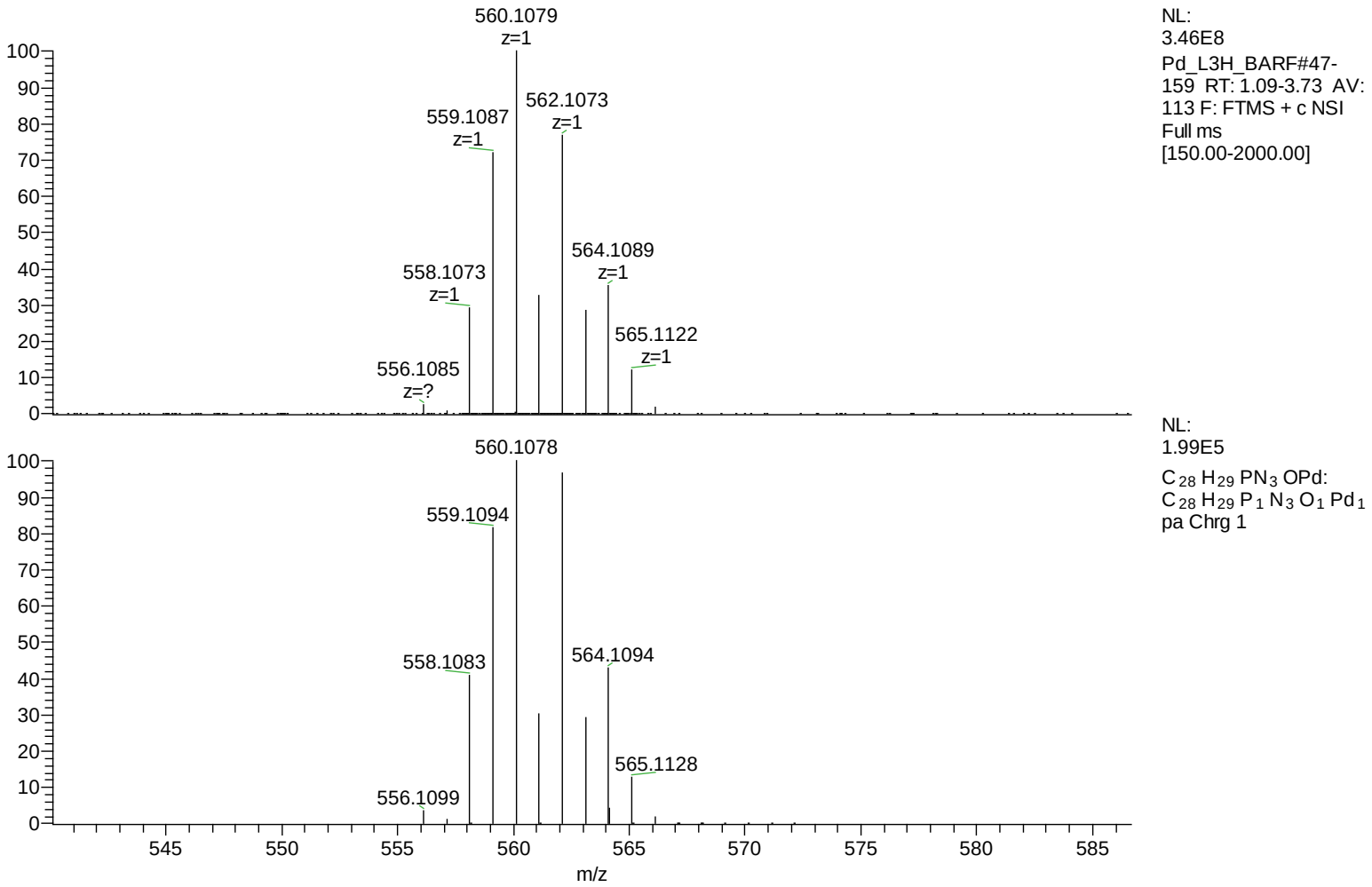

Figure S7. ESI-(HR)MS spectrum of MeCN solution of **1**-BAr^{F}_{4} (top) and simulated spectrum for $C_{28}H_{29}O_{1}N_{3}PPd^{+}$ (bottom).

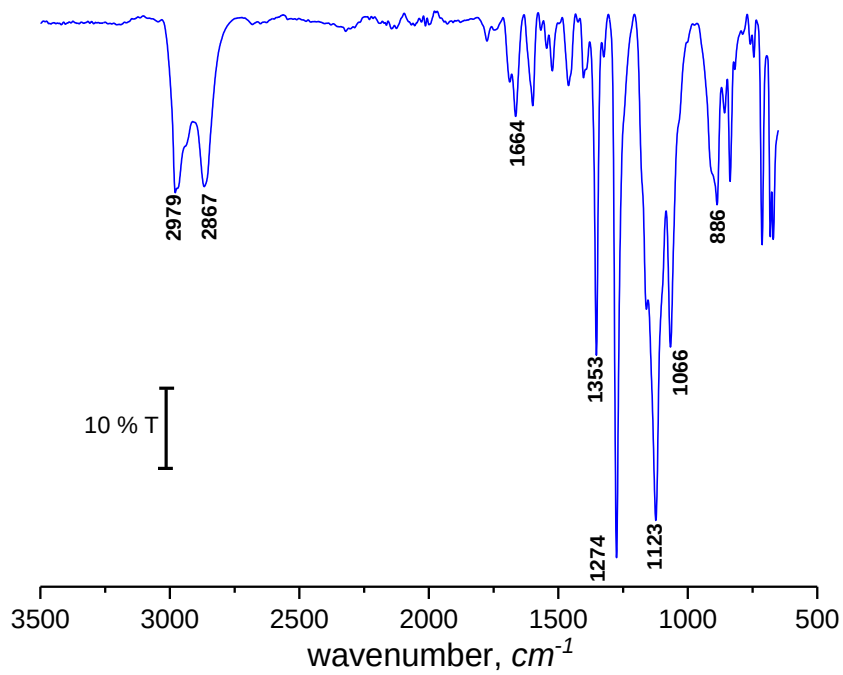

Figure S8. ATR FT-IR transmittance spectrum of **1**-BAr^{F}_{4}.

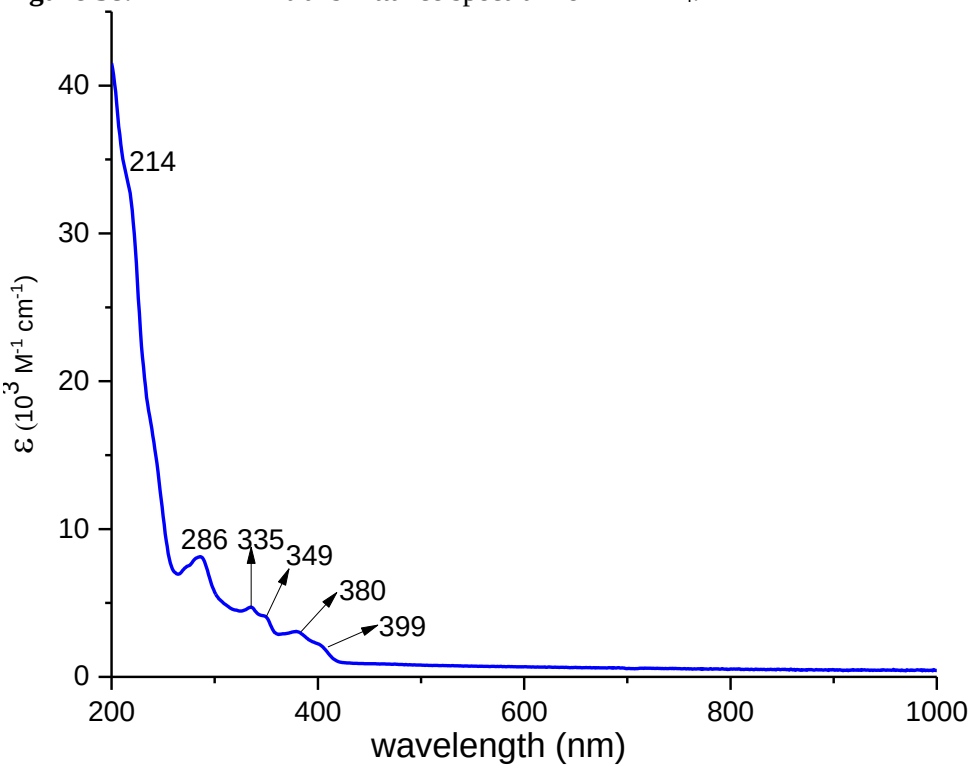

Figure S9. UV-vis absorbance spectrum for **1**-BAr^{F}_{4} in MeCN.

Synthesis of 1-OAc

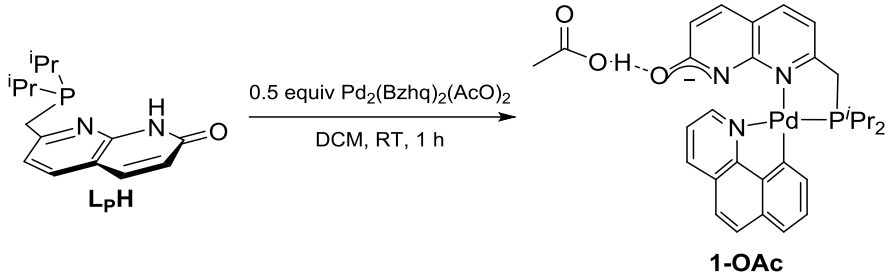

Scheme S2. Synthesis of **1**-OAc.

To a 20 mL vial containing palladium precursor $Pd_2(Bzhq)_2(AcO)_2$ (125.7 mg, 0.18 mmol) and $\mathbf{L_PH}$ (101.1 mg, 0.36 mmol) was added in DCM (4 mL) to give a yellow solution. The reaction was left to stir for 1 hour. Then the solvent was removed under vacuum and the desired complex was re-dissolved in DCM (1 mL). Cold hexane (5 x 2 mL) was added to precipitate the yellow powder. Solvent removal yields complex **1**-OAc quantitatively as a yellow solid, (157.5 mg, 0.25 mmol, 69% yield). Crystals suitable for X-ray diffraction study were grown via vapor diffusion technique in DCM/hexane solvent at -30 °C.

^{1}H NMR (600 MHz,CD_2Cl_2, 22 °C) δ: 8.72 (br s, 1H, N-H), 8.27 (d, $^3J_{HH}$ = 7.8 Hz, 1H, CH_{ar}), 7.87 (d, $^3J_{HH}$ = 7.8 Hz, 1H, CH_{ar}), 7.75 (d, $^3J_{HH}$ = 8.7 Hz, 1H, CH_{ar}), 7.66-7.62 (m, 4H, CH_{ar}), 7.55-7.51 (m, 1H, CH_{ar}), 7.40 (t, $^3J_{HH}$ = 7.5 Hz, 1H, CH_{ar}), 7.23 (d, $^3J_{HH}$ = 7.5 Hz, 1H, CH_{ar}), 6.74 (d, $^3J_{HH}$ = 9.1 Hz, 1H, CH_{ar}), 3.70 (d, $^2J_{PH}$ = 8.3 Hz, 2H, CH_2), 2.61-2.52 (m, 2H, C*H*$(CH_3)_2$),1.81 (s, 3H, OAc), 1.30 (d, $^3J_{PH}$ = 7.1 Hz, 3H, CH(C*H*$_3)_3$), 1.27 (d, $^3J_{PH}$ = 7.1 Hz, 3H, CH(C*H*$_3)_3$), 1.17-1.11(m, 6H, CH(C*H*$_3)_3$).

^{13}C{^{1}H} NMR (151 MHz, CD_2Cl_2, 22 °C) δ: 174.69 (C_{ar}), 171.76 (C_{ar}), 158.47 (C_{ar}), 157.06 (C_{ar}), 154.33 (C_{ar}), 153.16 (C_{ar}), 150.69 (C_{ar}), 143.07 (C_{ar}), 138.50 (C_{ar}), 137.92 (C_{ar}), 136.73-136.61 (m, C_{ar}), 134.40 (C_{ar}), 129.20 (d, J_{PC} =4.4 Hz, C_{ar}), 128.99 (C_{ar}), 127.11 (C_{ar}), 124.20 (C_{ar}), 123.88 (C_{ar}), 122.87 (C_{ar}), 121.75 (C_{ar}), 116.64 (C_{ar}), 114.36 (C_{ar}), 34.01(d, J_{PC} =26.1 Hz, CH_2), 24.72-24.15 (m, *C*H$(CH_3)_2$), 22.66 (OAc), 19.45 (d, J_{PC} =2.4 Hz, CH(*C*H$_3)_2$), 18.08 (CH(*C*H$_3)_2$).

^{31}P{^{1}H} NMR (162 MHz, CD_2Cl_2, 23 °C) δ: 67.15.

ESI-HRMS (m/z pos): Found (Calcd): $C_{28}H_{29}ON_3P_1Pd_1$: 560.1072 (560.1078).

FT-IR (ATR, solid): 2970 (br, w), 2854 (br, w), 1458 (s), 1068 (s), 907 (s) cm^{-1}.

UV-vis (MeCN), λ, nm (ε, $M^{-1}\cdot cm^{-1}$) : 463 (177), 394 (2060), 377 (2816), 287 (4978), 216 (15975).

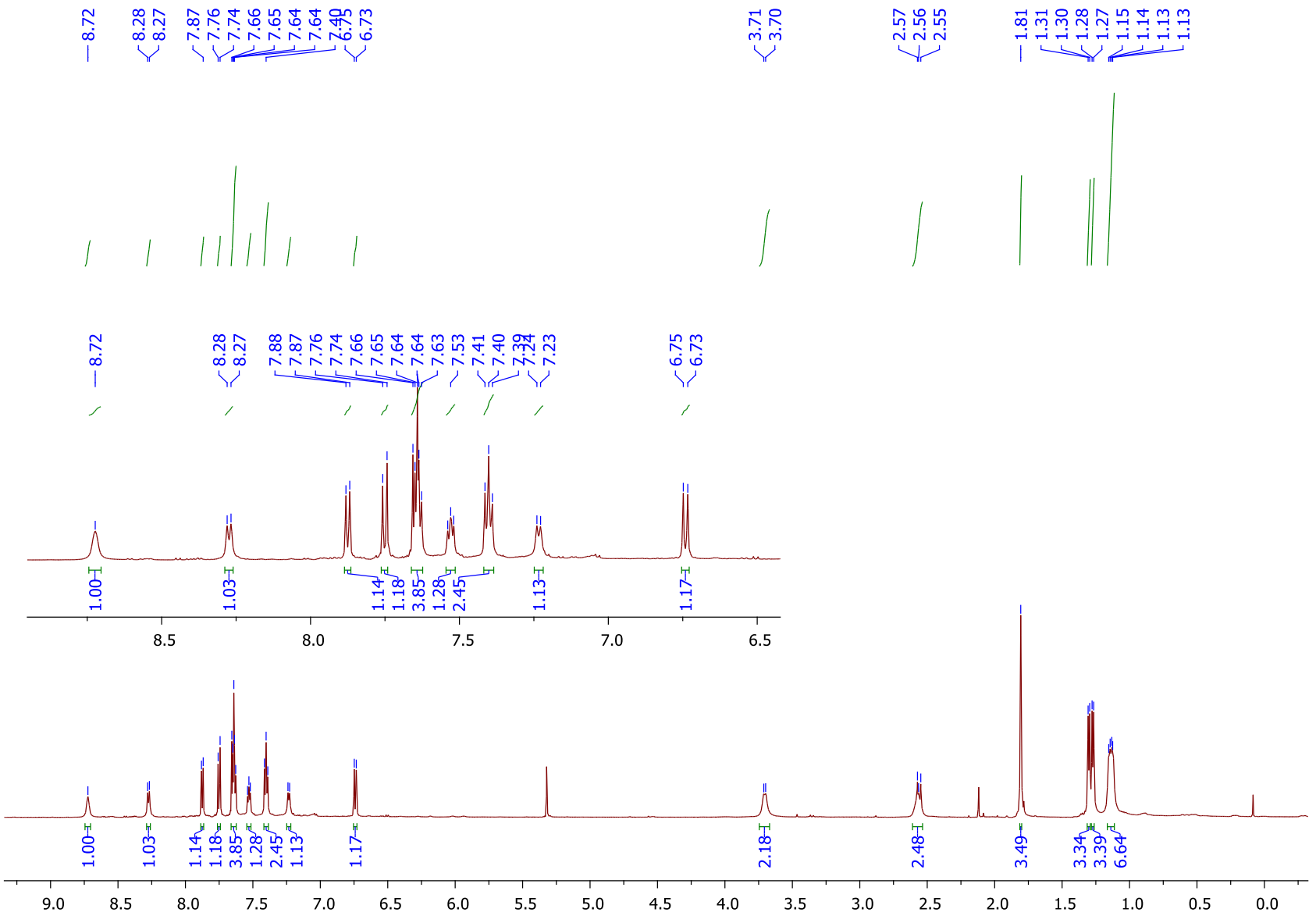

Figure S10.[1]H NMR spectrum of **1**-OAc in CD_2Cl_2 at 22 °C.

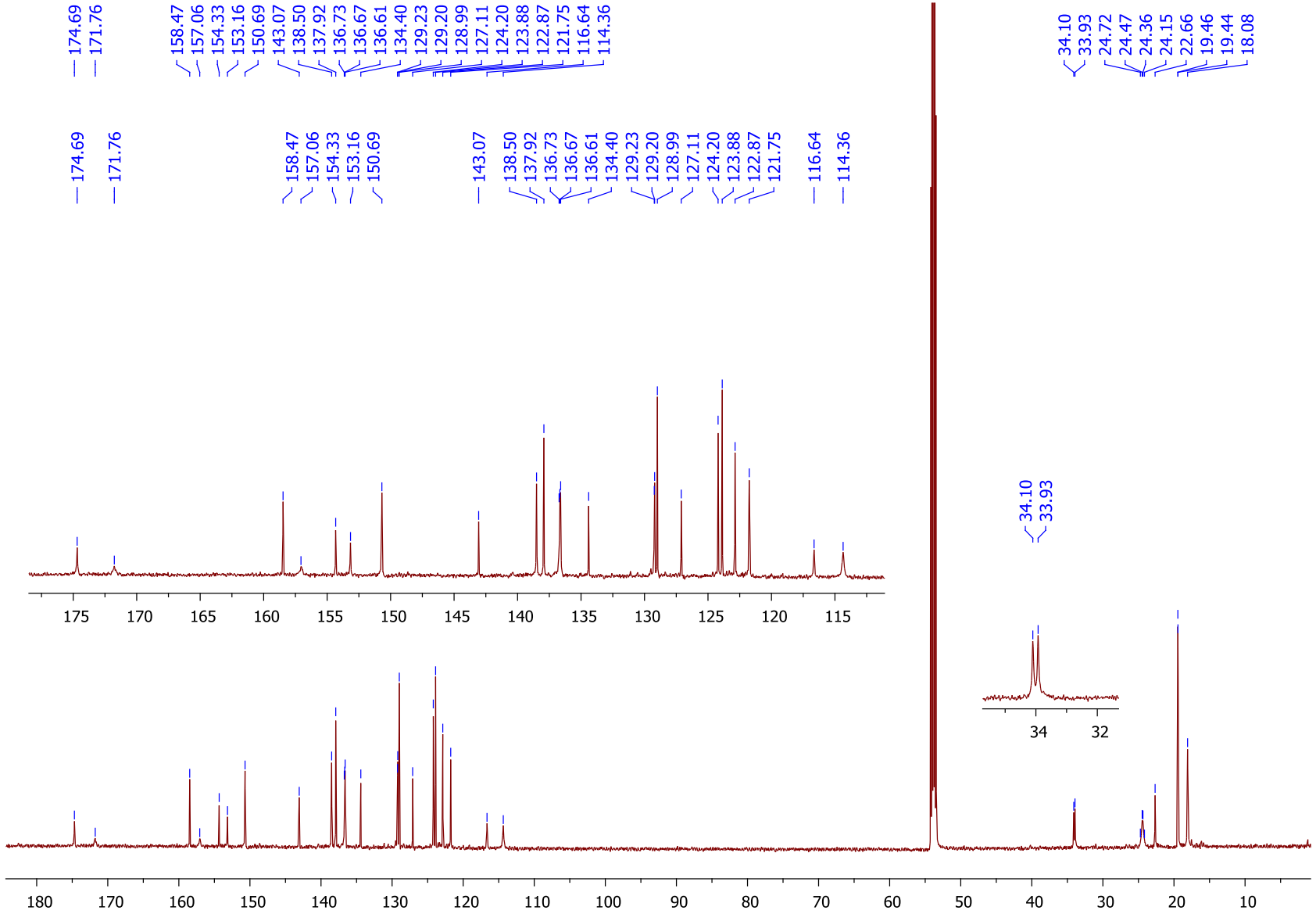

Figure S11.[13]C NMR spectrum of **1**-OAc in CD_2Cl_2 at 22 °C.

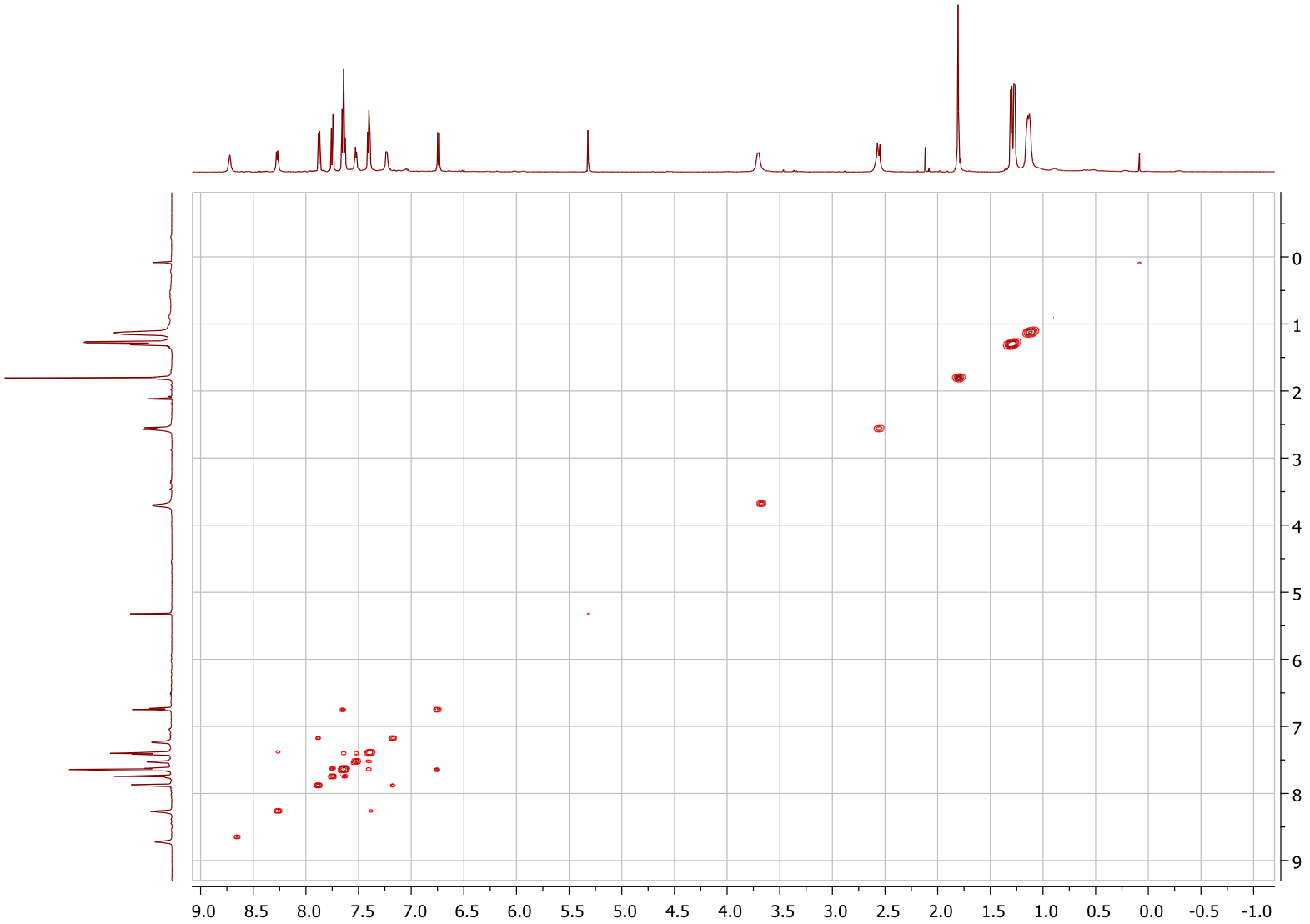

Figure S12. ^{1}H-^{1}H COSY spectrum of **1**-OAc in CD_2Cl_2 at 22 °C.

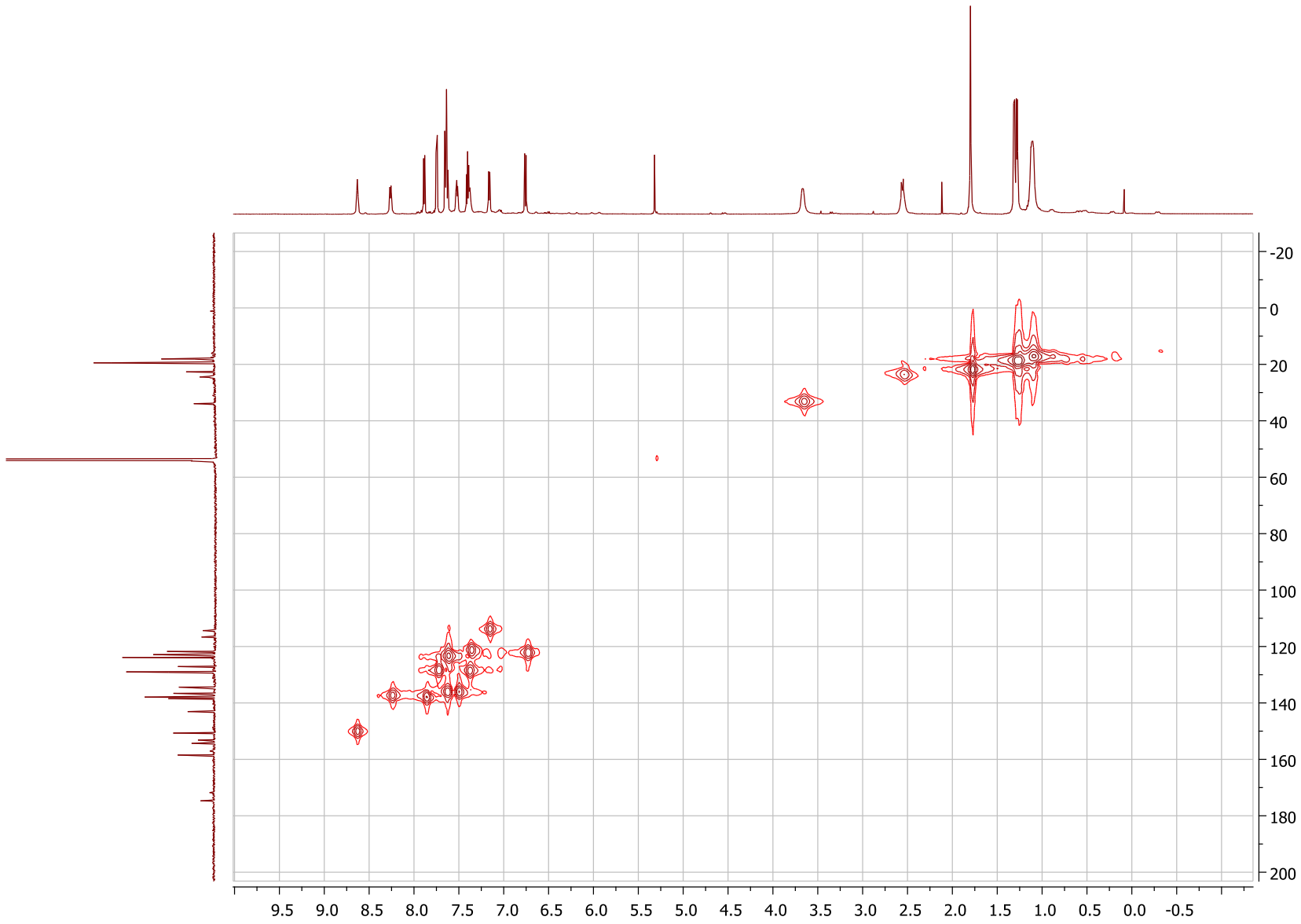

Figure S13. ^{1}H-^{13}C HMQC spectrum of **1**-OAc in CD_2Cl_2 at 23 °C.

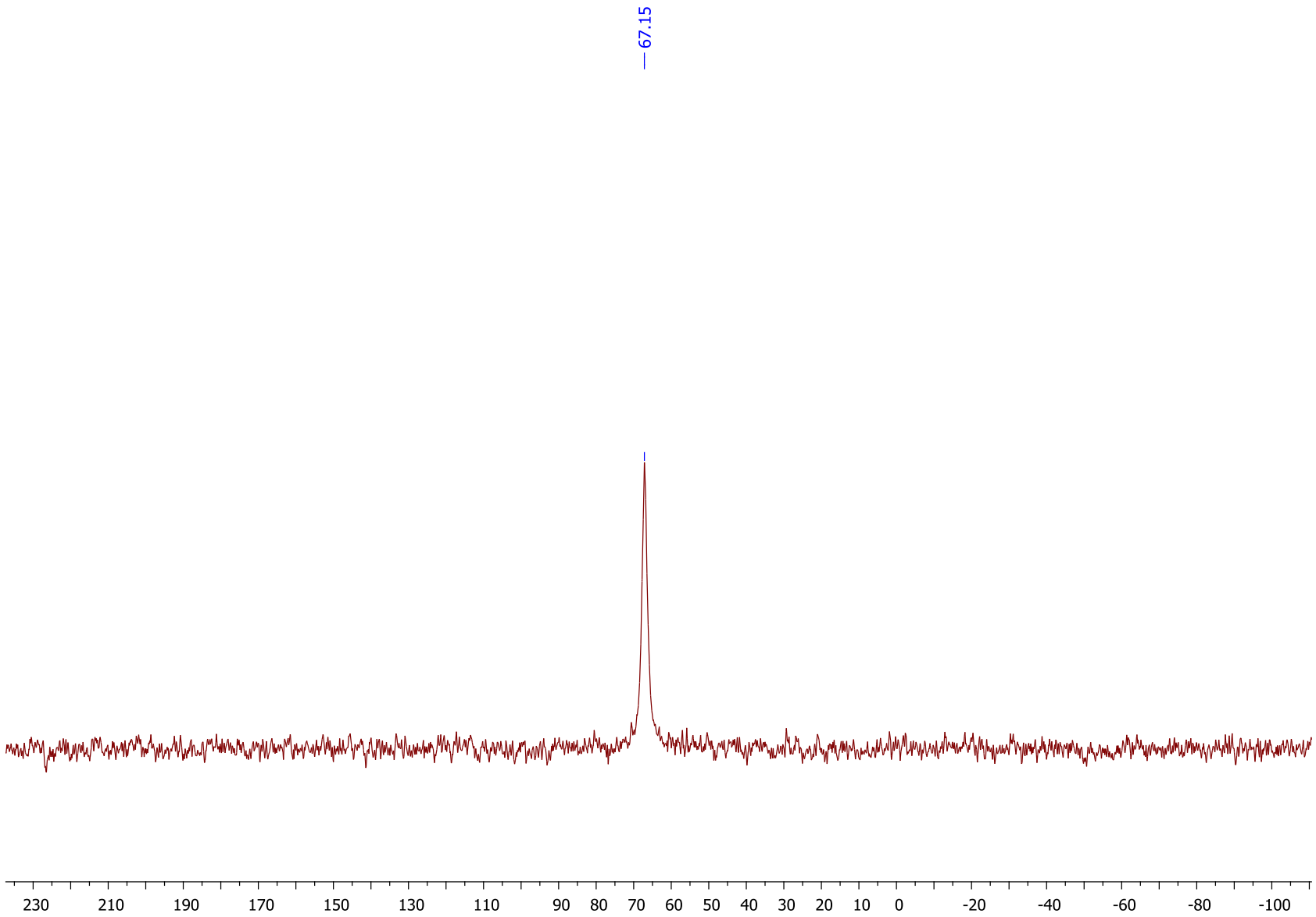

Figure S14. ^{31}P NMR spectrum of **1**-OAc in CD_2Cl_2 at 23 °C

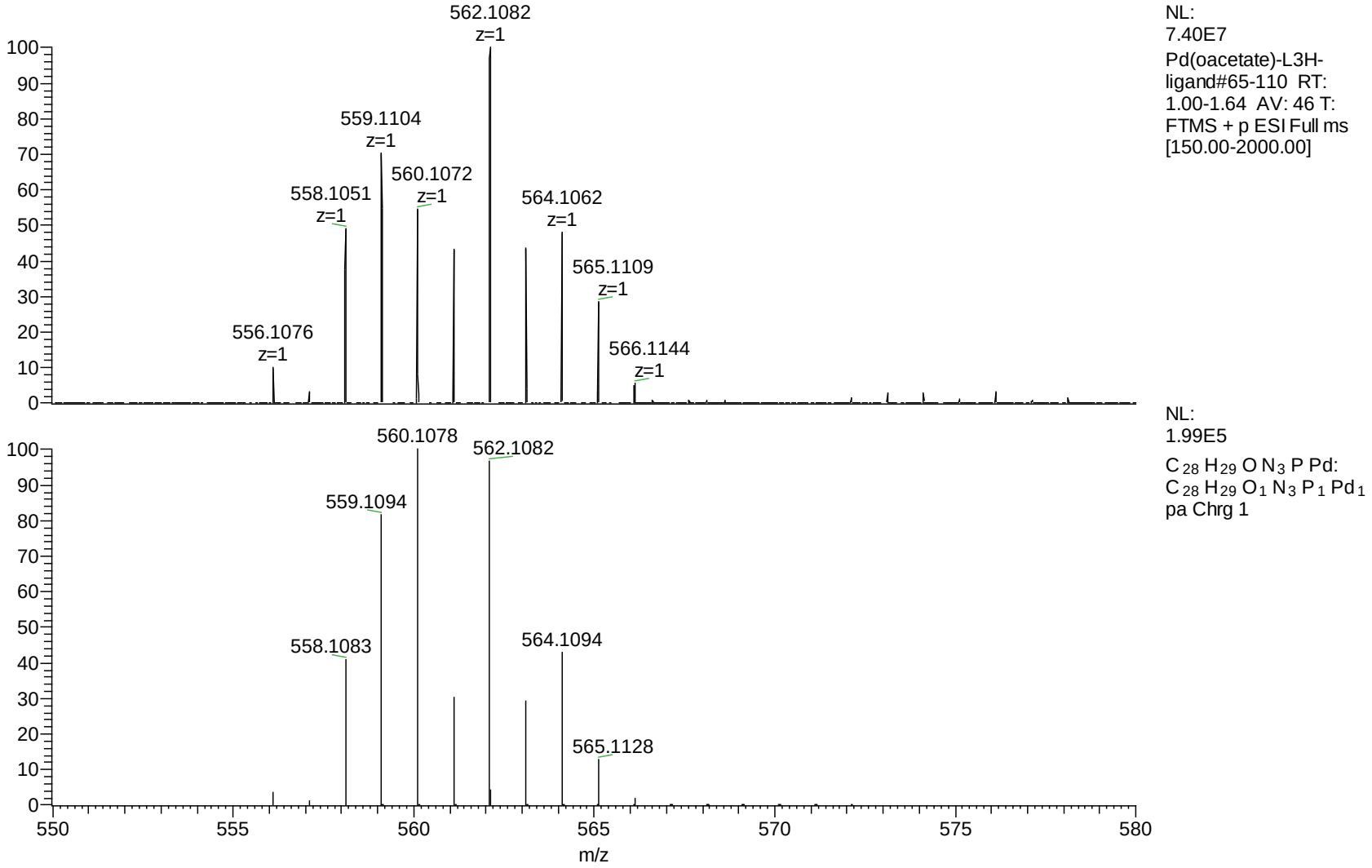

Figure S15. ESI-(HR)MS spectrum of a MeOH solution of **1**-OAc (top) and simulated spectrum for $C_{28}H_{29}ON_3P_1Pd_1$ (bottom).

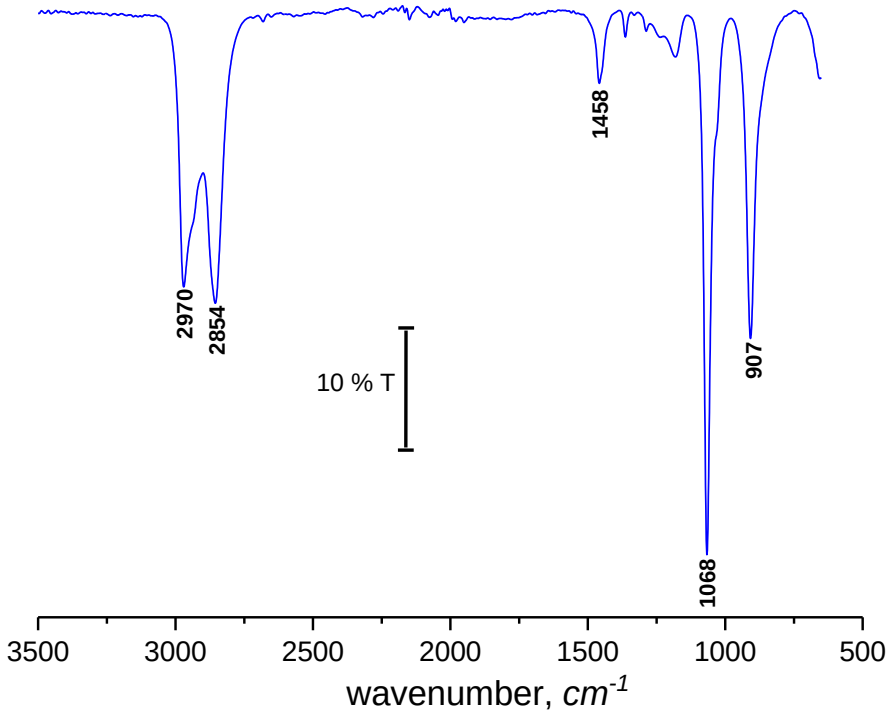

Figure S16. ATR FT-IR transmittance spectrum of **1**-OAc.

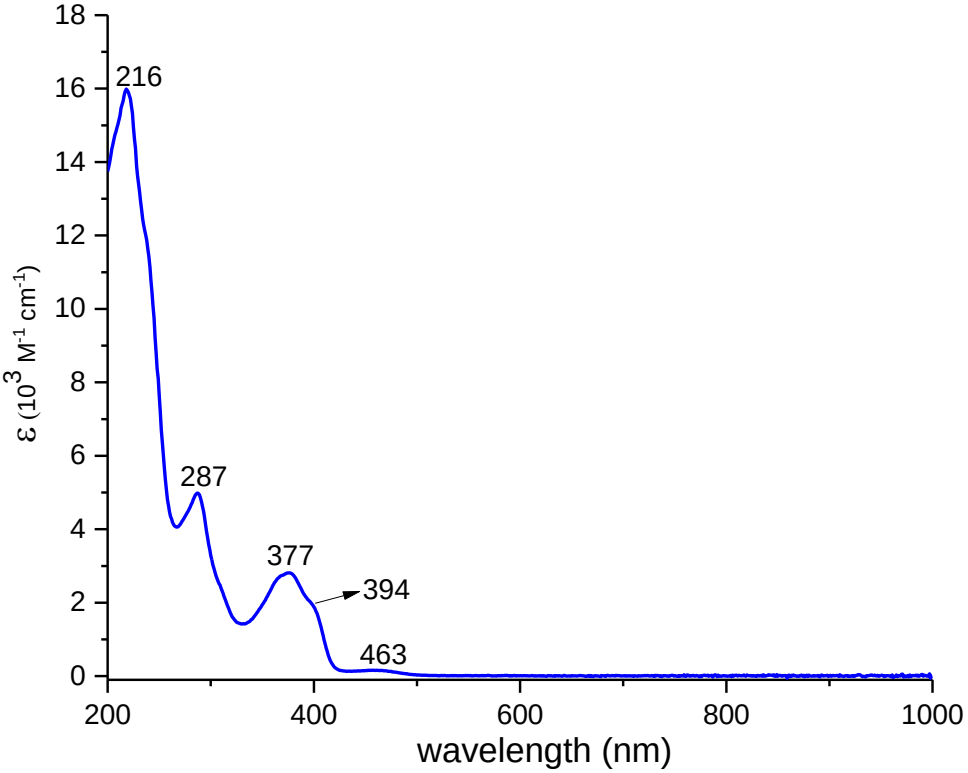

Figure S17. UV-vis absorbance spectrum for **1**-OAc in MeCN.

Synthesis of 2

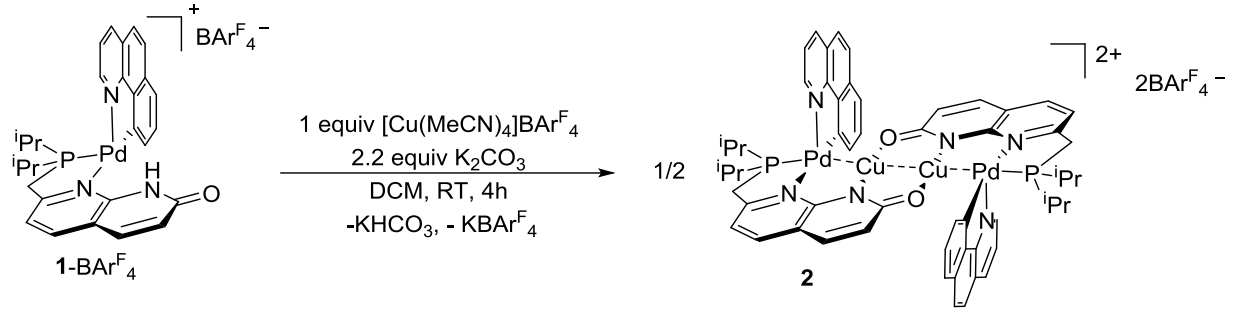

Scheme S3. Synthesis of **2**.

Complex **1**-BAr^F_4 (300 mg, 0.2 mmol), $[Cu(MeCN)_4]BAr^F_4$ (230 mg, 0.2 mmol) and K_2CO_3 (61 mg, 0.4 mmol) where placed in a 20 mL vial inside the glovebox. To the solid mixture 10 mL of diethyl ether were added and the mixture was left to stir for 4 h at room temperature. Then the solvent was removed under vacuum and the product was extracted from the remaining solid with dichloromethane (3 x 5 mL). The solution is preconcentrated and the crystals were obtained by layering with pentane (1:5 CH_2Cl_2 : pentane) at -30 ºC. Complex **2** was obtained in 60% yield, 355 mg.

^{1}H NMR (400 MHz, 20 ºC,CD_2Cl_2) δ: 8.04 (d, $^3J_{HH}$ = 8.0 Hz, 2H, CH_{ar}), 7.99 (d, $^3J_{HH}$ = 7.9 Hz, 2H, CH_{ar}), 7.71 (m, 20 H, *orto*-CH_{BARF} + CH_{ar}), 7.52 (m, 12H, *para*-CH_{BARF} + CH_{ar}), 7.49 (dd, $^3J_{HH}$ = 9.00 Hz, $^4J_{HH}$ = 1 Hz, 2H, CH_{ar}), 7.42 (m, 2H, CH_{ar}),7.38 (d, $^3J_{HH}$ = 8.7 Hz, 2H, CH_{ar}), 7.30 (d, $^3J_{HH}$ = 7.9 Hz, 2H, CH_{ar}), 7.10 (m, 2H, CH_{ar}), 5.60 (d, $^3J_{HH}$ = 9.0 Hz, 2H, CH_{ar}), 4.04 (dd, $^2J_{HH}$ = 17.9, $^2J_{HP}$ = 6.4 Hz, 2H, CH_2), 3.44 (dd, $^2J_{HH}$ = 17.8, $^2J_{HP}$ = 13.9 Hz, 2H, CH_2), 3.86 (m, 2H, C*H*(CH_3)$_2$), 2.43 (m, 2H, C*H*(CH_3)$_2$), 1.50 (dd, $^3J_{HP}$ = 18.4, $^3J_{HH}$ = 7.2 Hz, 6H, CH(C*H*$_3$)$_3$), 1.35 (dd, $^3J_{HP}$ = 13.6, $^3J_{HH}$ = 7.0 Hz, 6H, CH(C*H*$_3$)$_3$), 1.18 (dd, $^3J_{HP}$ = 19.6, $^3J_{HH}$ = 7.1 Hz, 6H, CH(C*H*$_3$)$_3$), 0.73 (dd, $^3J_{HP}$ = 16.9, $^3J_{HH}$ = 6.7 Hz, 6H, CH(C*H*$_3$)$_3$).

^{13}C{^{1}H} NMR (101 MHz, 20 ºC, CD_2Cl_2) δ: 173.0 (C_q), 161.77 (m, C_q, C_{BARF}), 160.02 (C_q), 154.41 (C_q), 153.24 (C_q), 148.0 (CH_{ar}), 147.28, 141.60 (C_q), 140.65 (CH_{ar}), 138.59 (d, CH_{ar}), 136.12 (d, $^3J_{CP}$ = 9.2 Hz, CH_{ar}), 134.81 (*orto*-CH_{BARF}), 130.20 (d, $^3J_{CP}$ = 5.2 Hz, CH_{ar}), 129.89 (CH_{ar}), 128.71 (m, C_q, C_{BARF}), 127.26 (C_q), 125.95, 124.55 (C_q, $^1J_{FC}$ = 272 Hz, C_{BARF}), 123.36, 123.24 (CH_{ar}), 121.57 (CH_{ar}), 120.92 (CH_{ar}), 120.53, 118.17 (C_q), 118.10 (C_q), 117.95 (CH_{ar}), 117.51 (C_q, C_{BARF}), 33.55 (d, $^1J_{CP}$ = 26.2 Hz, CH_2), 26.03 (d, $^1J_{CP}$ = 21.3 Hz, *C*H(CH_3)$_2$), 21.72 (d, $^1J_{CP}$ = 27.3 Hz, *C*H(CH_3)$_2$), 20.11 (CH(*C*H$_3$)$_2$), 19.09 (d, $^2J_{CP}$ = 4.28 Hz CH(*C*H$_3$)$_2$), 19.01 (CH(*C*H$_3$)$_2$), 16.04 (d, $^2J_{CP}$ = 6.8 Hz, CH(*C*H$_3$)$_2$).

^{31}P{^{1}H} NMR (262 MHz, CD_2Cl_2, 22 °C) δ: 72.98.

Elemental Analysis: Expt (Calc): $C_{120}H_{82}NB_2F_{48}N_6O_2Pd_2Cu_2$: C 48.05(48.47) H 2.63(2.71) N 2.80(2.83).

ESI-HRMS (m/z pos): The observed spectrum is a combination of two overlapping signals from expected tetranuclear 2+ charged complex complex and a binuclear +1 charged species that could be formed under ESI conditions (according to NMR, only one type of species is present).
Found (Calcd): *m/z* $C_{56}H_{56}O_2N_6P2Pd_2Cu_2^{2+}$ 624.0298 (624.0288).
Found (Calcd): *m/z* $C_{28}H_{28}ON_3PPdCu^+$ 622.0305 (622.0301).

FT-IR (ATR, solid): 2963 (br, w), 1612 (s), 1510 (m), 1351 (s), 1273 (s), 1110 (s), 884 (m), 837 (s) 711 (s) cm^{-1}.

UV-vis (MeCN), λ, nm (ε, $M^{-1}\cdot cm^{-1}$) : 377 (4691), 282 (10322), 271 (9744), 205 (73405).

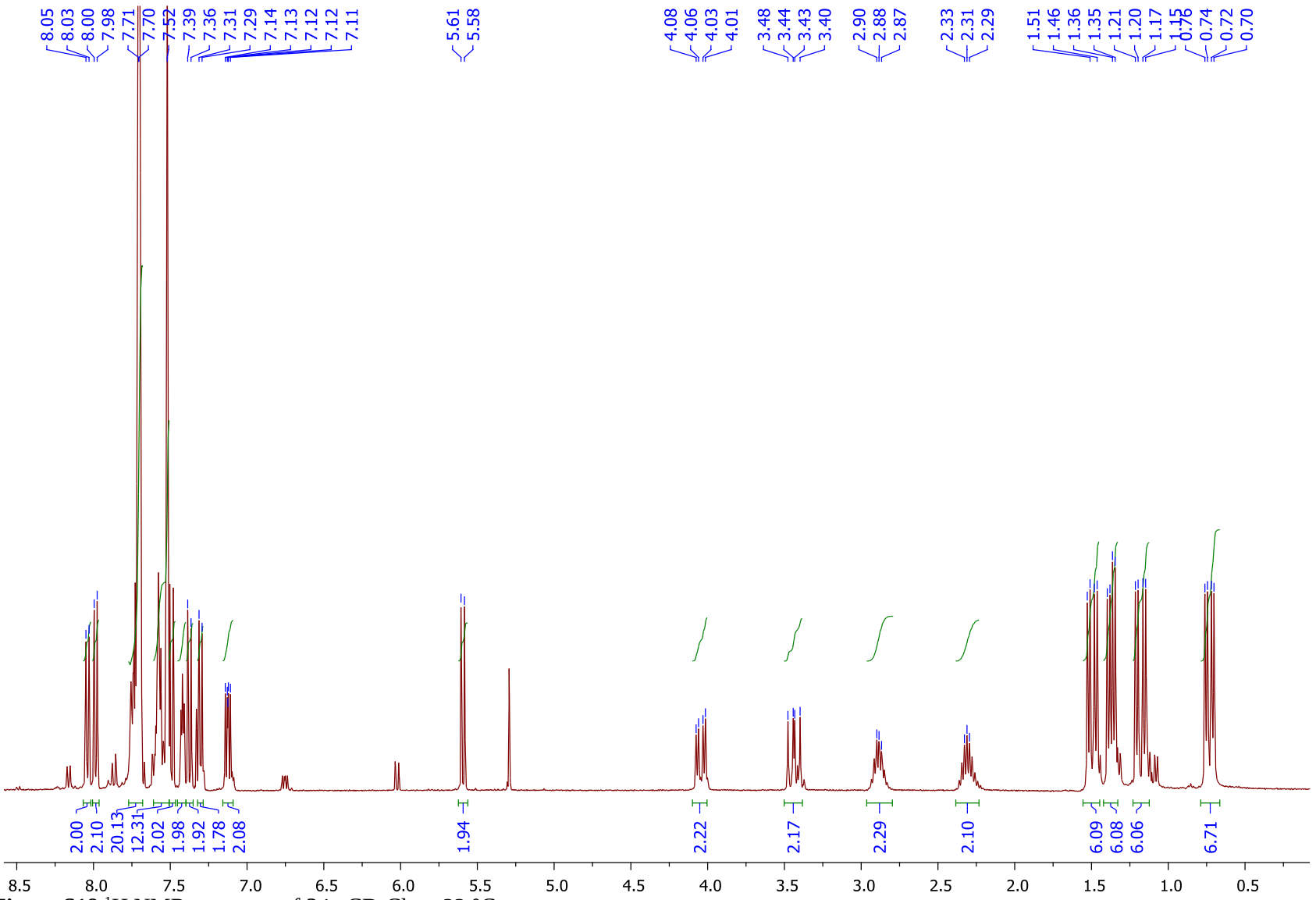

Figure S18.[1]H NMR spectrum of **2** in CD_2Cl_2 at 22 °C.

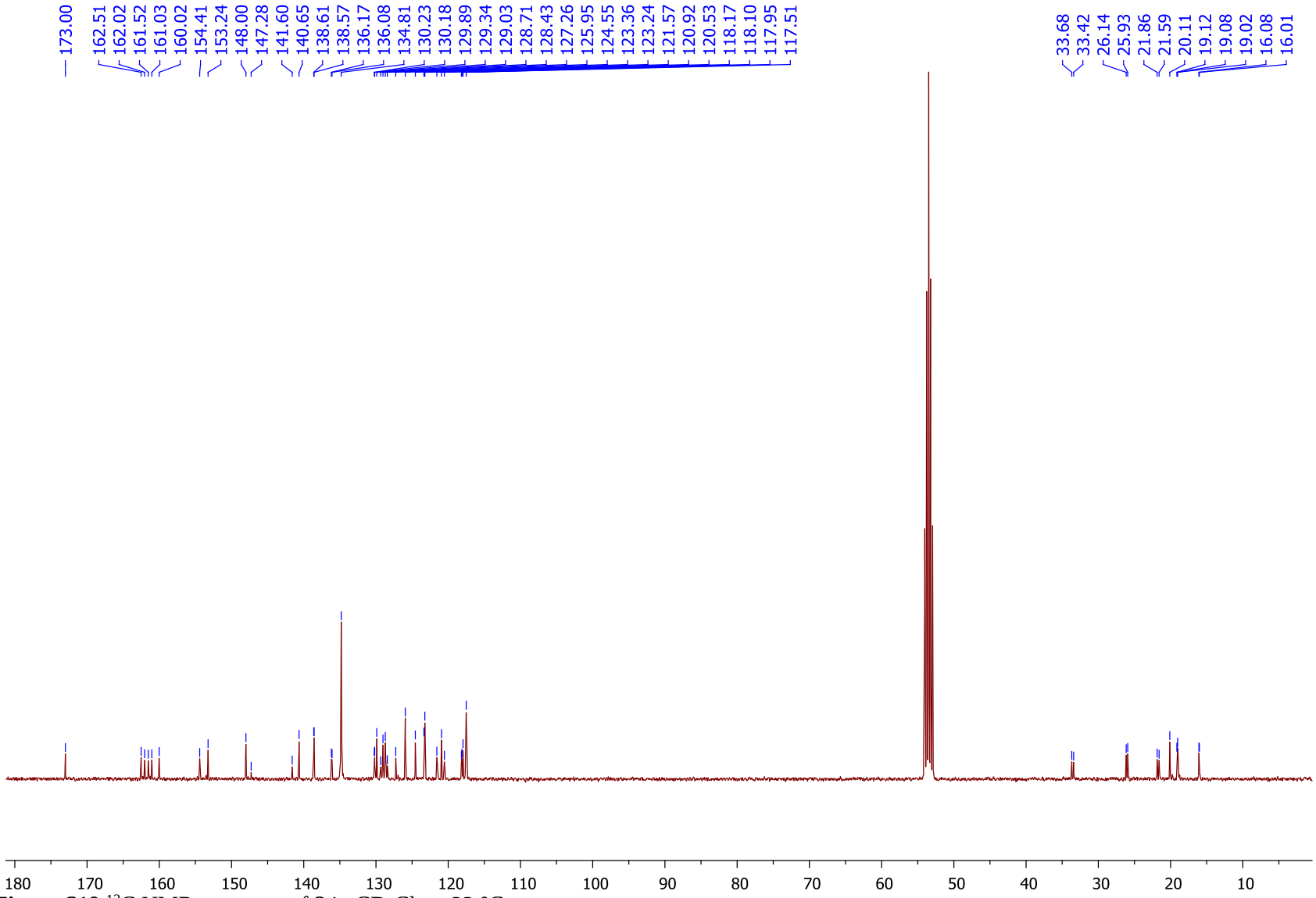

Figure S19.[13]C NMR spectrum of **2** in CD_2Cl_2 at 22 °C.

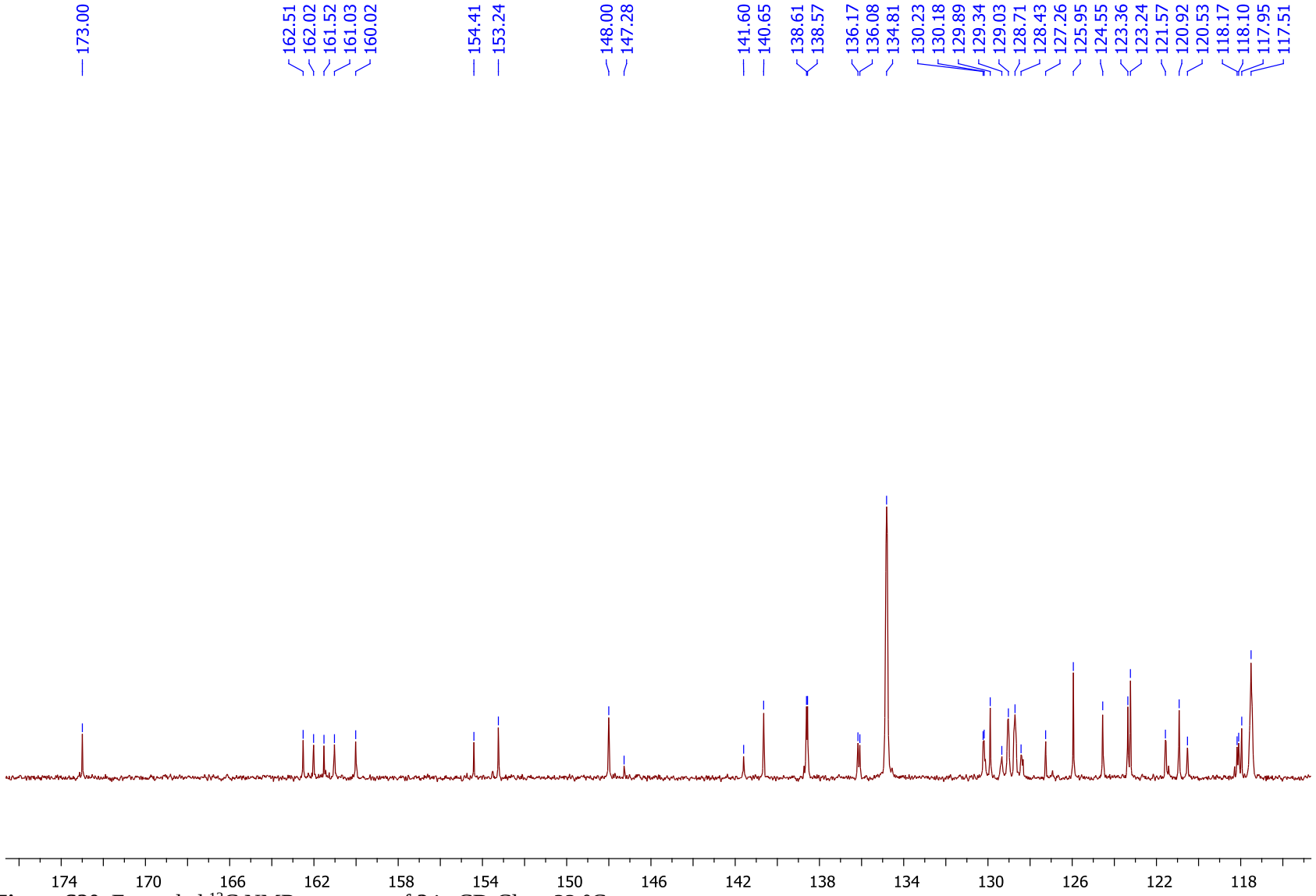

Figure S20. Expanded ^{13}C NMR spectrum of **2** in CD_2Cl_2 at 22 °C.

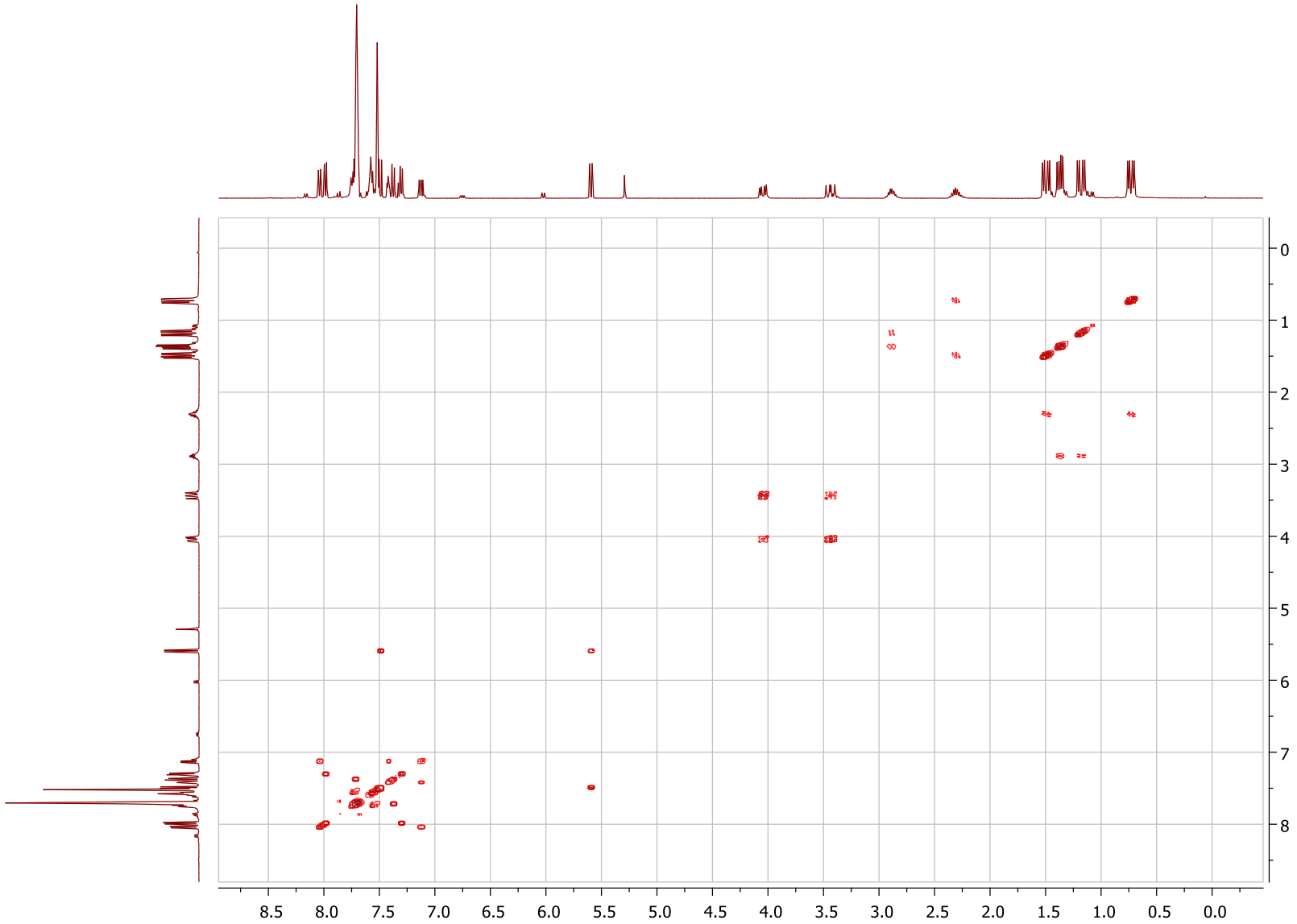

Figure S21. ^{1}H-^{1}H COSY spectrum of **2** in CD_2Cl_2 at 22 °C.

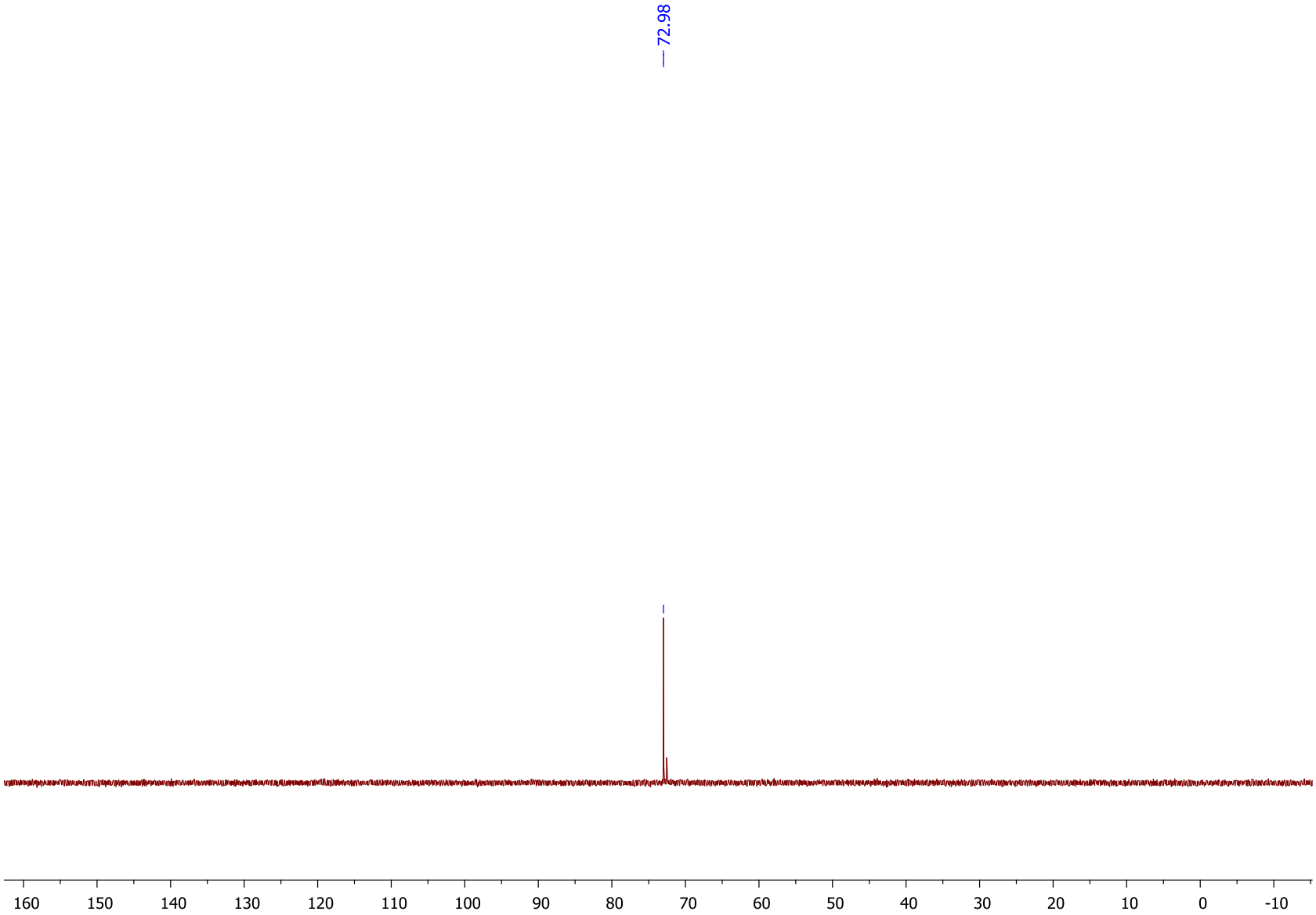

Figure S22.^{31}P NMR spectrum of **2** in CD_2Cl_2 at 22 °C.

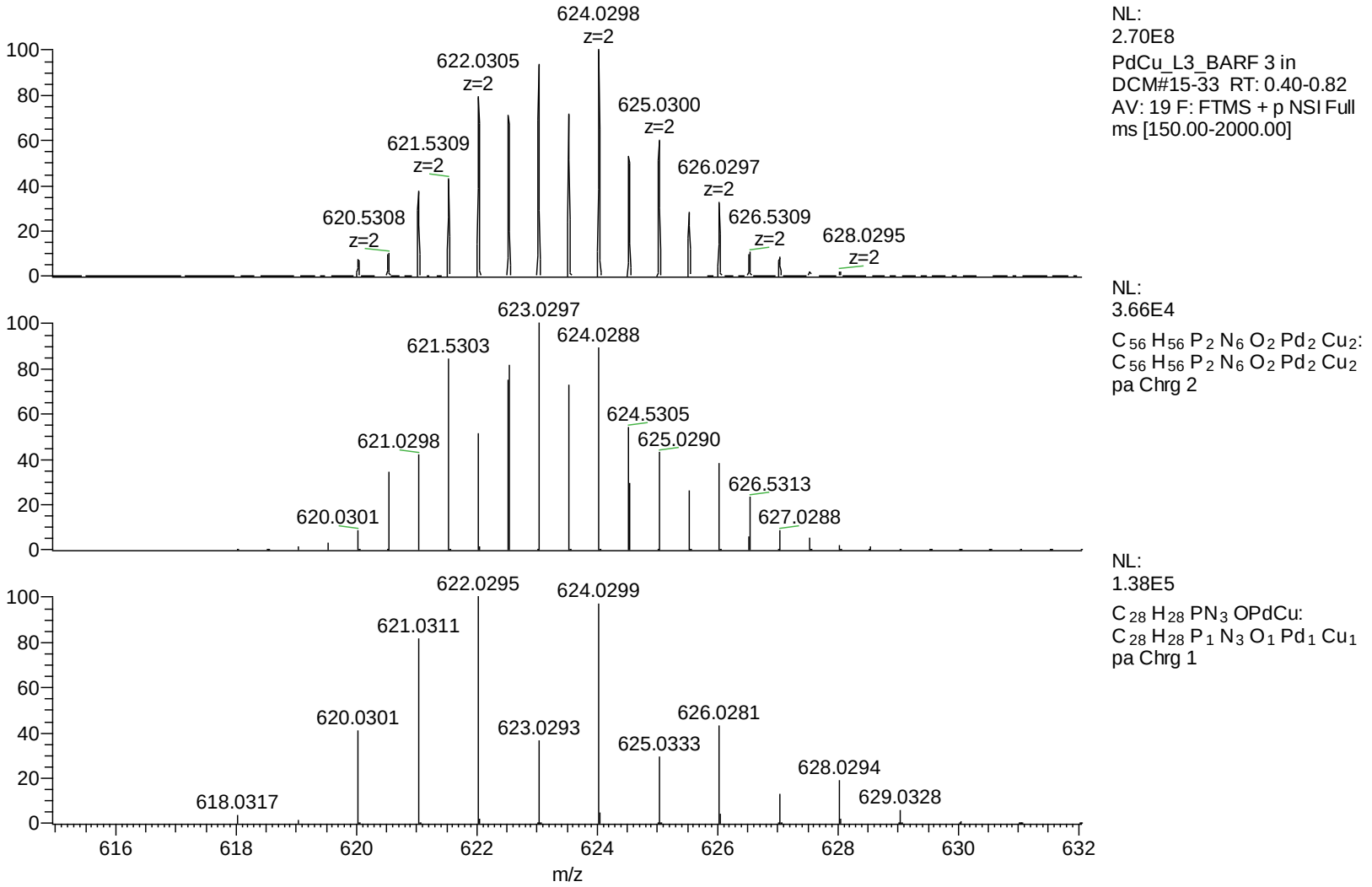

Figure S23. ESI-(HR)MS spectrum of CH_2Cl_2 solution of **2** (top), simulated spectrum for $C_{56}H_{56}O_2N_6P2Pd_2Cu_2^{2+}$ and simulated spectrum for $C_{28}H_{28}ON_3PPdCu^+$ (below).

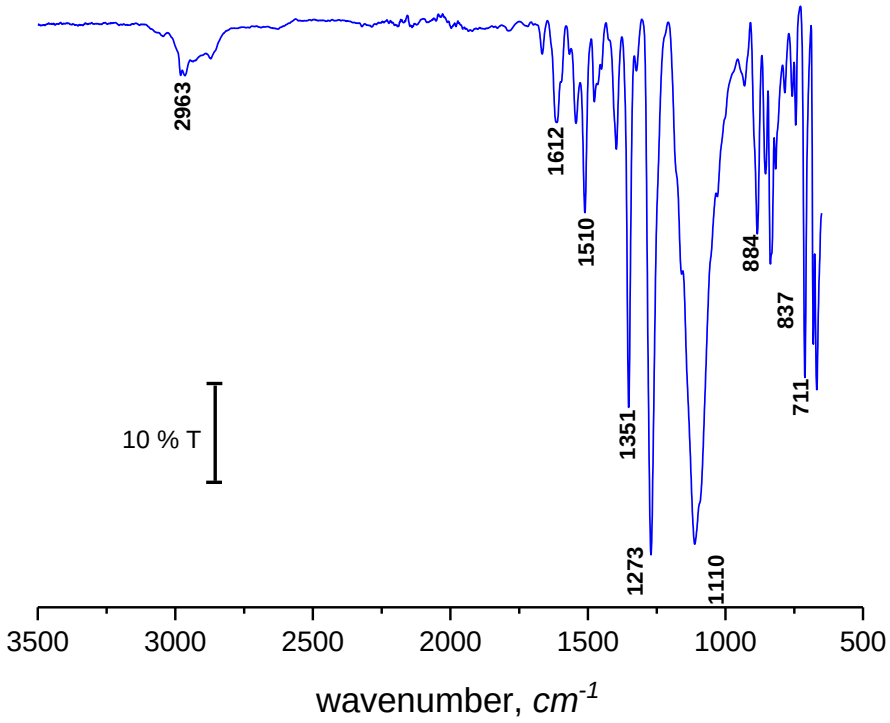

Figure S24. ATR FT-IR transmittance spectrum of **2**.

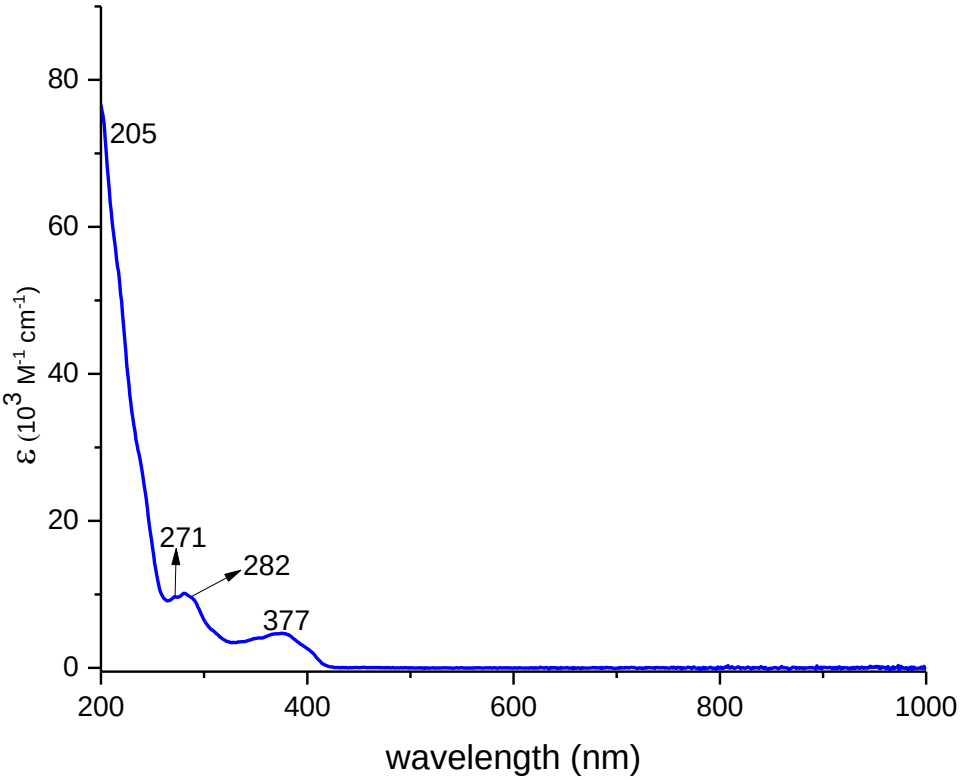

Figure S25. UV-vis absorbance spectrum for **2** in MeCN.

Synthesis of 3

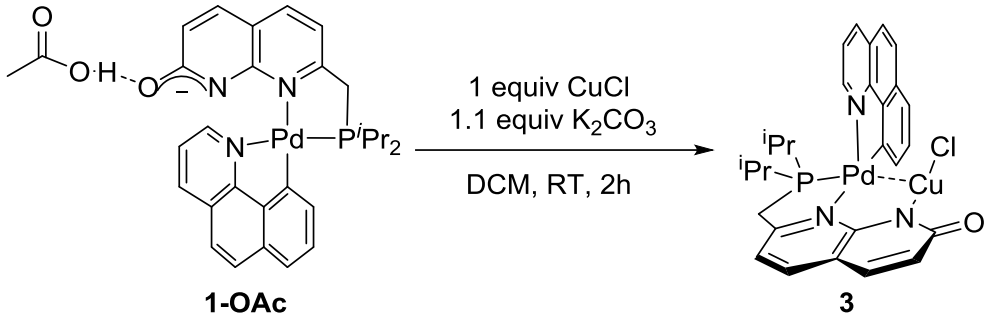

Scheme S4. Synthesis of **3**.

To a 20 mL vial containing **1**-OAc (158.5 mg, 0.25 mmol), CuCl (25.3 mg, 0.25 mmol) and K_2CO_3 (38.8 mg, 0.28 mmol) was added in DCM (4 mL) to give a yellow solution. The reaction was left to stir for 2 hours. Then the solvent was removed under vacuum and the desired complex was re-dissolved in DCM (1 mL), then precipitated with cold pentane (5 x 2 mL) to crash out the yellow powder. Solvent removal yields complex **3** as a yellow solid, 110.7 mg, 0.16 mmol, 66% yield. Crystals suitable for X-ray diffraction study were obtained by vapor diffusion of pentane into a DCM solution at – 30 °C.

^{1}H NMR (600 MHz,CD_2Cl_2, -25 °C) δ: 8.29 (d, $^3J_{HH}$ = 8.1 Hz, 1H, CH_{ar}), 7.93 (d, $^3J_{HH}$ = 7.5 Hz, 1H, CH_{ar}), 7.85 (br.s, 1H, CH_{ar}), 7.80 (d, $^3J_{HH}$ = 8.7 Hz, 1H, CH_{ar}), 7.70-7.62 (m, 4H, CH_{ar}), 7.48 (t, $^3J_{HH}$ = 7.5 Hz, 1H, CH_{ar}), 7.35-7.30 (m, 1H, CH_{ar}), 7.08 (d, $^3J_{HH}$ = 7.5 Hz, 1H, CH_{ar}), 6.72 (d, $^3J_{HH}$ = 9.1 Hz, 1H, CH_{ar}), 3.92 (dd, $^2J_{HH}$ = 17.1 Hz, $^2J_{PH}$ = 6.1 Hz, 1H, CH_2), 3.34 (dd, $^2J_{HH}$ = 17.1 Hz, $^2J_{PH}$ = 14.4 Hz, 1H, CH_2), 2.91-2.81 (m, 1H, C*H*$(CH_3)_2$), 2.29-2.20 (m, 1H, C*H*$(CH_3)_2$), 1.66-1.59 (m, 3H, CH(C*H*$_3)_3$), 1.35-1.30 (m, 3H, CH(C*H*$_3)_3$), 1.06-0.95 (m, 6H, CH(C*H*$_3)_3$).

^{13}C{^{1}H} NMR (151 MHz, CD_2Cl_2, -25 °C) δ: 171.25 (C_{ar}), 158.29 (C_{ar}), 157.83 (C_{ar}), 155.62 (C_{ar}), 154.06 (C_{ar}), 148.55 (C_{ar}), 141.85 (C_{ar}), 138.72 (C_{ar}), 138.12 (C_{ar}), 136.21 (d, J_{PC} =8.7 Hz, C_{ar}), 136.01 (C_{ar}), 134.36 (C_{ar}), 129.71-129.57 (m, C_{ar}), 127.60 (C_{ar}), 124.30 (C_{ar}), 123.90 (C_{ar}), 123.59 (C_{ar}), 121.73 (C_{ar}), 117.21 (C_{ar}), 113.92 (d, J_{PC} =8.1 Hz, C_{ar}), 111.41 (C_{ar}), 33.53 (d, $^1J_{PC}$ =26.3 Hz, CH_2), 26.83 (d, $^1J_{PC}$ =21.2 Hz, *C*H$(CH_3)_2$), 20.95 (d, $^1J_{PC}$ =27.1 Hz, *C*H$(CH_3)_2$), 19.75 (CH(*C*H$_3)_2$), 19.13 (CH(*C*H$_3)_2$), 18.36 (CH(*C*H$_3)_2$), 18.08 (CH(*C*H$_3)_2$), 16.18 (d, J_{PC} =6.5 Hz, CH(*C*H$_3)_2$).

^{31}P{^{1}H} NMR (262 MHz, CD_2Cl_2, 22 °C) δ: 66.33

ESI-HRMS (m/z pos): Found (Calcd $C_{28}H_{28}O_1N_3P_1Pd_1Cu_1$: 622.0263 (622.0295).

FT-IR (ATR, solid): 2959 (br, w), 2924 (br, w), 1558 (s), 1402 (br, s), 1259 (s), 1087 (br, w), 1020 (br, s), 798 (s) cm^{-1}.

UV-vis (MeCN), λ, nm (ε, $M^{-1}\cdot cm^{-1}$) : 368 (1805), 288 (3424), 218 (12055).

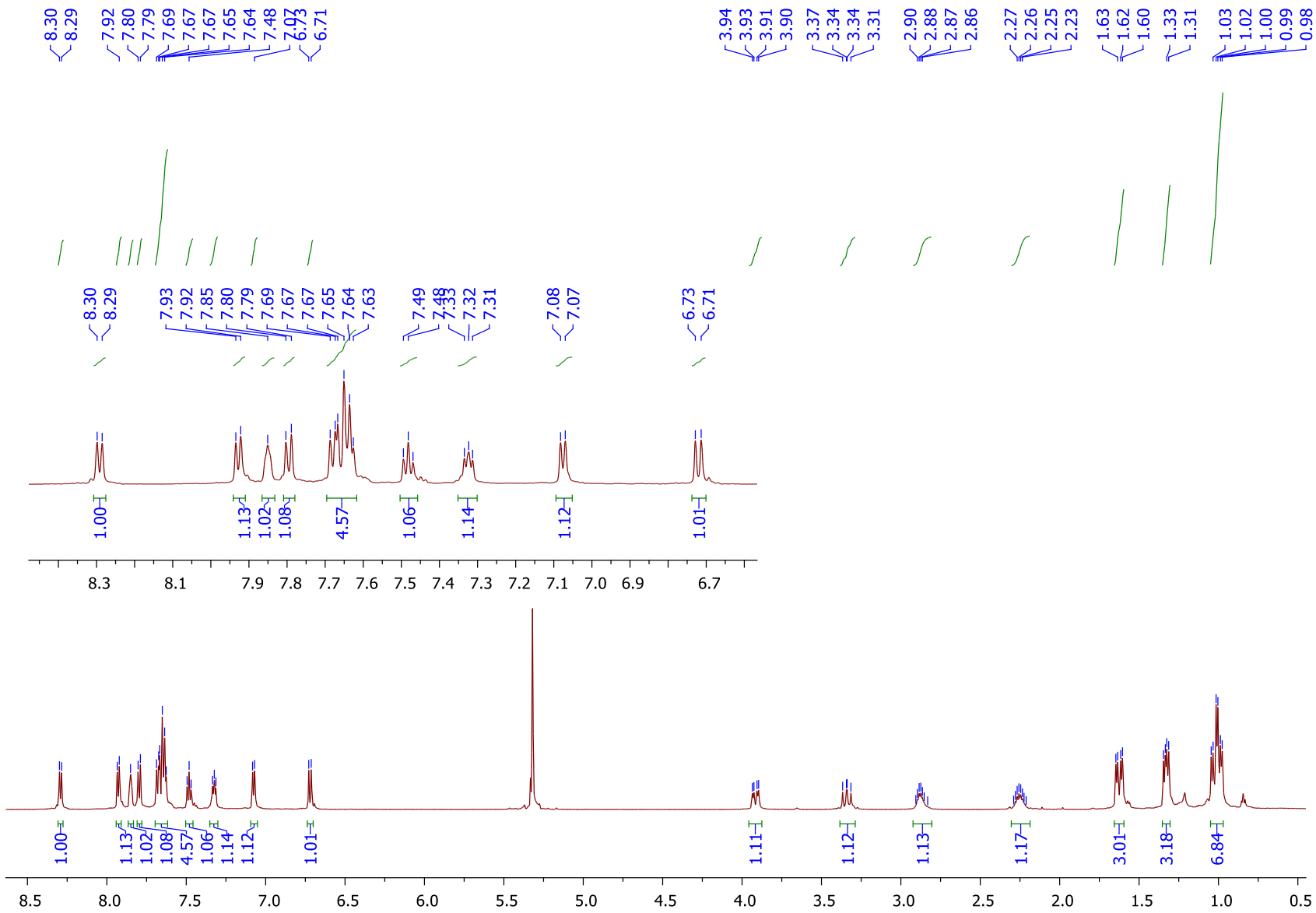

Figure S26.[1]H NMR spectrum of **3** in CD_2Cl_2 at -25 °C.

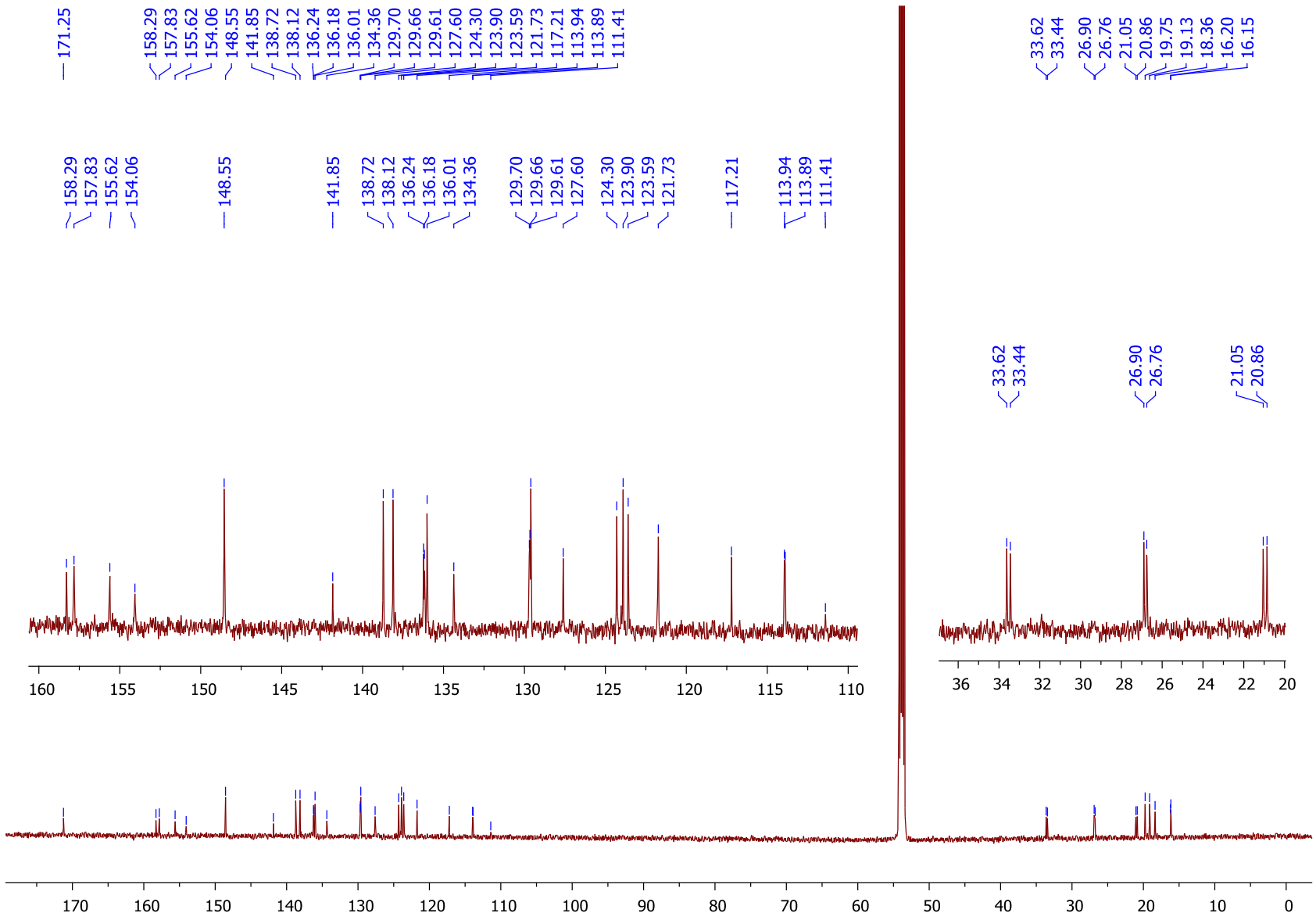

Figure S27.[13]C NMR spectrum of **3** in CD_2Cl_2 at -25 °C.

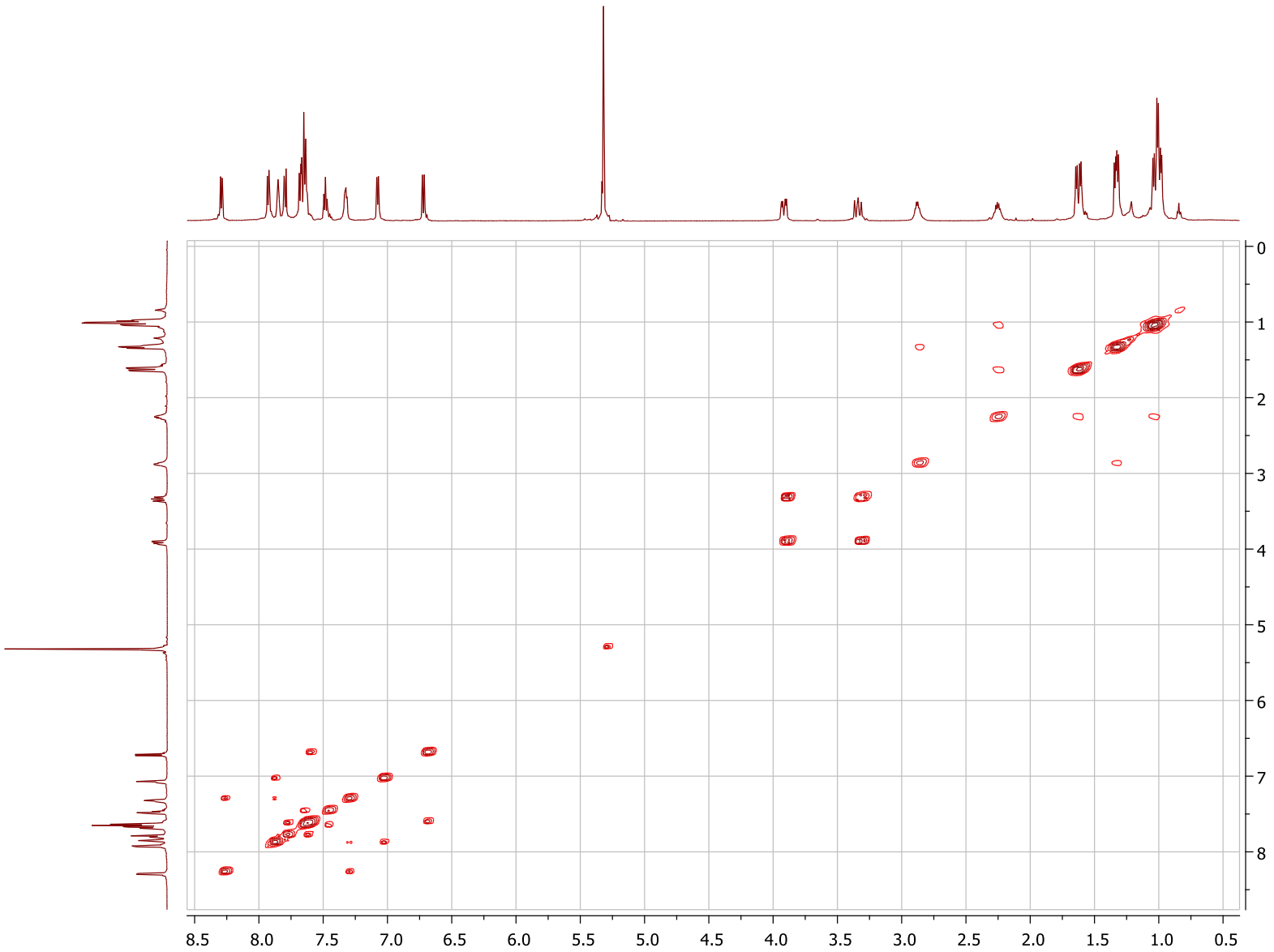

Figure S28. ^{1}H-^{1}H COSY spectrum of **3** in CD_2Cl_2 at -25 °C.

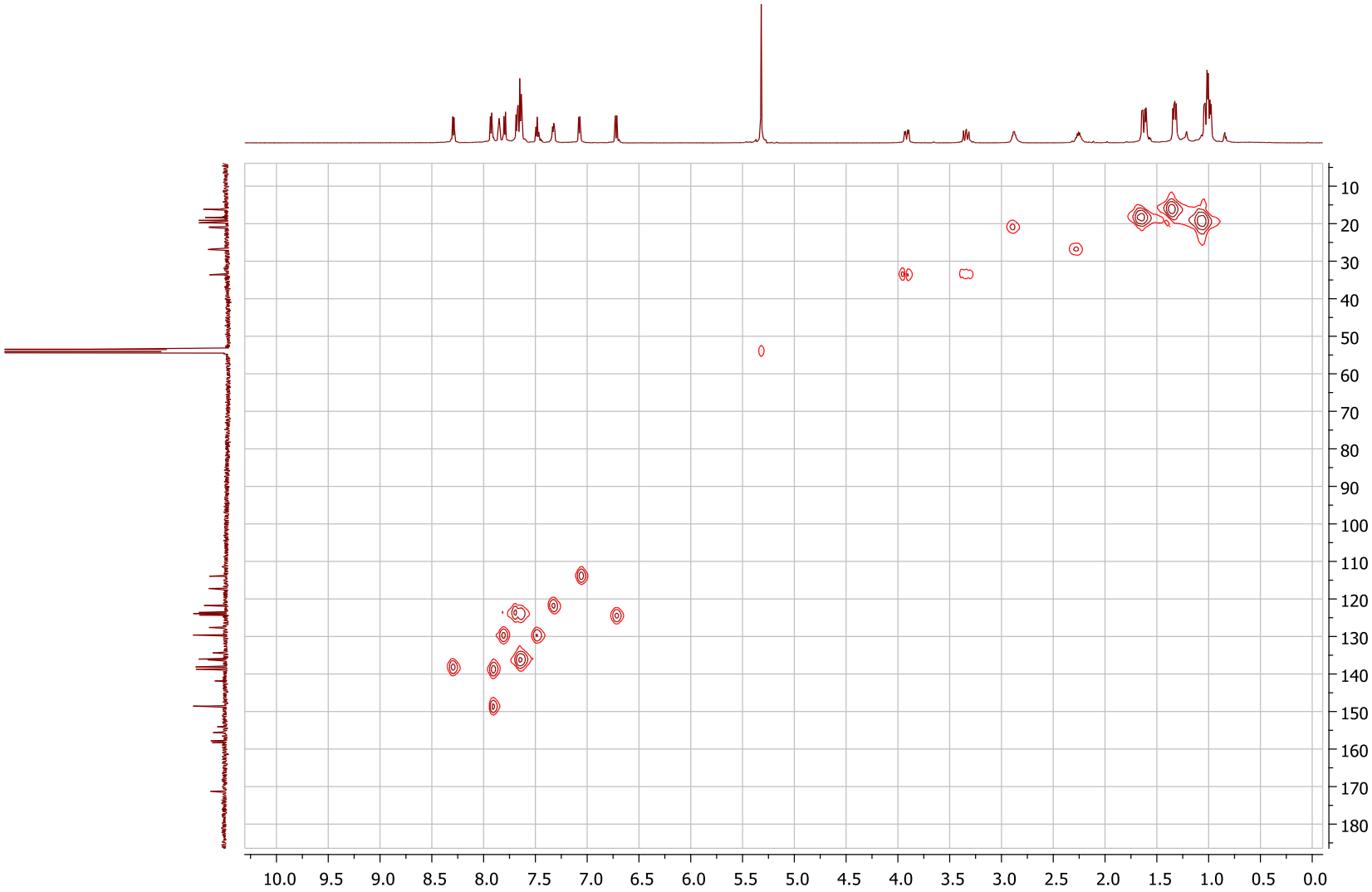

Figure S29. ^{1}H-^{13}C HMQC spectrum of **3** in CD_2Cl_2 at -25 °C.

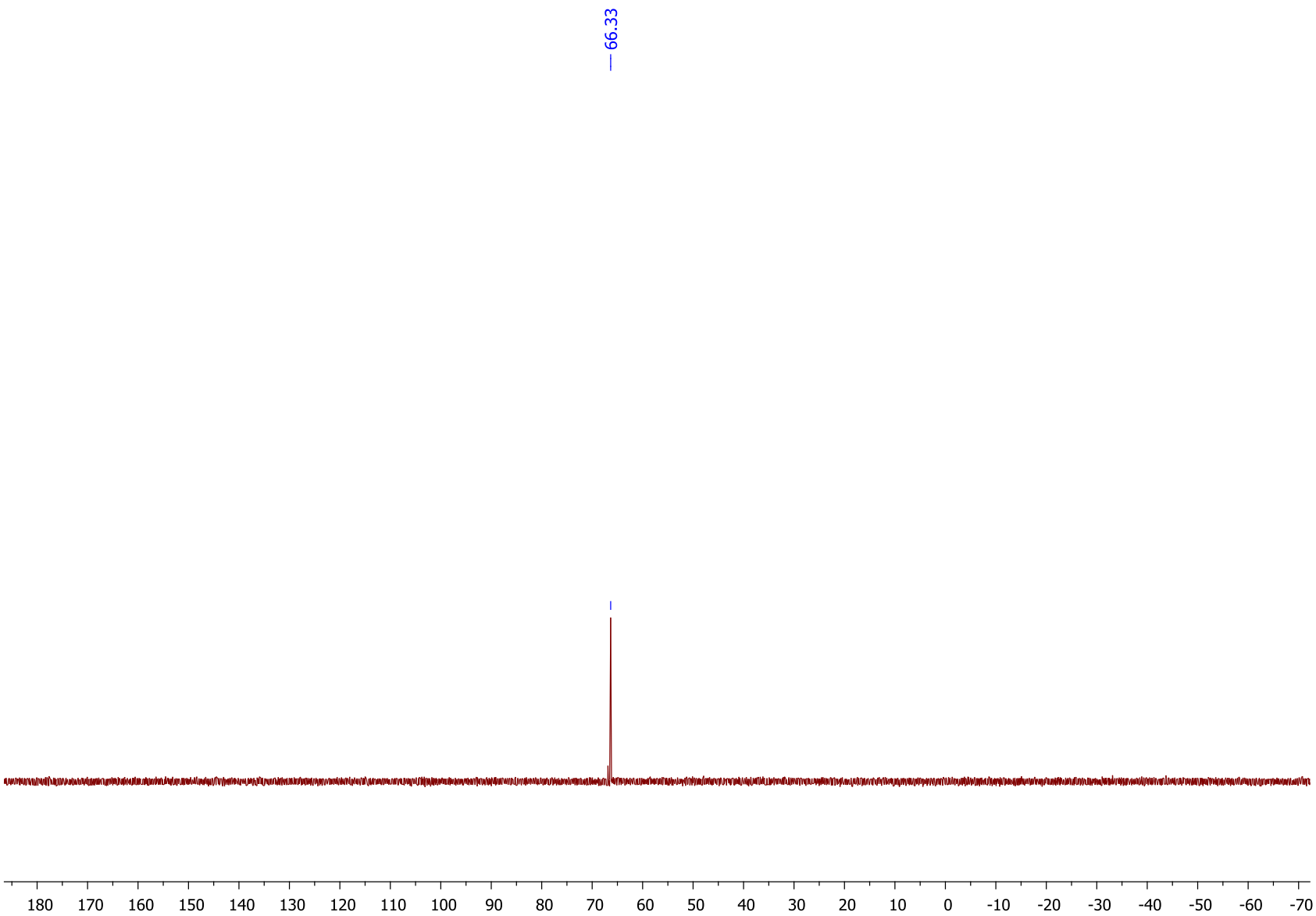

Figure S30. ^{31}P spectrum of **3** in CD_2Cl_2 at -25 °C.

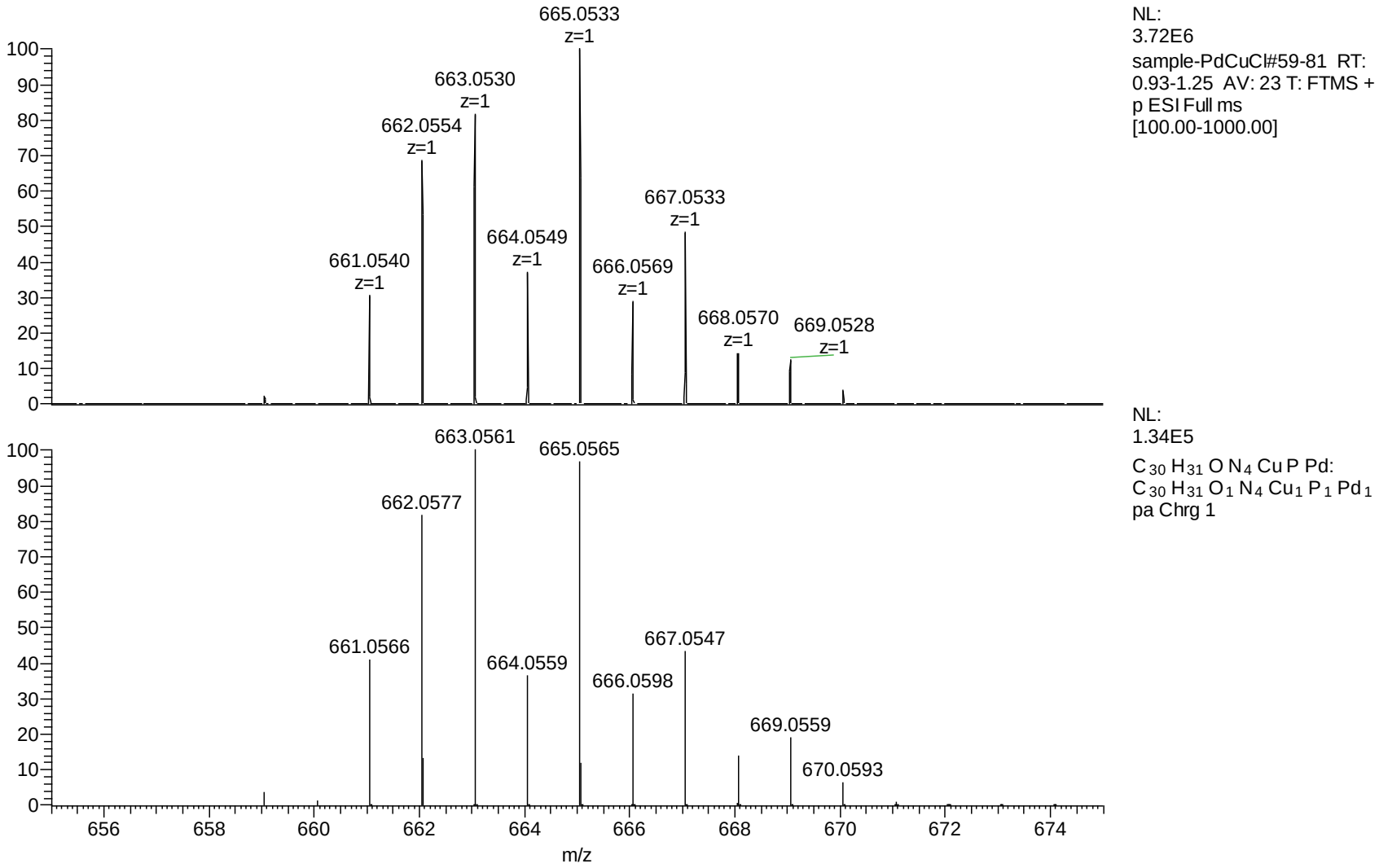

Figure S31. ESI-(HR)MS spectrum of a MeCN solution of **3** (top) and simulated spectrum for $C_{28}H_{28}O_1N_3P_1Pd_1Cu_1$ (bottom).

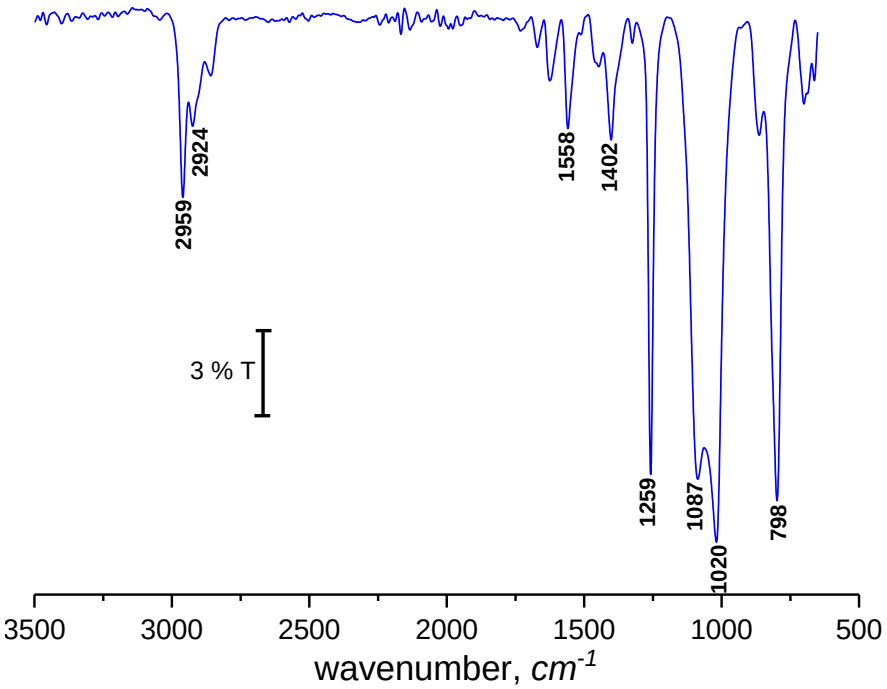

Figure S32. ATR FT-IR transmittance spectrum of **3**.

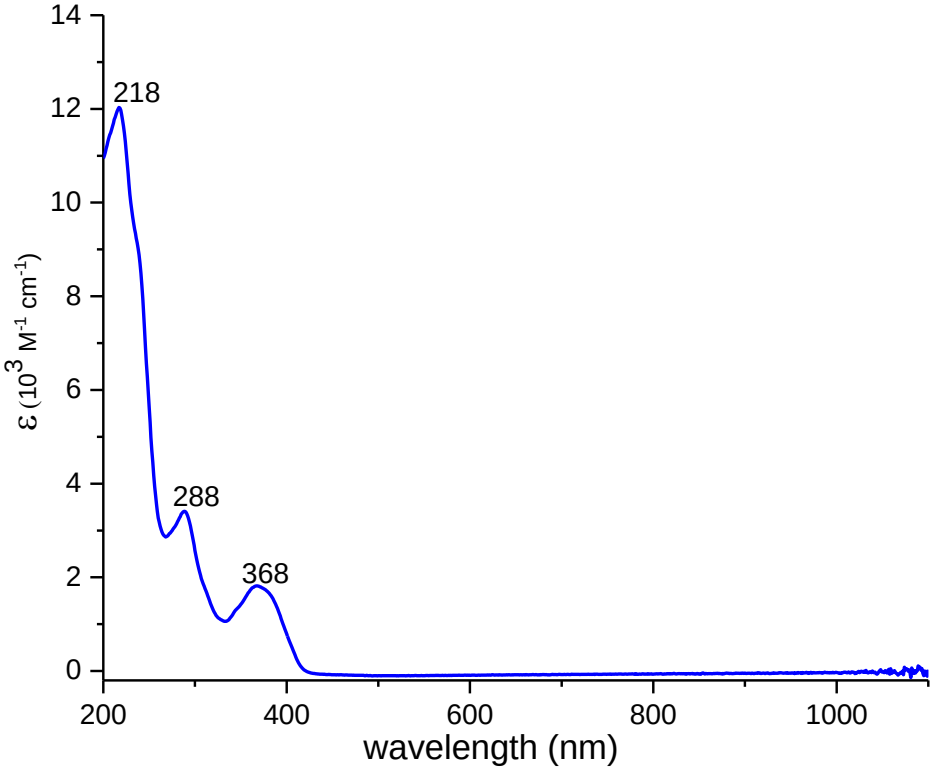

Figure S33. UV-vis absorbance spectrum for **3** in MeCN.

Synthesis of 4

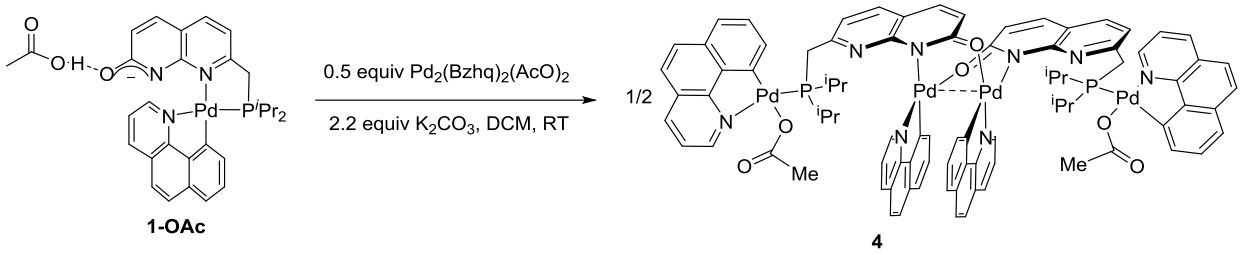

Scheme S5. Synthesis of **4.**

Under inert atmosphere to a 20 mL vial containing **1**-OAc (103.5 mg, 0.16 mmol), palladium precursor $[Pd(Bzhq)(AcO)]_2$ (57.3 mg, 0.08 mmol) and K_2CO_3 (50.7 mg, 0.36 mmol) were added in cold DCM (5 mL) to give a yellow solution. The reaction was left to stir for 2 hours. Then the solvent was removed under vacuum and the desired complex was re-dissolved in DCM (1 mL) and precipitated with cold hexane (5 x 2 mL) to give yellow powder. Solvent removal yields complex **4** as a yellow solid, 155.7 mg, 0.08 mmol, 51% yield. Crystals suitable for X-ray diffraction study were obtained by vapor diffusion of hexane into a toluene solution at room temperature.

^{1}H NMR (600 MHz,CD_2Cl_2, 23 °C) δ: 8.70-8.68 (m, 2H, CH_{ar}), 8.30 (dd, $^3J_{HH}$ = 8.3 Hz, 1.3 Hz, 2H, CH_{ar}), 8.08 (d, $^3J_{HH}$ = 4.3 Hz, 2H, CH_{ar}), 7.73-7.68 (m, 4H, CH_{ar}), 7.64 (d, $^3J_{HH}$ = 8.7 Hz, 2H, CH_{ar}), 7.60 (d, $^3J_{HH}$ = 8.7 Hz, 2H, CH_{ar}), 7.57-7.53 (m, 2H, CH_{ar}), 7.51 (d, $^3J_{HH}$ = 8.3 Hz, 2H, CH_{ar}), 7.47-7.43 (m, 4H, CH_{ar}), 7.31 (d, $^3J_{HH}$ = 8.7 Hz, 2H, CH_{ar}), 7.24-7.21 (m, 4H, CH_{ar}), 7.18 (br.s, 2H, CH_{ar}), 7.07-7.05 (br.s, 2H, CH_{ar}), 6.97 (t, $^3J_{HH}$ = 7.4 Hz, 2H, CH_{ar}), 6.85 (d, $^3J_{HH}$ = 8.7 Hz, 2H, CH_{ar}), 6.42 (dd, $^3J_{HH}$ = 8.3 Hz, 5.1 Hz, 2H, CH_{ar}), 6.08 (d, $^3J_{HH}$ = 7.4 Hz, 2H, CH_{ar}), 3.89-3.79 (m, 4H, CH_2), 3.14-3.05 (m, 2H, C*H*$(CH_3)_2$), 2.95-2.84 (m, 2H, C*H*$(CH_3)_2$), 2.03 (s, 6H, OAc anion), 1.28 (dd, $^3J_{PH}$ = 7.1 Hz, $^3J_{HH}$ = 15.6 Hz , 6H, CH(C*H*$_3)_3$), 0.94 (dd, $^3J_{PH}$ = 7.1 Hz, $^3J_{HH}$ = 16.4 Hz, 6H, CH(C*H*$_3)_3$), 0.78 (dd, $^3J_{PH}$ = 7.1 Hz, $^3J_{HH}$ = 16.4 Hz, 6H, CH(C*H*$_3)_3$), 0.68 (dd, $^3J_{PH}$ = 7.1 Hz, $^3J_{HH}$ = 15.6 Hz , 6H, CH(C*H*$_3)_3$).

^{13}C{^{1}H} NMR (151 MHz, CD_2Cl_2, -25 °C) δ: 177.10 (C_{ar}), 173.02 (C_{ar}), 158.54 (d, J_{PC} =6.5 Hz, C_{ar}), 156.38 (C_{ar}), 153.33 (C_{ar}), 152.21 (C_{ar}), 151.12 (C_{ar}), 149.46 (C_{ar}), 148.01 (C_{ar}), 147.15 (C_{ar}), 142.91 (C_{ar}), 139.98 (C_{ar}), 137.58 (C_{ar}), 136.78 (C_{ar}), 136.13 (C_{ar}), 135.93 (C_{ar}), 134.93 (C_{ar}), 133.75 (C_{ar}), 132.25 (C_{ar}), 130.02 (C_{ar}), 129.03 (d, J_{PC} =6.5 Hz, C_{ar}) 128.26 (C_{ar}), 128.12 (C_{ar}), 127.84 (C_{ar}), 127.36 (C_{ar}), 126.71 (C_{ar}), 125.32 (C_{ar}), 124.41 (C_{ar}), 123.32 (C_{ar}), 122.99 (d, J_{PC} =7.7 Hz, C_{ar}), 121.60 (d, J_{PC} =14.8 Hz, C_{ar}), 121.30 (C_{ar}), 119.30 (C_{ar}), 116.12 (Ar-*C*), 34.25 (CH_2), 25.45 (OAc anion), 23.47 (d, $^1J_{PC}$ =22.6 Hz, *C*H$(CH_3)_2$), 22.81 (d, $^1J_{PC}$ =17.5 Hz, *C*H$(CH_3)_2$), 21.36 (CH(*C*H$_3)_2$), 18.81 (d, J_{PC} =6.1 Hz, CH(*C*H$_3)_2$), 18.35 (CH(*C*H$_3)_2$), 17.52 (CH(*C*H$_3)_2$).

^{31}P{^{1}H} NMR (262 MHz, CD_2Cl_2, 23 °C) δ: 49.48.

ESI-HRMS (m/z pos): Found (Calcd): $C_{82}H_{72}O_2N_8P_2Pd_4$: 1686.1362 (1686.1387). During the analysis binuclear species were also observed in HRMS follows as $C_{41}H_{36}ON_4P_1Pd_2$: 843.0747 (843.0691).

FT-IR (ATR, solid): 2959 (br, w), 2924 (br, w), 1558 (br, s), 1402 (br, s), 1259 (s), 1087 (br, s), 1020 (s), 798 (s) cm^{-1}.

UV-vis (MeCN), λ, nm (ε, $M^{-1}\cdot cm^{-1}$) : 459 (644), 364 (5964), 288 (11607), 235 (32080), 217 (42284).

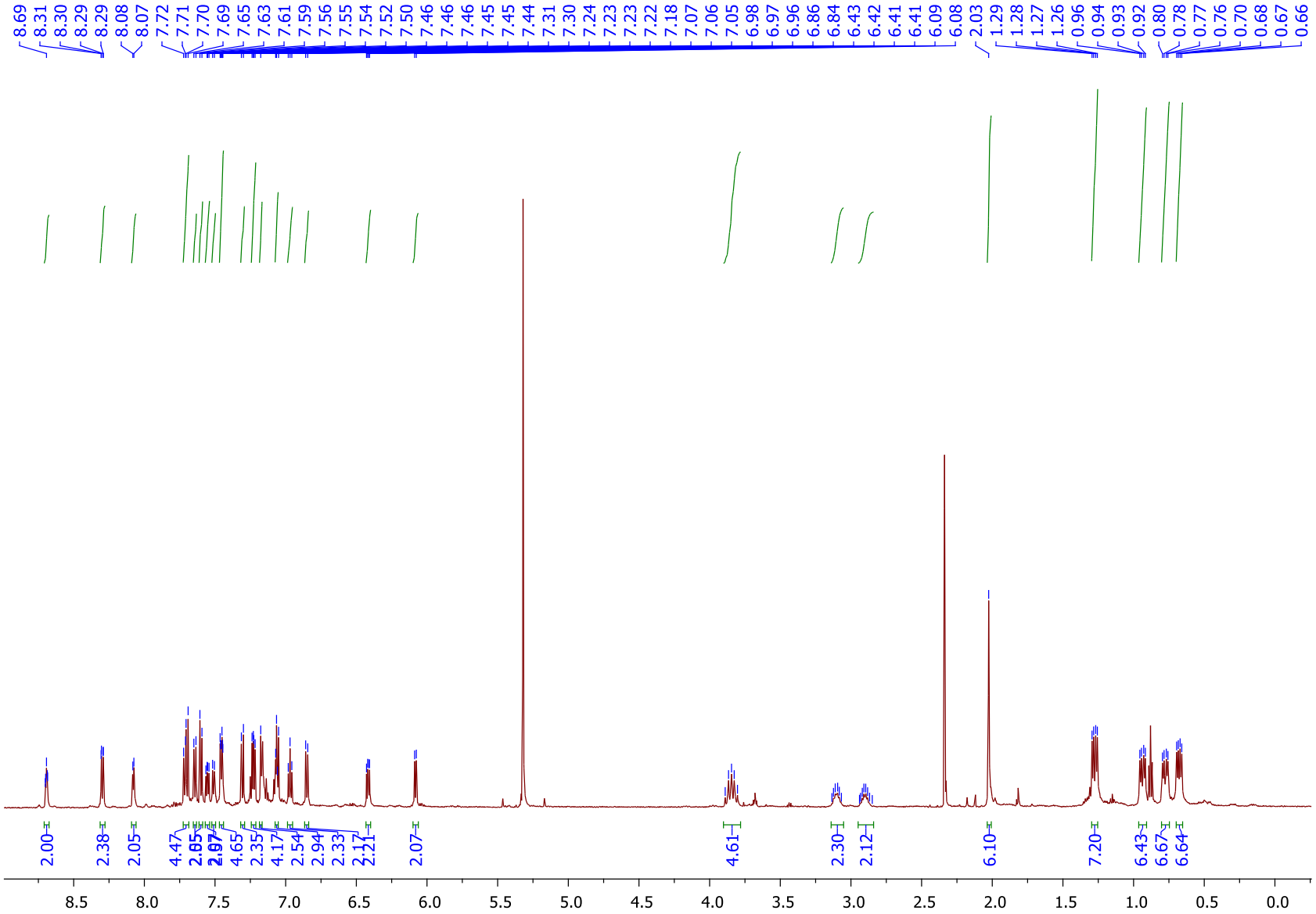

Figure S34.[1]H NMR spectrum of **4** in CD_2Cl_2 at 23 °C.

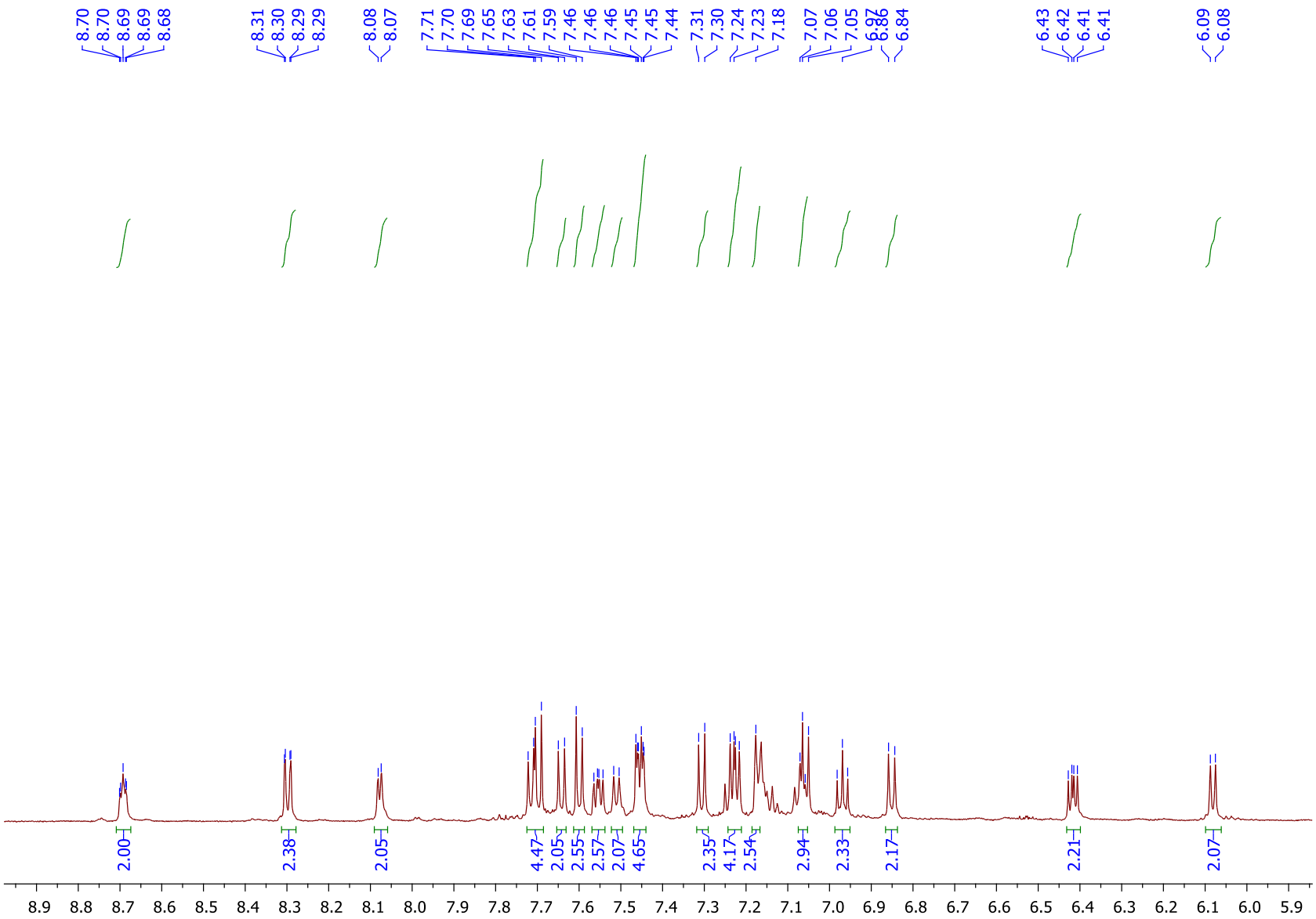

Figure S35. Expanded aromatic region of ^{1}H NMR spectrum of **4** in CD_2Cl_2 at 23 °C.

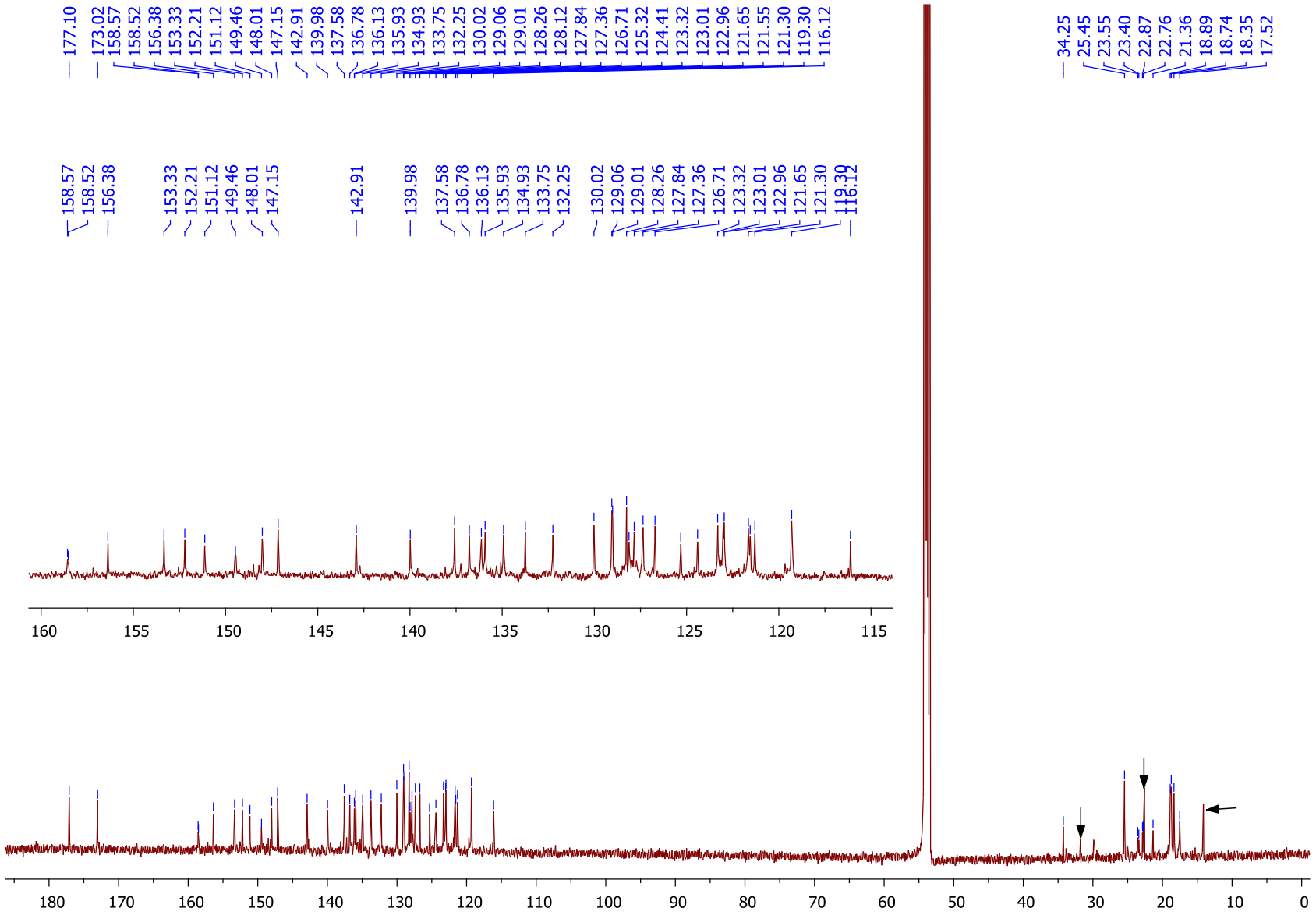

Figure S36.[13]C NMR spectrum of **4** in CD_2Cl_2 at - 25 °C. The peaks marked by arrows corresponds to residual hexane.

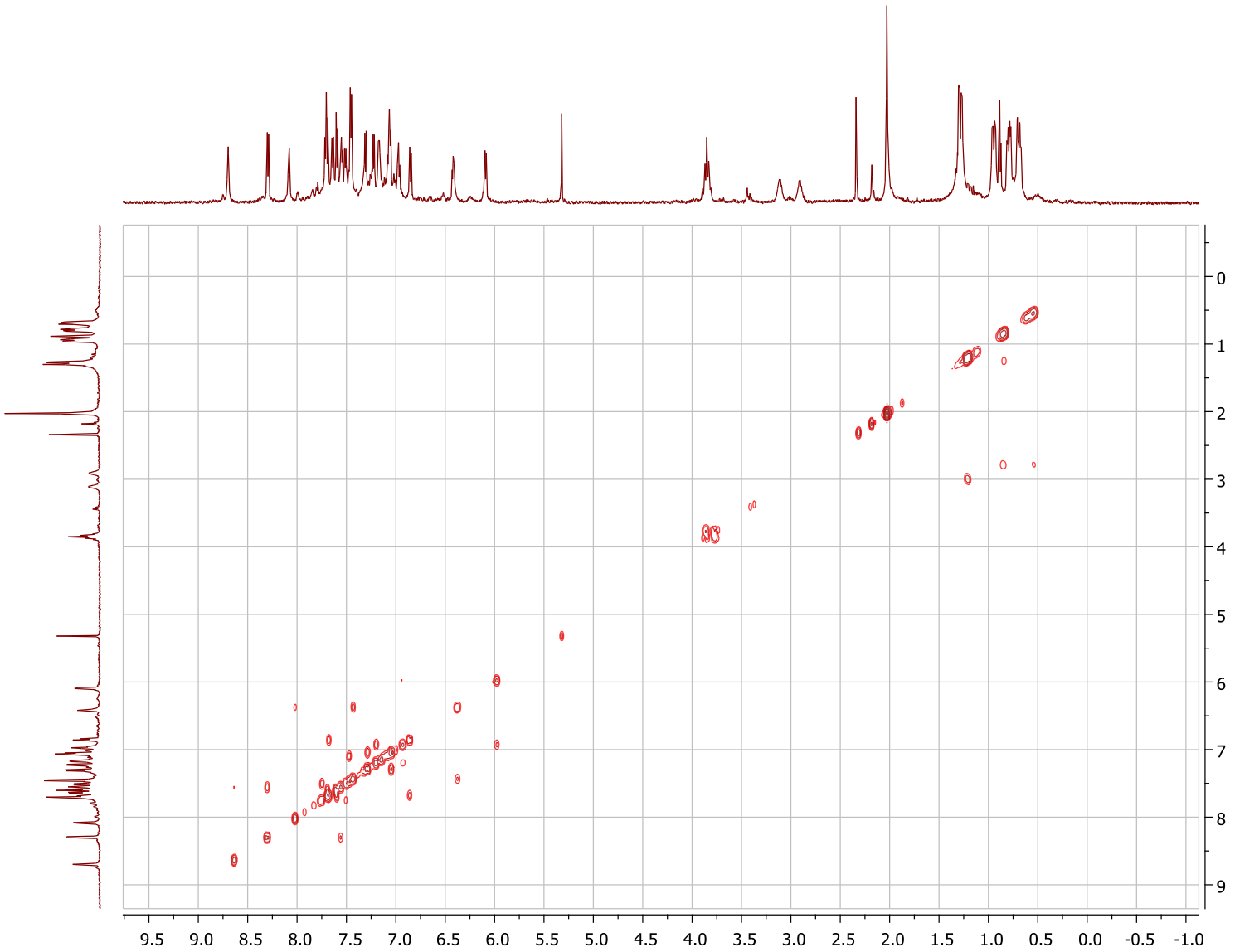

Figure S37. ^{1}H-^{1}H COSY spectrum of **4** in CD_2Cl_2 at -25 °C.

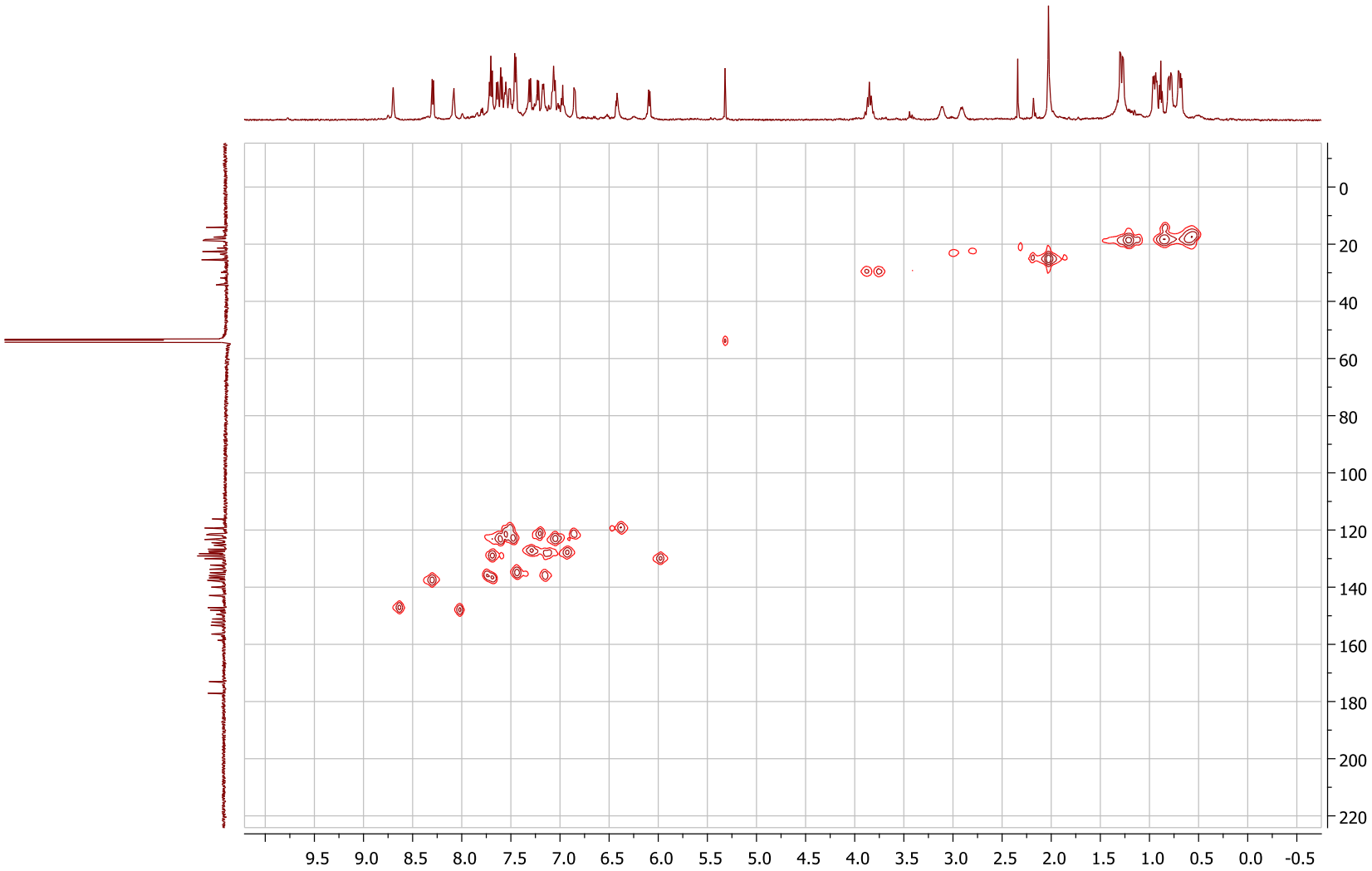

Figure S38. ^{1}H-^{13}C HMQC spectrum of **4** in CD_2Cl_2 at -25 °C.

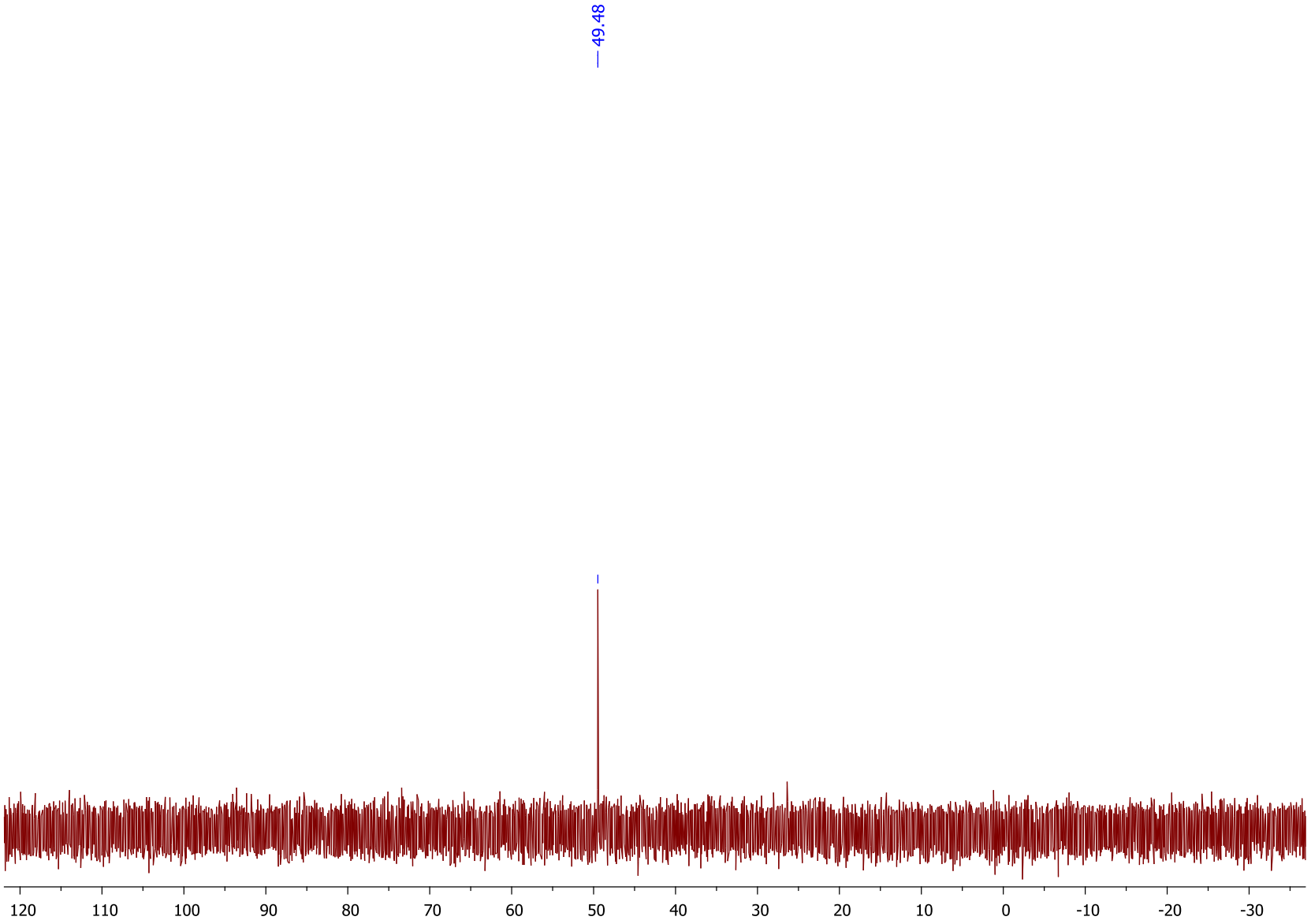

Figure S39. ^{31}P NMR spectrum of **4** in CD_2Cl_2 at 23 °C.

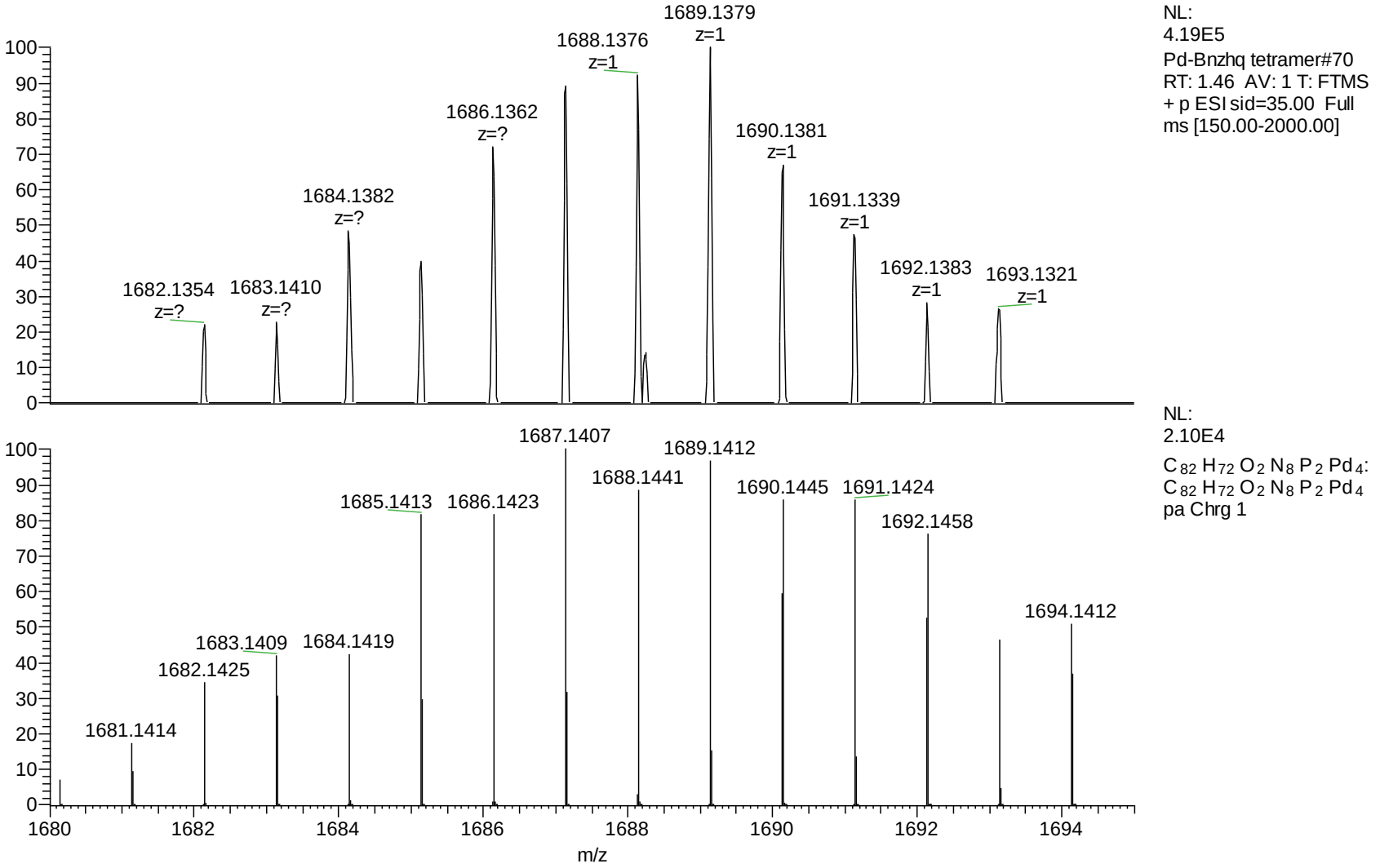

Figure S40. ESI-(HR)MS spectrum of a DCM solution of **4** (top) and simulated spectrum for $C_{82}H_{72}O_2N_8P_2Pd_4$ (bottom).

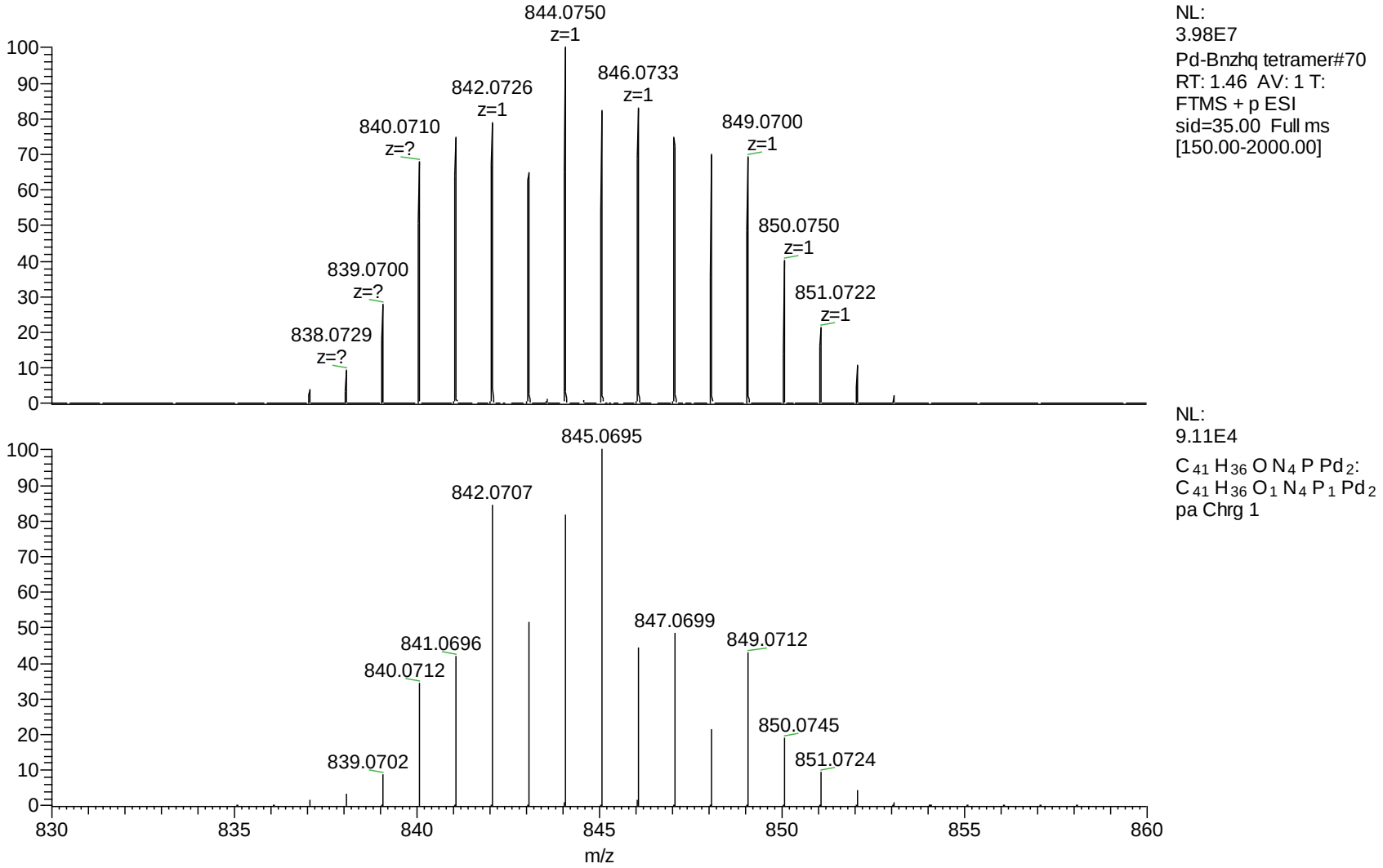

Figure S41. ESI-(HR)MS spectrum of a DCM solution of **4** (top) and simulated spectrum for $C_{41}H_{36}ON_4P_1Pd_2$ (bottom).

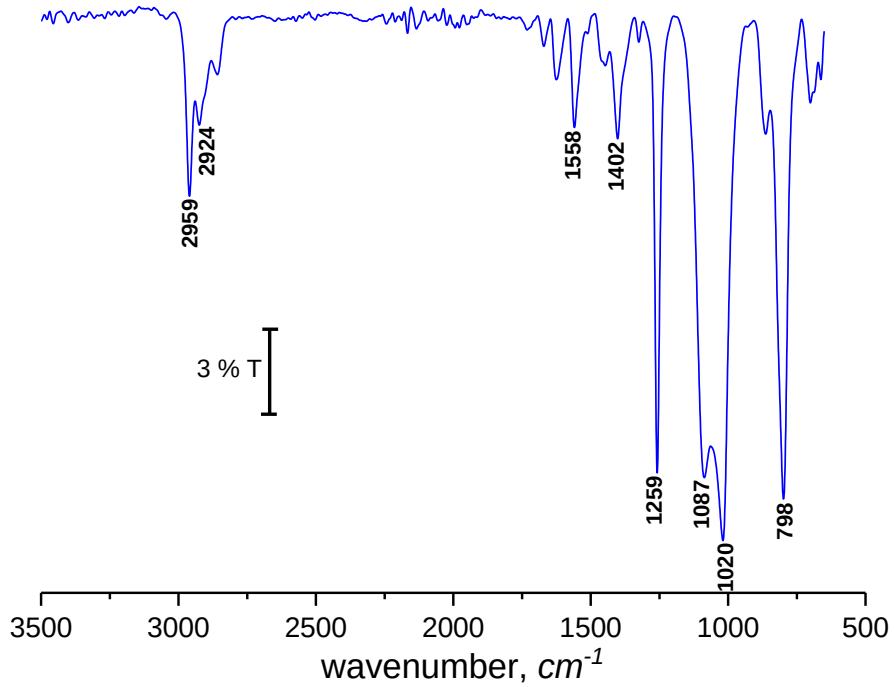

Figure S42. ATR FT-IR transmittance spectrum of **4**.

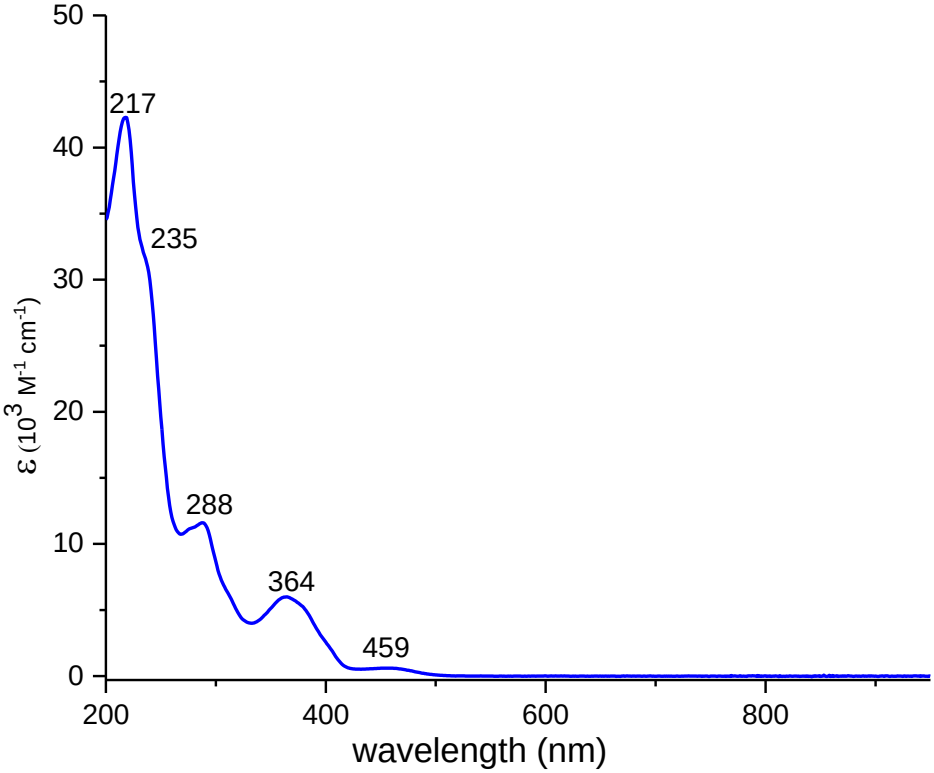

Figure S43. UV-vis absorbance spectrum for **4** in MeCN

Synthesis of 5

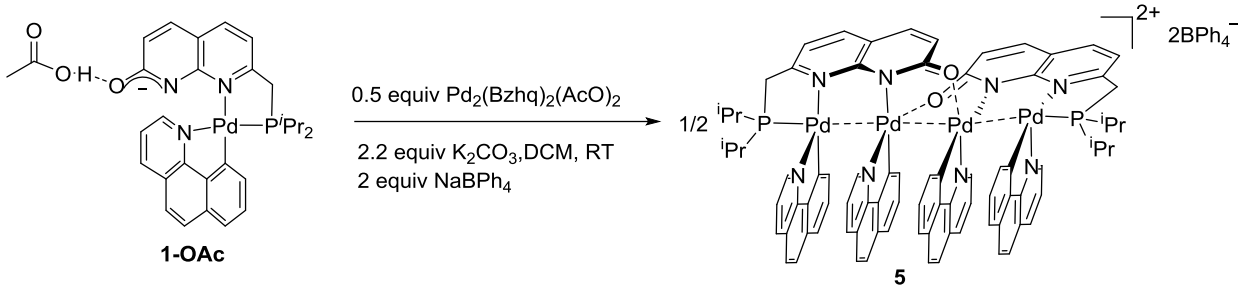

Scheme S6. Synthesis of **5**.

To a 20 mL vial containing **1**-OAc (100.2 mg, 0.16 mmol), palladium precursor $Pd_2(Bzhq)_2(AcO)_2$ (55.5 mg, 0.08 mmol), sodium tetraphenyl borate (110.6 mg, 0.32 mmol) and K_2CO_3 (49.1 mg, 0.35 mmol) were added in cold DCM (4 mL) to give yellow solution. The reaction mixture was left to stir for 2 hours at room temperature. Then the solvent was removed under vacuum and the desired complex was extracted in THF (1 mL), then precipitated with cold pentane (5 x 2 mL) to give yellow powder. Solvent removal yields complex **5** as a yellow solid, 221.5 mg, 0.09 mmol, 56 % yield. Crystals suitable for X-ray diffraction study were obtained by vapor diffusion of cyclohexane into a THF solution at room temperature.

^{1}H NMR (600 MHz,CD_2Cl_2, 0 °C) δ: 8.43 (d, $^3J_{HH}$ = 7.8 Hz, 2H, CH_{ar}), 7.93-7.88 (br. m, 4H, CH_{ar}), 7.80 (d, $^3J_{HH}$ = 7.8 Hz, 2H, CH_{ar}), 7.55-7.46 (m, 8H, CH_{ar}), 7.36 (br. s, 16H, CH_{ar}), 7.20-7.16 (m, 2H, CH_{ar}), 7.09-6.97 (m, 22H, CH_{ar}), 6.88-6.83 (br. m, 8H, CH_{ar}), 6.72 (t, $^3J_{HH}$ = 7.4 Hz, 2H, CH_{ar}), 6.62 (t, $^3J_{HH}$ = 7.4 Hz, 2H, CH_{ar}), 6.20-6.16 (m, 2H, CH_{ar}), 6.11 (d, $^3J_{HH}$ = 5.1 Hz, 2H, CH_{ar}), 5.98 (t, $^3J_{HH}$ = 6.3 Hz, 2H, CH_{ar}), 5.89 (t, $^3J_{HH}$ = 7.8 Hz, 2H, CH_{ar}), 5.28 (d, $^3J_{HH}$ = 9.1 Hz, 2H, CH_{ar}), 4.48 (d, $^3J_{HH}$ = 7.3 Hz, 2H, CH_{ar}), 3.57 (d, $^3J_{HH}$ = 6.8 Hz, 1H, CH_2), 3.54 (d, $^3J_{HH}$ = 6.8 Hz, 1H, CH_2), 3.18-3.05 (m, 2H, CH_2), 2.06-1.95 (m, 2H, C*H*$(CH_3)_2$), 0.88 (dd, $^3J_{PH}$ = 6.9 Hz, $^3J_{HH}$ = 13.1 Hz , 6H, CH(C*H*$_3)_3$), 0.57 (dd, $^3J_{PH}$ = 6.9 Hz, $^3J_{HH}$ = 18.7 Hz, 6H, CH(C*H*$_3)_3$), 0.42-0.33 (m, 2H, C*H*$(CH_3)_2$), 0.22 (dd, $^3J_{PH}$ = 7.1 Hz, $^3J_{HH}$ = 14.7 Hz, 6H, CH(C*H*$_3)_3$), - 0.32 (dd, $^3J_{PH}$ = 7.1 Hz, $^3J_{HH}$ = 16.7 Hz , 6H, CH(C*H*$_3)_3$).

^{13}C{^{1}H} NMR (151 MHz, CD_2Cl_2, -20 °C) δ: 171.76 (C_{ar}), 164.05 (m, C_{ar}), 159.68 (C_{ar}), 157.39 (C_{ar}), 154.15 (C_{ar}), 153.12 (C_{ar}), 152.28 (C_{ar}), 148.37 (C_{ar}), 147.45 (C_{ar}), 145.56 (C_{ar}), 140.86 (C_{ar}), 139.69 (C_{ar}), 139.27 (C_{ar}), 137.56 (C_{ar}), 137.10 (C_{ar}), 136.32 (C_{ar}), 135.91 (C_{ar}), 134.48 (d, *J* = 10 Hz, C_{ar}), 134.09 (C_{ar}), 132.05 (C_{ar}), 130.55 (C_{ar}), 129.42 (d, *J* = 5.3 Hz, C_{ar}), 129.25 (C_{ar}), 128.03 (C_{ar}), 127.25 (C_{ar}), 127.10 (C_{ar}), 125.91 (br.s, C_{ar}), 125.75 (C_{ar}), 124.20 (C_{ar}), 123.16 (C_{ar}), 123.06 (C_{ar}), 122.45 (C_{ar}), 122.12 (C_{ar}), 121.97 (C_{ar}), 121.62 (C_{ar}), 121.25 (C_{ar}), 119.46 (C_{ar}), 117.29 (d, *J* = 8.1 Hz, C_{ar}), 32.96 (d, $^1J_{PC}$ =24.2 Hz, CH_2), 24.98 (d, $^1J_{PC}$ =16.1 Hz, (*C*H$(CH_3)_2$)), 21.34 (d, $^1J_{PC}$ =24.2 Hz, (*C*H$(CH_3)_2$)), 19.18 (br.s), 17.38 (d, J_{PC} =3.9 Hz, CH(*C*H$_3)_2$), 17.27 (d, J_{PC} =6.7 Hz, CH(*C*H$_3)_2$), 15.77 (CH(*C*H$_3)_2$).

^{31}P{^{1}H} NMR (262 MHz, CD_2Cl_2, 0 °C) δ: 52.49

ESI-HRMS (m/z pos): Found (Calcd): $C_{82}H_{72}O_2N_8P_2Pd_4$: 1686.1385 (1686.1387).

FT-IR (ATR, solid): 2972 (br, w), 2853 (br, w), 1457 (br, s), 1066 (s), 908 (br, s), 730 (s) cm^{-1}.

UV-vis (MeCN), λ, nm (ε, $M^{-1}\cdot cm^{-1}$) : 463 (447), 355(3349), 277 (33050), 201 (4740).

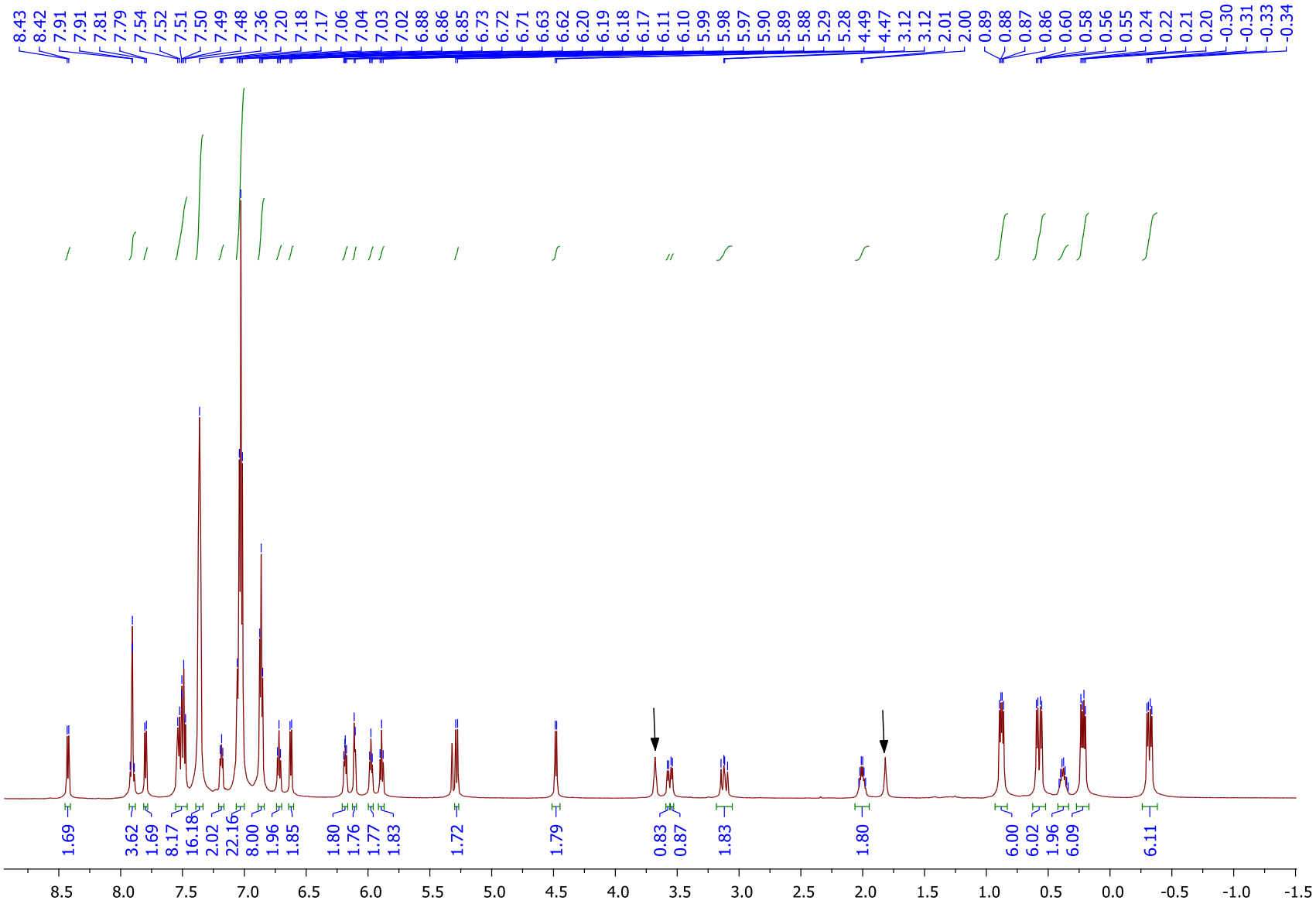

Figure S44.[1]H NMR spectrum of **5** in CD_2Cl_2 at 0 °C. Arrows indicate the peaks of residual THF solvent.

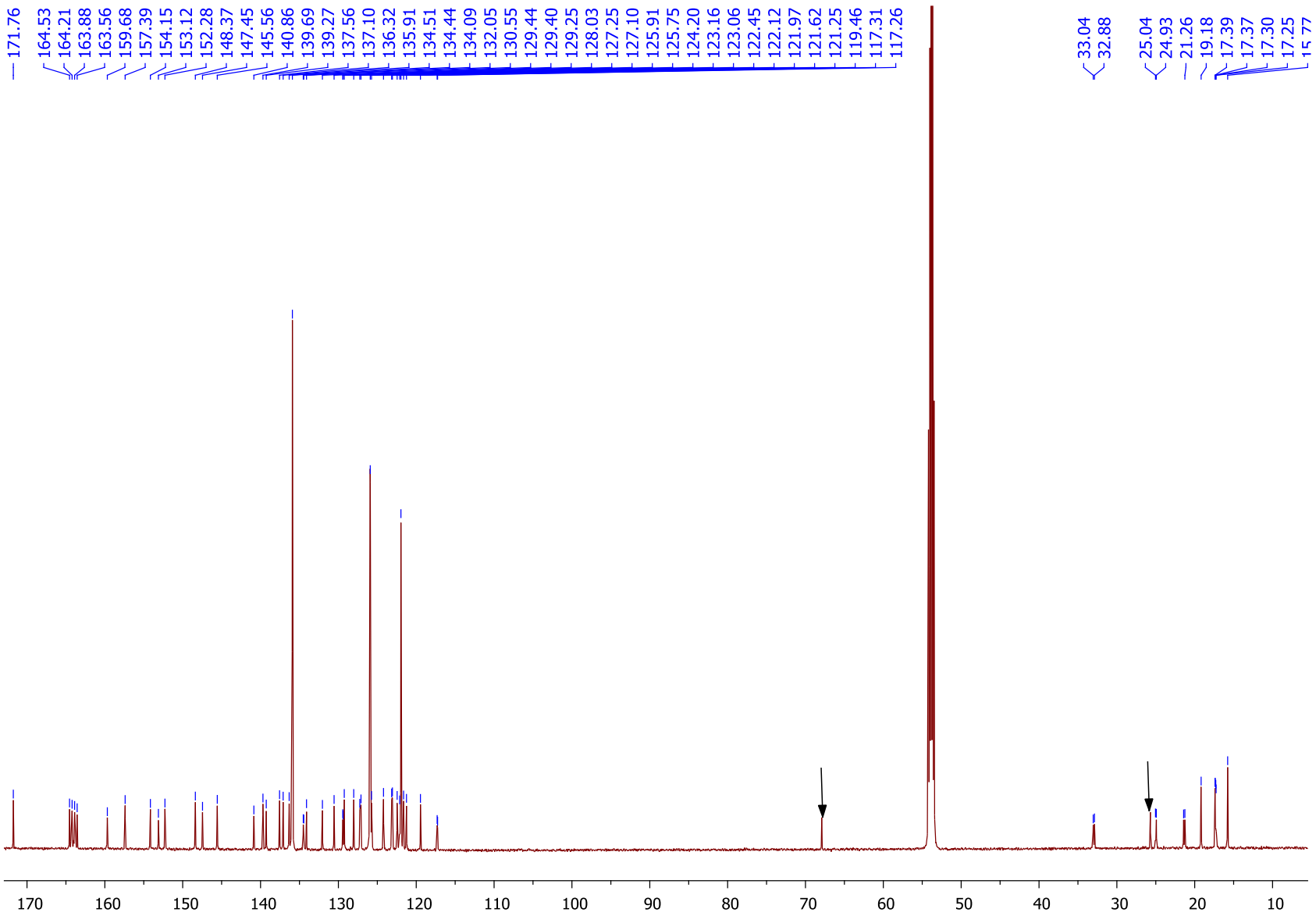

Figure S45.[13]C NMR spectrum of **5** in CD_2Cl_2 at -20 °C. Arrows indicate the peaks of residual THF solvent.

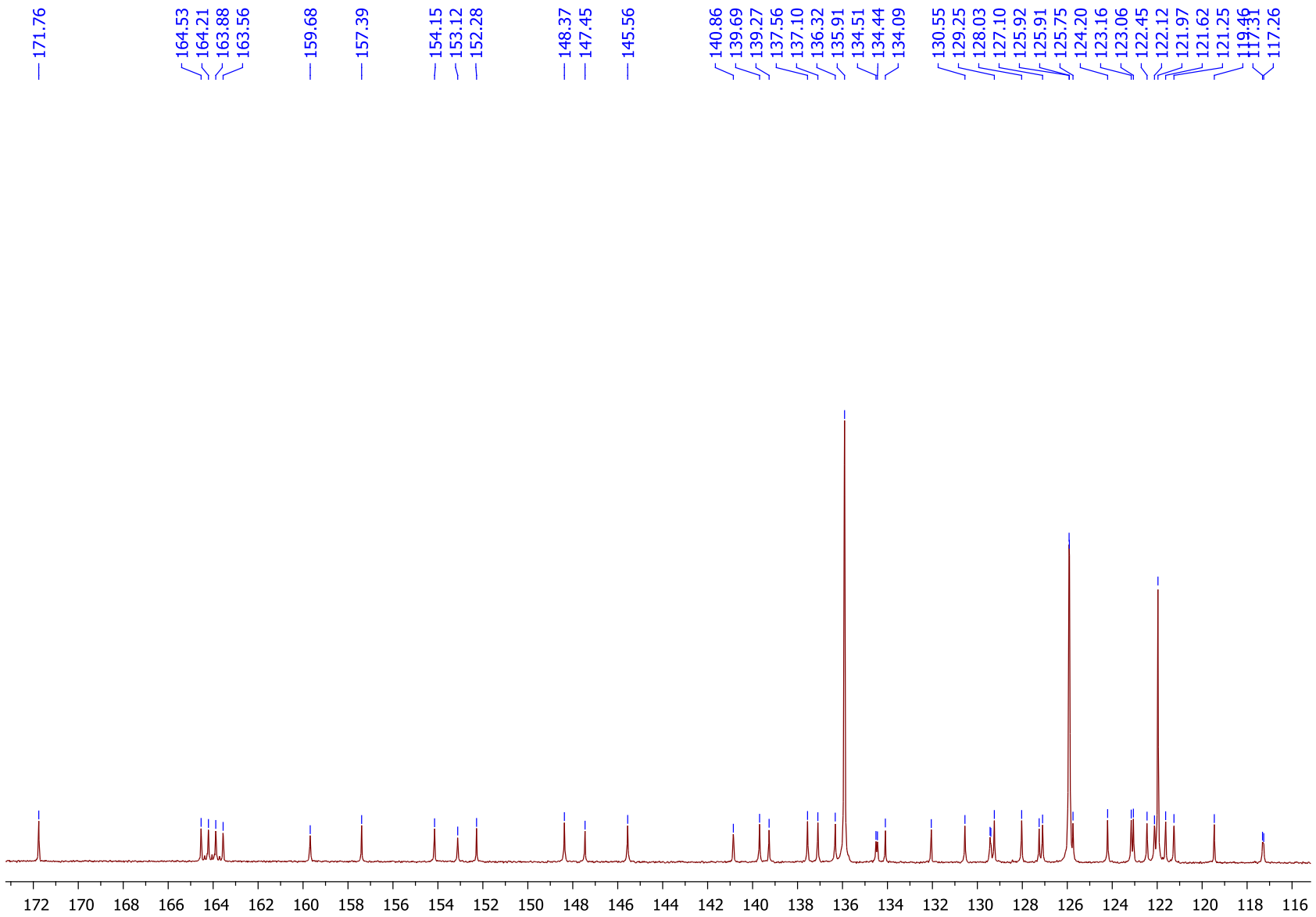

Figure S46. Expanded ^{13}C NMR spectrum of **5** in CD_2Cl_2 at -20 °C.

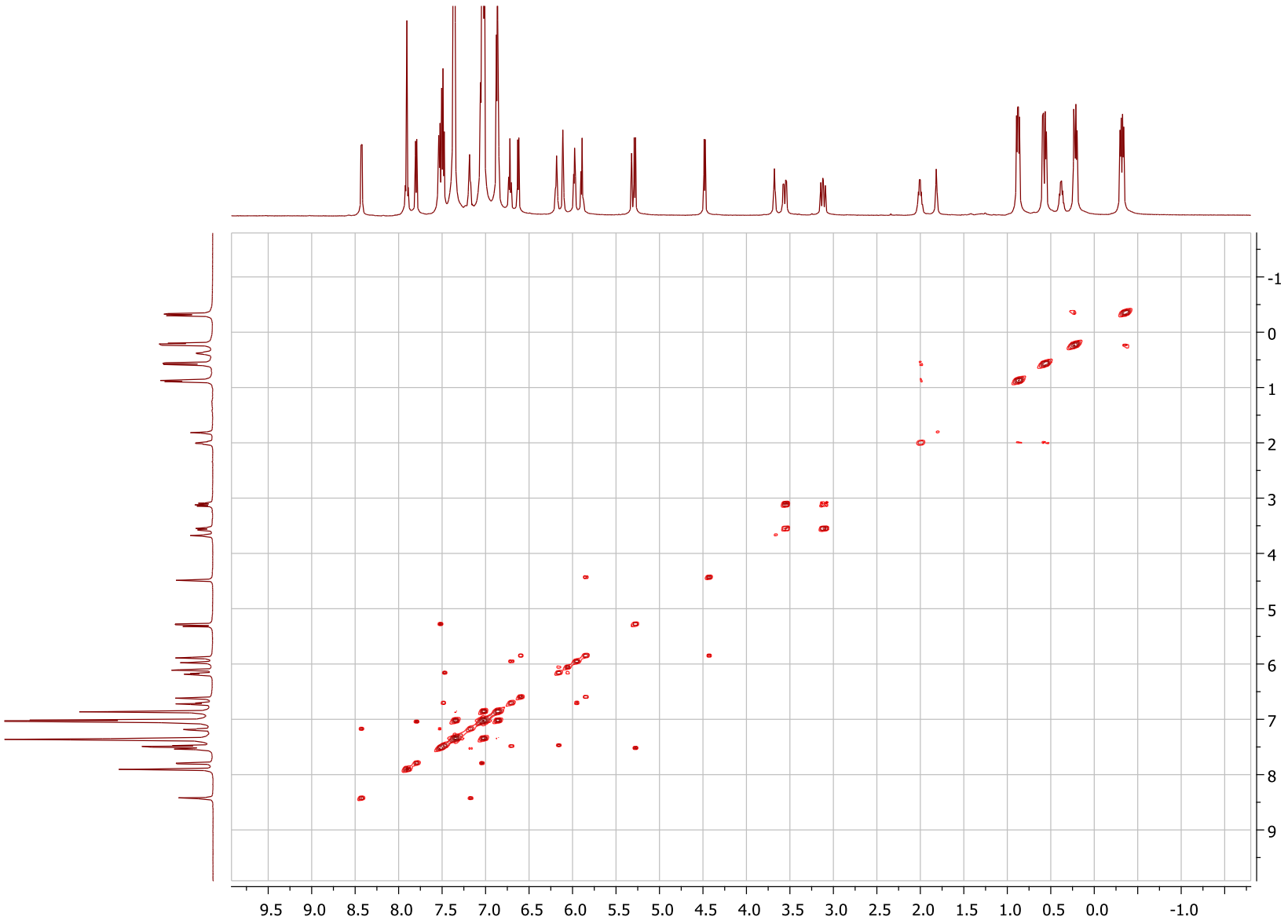

Figure S47.. ^{1}H-^{1}H COSY spectrum of **5** in CD_2Cl_2 at -20 °C.

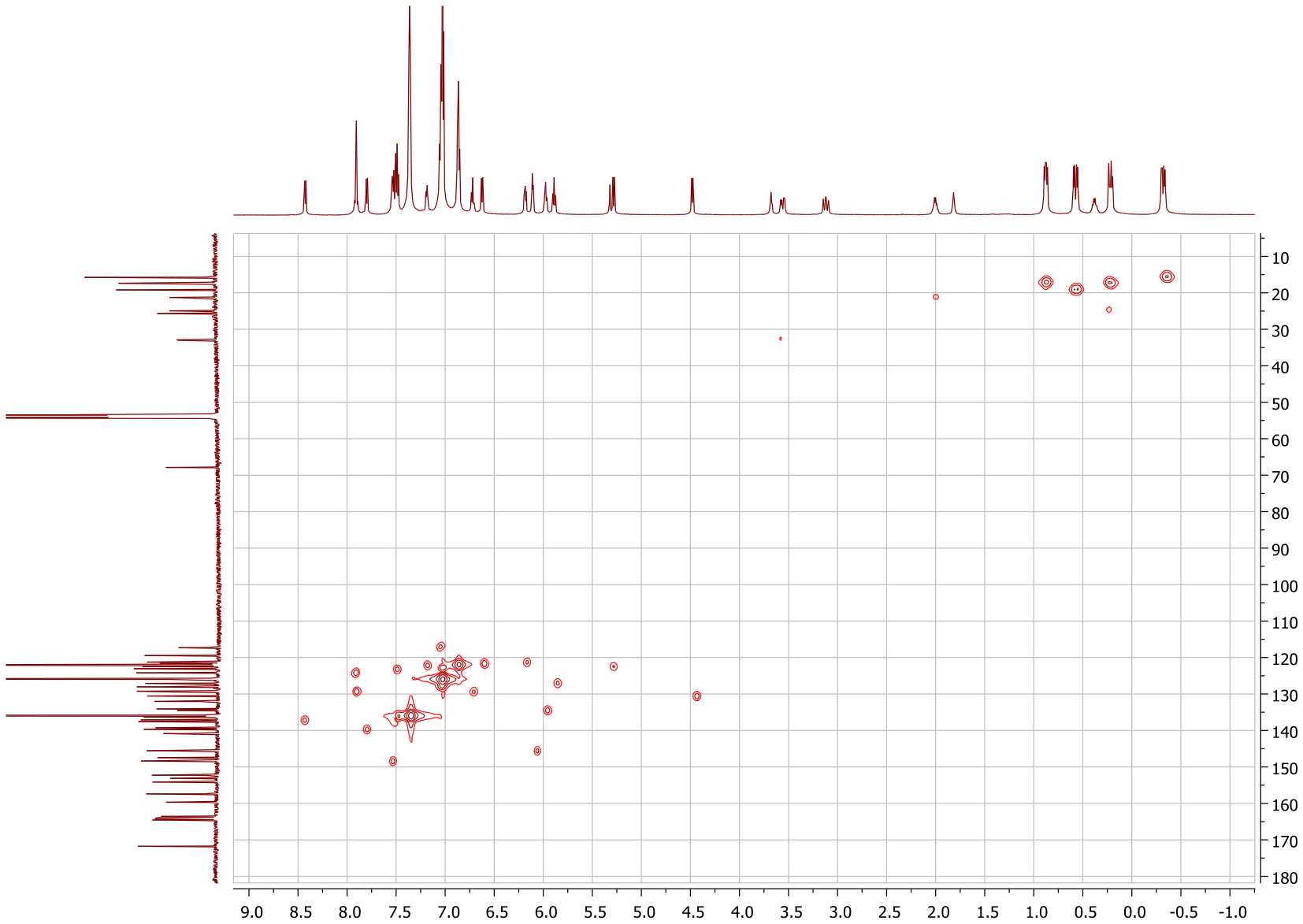

Figure S48. ^{1}H-^{13}C HMQC spectrum of **5** in CD_2Cl_2 at -20 °C.

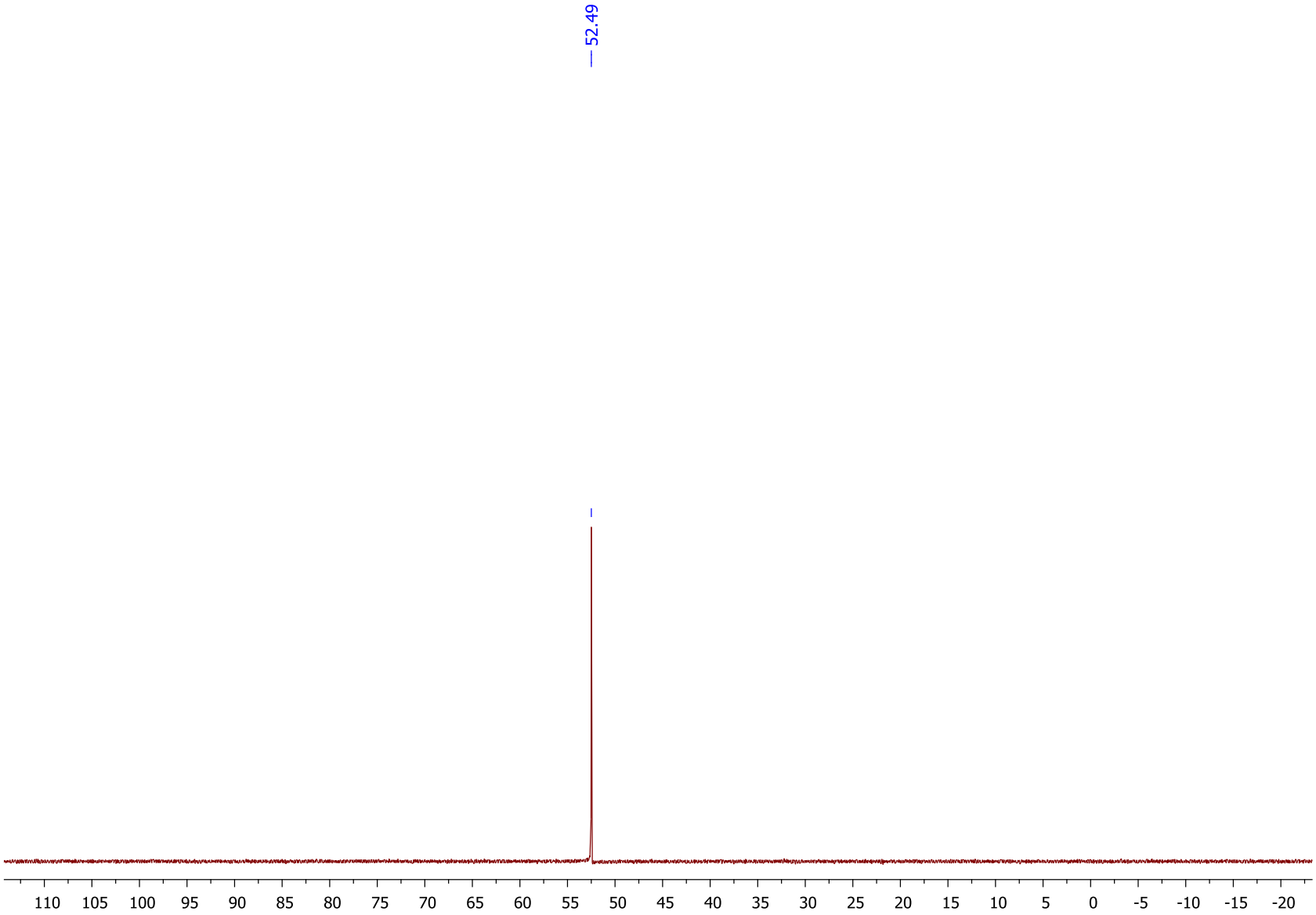

Figure S49. ^{31}P spectrum of **5** in CD_2Cl_2 at -20 °C.

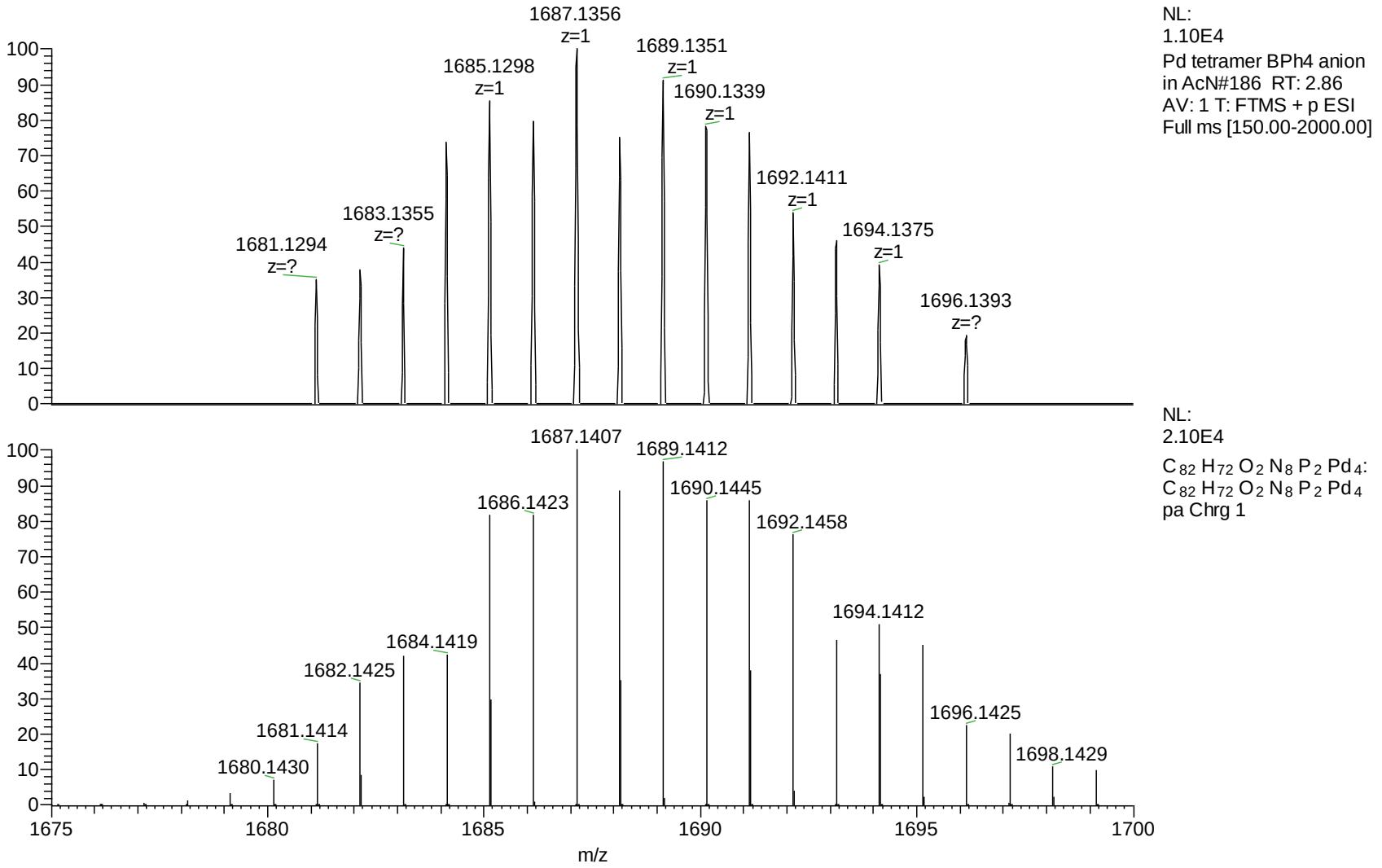

Figure S50. ESI-(HR)MS spectrum of a MeCN solution of **5** (top) and simulated spectrum for $C_{82}H_{72}O_2N_8P_2Pd_4$ (bottom).

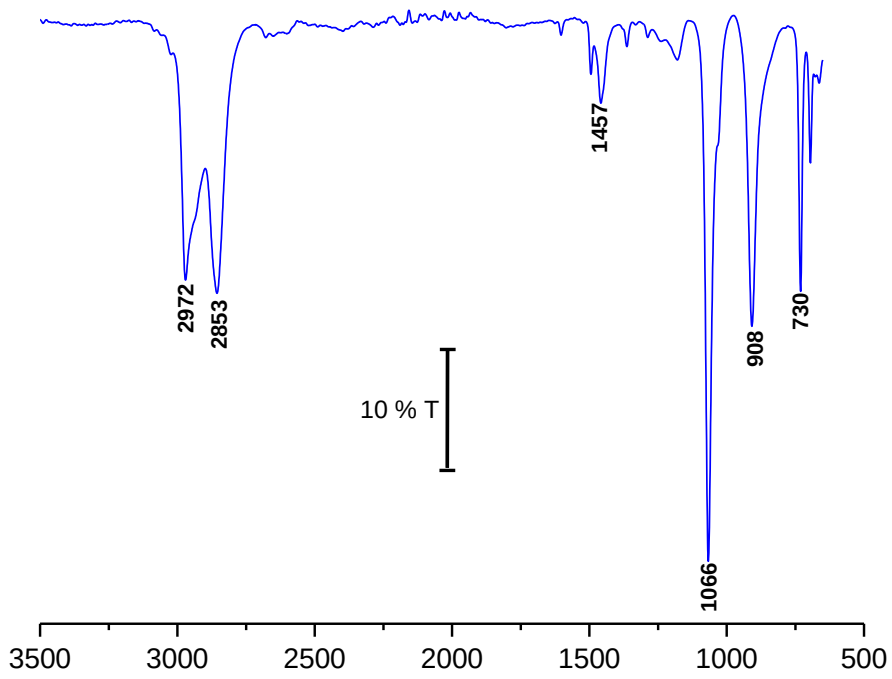

Figure S51. ATR FT-IR transmittance spectrum of **5**.

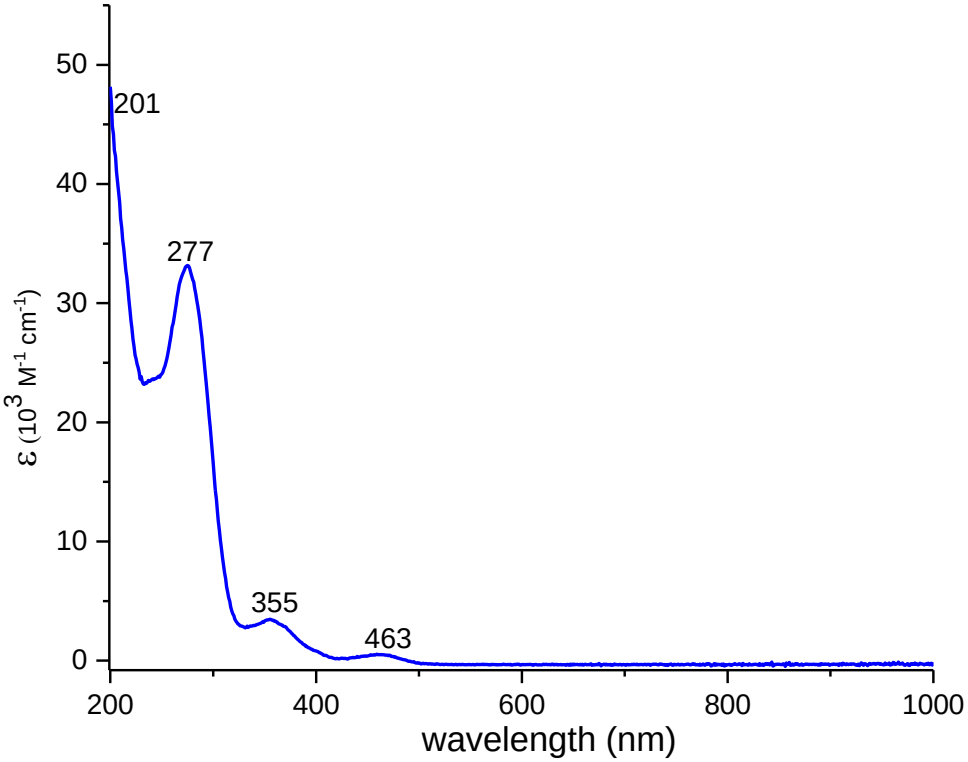

Figure S52. UV-vis absorbance spectrum for **5** in MeCN.

Synthesis of 6

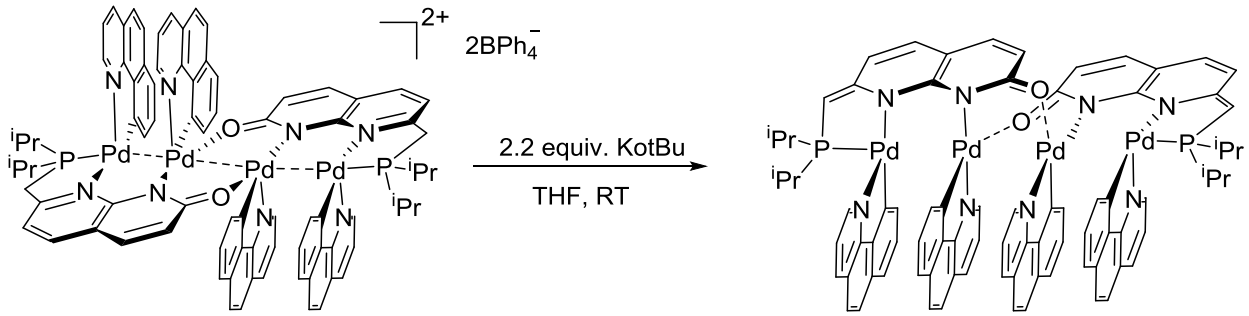

5 **6**

Scheme S7. Synthesis of **6**.

In a 20 mL vial **5** (50.7 mg, 0.020 mmol), KO^{t}Bu (5.1 mg, 0.046 mmol) were dissolved in THF (4 mL) giving a red solution which was stirred at RT for 30 minutes. Inorganic salts were removed via filtration and the solvent is removed under vacuum. The red color viscous solid was dissolved again in ether and left for crystallization at -30 °C to obtain red color crystals suitable for XRD analysis. The NMR analysis could not be performed due to low stability of the complex in solution. Complex **6** can be obtained by al alternative method by treating complex **4** with 2.2 equivalent of KO^{t}Bu; the product of this reaction was crystallized in ether, and XRD showed the identical unit cell as for the product obtained from **5**.
The complex decomposes in solution at room temperature in aprotic solvents (toluene) even without protic additives, which prevented the reactivity study with weak proton sources. The product could only be obtained as crystals that could be kept at -20 °C under a layer of mother liquor, but it decomposes during filtration through Celite and evaporation of the solvent leading to color changes.

Reaction of 2 with phenylacetylene

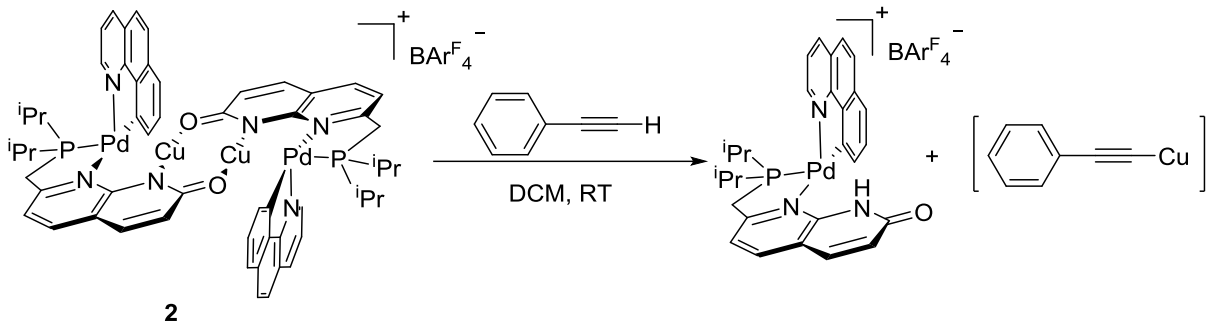

2

Scheme S8. Reaction of **2** with phenylacetylene.

Complex **2** (9.2 mg, 0.003 mmol) was dissolved in DCM-d_2 (400 μL) in a Teflon sealed J. Young NMR tube in the presence of internal standard mesitylene (1.2 μL, 0.009 mmol). After this the first NMR spectrum was recorded. Further the J. Young NMR tube was cooled down to -50 °C, phenyl acetylene (6.7 μL, 0.061 mmol,) was added and the NMR tube was quickly transferred to the NMR with pre-cooled probe. at -25 °C. Formation of complex **1**-BAr$^F_4$ was observed and the NMR spectrum was recorded. Based on integration of one of the methylene's CHH peaks, estimated yield is 68%, also consistent with integration of NH peak.

Isolation of copper acetylide

The modified literature procedure was followed to isolate copper acetylide species.[4] Inside the glovebox in a round bottom flask complex **2** (100.3 mg, 0.03 mmol) was dissolved in 10 mL of DCM. Phenylacetylene (18.4 μL, 0.16 mmol) was added at room temperature and the reaction mixture was stirred for five minutes. The ammonium hydroxide (28% NH_3 solution, 5 mL) was added to the reaction mixture resulting in precipitation of yellow powder. The powder was collected by filtration. The bright yellow solid was washed with cold water : ethanol mixture (10:10 mL) and the solid was dried under vacuum for 10 hours. Yield 12.6 mg; yellow solid. The NMR spectrum could not be measured because of low solubility. FT-IR spectrum matched with IR spectra of Cu phenylacetylide reported in the literature. [5-8]

FT-IR (ATR, solid): 3045 (w), 2456 (w), 1928 (w), 1593 (w), 1569 (w), 1479 (m), 1438 (m), 1155 (w), 1067 (m), 1024 (m), 904 (m), 745 (s), 681 (s) cm^{-1}.

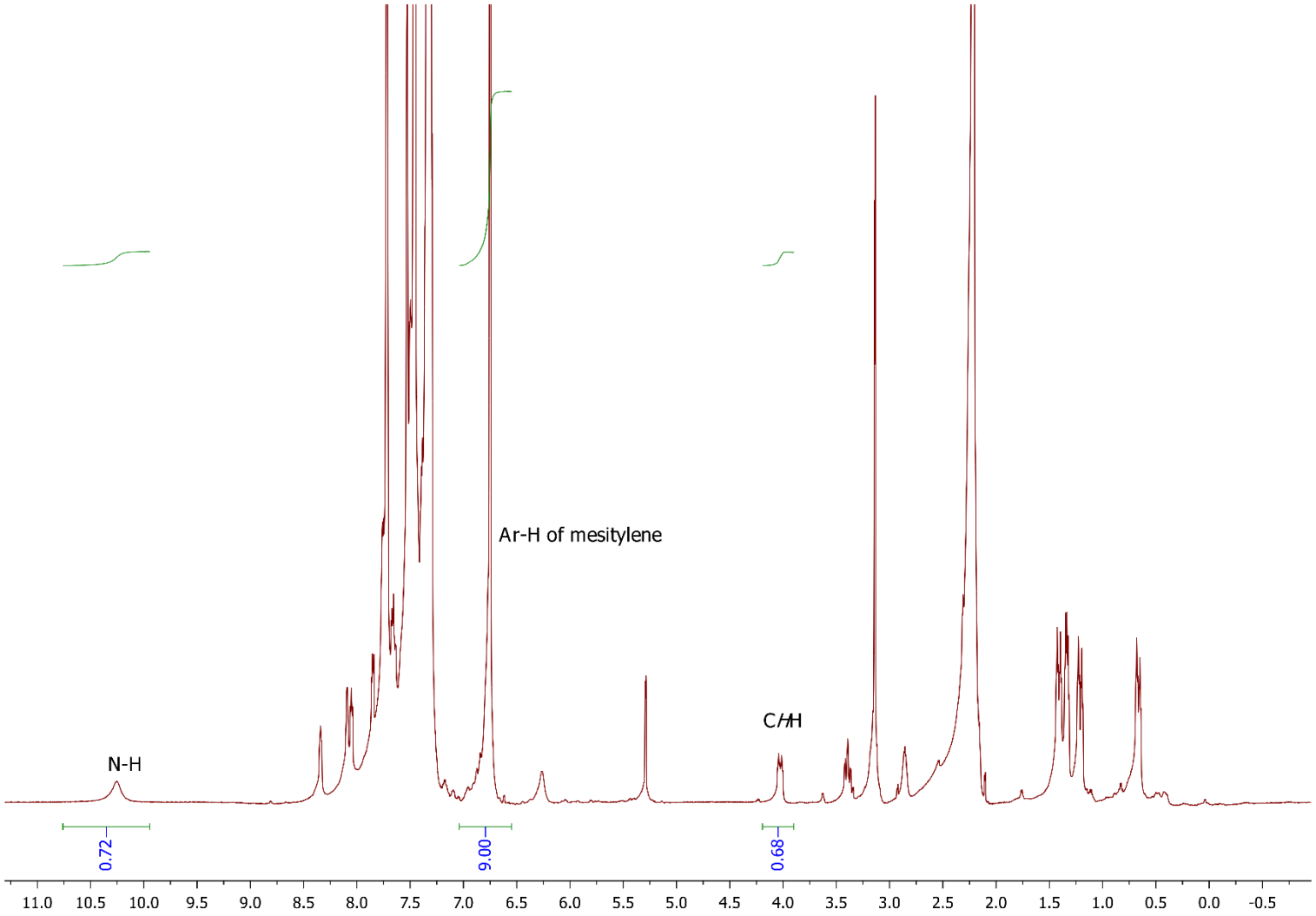

Figure S53.[1]H NMR spectrum of **2** in presence of phenyl acetylene to form **1**-BAr^F_4 in CD_2Cl_2 at -25 °C.

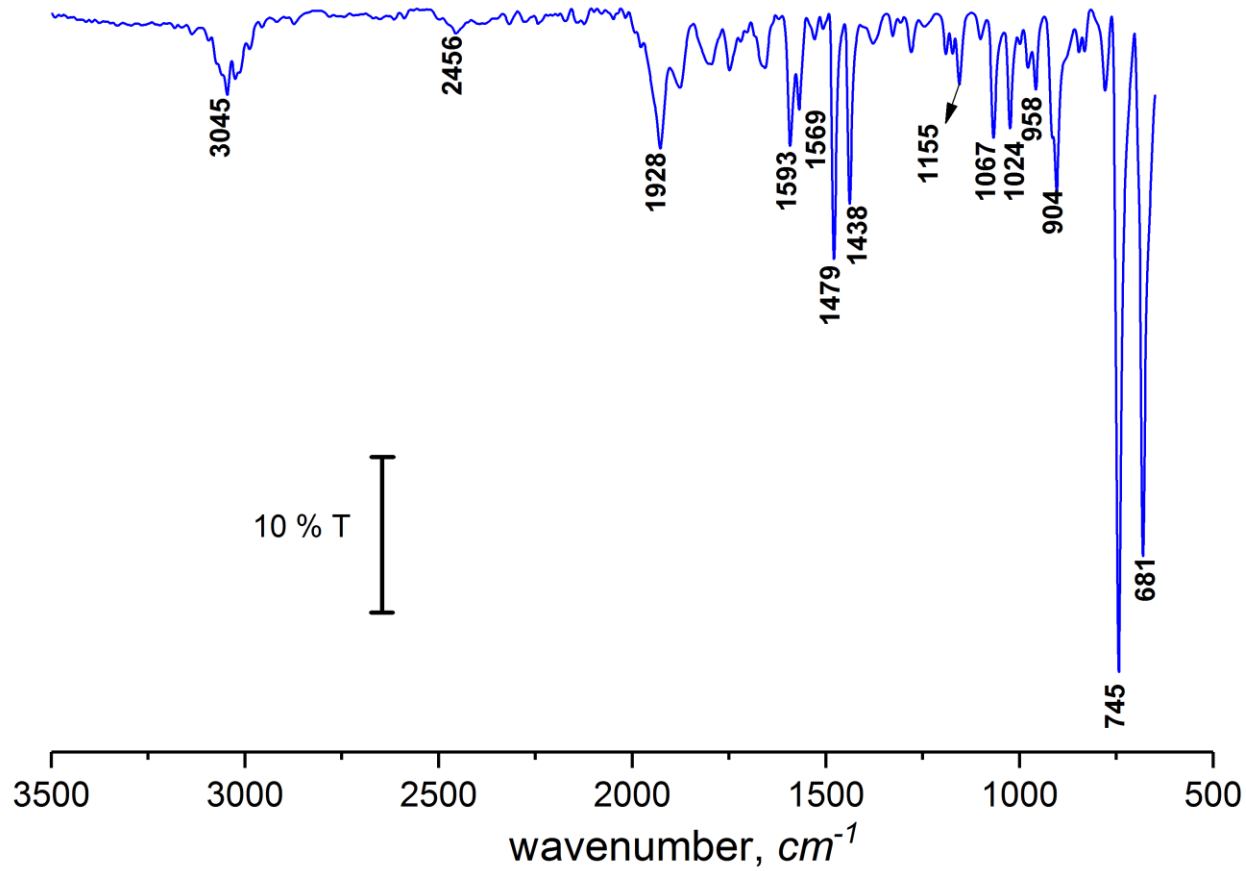

Figure S54. ATR FT-IR transmittance spectrum of copper phenylacetylide product.

Reaction of 2 with phenylacetylene-*d*

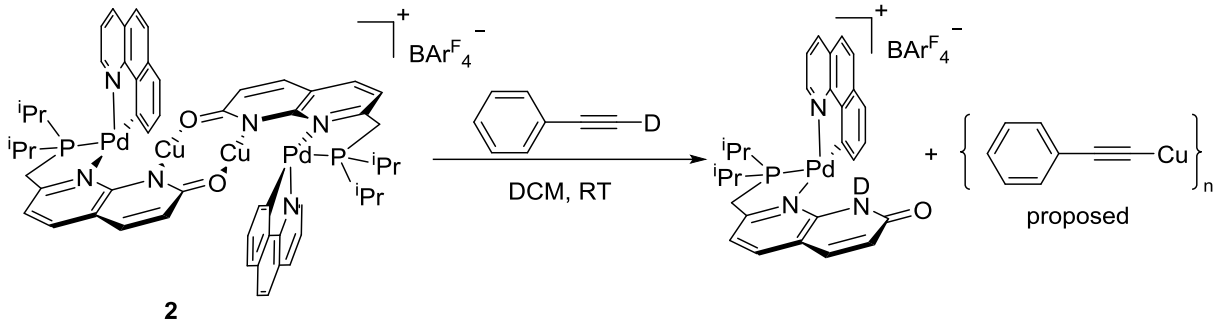

2

Scheme S9. Reaction of **2** with phenylacetylene-*d*.

Inside the glovebox, complex **2** (8.7 mg, 0.002 mmol) was dissolved in CH_2Cl_2 (400 μL) in a J. Young NMR tube in the presence of deuterated phenylacetylene-*d* (1.5 μL, 0.014 mmol) and the reaction mixture was stirred for five minutes at room temperature. The ^{1}H and ^{2}H NMR spectra was recorded suggesting the formation of complex **1**-BAr$^F_4$-*d* based on the presence of an ND peak as a broad singlet at 9.63 ppm in ^{2}H NMR spectrum and the absence of NH signal in ^{1}H NMR spectrum; other peaks were identical to those for complex obtained by reaction with phenylacetylene.

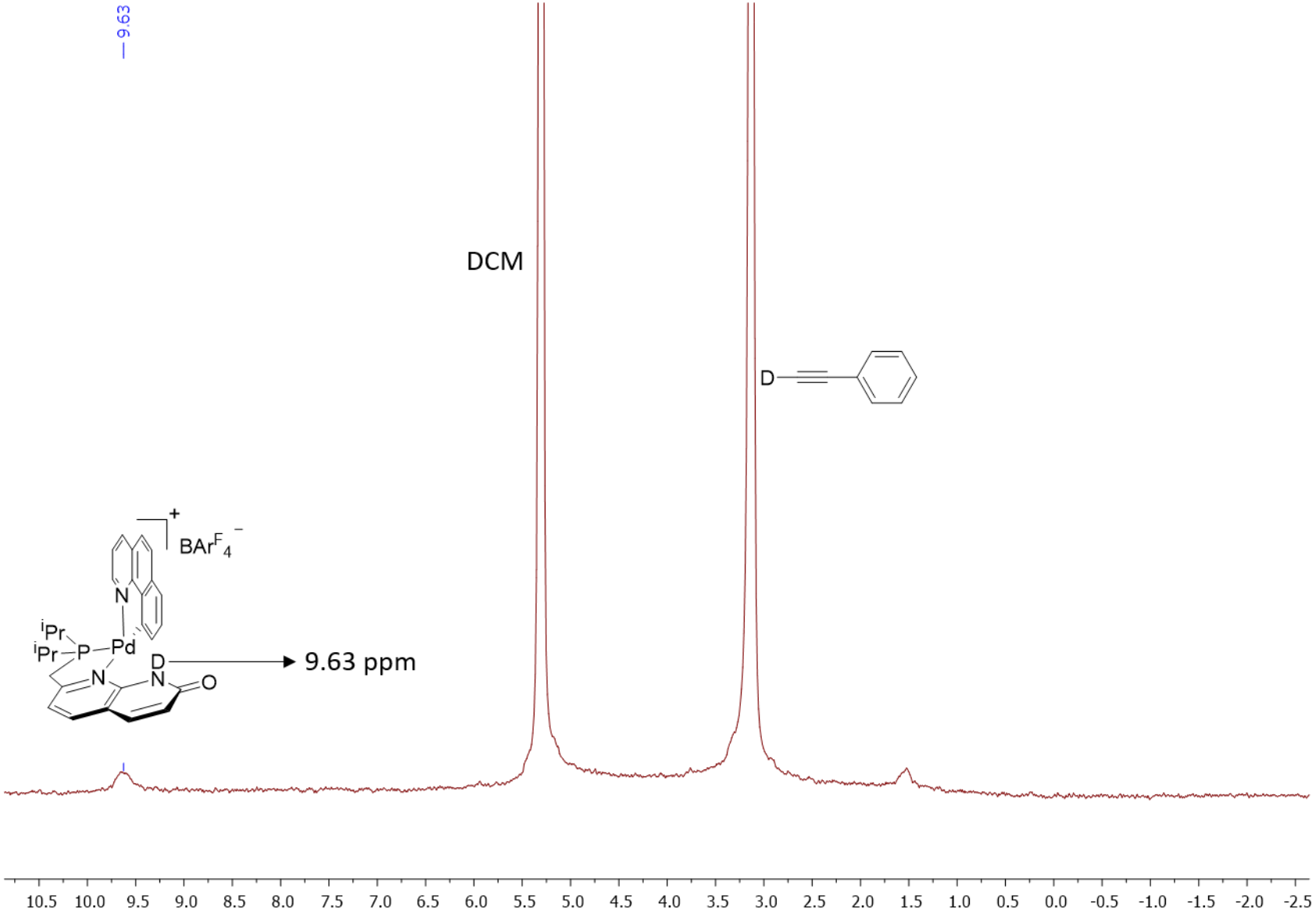

Figure S55. ^{2}H NMR spectrum of **2** after reaction with phenylacetylene-*d*.

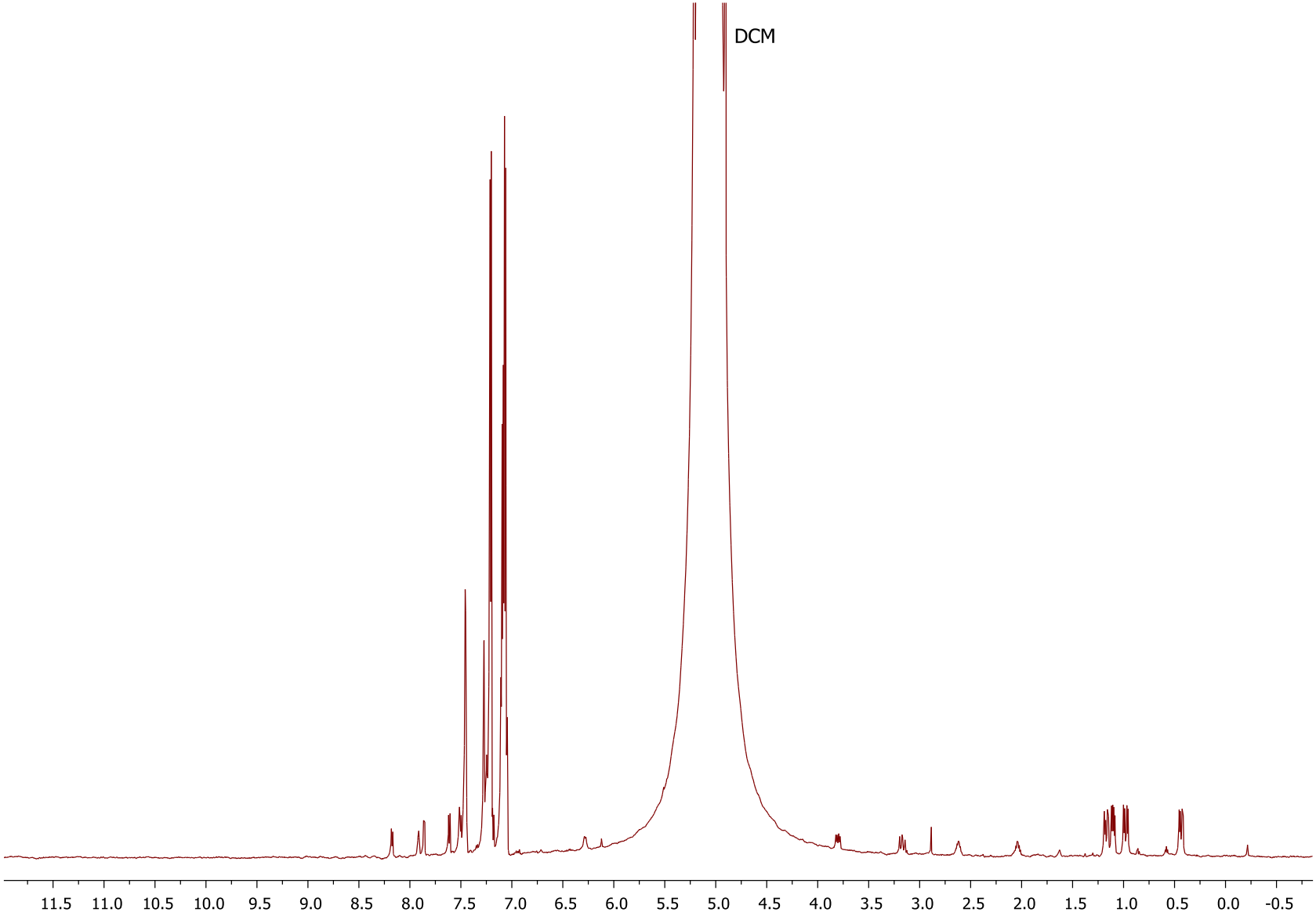

Figure S56. ^{1}H NMR spectrum of **2** after reaction with phenylacetylene-*d* (in CH_2Cl_2).

Catalytic alkyne dimerization.

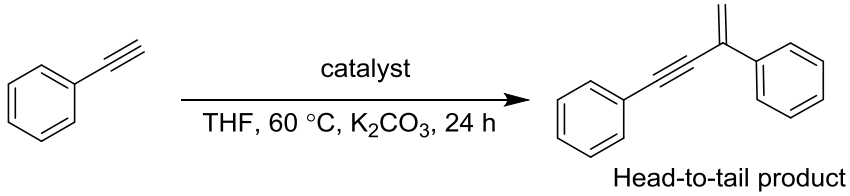

Control experiments using simple Pd and Cu precursors.
General Procedure. In a nitrogen filled glovebox , a 5 mL glass vial equipped with a stirring bar was charged with phenyl acetylene (0.1 mmol), Pd or Cu precursor and/or other additives; the anhydrous solvent was added (1 mL). Then the reaction vial was sealed and stirred inside the glovebox for 24 h at RT. Mesitylene (0.1 mmol) was added and the reaction mixture was analyzed by ^{1}H NMR spectroscopy. The control experiments in the presence of simple Pd and Cu precursors not ligated to **L_P(H)** ligand showed no product formation either at RT or upon heating.

Table S1. Control experiments for alkyne dimerization using various additives.

Entry	Pd or Cu additive (mol%)[a]	Other additives (mol%)[a]	Solvent	Time (h)	Temperature (°C)	Product
1	none	$NaBAr^F_4$ (1.0)	THF	24	23	n.d. [b]
2	none	**L_PH** (1.0)	THF	24	23	n.d.
3	$Pd_2(Bzhq)_2(AcO)_2$ (0.5)	none	THF	24	23	n.d.
4	$Pd_2(Bzhq)_2(AcO)_2$ (0.5)	$NaBAr^F_4$ (1.0), **L_PH** (1.0)	THF	24	23	n.d.
5	$Pd_2(Bzhq)_2(AcO)_2$ (0.5)	$NaBAr^F_4$ (1.0), **L_PH** (1.0), K_2CO_3 (120)	THF	24	23	n.d.
6	$[Cu(MeCN)_4]BAr^F_4$ (0.5)	K_2CO_3 (120)	THF	24	23	n.d.
7	$Pd_2(Bzhq)_2(AcO)_2$ (0.5)	none	MeCN	24	23	n.d.
8	$[Cu(MeCN)_4]BAr^F_4$ (1)	K_2CO_3 (120)	THF	24	60	n.d.
9	$Pd_2(Bzhq)_2(AcO)_2$ (1)	K_2CO_3 (120)	THF	24	60	n.d.

[a] Relative to phenylacetylene. [b]n.d = not detected

*Comparison of Pd and Pd/Cu complexes with **L_P(H)**.*
General Procedure. In a glovebox, phenylacetylene (10.9 μL, 0.1 mmol), K_2CO_3 (16.5 mg, 0.12 mmol) and catalyst (1 mol%) were dissolved in THF (1 mL) in a septum-sealed pressure tube in the presence of mesitylene (13.9 μL, 0.1 mmol; internal standard). Then the reaction tube was transferred to a constant temperature heating bath at 60 °C. The reaction was stirred for 24 hours at 60 °C. Then 50 μL of reaction mixture was sampled and dissolved in 500 μL of $CDCl_3$. The reaction mixture was analyzed ^{1}H NMR spectroscopy. During initial optimization, NMR yield was determined. No other isomers were present and only head-to-tail product formed unless indicated otherwise. These experiments showed that although 2 is catalytically active under these conditions, such reactivity likely results from the catalytic activity of complex **1**-BAr^F_4 formed under these conditions as shown by stoichiometric experiments.

Table S2. Comparison of Pd and Pd/Cu complexes in alkyne dimerization.

Entry	Catalyst (mol%)[a]	Other additives (equiv)[a]	Solvent (ml)	Time (h)	Temperature (°C)	Product, % yield
1	**1**-BAr^F_4 (1)	K_2CO_3 (1.2)	THF	24	60	98
2	**2** (1)	K_2CO_3 (1.2)	THF	24	60	90
3	**3** (1)	K_2CO_3 (1.2)	THF	24	60	11
4	**4** (1)	K_2CO_3 (1.2)	THF	24	60	10

[a]Relative to phenylacetylene.

Table S3. Screening of solvents, base additives and temperature in a reaction catalyzed by **1**-BAr^F_4.

Entry	Catalyst (mol%)[a]	Other additives (equiv)[a]	Solvent	Time (h)	Temperature (°C)	Product, % yield
1	**1**-BAr^F_4 (1)	none	THF	24	23	52
2	**1**-BAr^F_4 (1)	none	MeCN	24	23	n.d
3	**1**-BAr^F_4 (1)	none	MeOH	24	23	n.d
4	**1**-BAr^F_4 (1)	Cs_2CO_3 (1.2)	THF	24	23	n.d
5	**1**-BAr^F_4 (1)	K_2CO_3 (1.2)	THF	24	23	73
6	**1**-BAr^F_4 (1)	K_2CO_3 (1.2)	THF	24	40	82
7	**1**-BAr^F_4 (1)	K_2CO_3 (1.2)	THF	24	60	98

[a]Relative to phenylacetylene.

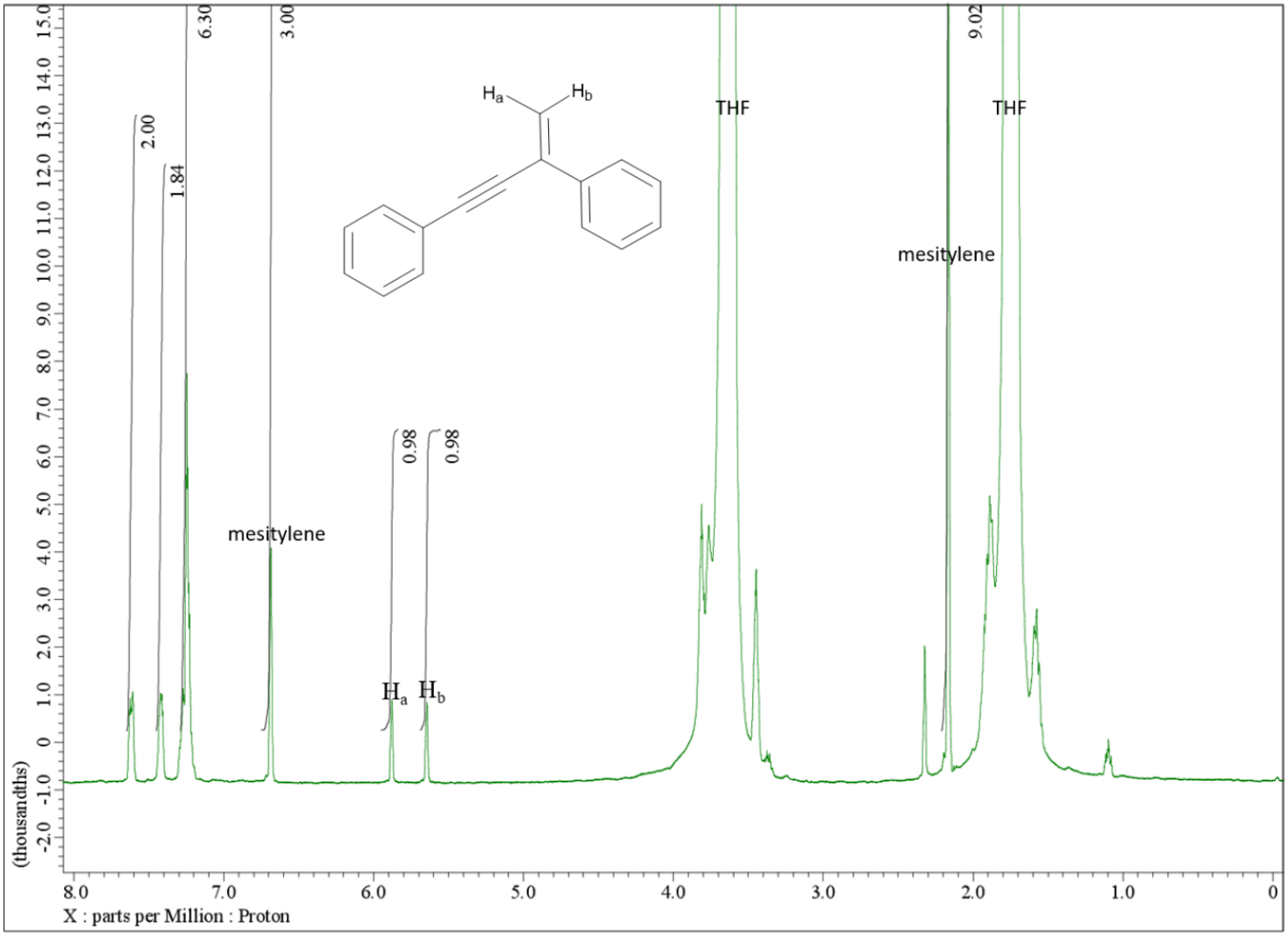

Figure S57. Representative ^{1}H NMR spectrum of an aliquot from the reaction mixture dissolved in $CDCl_3$ for catalytic dimerization catalyzed by **1**-BAr^{F}_{4} after 24 hours of reaction at 60 °C (entry 1, Table S2).

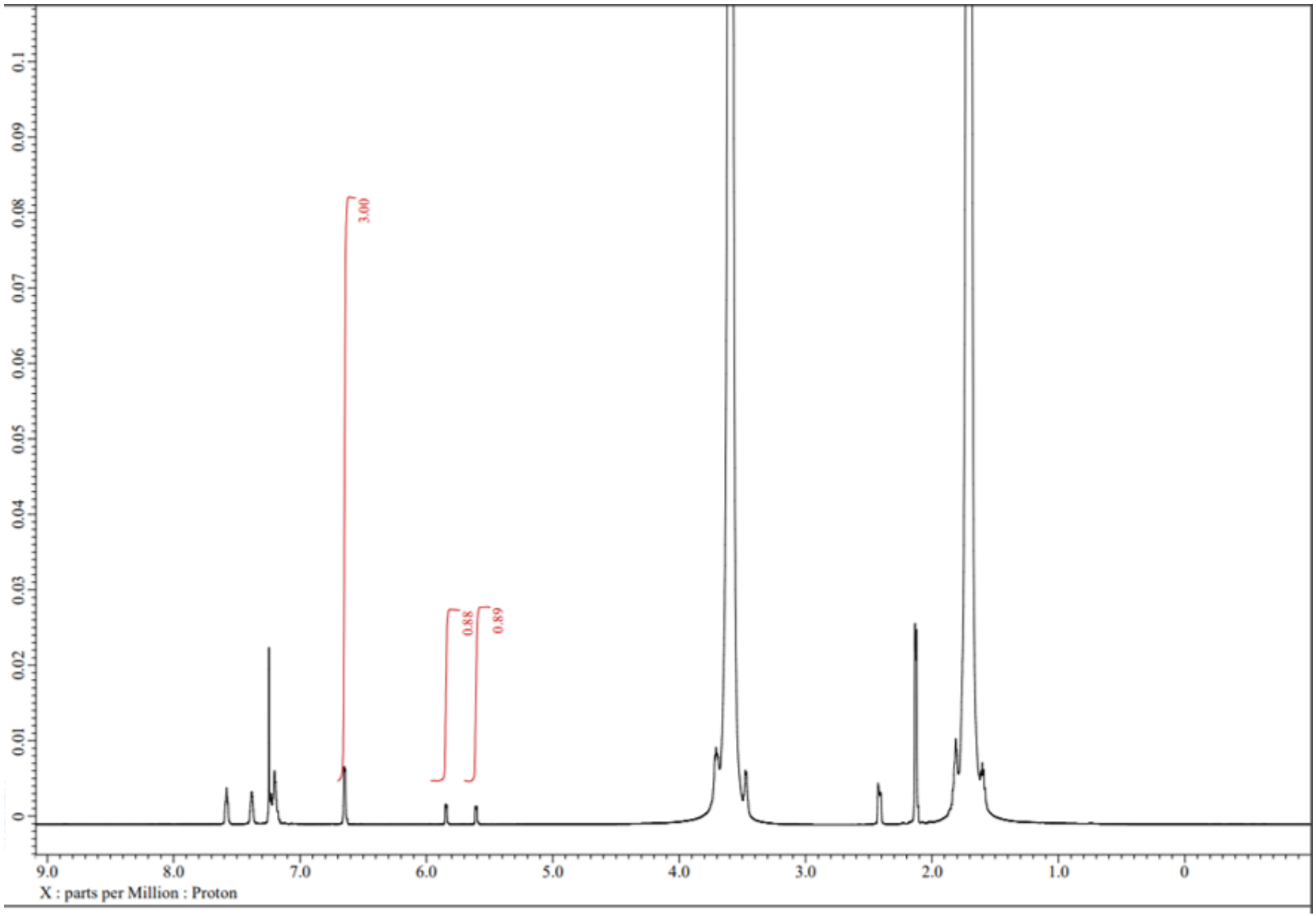

Figure S58. Representative ^{1}H NMR spectrum of an aliquot from the reaction mixture dissolved in $CDCl_3$ for catalytic dimerization catalyzed by **2** after 24 hours of reaction at 60 °C (entry 2, Table S2).

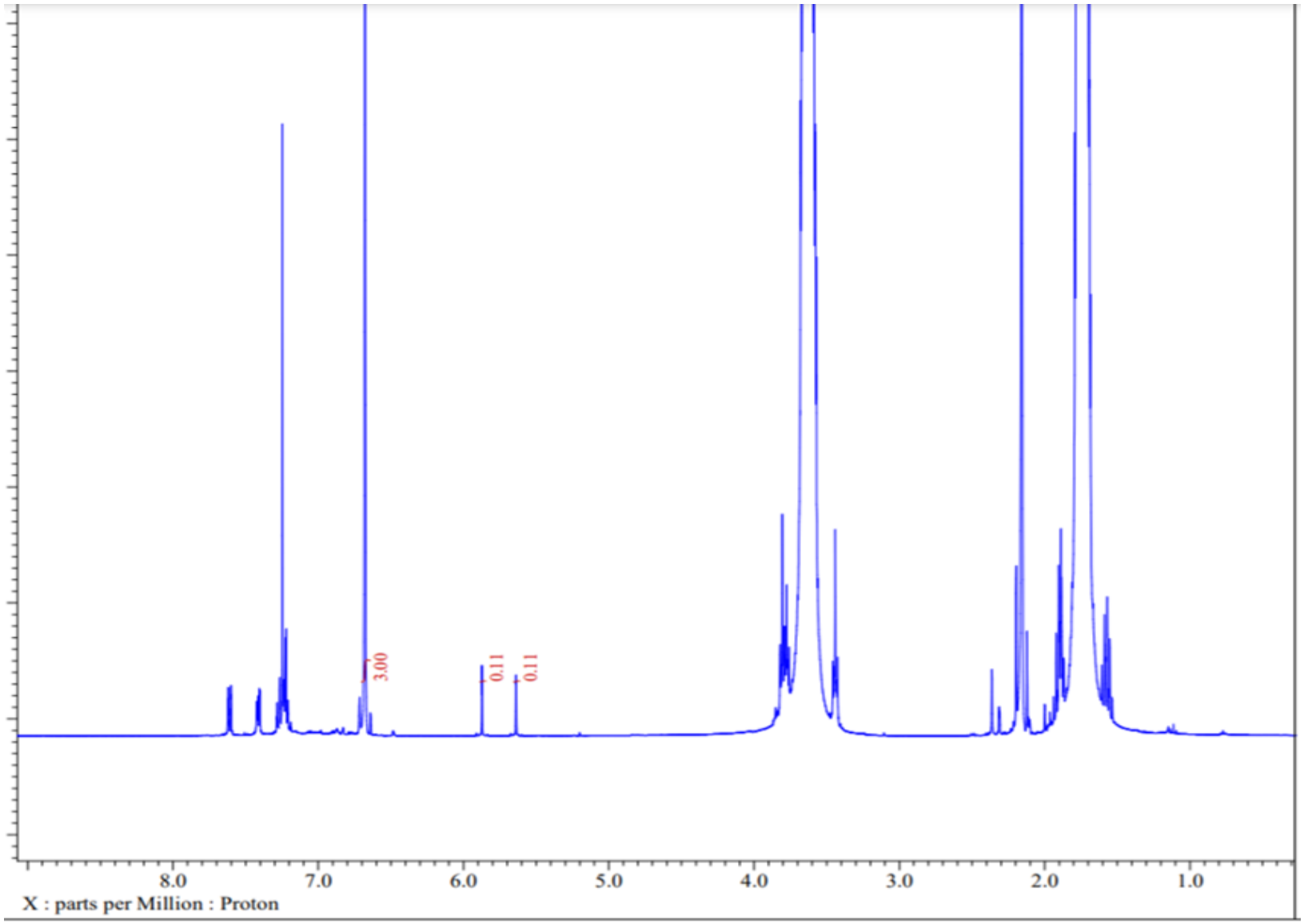

Figure S59. Representative ^{1}H NMR spectrum of an aliquot from the reaction mixture dissolved in $CDCl_3$ for catalytic dimerization catalyzed by **3** after 24 hours of reaction at 60 °C (entry 3, Table S2).

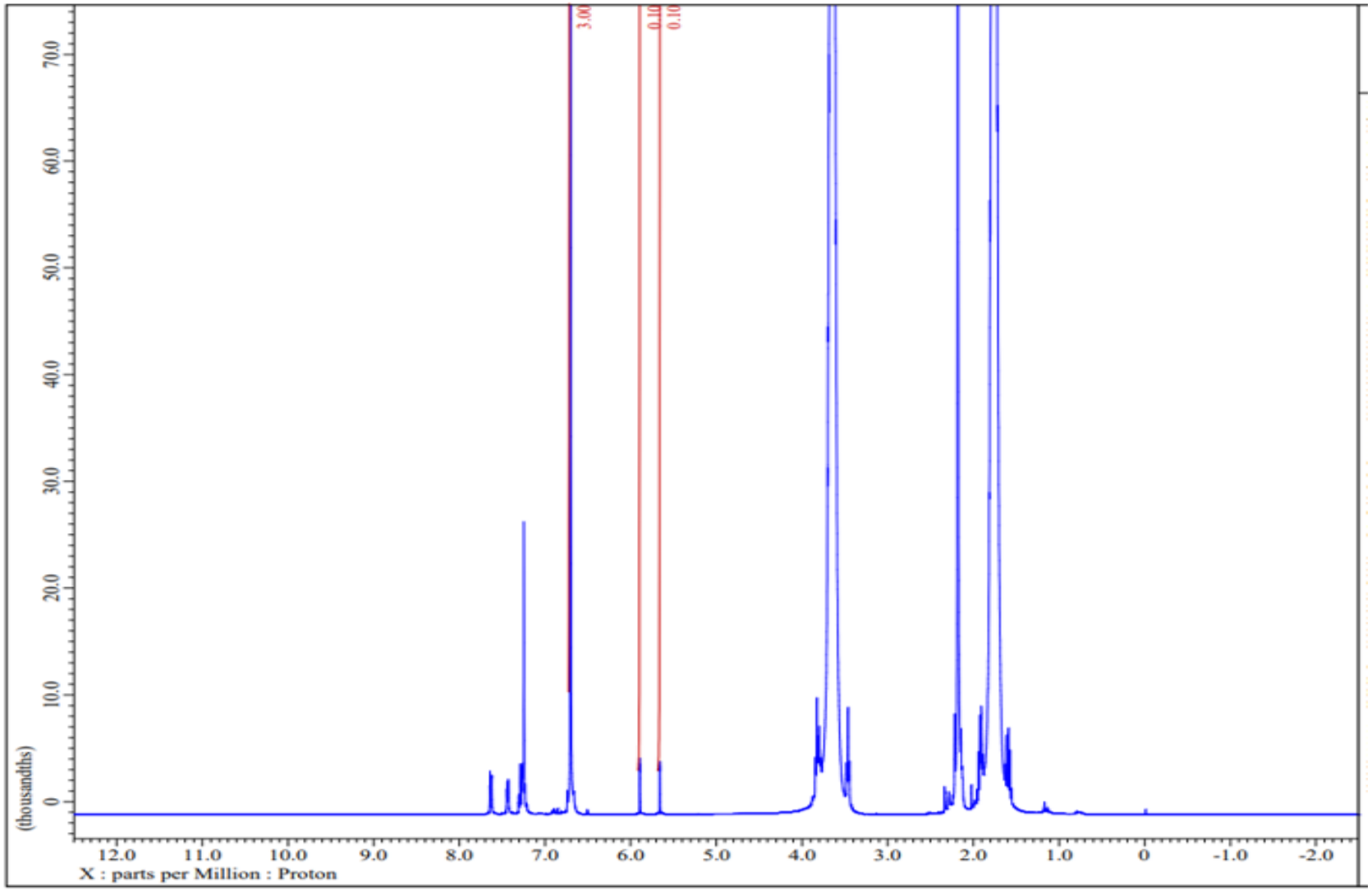

Figure S60. Representative ^{1}H NMR spectrum of an aliquot from the reaction mixture dissolved in $CDCl_3$ for catalytic dimerization catalyzed by **4** after 24 hours of reaction at 60 °C (entry 4, Table S2).

Catalytic dimerization of alkynes catalyzed by 1-BAr^F_4: product isolation and characterization

Complex **1**-BAr^F_4 (1 mol%, 0.01 mmol), K_2CO_3 (1.2 mmol), and alkyne substrate (1 mmol) were added into a 50 mL Schlenk flask in a nitrogen-filled glovebox. To this mixture 5 mL of THF was added. The reaction mixture was stirred for 24 hours at 60 °C. The solvent was removed under vacuum and the crude product was purified by flash chromatography (see details below).

Characterization of isolated enynes

The yields of isolated products after flash chromatography are reported. Products were identified by ^{1}H NMR spectra that matched those reported in the literature.[9-10]

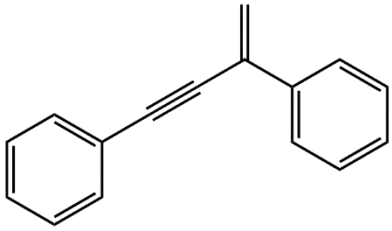

2,4-Diphenylbut-1-en-3-yne (Light yellow oil, Eluent: hexane), (190.7 mg, 93% isolated yield). ^{1}H NMR (600 MHz, $CDCl_3$, 23 °C) δ: 7.74 – 7.71 (m, 2H), 7.55-7.52 (m, 2H), 7.40 – 7.33 (m, 6H), 5.99 (s, 1H), 5.77 (s,1H).

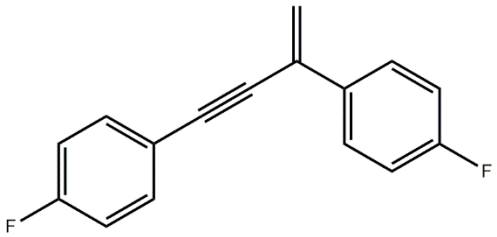

2,4-Bis(4-fluorophenyl)but-1-en-3-yne (Light yellow oil, Eluent: hexane) (219.7 mg, 91% isolated yield). ^{1}H NMR (600 MHz, $CDCl_3$, 23°C) δ: 7.70 – 7.66 (m, 2H), 7.53-7.49 (m, 2H), 7.09 – 7.03 (m, 4H), 5.92 (s, 1H), 5.73 (s,1H). ^{19}F NMR (564 MHz, $CDCl_3$, 23 ℃) δ −111.36, −114.49.

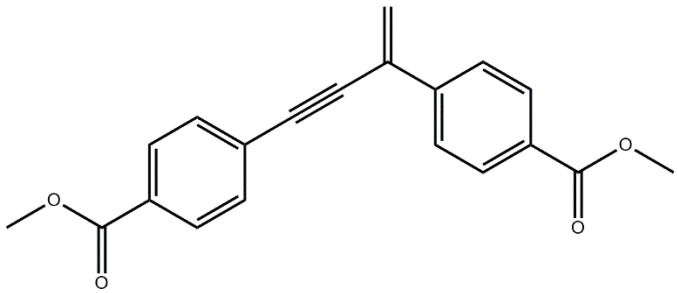

Dimethyl 4,4'-(but-3-en-1-yne-1,3-diyl) dibenzoate (White solid, Eluent: ethyl acetate/ hexane, v/v=1/1) (286.7 mg, 89% isolated yield). ^{1}H NMR (600 MHz, $CDCl_3$, 23 °C) δ: 8.07 – 8.03 (m, 4H), 7.78 – 7.76 (m, 2H), 7.60 – 7.58 (m, 2H), 6.13 (s, 1H), 5.91 (s, 1H), 3.94 (s, 6H).

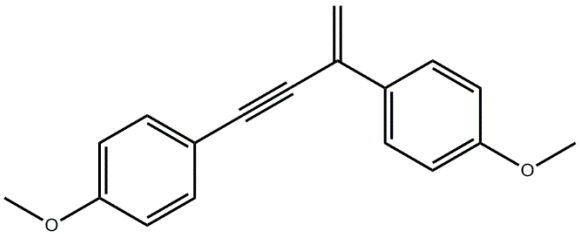

4,4'-(But-3-en-1-yne-1,3-diyl)bis(methoxybenzene) (Light yellow oil, Eluent: ethyl acetate/ hexane, v/v=1/1) (225.7 mg, 85% isolated yield). ^{1}H NMR (600 MHz, $CDCl_3$, 23 °C) δ: 7.66 (d, $^{3}J_{HH}$ = 8.5 Hz, 2H), 7.47 (d, $^{3}J_{HH}$ = 8.5 Hz, 2H), 6.90 (d, $^{3}J_{HH}$ = 8.5 Hz, 2H), 6.88 (d, $^{3}J_{HH}$ = 8.5 Hz, 2H), 5.84 (s, 1H), 5.62 (s, 1H), 3.84-3.83 (m, 6H, two overlapping signals).

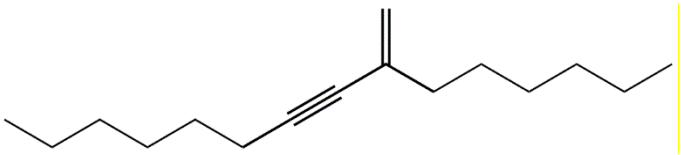

9-Methylenepentadec-7-yne (Colorless oil, Eluent: ethyl acetate/ hexane, v/v=1/1) (190.4 mg, 86% isolated yield). ^{1}H NMR (600 MHz, $CDCl_3$, 23 °C) δ: 5.20 (s, 1H), 5.11 (s, 1H), 2.30 (t, $^{3}J_{HH}$ = 7.1 Hz, 2H), 2.11 (t, $^{3}J_{HH}$ = 7.6 Hz, 2H), 1.55 – 1.48 (m, 4H), 1.43 – 1.38 (m, 2H), 1.33 – 1.27 (m, 10H), 0.91 – 0.88 (m, 6H).

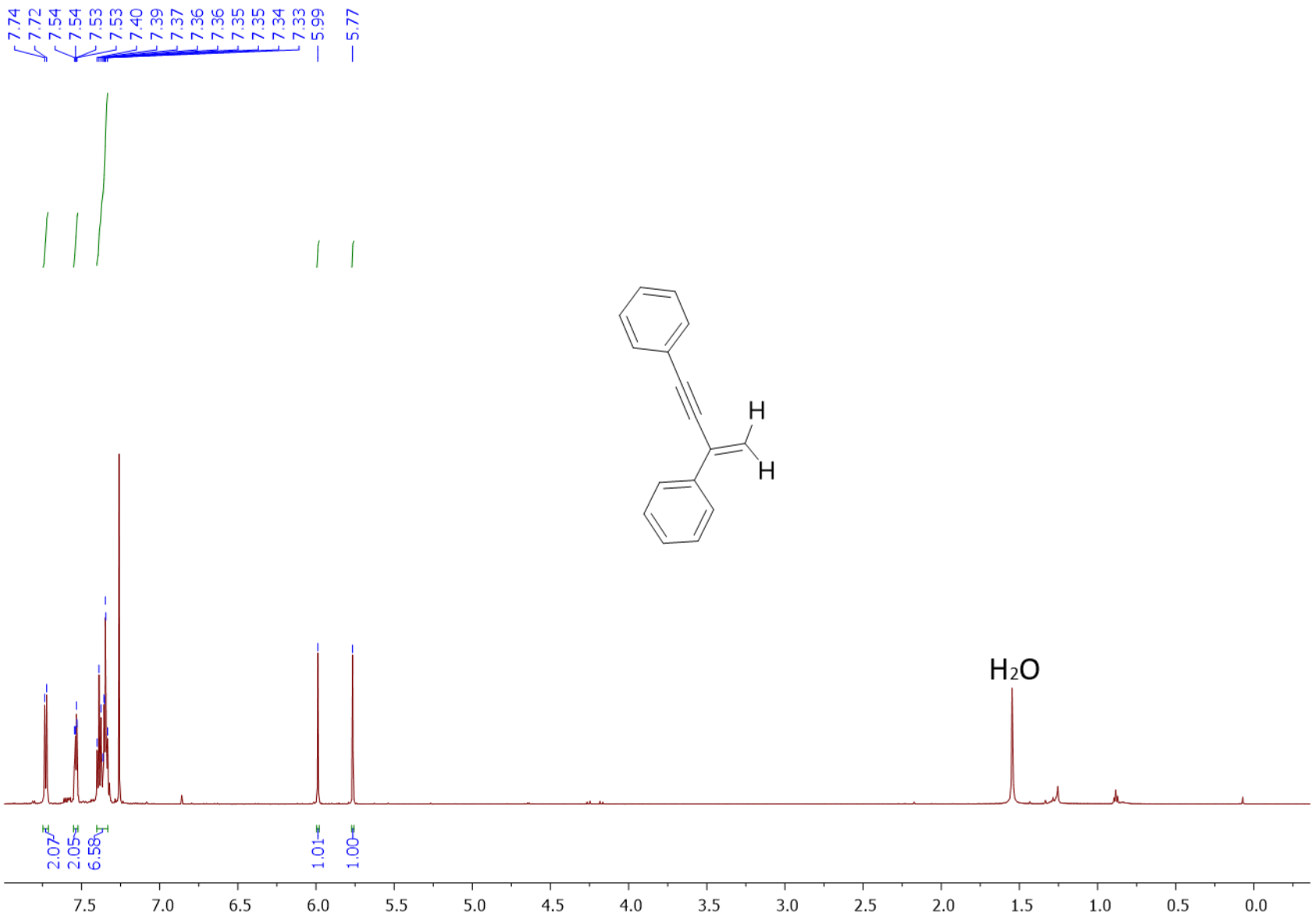

Figure S61. ^{1}H NMR spectrum of 2,4-diphenylbut-1-en-3-yne in $CDCl_3$ at 23 °C.

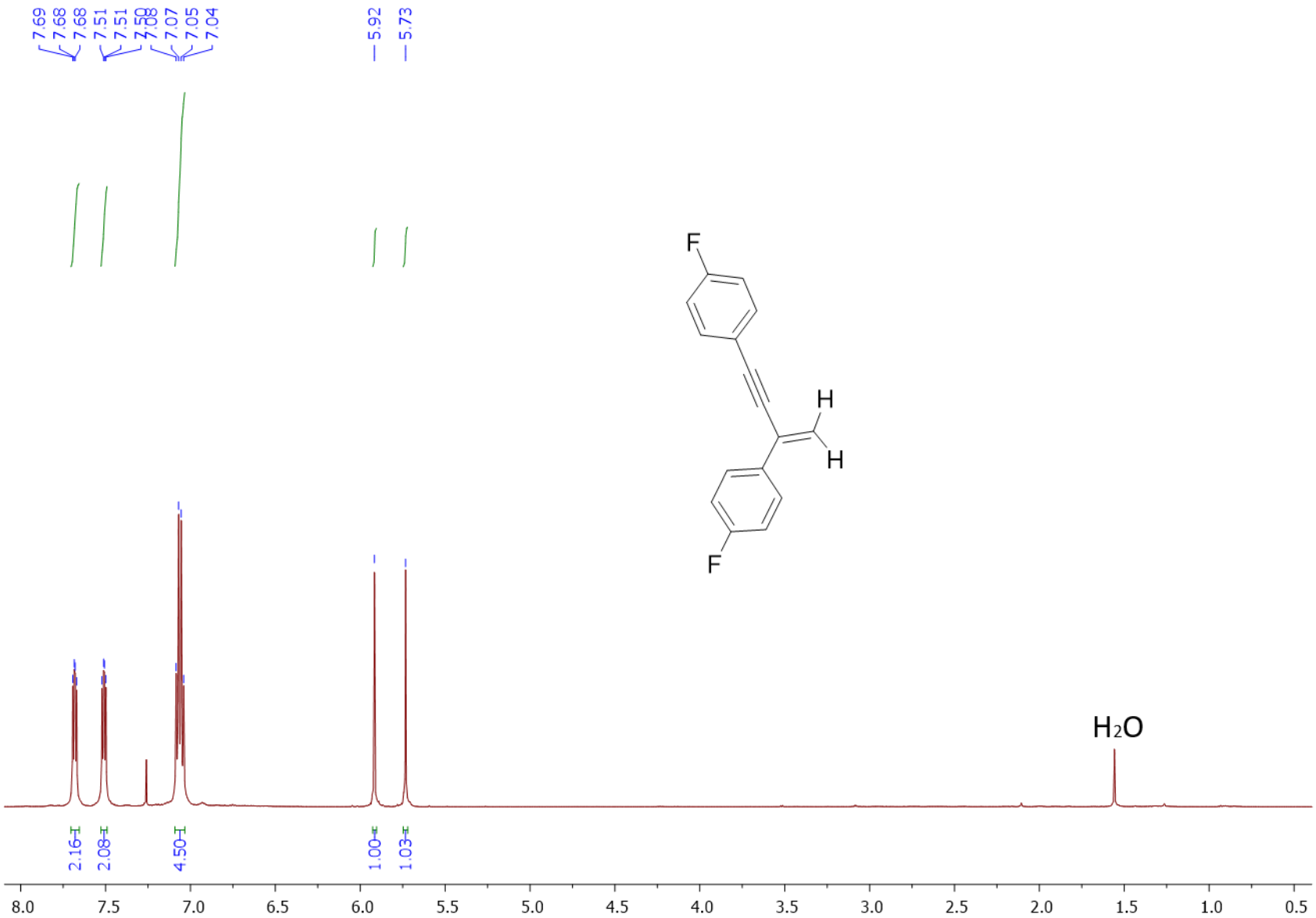

Figure S62. ^{1}H NMR spectrum of 2,4-bis(4-fluorophenyl)but-1-en-3-yne) in $CDCl_3$ at 23 °C.

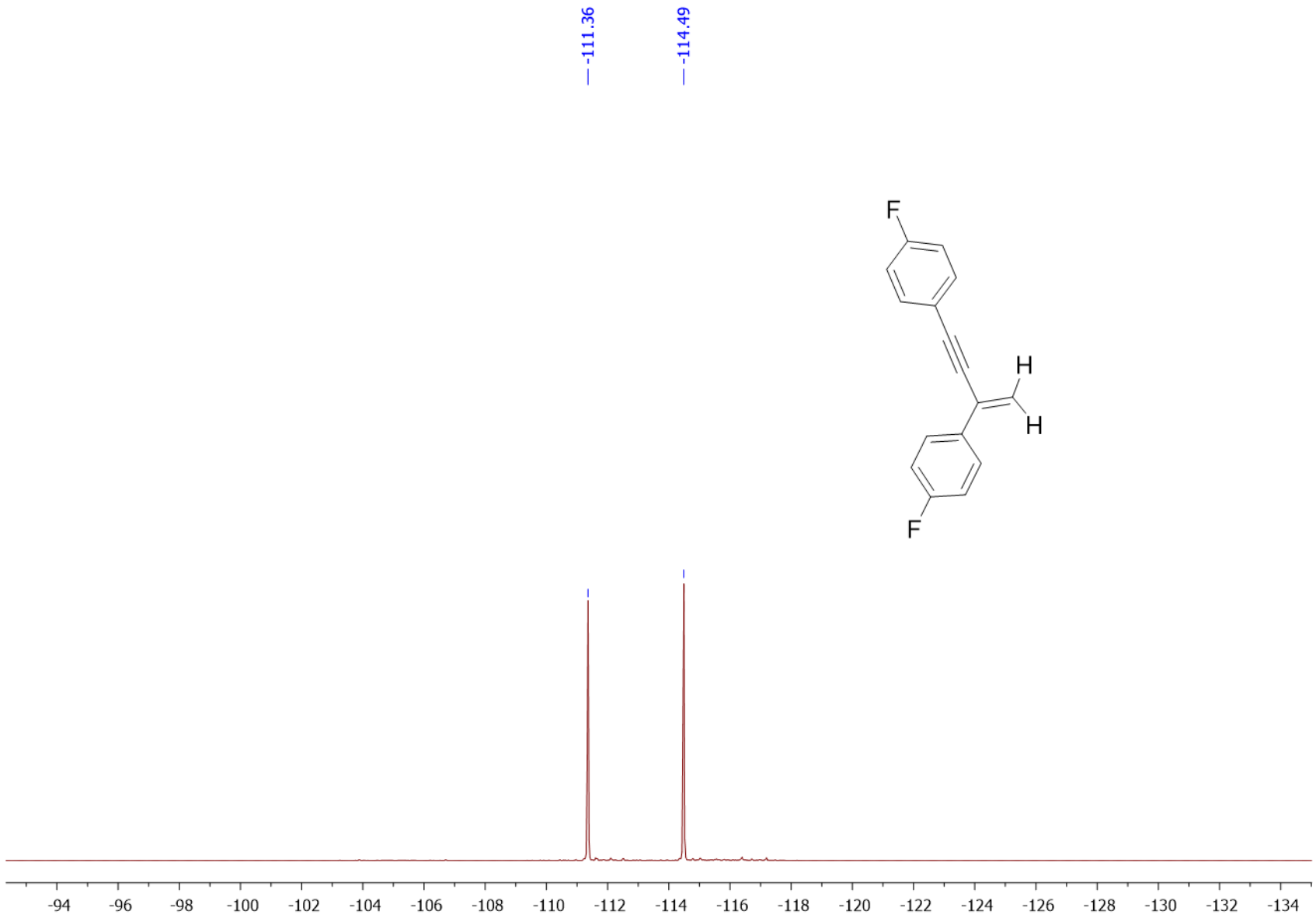

Figure S63. ^{19}F NMR spectrum of 2,4-bis(4-fluorophenyl)but-1-en-3-yne) in $CDCl_3$ at 23 °C.

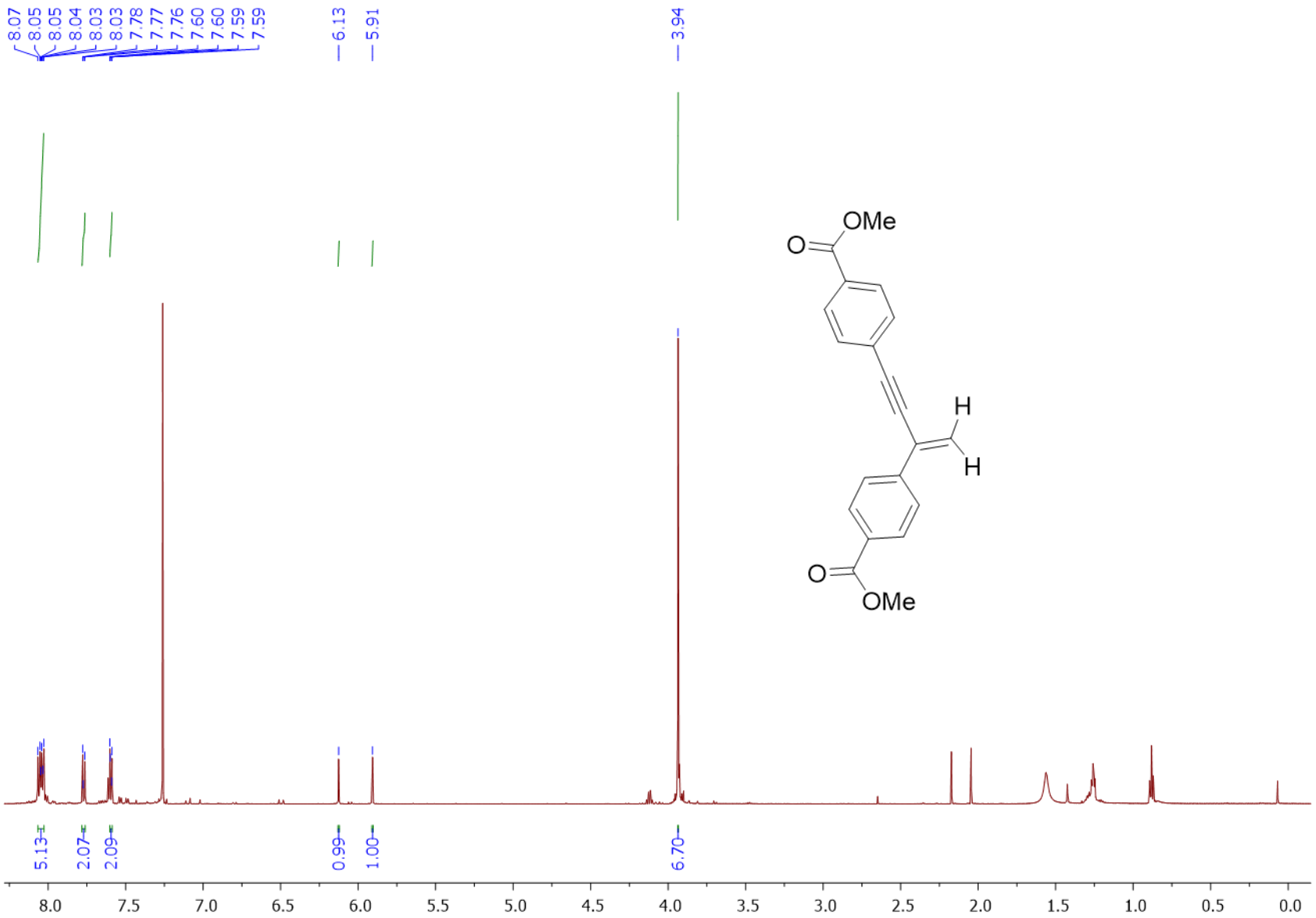

Figure S64. ^{1}H NMR spectrum of dimethyl 4,4'-(but-3-en-1-yne-1,3-diyl)dibenzoate in $CDCl_3$ at 23 °C.

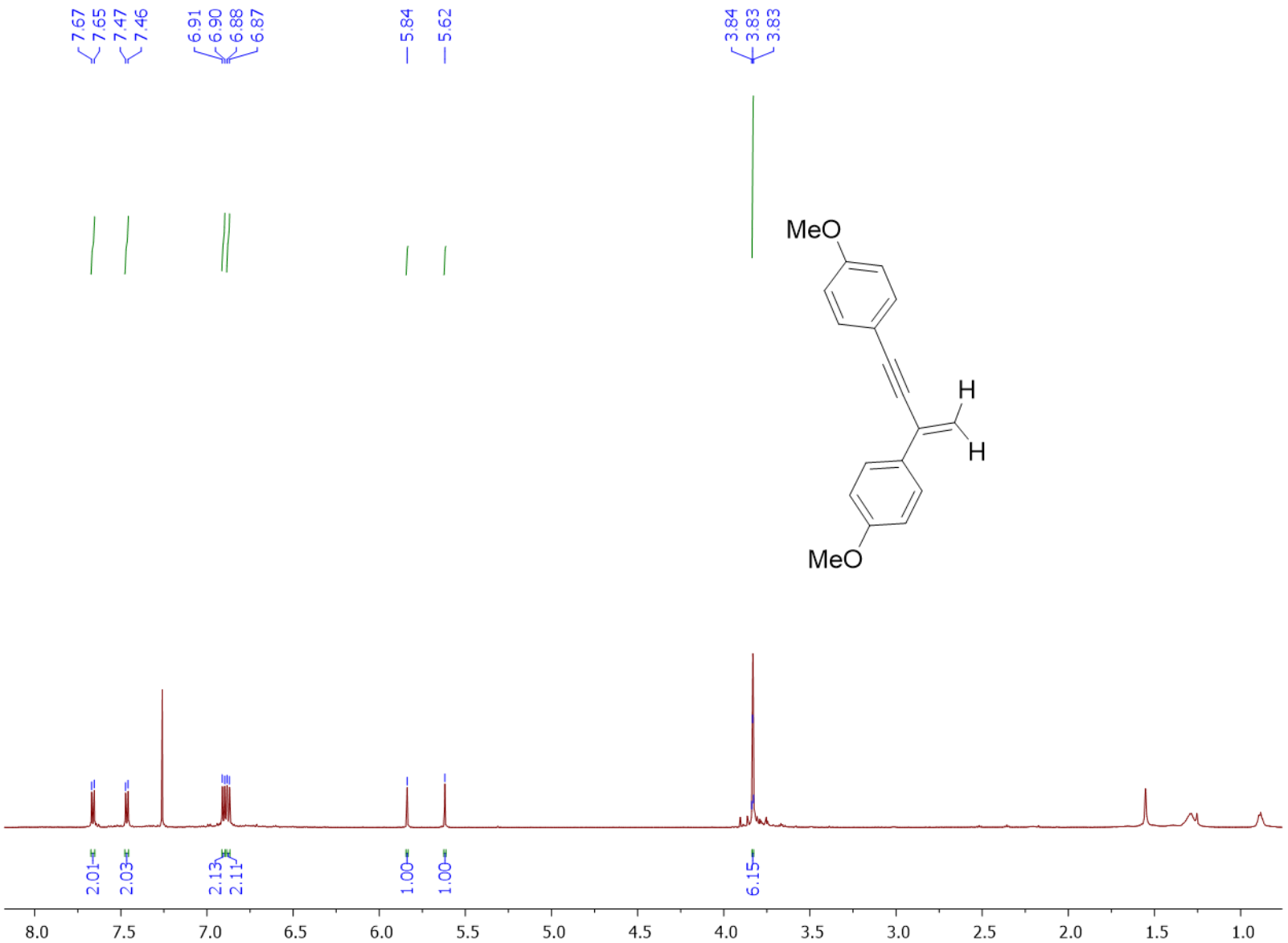

Figure S65. ^{1}H NMR spectrum of 2,4-bis(4-methoxyphenyl)but-1-en-3-yne in $CDCl_3$ at 23 °C.

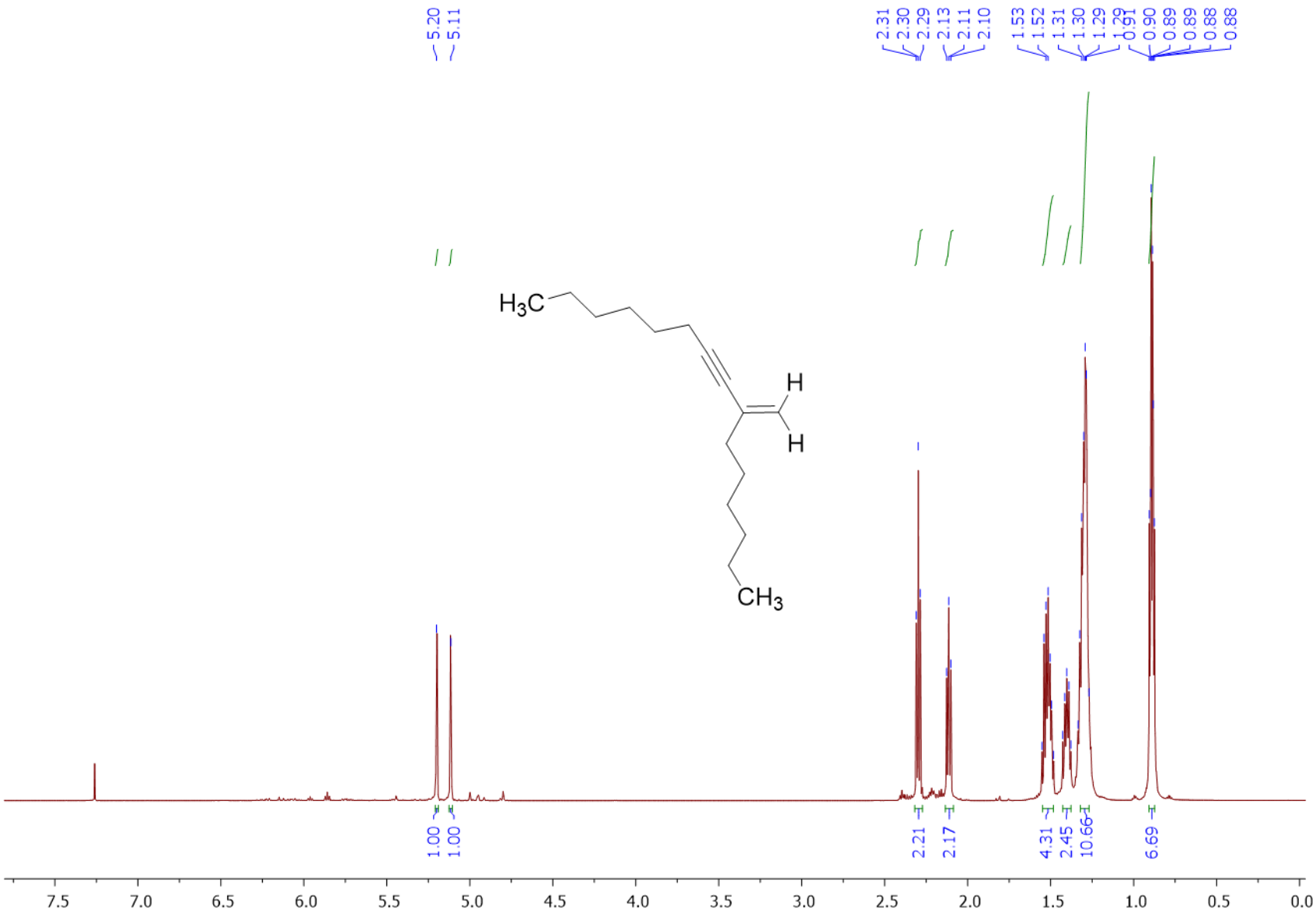

Figure S66. ^{1}H NMR spectrum of 9-methylenepentadec-7-yne in $CDCl_3$ at 23 °C.

Ar-OH elimination under oxidative conditions

Formation and isolation of 10-hydroxybenzo[h]quinoline.

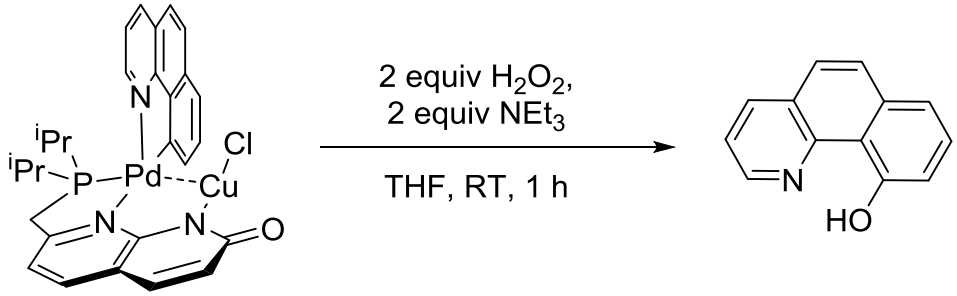

A 50 mL Schlenk flask was charged with crystalline complex **3** (400.4 mg, 0.6076 mmol) dissolved in superdehydrated THF (10 mL). Triethylamine (169 μL, 1.21 mmol), and 30% hydrogen peroxide (28 μL, 1.2 mmol) were added. The Schlenk flask was stirred at room temperature for 1 hour. There was a visual change in the color of solution from yellow to pale green. During the course of reaction black precipitate formation was observed. Solvent was removed under vacuum and the crude product was purified by flash chromatography to obtain 21.8 mg of pure 10-hydroxybenzo[h]quinoline as colorless powder, 18% isolated yield. ^{1}H NMR spectrum corresponds to that reported in the literature.[11]

10-Hydroxybenzo[h]quinoline (colorless solid, eluent: hexane: ether). ^{1}H NMR (400 MHz, $CDCl_3$, 23 °C) δ: 8.82 (dd, *J* = 4.7 Hz, 1.7 Hz, 1H), 8.24 (dd, *J* = 8 Hz, 1.7 Hz, 1H), 7.80 (d, *J* = 8.9 Hz, 1H), 7.65-7.54 (m, 2H), 7.55 (dd, *J* = 8 Hz, 4.7 Hz, 1H), 7.41 (dd, *J* = 7.9 Hz, 0.9 Hz, 1H), 7.26 (dd, *J* = 8 Hz, 1 Hz, 1H). ^{13}C NMR (101 MHz, $CDCl_3$, 23 °C) δ: 159.55, 148.44, 145.10, 136.38, 135.18, 130.05, 129.29, 126.41, 124.67, 120.93, 118.23, 116.04, 114.11.
ESI-HRMS (m/z pos): Found (Calcd $C_{13}H_{10}O_1N_1$: 196.0746 (196.0757).

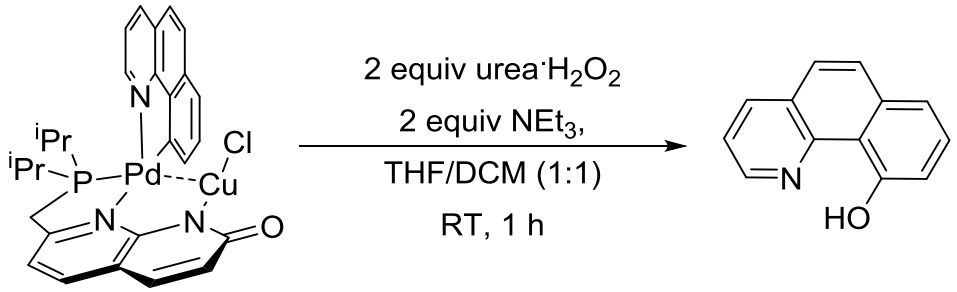

A Schlenk flask (50 mL) was charged with crystalline complex **3** (304.5 mg, 0.4621 mmol) dissolved in superdehydrated THF/DCM (1:1) mixture (10 mL). Triethylamine (129 μL, 0.924 mmol) and urea-hydrogen peroxide adduct (86.9 mg, 0.9242 mmol) were added. The reaction mixture was stirred at room temperature for 1 hour. Black precipitate formation was observed, and the solution changed color from yellow to dark green. After the completion of the reaction, the solvent was removed under vacuum and the crude product was purified by flash chromatography to obtain 20.5 mg of colorless powder, 23% isolated yield. The NMR spectra corresponds to that of 1-hydroxybenzo[h]quinoline obtained by reacting with aqueous H_2O_2 as described above and matches the spectrum reported in the literature.

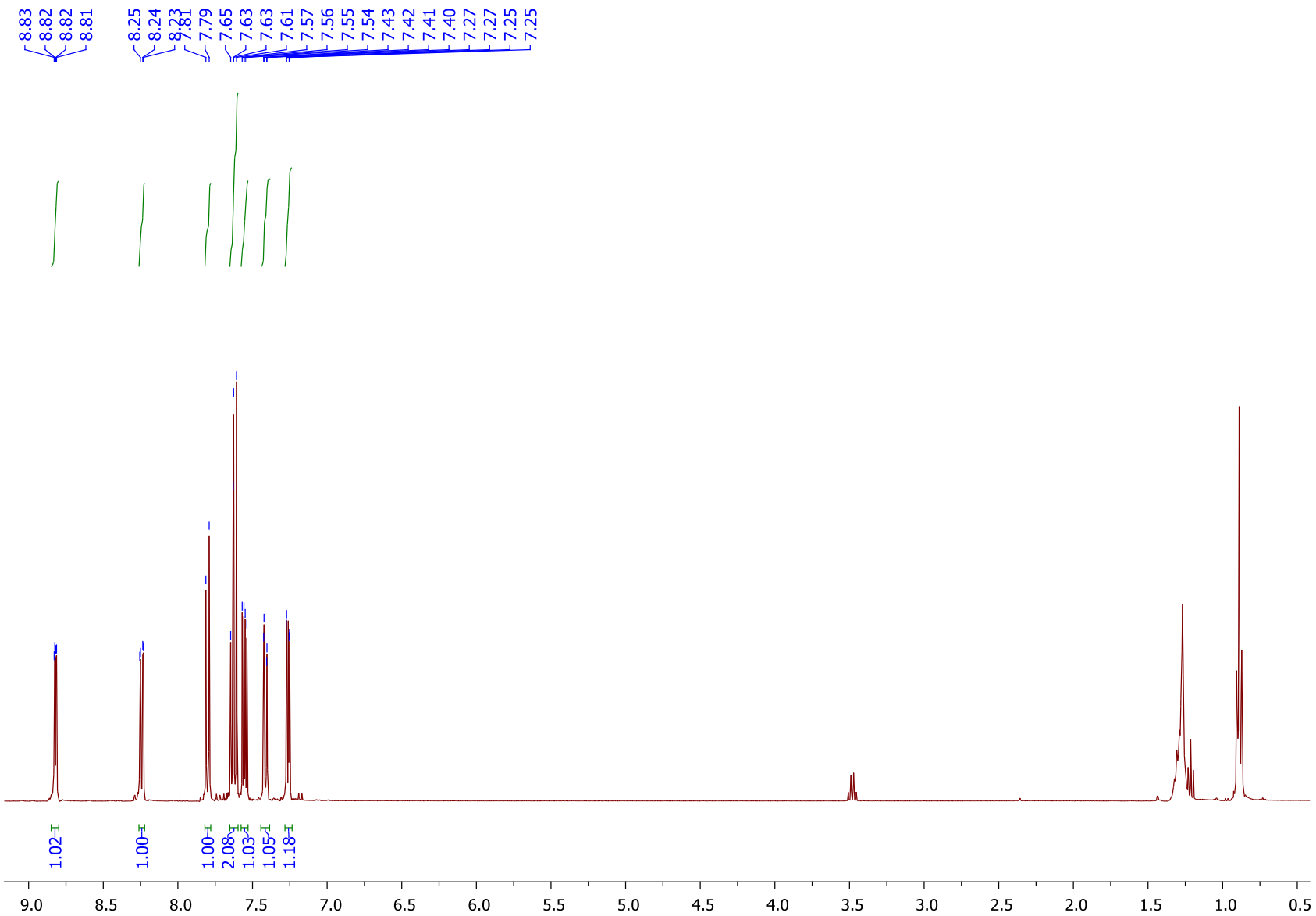

Figure S67. ^{1}H NMR spectrum of 10-hydroxybenzo[h]quinoline in $CDCl_3$ at 23 °C.

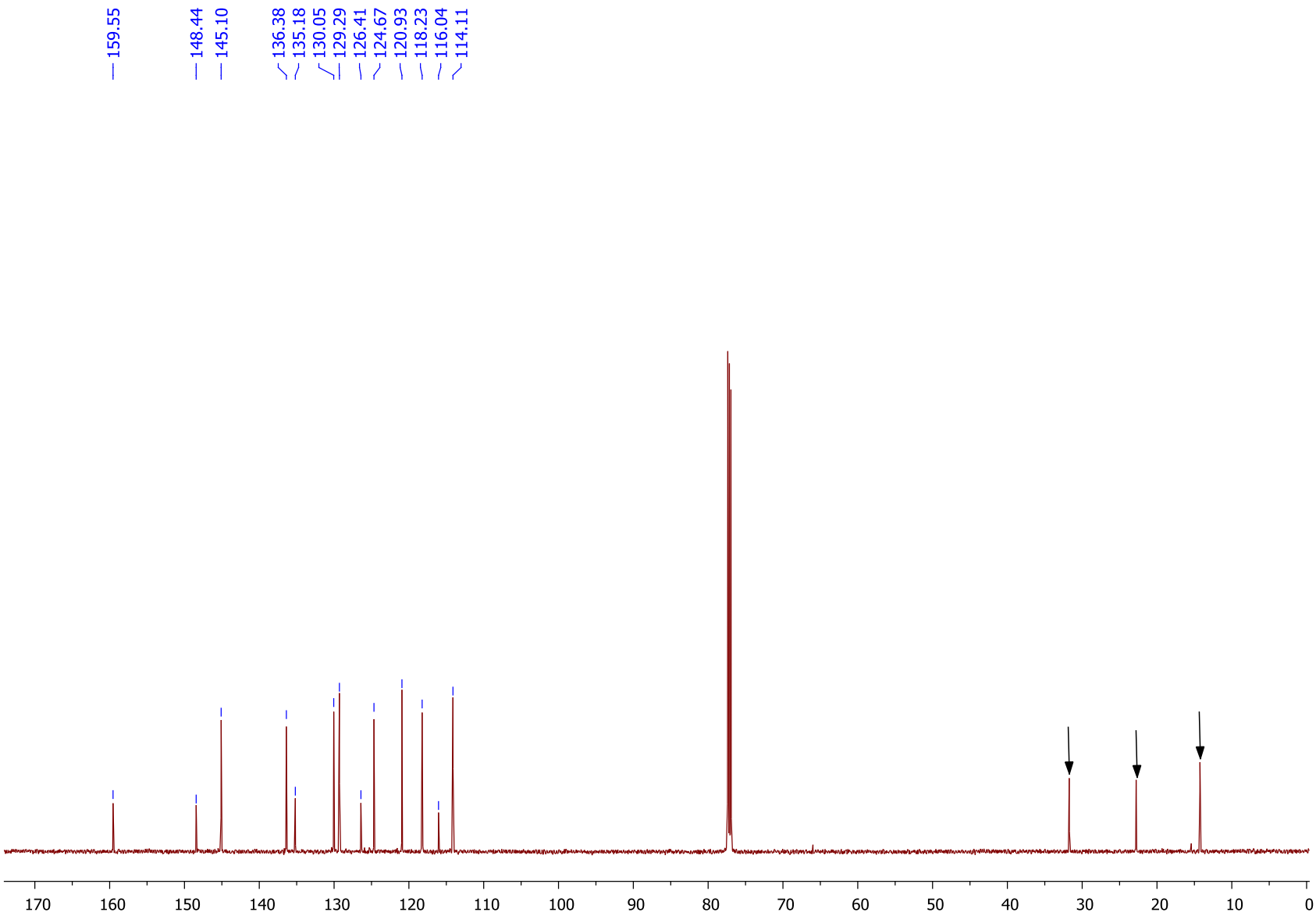

Figure S68. ^{13}C NMR spectrum of 10-hydroxybenzo[h]quinoline in $CDCl_3$ at 23 °C. The peaks marked by arrows correspond to residual hexane.

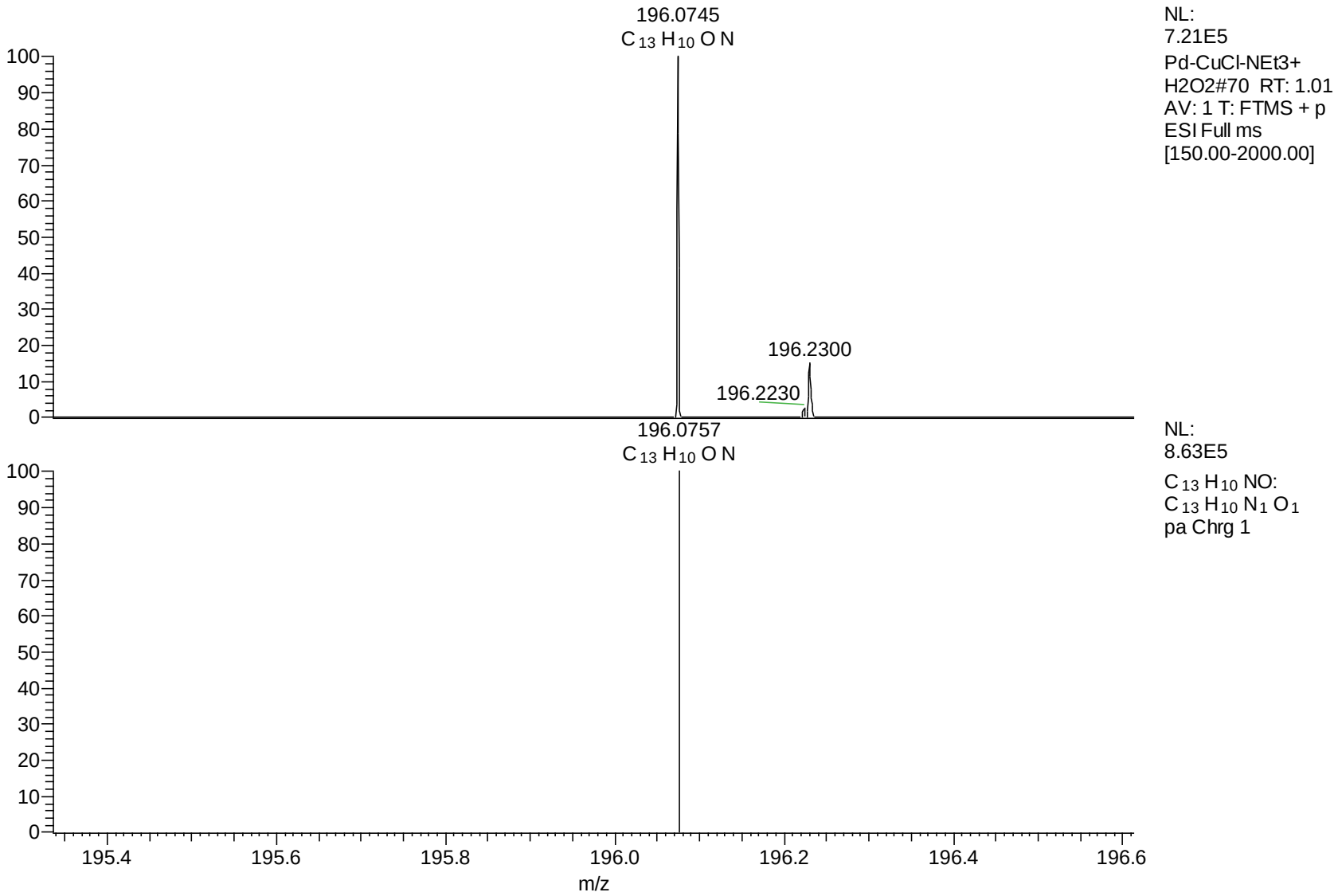

Figure S69. ESI-(HR)MS spectrum of a MeOH solution of benzo[h]quinoline-10-ol (top) and simulated spectrum for $C_{13}H_{10}O_1N_1$ (bottom).

Attempted reactivity of 1-OAc with H_2O_2 / NEt_3

In a glovebox, complex **1-OAc** (25.6 mg , 0.041 mmol) was dissolved in deuterated CD_2Cl_2 (1 mL). Triethylamine (11.5 μL, 0.082 mmol), and 30% aqueous hydrogen peroxide (2.0 μL, 0.082 mmol) were added. The reaction was stirred for 12 hours at room temperature. The reaction mixture was analyzed ^{1}H NMR and ^{31}P NMR spectroscopy. According to ^{1}H NMR, the starting material remains mostly unreacted. Only a small amount of a new product is formed as evidence by appearance of a new peak in ^{31}P NMR, which could correspond to phosphine oxide formed by ligand oxidation.

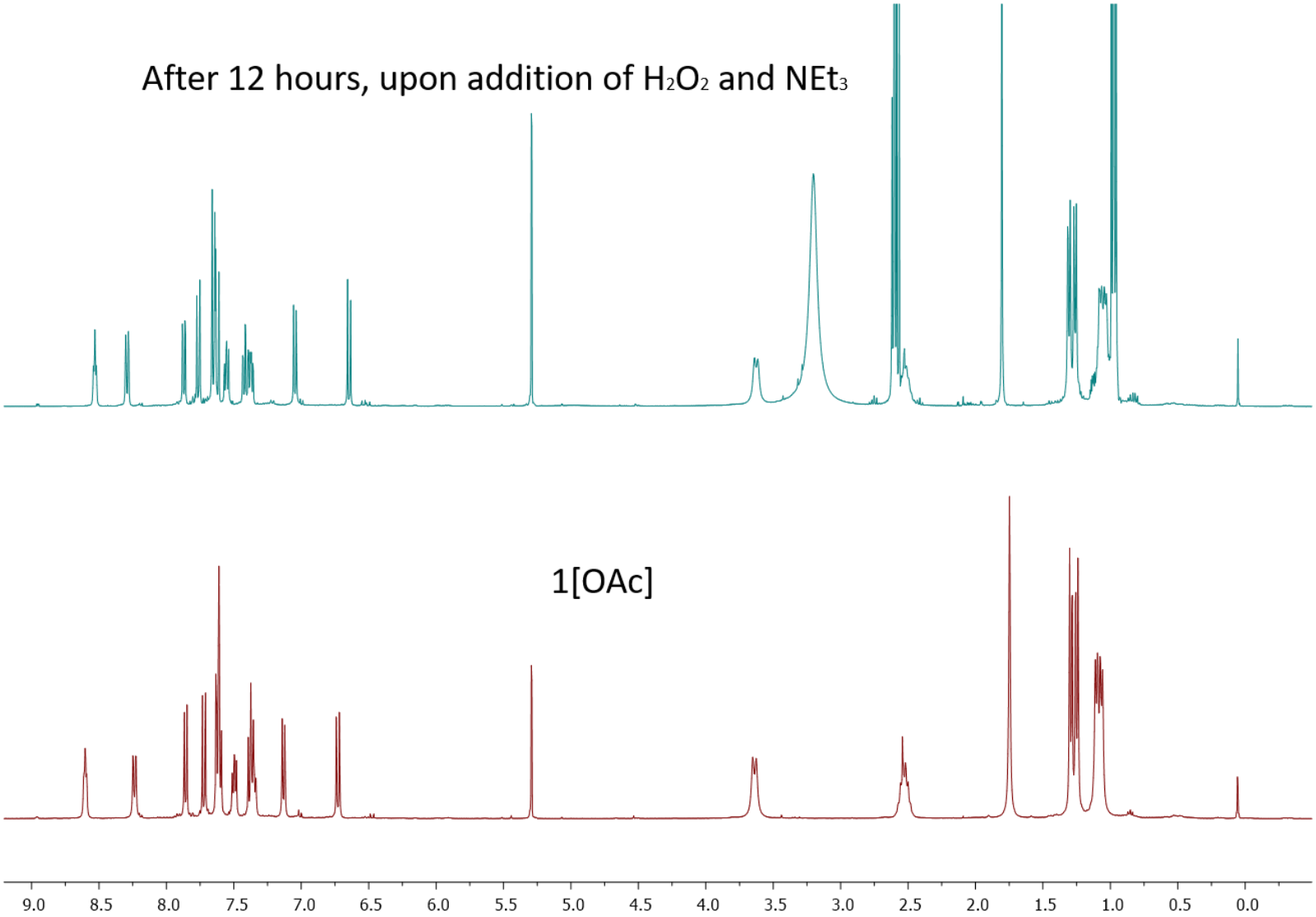

Figure S70. ^{1}H NMR spectrum of the reaction mixture containing **1**-OAc before and after addition of 2 equivalents of H_2O_2 and NEt_3 after 12 h at RT (23 °C, CD_2Cl_2).

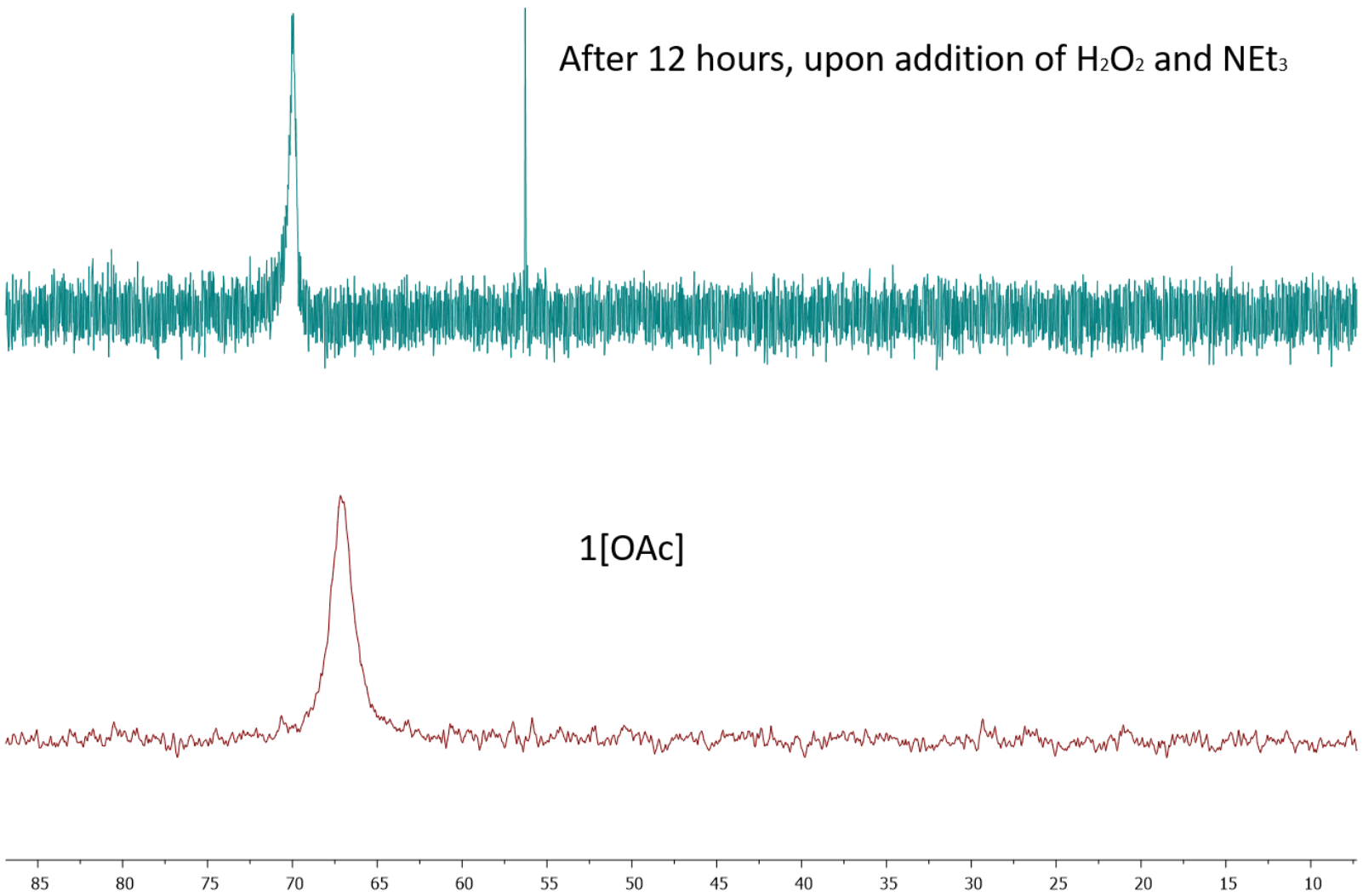

Figure S71. ^{31}P NMR spectrum of the reaction mixture containing **1**-OAc before and after addition of 2 equivalents of H_2O_2 and NEt_3 after 12 h at RT (23 °C, CD_2Cl_2).

Synthesis of 7

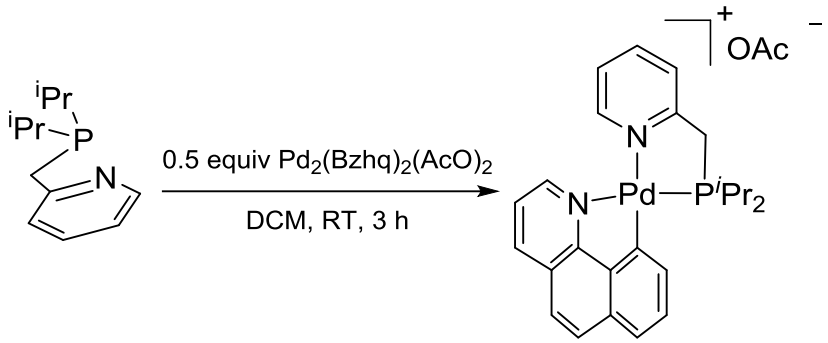

Scheme S10. Synthesis of 7.

The (2-picolyl)-di(isopropyl)phosphine ligand (50.1 mg, 0.23 mmol) was added to a 20 mL vial containing a solution of a palladium precursor $Pd_2(Bzhq)_2(AcO)_2$ (82.2 mg, 0.11 mmol) in DCM (4 mL) to give a yellow-green solution. The reaction was left to stir for 3 hours. Then the solvent was removed under vacuum and the desired complex was re-dissolved in a small amount of DCM (1 mL). Cold pentane (5 x 2 mL) was added to precipitate the powder. Solvent removal yields complex **7** as a yellow-green solid, (78.2 mg, 0.14 mmol, 59% yield).

^{1}H NMR (600 MHz,CD_2Cl_2, 22 °C) δ: 8.78 (d, $^3J_{HH}$ = 4.7 Hz, 1H, CH_{ar}), 8.75 (d, $^3J_{HH}$ = 4.7 Hz, 1H, CH_{ar}), 8.53 (d, $^3J_{HH}$ = 7.5 Hz, 1H, CH_{ar}), 8.13-8.07 (m, 2H, CH_{ar}), 7.87 (d, $^3J_{HH}$ = 9.2 Hz, 1H, CH_{ar}), 7.83-7.79 (m, 1H, CH_{ar}), 7.76 (d, $^3J_{HH}$ = 8.4 Hz, 1H, CH_{ar}), 7.73-7.67 (m, 2H, CH_{ar}), 7.55 (t, $^3J_{HH}$ = 7.5 Hz, 1H, CH_{ar}), 7.48 (d, $^3J_{HH}$ = 7.1 Hz, 1H, CH_{ar}), 4.07 (d, $^2J_{PH}$ = 11.1 Hz, 2H, CH_2), 2.75-2.64 (m, 2H, C*H*$(CH_3)_2$), 2.08 (s, 3H, OAc), 1.40 (d, $^3J_{PH}$ = 6.9 Hz, 3H, CH(C*H*$_3)_3$), 1.37 (d, $^3J_{PH}$ = 6.9 Hz, 3H, CH(C*H*$_3)_3$), 1.16 (d, $^3J_{PH}$ = 6.9 Hz, 3H, CH(C*H*$_3)_3$), 1.13 (d, $^3J_{PH}$ = 6.9 Hz, 3H, CH(C*H*$_3)_3$).

^{13}C{^{1}H} NMR (151 MHz, CD_2Cl_2, 22 °C) δ: 169.89 (OAc), 160.73 (C_{ar}), 154.15 (C_{ar}), 151.27 (C_{ar}), 150.38 (C_{ar}), 148.04 (C_{ar}), 142.31 (C_{ar}), 140.91 (C_{ar}), 139.38 (C_{ar}), 137.43 (C_{ar}, J_{PC} = 8.7 Hz), 134.86 (C_{ar}), 130.13 (C_{ar}), 129.64 (d, J_{PC} =4.5 Hz, C_{ar}), 127.90 (C_{ar}), 125.95 (C_{ar}, J_{PC} = 7.6 Hz), 125.04 (C_{ar}), 124.74 (C_{ar}), 124.29 (C_{ar}), 123 (C_{ar}, J_{PC} = 2.4 Hz C_{ar}), 34.12 (d, J_{PC} =26.3 Hz, CH_2), 24.43 (d, J_{PC} =24.8 Hz, CH(*C*$H_3)_2$), 20.87 (OAc), 19.61 (d, J_{PC} =3.5 Hz, CH(*C*$H_3)_2$) 18.08 (CH(*C*$H_3)_2$).

^{31}P{^{1}H} NMR (162 MHz, CD_2Cl_2, 23 °C) δ: 73.55.

ESI-HRMS (m/z pos): Found (Calcd): $C_{25}H_{28}N_2P_1Pd_1$: 493.1019 (493.1019).

FT-IR (ATR, solid): 2970 (br, w), 2968 (br, w), 2862 (br, s), 1764 (s),1565 (s), 1460 (m), 1197 (s), 1063 (s), 908 (br, s), 837 (s), 717 (s) cm^{-1}.

UV-vis (MeCN), λ, nm (ε, $M^{-1}\cdot cm^{-1}$) : 379 (178), 290 (1626), 236 (6042), 200 (18527).

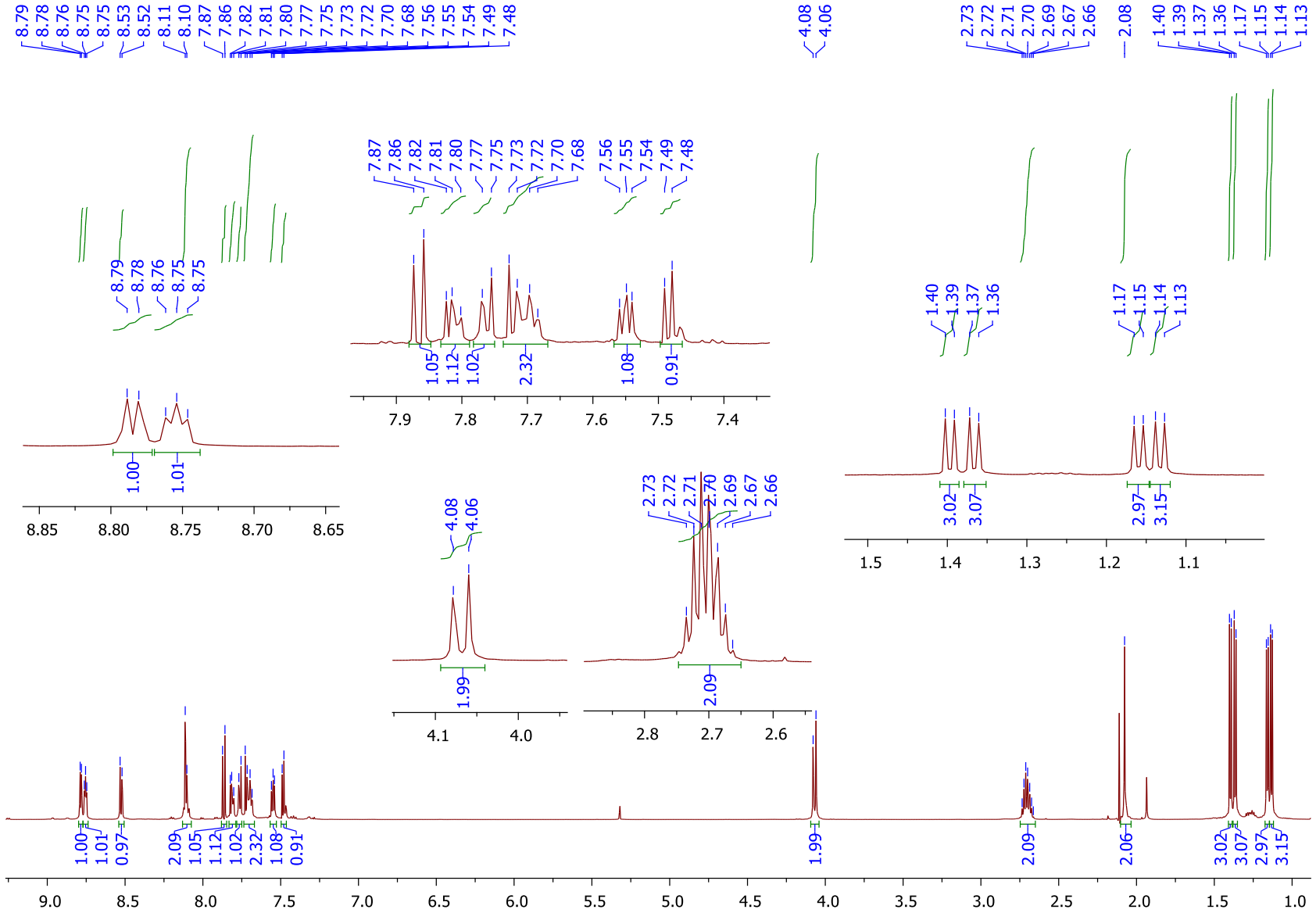

Figure S72. ^{1}H NMR spectrum of **7** in CD_2Cl_2 at 23 °C.

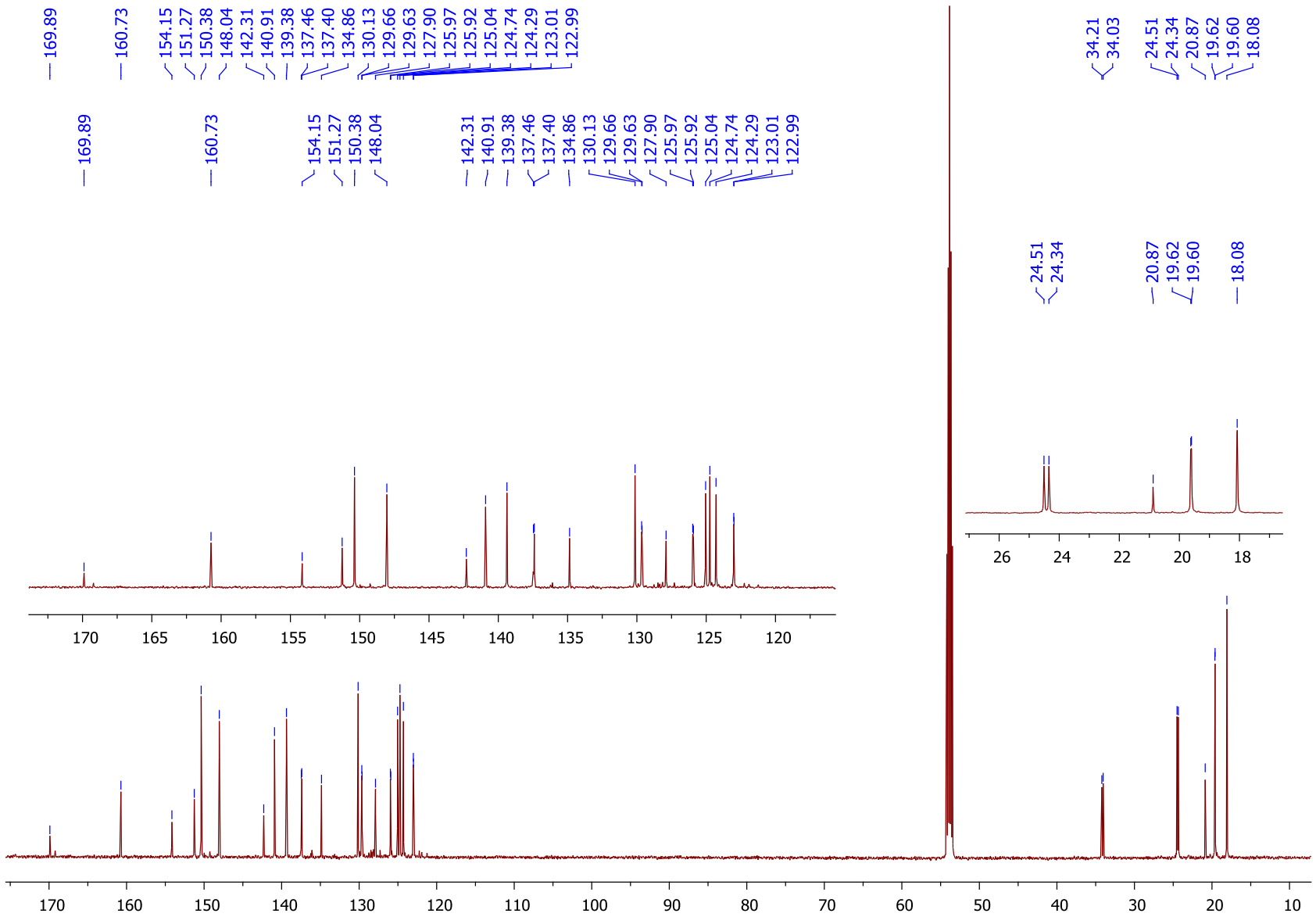

Figure S73. ^{13}C NMR spectrum of **7** in CD_2Cl_2 at 23 °C.

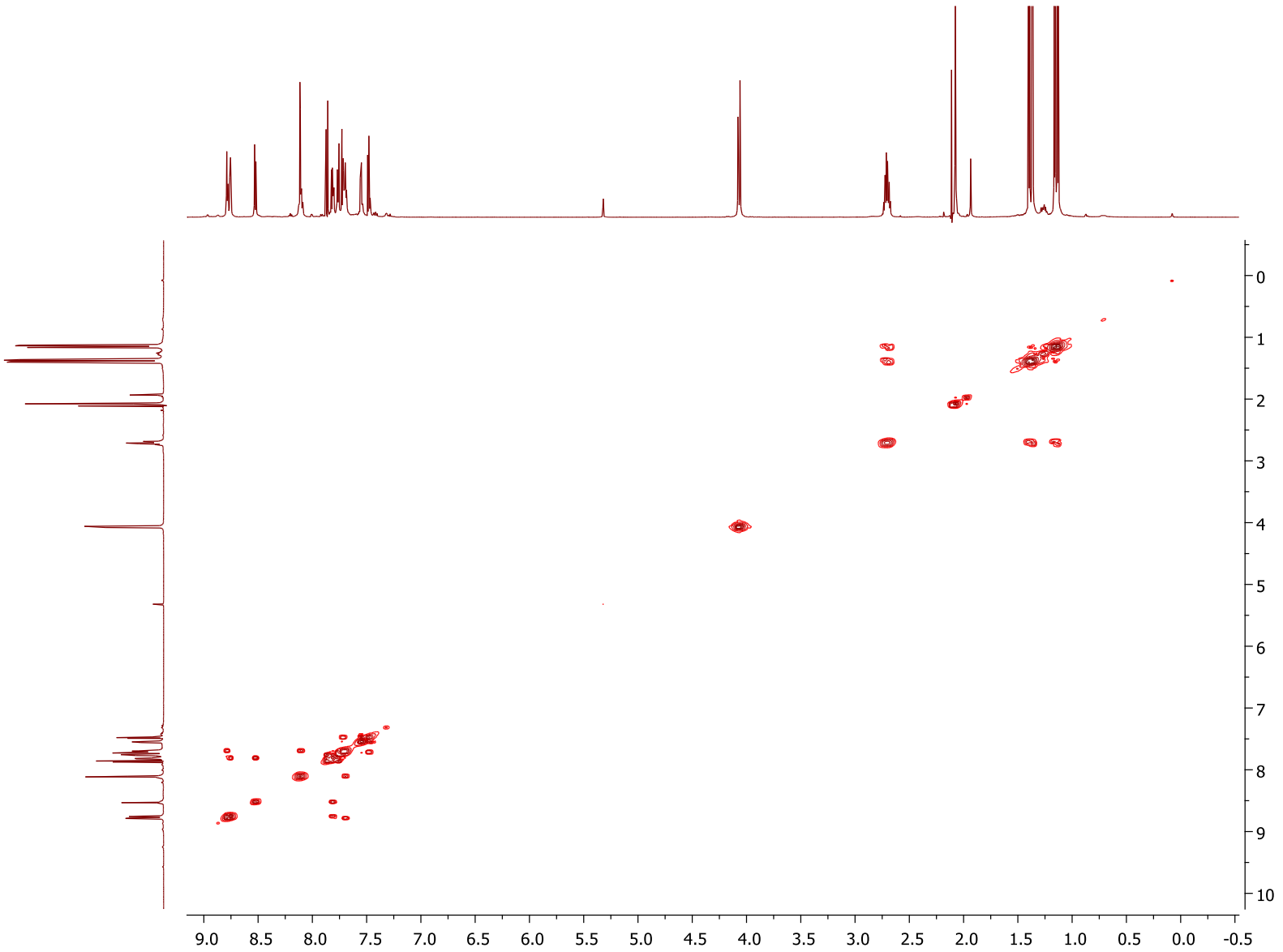

Figure S74. ^{1}H-^{1}H COSY spectrum of **7** in CD_2Cl_2 at 23 °C.

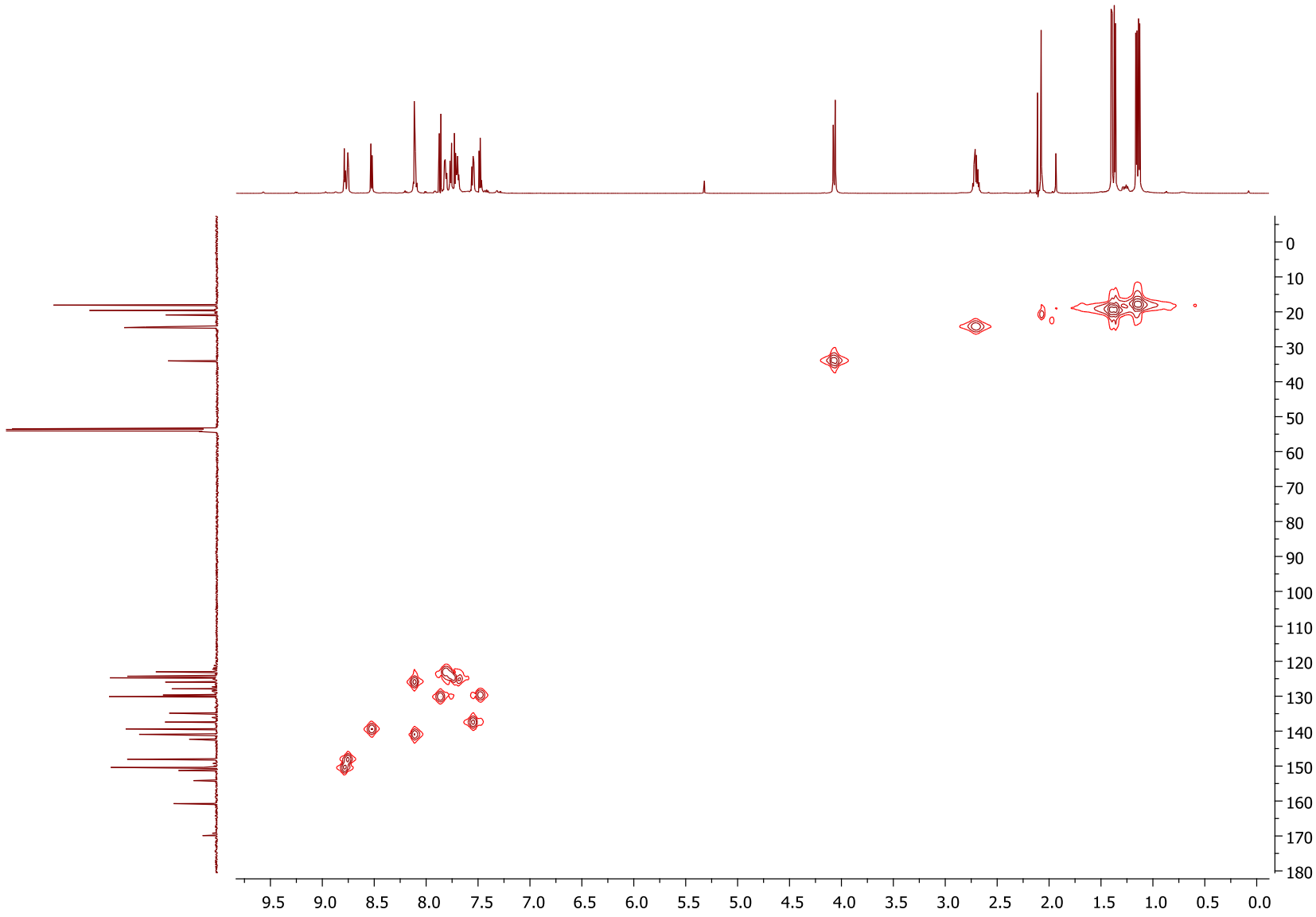

Figure S75. ^{1}H-^{13}C HMQC spectrum of **7** in CD_2Cl_2 at 23 °C.

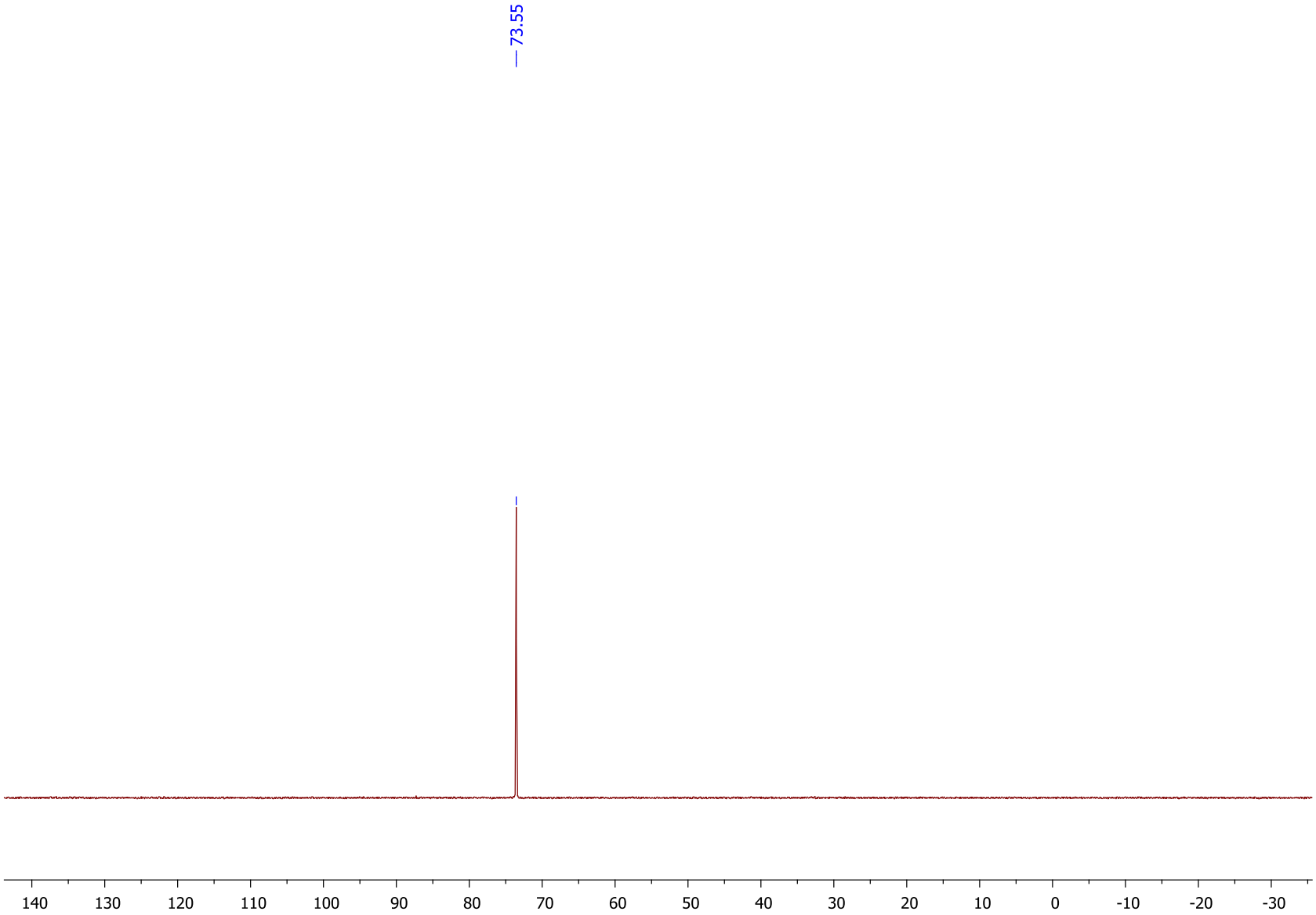

Figure S76. ^{31}P NMR spectrum of **7**· in CD_2Cl_2 at 23 °C.

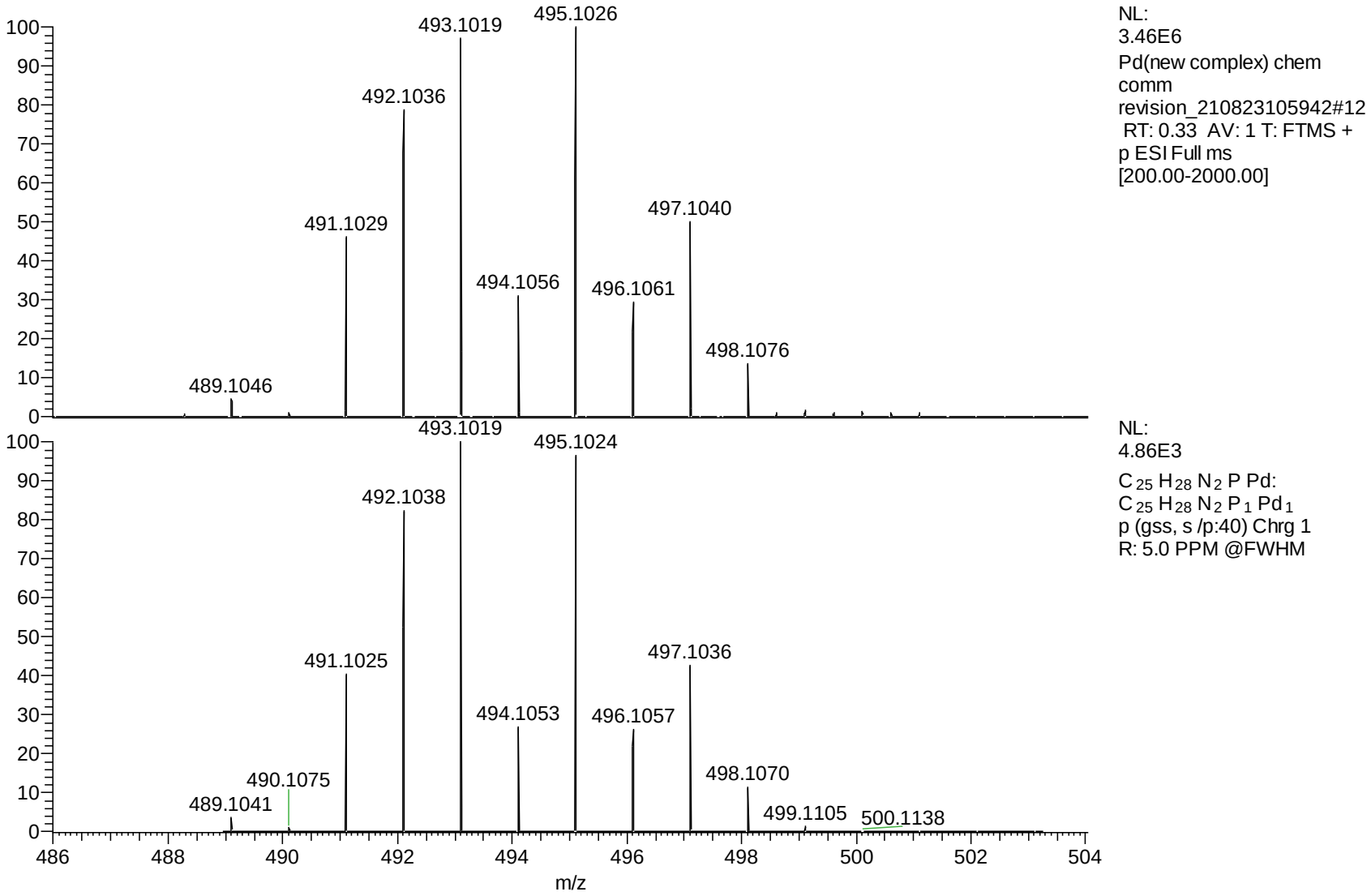

Figure S77. ESI-(HR)MS spectrum of MeOH solution of **7** (top) and simulated spectrum for $C_{25}H_{28}N_2PPd^+$ (bottom).

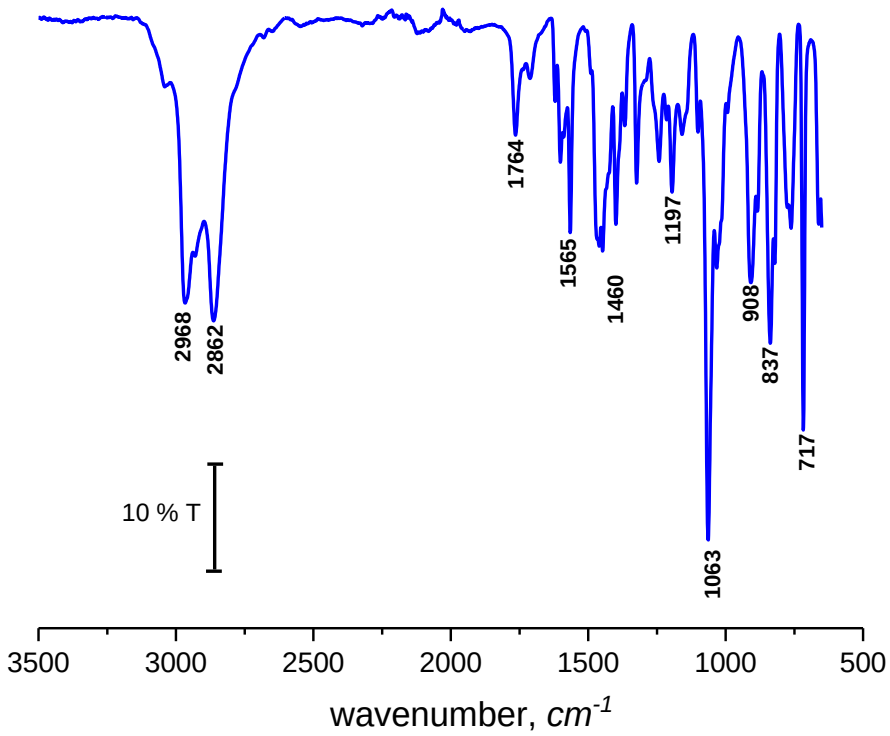

Figure S78. ATR FT-IR transmittance spectrum of **7**.

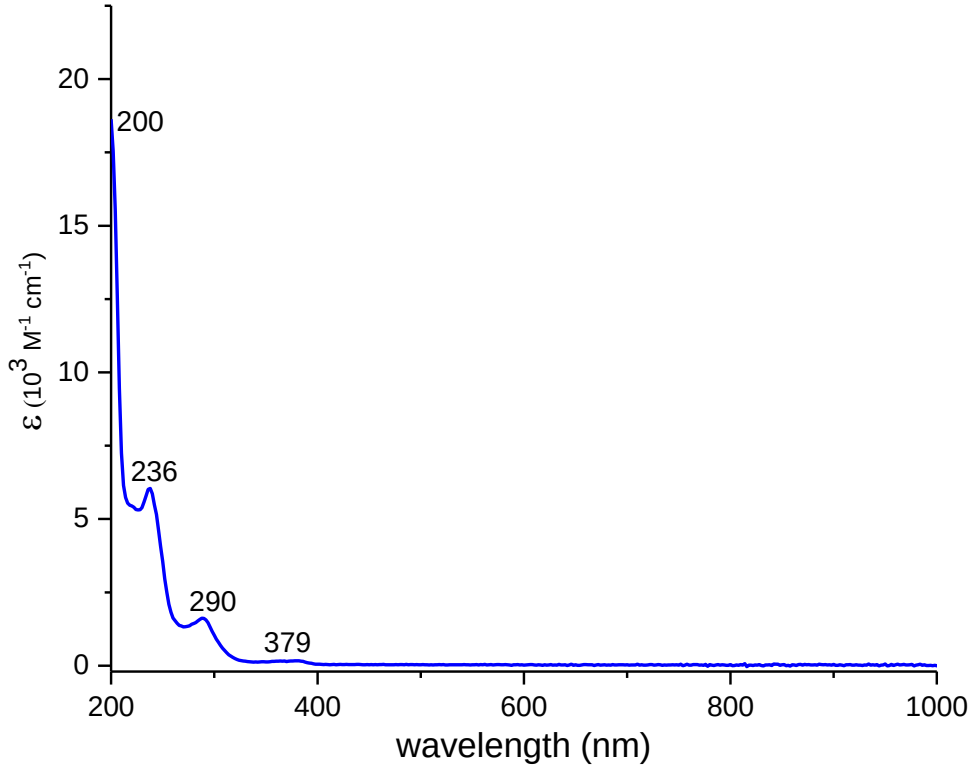

Figure S79. UV-vis absorbance spectrum for **7** in MeCN.

Attempted reactivity of 7 with H_2O_2 / NEt_3 in presence of CuCl.
In a glovebox, complex **7** (20.1 mg , 0.036 mmol) and copper chloride (7.1 mg, 0.072 mmol) were dissolved in CD_2Cl_2 (1 mL). Triethylamine (10.1 µL, 0.082 mmol) and 30% aqueous hydrogen peroxide (1.7 µL, 0.072 mmol) were added. The reaction was stirred for 2 hours at room temperature. The reaction mixture was analyzed ^1H NMR and ^{31}P NMR spectroscopy. According to ^1H NMR and ^{31}P NMR, the starting material remains mostly unreacted.

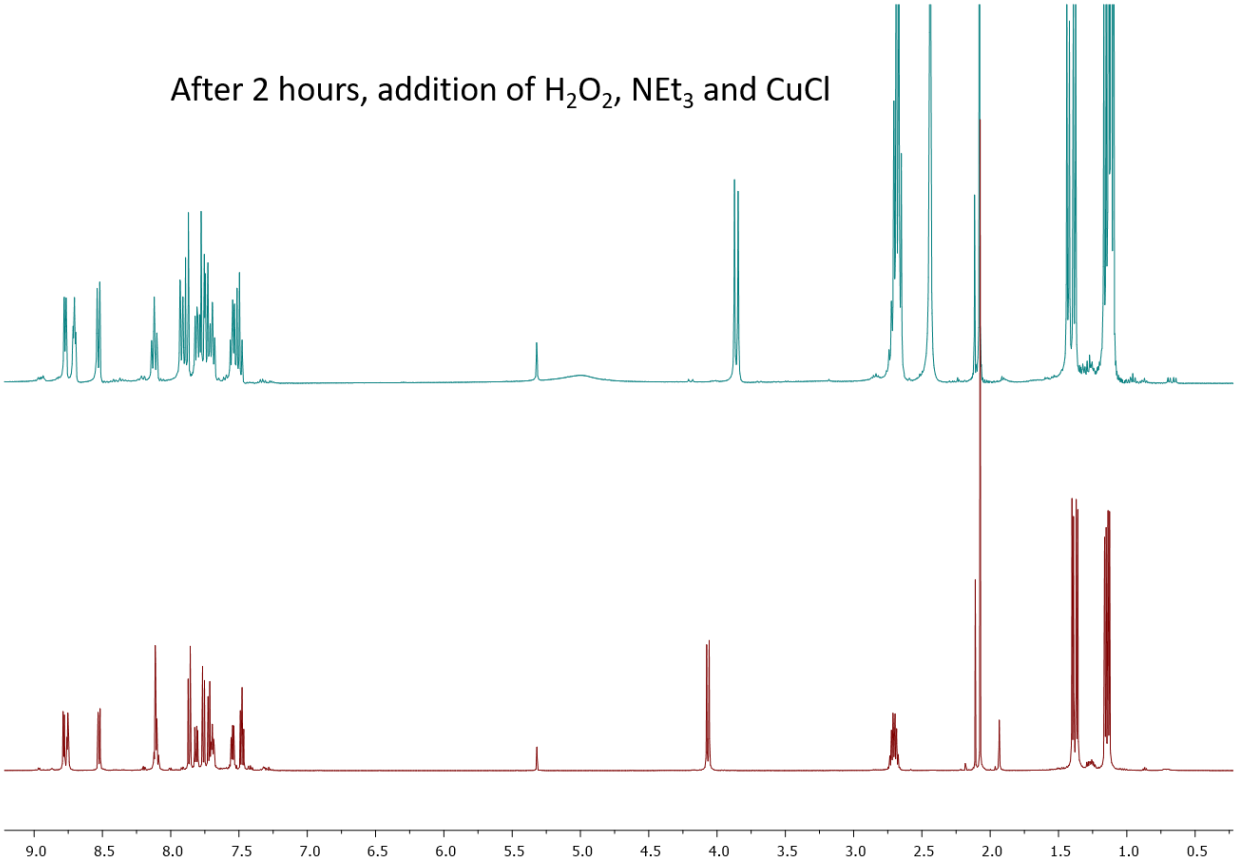

Figure S80. ^1H NMR spectrum of the reaction mixture containing **7** before and after addition of 2 equivalents of CuCl, H_2O_2 and NEt_3 after 2 h at RT (23 °C, CD_2Cl_2).

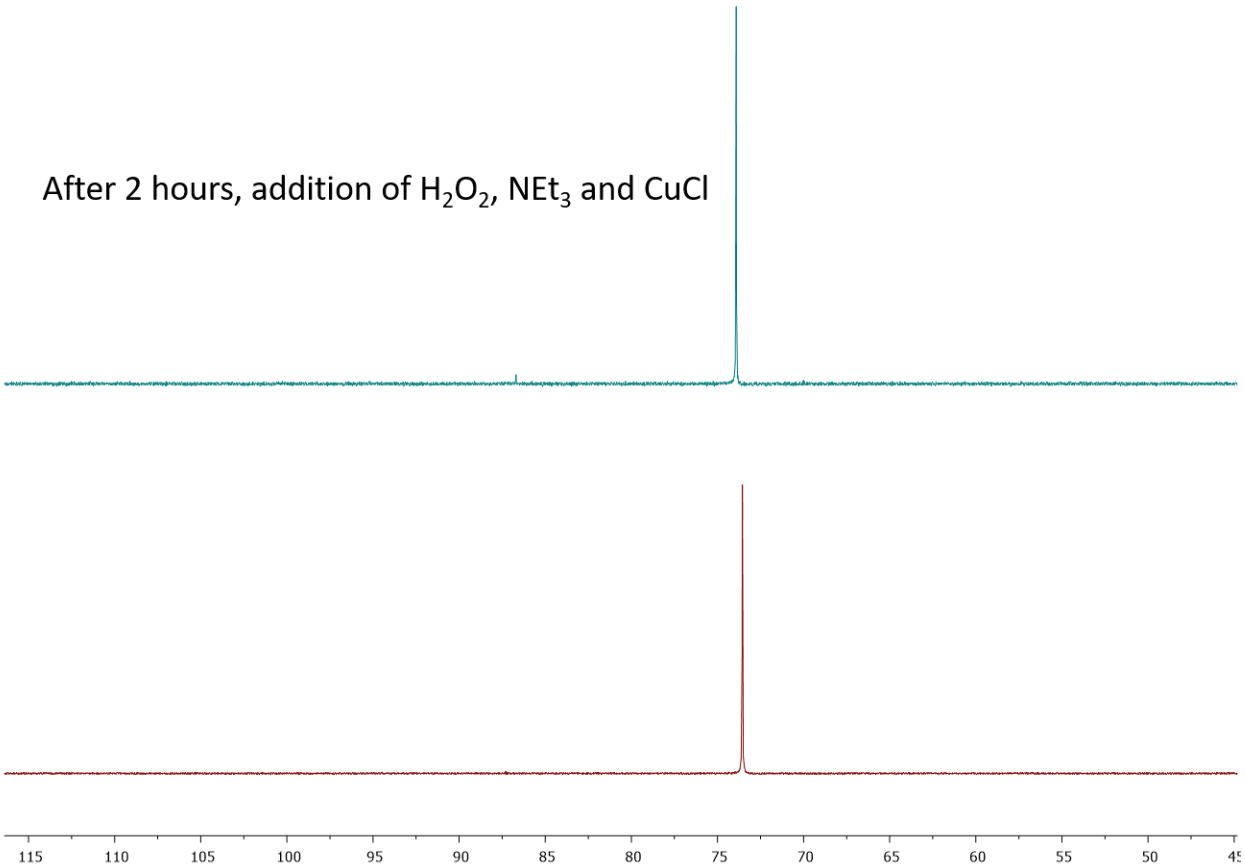

Figure S81. ^{31}P NMR spectrum of the reaction mixture containing **7** before and after addition of 2 equivalents of CuCl, H_2O_2 and NEt_3 after 2 h at RT (23 °C, CD_2Cl_2).

II. The X-ray structure determination details

The X-ray diffraction data for the single crystals were collected on a Rigaku XtaLab PRO instrument (κ-goniometer) with a PILATUS3 R 200K hybrid pixel array detector using Mo-*K*α (0.71073 Å) or Cu-*K*α (1.54184 Å) radiation monochromated by means of multilayer optics. The performance mode of MicroMax^{TM}-003 microfocus sealed X-ray tubes was 50 kV, 0.60 mA. The diffractometer was equipped with a Rigaku GN2 system for low temperature experiments. Suitable crystals of appropriate dimensions were mounted on MiTeGen loops in random orientations. Preliminary unit cell parameters were determined with three sets of a total of 10 narrow frame scans in the case of a Mo-source and six sets of a total of 10 narrow frame scans at two different 2θ positions in the case of a Cu-source. The data were collected according to recommended strategies in an ω scan mode. Final cell constants were determined by global refinement of reflections from the complete data sets using the Lattice wizard module. Images were indexed and integrated with "smart" background evaluation using the *CrysAlisPro* data reduction package (1.171.39.20a-1.171.40.82a, Rigaku Oxford Diffraction). Analysis of the integrated data did not show any decay. Data were corrected for systematic errors and absorption using the *ABSPACK* module: Numerical absorption correction based on Gaussian integration over a multifaceted crystal model and empirical absorption correction based on spherical harmonics according to the point group symmetry using equivalent reflections. The *GRAL* module and the *ASSIGN SPACEGROUP* routine of the *WinGX* suite were used for analysis of systematic absences and space group determination.

The structures were solved by the direct methods using *SHELXT*-2018/2[12] and refined by the full-matrix least-squares on F^2 using *SHELXL*-2018/3,[13] which uses a model of atomic scattering based on spherical atoms. Calculations were mainly performed using the *WinGX*-2021.1 suite of programs.[14] Non-hydrogen atoms were refined anisotropically. The positions of hydrogen atoms [O11–]H11 of co-crystallized acetic acid in crystal **1**-OAc and [N12–]H12 in crystal **1**-B(Ar^F)$_4$ were determined by difference Fourier maps; these atoms were refined isotropically. The positions of hydrogen atoms of methyl groups were found using rotating group refinement with idealized tetrahedral angles. The other hydrogen atoms were inserted at the calculated positions and refined as riding atoms. The disorder, if present, was resolved using free variables and reasonable restraints on geometry and anisotropic displacement parameters. All the compounds studied have no unusual bond lengths and angles. The absolute structure of the crystal **1**-OAc was determined based on the Flack parameter calculated by Parsons' method.[15] The unit cell of **4** contains highly disordered solvent molecules of toluene and cyclohexane, which were treated as a diffuse contribution to the overall scattering without specific atom positions by *PLATON*/SQUEEZE-130220.[16] Squeezed solvent info is not included in the formulae and related items such as molecular weights and calculated densities.

Crystallographic data for 1-B(Ar^F)$_4$

$C_{28}H_{29}N_3OPPd^{1+}$ $C_{32}H_{12}BF_{24}^{1-}$ × 1.5(CH_2Cl_2), light yellow prism (0.302 × 0.191 × 0.158 mm^3), formula weight 1551.52; triclinic, $P\bar{1}$ (No. 2), a = 13.38647(13) Å, b = 14.66903(16) Å, c = 18.73570(19) Å, α = 108.0714(9)°, β = 94.0455(8)°, γ = 112.8323(10)°, V = 3146.06(6)Å^3, Z = 2, Z' = 1, T = 93(2) K, d_{calc} = 1.638 g cm^{-3}, μ(Mo-*K*α) = 0.564 mm^{-1}, F(000) = 1550; $T_{max/min}$ = 1.000/0.316; 254932 reflections were collected (2.258° ≤ θ ≤ 31.000°, index ranges: –19 ≤ h ≤ 19, –21 ≤ k ≤ 21, –27 ≤ l ≤ 27), 20078 of which were unique, R_{int} = 0.0599, $R_σ$ = 0.0229; completeness to $θ_{max}$ 99.9 %. The refinement of 967 parameters with 245 restraints converged to R_1 = 0.0474 and wR_2 = 0.1069 for 16247 reflections with $I > 2σ(I)$ and R_1 = 0.0688 and wR_2 = 0.1274 for all data with S = 1.124 and residual electron density, $ρ_{max/min}$ = 1.530 and –0.727 e Å^{-3}. The crystals were grown by layering in a DCM/hexane system at r.t.

Crystallographic data for 1-OAc.

$C_{28}H_{28}N_3OPPd$ × $C_2H_4O_2$ × CH_2Cl_2, yellow prism (0.171 × 0.052 × 0.026 mm^3), formula weight 704.88; monoclinic, *Pc* (No. 7), a = 7.78647(4)Å, b = 13.20388(5) Å, c = 15.31398(7) Å, β = 104.0699(5)°, V = 1527.222(12) Å^3, Z = 2, Z' = 1, T = 94(2) K, d_{calc} = 1.533 g cm^{-3}, μ(Cu-*K*α) = 7.307 mm^{-1}, F(000) = 720; $T_{max/min}$ = 1.000/0.420; 34807 reflections were collected (4.480° ≤ θ ≤ 79.825°, index ranges: –9 ≤ h ≤ 9, –

$16 \le k \le 16$, $-19 \le l \le 18$), 5974 of which were unique, R_{int} = 0.0422, R_σ = 0.0335; completeness to θ_{max} 89.9 % for the point group 2 and 97.9 % for the Laue group *m*. The refinement of 407 parameters with 89 restraints converged to R_1 = 0.0320 and wR_2 = 0.0876 for 5919 reflections with $I > 2\sigma(I)$ and R_1 = 0.0323 and wR_2 = 0.0878 for all data with S = 1.144 and residual electron density, $\rho_{max/min}$ = 1.324 and –0.828 e Å^{-3}. Flack parameter x = –0.019(4) determined using 2624 selected quotients by Parsons' method. The crystals were grown by vapor diffusion in a DCM/pentane system at –30°C.

Crystallographic data for 2.

$C_{56}H_{56}Cu_2N_6O_2P_2Pd_2^{2+}$ $2(C_{32}H_{12}BF_{24}^{1-})$, yellow plank (0.221 × 0.176 × 0.062 mm^3), formula weight 2973.34; monoclinic, $P2_1/n$ (No. 14), a = 10.34121(11) Å, b = 20.0511(2) Å, c = 28.2805(3) Å, β = 91.8270(9)°, V = 5861.05(10) Å^3, Z = 2, Z' = 0.5, T = 94(2) K, d_{calc} = 1.685 g cm^{-3}, μ(Mo-*K*α) = 0.819 mm^{-1}, F(000) = 2960; $T_{max/min}$ = 1.000/0.484; 410107 reflections were collected (2.119° ≤ θ ≤ 31.000°, index ranges: $-14 \le h \le 14$, $-29 \le k \le 29$, $-40 \le l \le 40$), 18640 of which were unique, R_{int} = 0.0568, R_σ = 0.0178; completeness to θ_{max} 99.9 %. The refinement of 889 parameters with 156 restraints converged to R_1 = 0.0306 and wR_2 = 0.0805 for 16870 reflections with $I > 2\sigma(I)$ and R_1 = 0.0350 and wR_2 = 0.0826 for all data with S = 1.036 and residual electron density, $\rho_{max/min}$ = 1.026 and –0.386 e Å^{-3}. The crystals were grown by layering in a DCM/pentane system at –30°C.

Crystallographic data for 2 (solvate).

$C_{56}H_{56}Cu_2N_6O_2P_2Pd_2^{2+}$ $2(C_{32}H_{12}BF_{24}^{1-}) \times 0.75(C_6H_{14}) \times 2.5(CH_2Cl_2)$, yellow plank (0.262 × 0.054 × 0.046 mm^3), formula weight 3250.28; triclinic, $P\bar{1}$ (No. 2), a = 10.15573(12) Å, b = 17.53056(19) Å, c = 19.68740(20) Å, α = 68.2328(10)°, β = 84.5431(9)°, γ = 84.2304(9)°, V = 3232.30(7) Å^3, Z = 1, Z' = 0.5, T = 93(2) K, d_{calc} = 1.670 g cm^{-3}, μ(Mo-*K*α) = 0.850 mm^{-1}, F(000) = 1622; $T_{max/min}$ = 1.000/0.546; 122755 reflections were collected (2.245° ≤ θ ≤ 31.499°, index ranges: $-14 \le h \le 14$, $-25 \le k \le 25$, $-28 \le l \le 28$), 20916 of which were unique, R_{int} = 0.0647, R_σ = 0.0428; completeness to θ_{max} 97.3 %. The refinement of 1023 parameters with 367 restraints converged to R_1 = 0.0375 and wR_2 = 0.0944 for 17625 reflections with $I > 2\sigma(I)$ and R_1 = 0.0484 and wR_2 = 0.0993 for all data with S = 1.020 and residual electron density, $\rho_{max/min}$ = 1.081 and –0.828 e Å^{-3}. The crystals were grown by layering in a DCM/hexane system at –30°C.

Crystallographic data for 3.

$C_{28}H_{28}ClCuN_3OPPd \times 2.5(CH_2Cl_2)$, yellow prism (0.593 × 0.301 × 0.197 mm^3), formula weight 871.21; monoclinic, $P2_1/c$ (No. 14), a = 20.5675(4) Å, b = 16.21405(19) Å, c = 21.6642(4) Å, β = 108.286(2)°, V = 6859.8(2) Å^3, Z = 8, Z' = 2, T = 95(2) K, d_{calc} = 1.687 g cm^{-3}, μ(Cu-*K*α) = 9.980 mm^{-1}, F(000) = 3496; $T_{max/min}$ = 1.000/0.021; 68466 reflections were collected (3.471° ≤ θ ≤ 68.248°, index ranges: $-24 \le h \le 22$, $-19 \le k \le 19$, $-26 \le l \le 26$), 12362 of which were unique, R_{int} = 0.0895, R_σ = 0.0463; completeness to θ_{max} 98.4 %. The refinement of 820 parameters with 90 restraints converged to R_1 = 0.0810 and wR_2 = 0.2324 for 11291 reflections with $I > 2\sigma(I)$ and R_1 = 0.0857 and wR_2 = 0.2378 for all data with S = 1.070 and residual electron density, $\rho_{max/min}$ = 3.828 and –1.613 e Å^{-3}. The crystals were grown by vapor diffusion in a DCM/hexane system at –30°C.

Crystallographic data for 4.

The unit cell contains highly disordered solvent molecules of toluene and cyclohexane, which were treated as a diffuse contribution to the overall scattering without specific atom positions by *PLATON*/SQUEEZE-130220. Squeezed solvent info is not included in the formulae and related items such as molecular weights and calculated densities. $C_{86}H_{78}N_8O_6P_2Pd_4 \times 1.1(C_7H_8)$, yellow plate (0.055 × 0.032 × 0.009 mm^3), formula weight 1908.45; monoclinic, $P2_1/n$ (No. 14), a = 18.3023(3) Å, b = 24.7637(3) Å, c = 21.0668(4) Å, β = 99.1506(17)°, V = 9426.6(3) Å^3, Z = 4, Z' = 1, T = 95(2) K, d_{calc} = 1.345 g cm^{-3}, μ(Cu-*K*α) = 6.800 mm^{-1}, F(000) = 3868; $T_{max/min}$ = 1.000/0.816; 79378 reflections were collected (2.774° ≤ θ ≤ 68.446°, index ranges: $-20 \le h \le 22$, $-29 \le k \le 29$, $-25 \le l \le 21$), 17050 of which were unique, R_{int} = 0.0848, R_σ = 0.0647; completeness to θ_{max} 98.5 %. The refinement of 1220 parameters with 1159 restraints converged to R_1 = 0.0646 and wR_2 = 0.1714 for 11707 reflections with $I > 2\sigma(I)$ and R_1 = 0.0935 and wR_2 = 0.1932 for all data with S = 0.987 and residual electron density, $\rho_{max/min}$ = 1.897 and –1.891 e Å^{-3}. The crystals were grown vapor diffusion of a toluene/cyclohexane solution at r.t.

Crystallographic data for 5.

$C_{82}H_{72}N_8O_2P_2Pd_4^{2+}$ $2(C_{24}H_{20}B^{1-})$ × $2(C_6H_{12})$ × $5(C_4H_8O)$, yellow prism (0.197 × 0.139 × 0.068 mm^3), formula weight 2856.26; triclinic, $P\bar{1}$ (No. 2), a = 14.63077(10) Å, b = 18.4543(2) Å, c = 27.6768(2) Å, α = 72.6084(8)°, β = 86.4096(6)°, γ = 71.5611(8)°, V = 6760.85(11) Å^3, Z = 2, Z' = 1, T = 95(2) K, d_{calc} = 1.403 g cm^{-3}, μ(Cu-Kα) = 4.935 mm^{-1}, F(000) = 2968; $T_{max/min}$ = 1.000/0.485; 136477 reflections were collected (2.641° ≤ θ ≤ 79.893°, index ranges: –18 ≤ h ≤ 15, –23 ≤ k ≤ 23, –35 ≤ l ≤ 32), 28766 of which were unique, R_{int} = 0.0393, $R_σ$ = 0.0300; completeness to $θ_{max}$ 97.6 %. The refinement of 1812 parameters with 992 restraints converged to R_1 = 0.0497 and wR_2 = 0.1367 for 27281 reflections with $I > 2σ(I)$ and R_1 = 0.0512 and wR_2 = 0.1380 for all data with S = 1.037 and residual electron density, $ρ_{max/min}$ = 1.652 and –1.420 e Å^{-3}. The crystals were grown by slow evaporation of a THF/cyclohexane solution at r.t.

Crystallographic data for 6.

$C_{82}H_{70}N_8O_2P_2Pd_4$ × $2(C_4H_{10}O)$, red plate (0.063 × 0.037 × 0.017 mm^3), formula weight 1835.23; orthorhombic, *Pnna* (No. 52), a = 23.1971(3) Å, b = 31.5985(5) Å, c = 10.45124(16) Å, V = 7660.69(19) Å^3, Z = 4, Z' = 0.5, T = 93(2) K, d_{calc} = 1.591 g cm^{-3}, μ(Cu-Kα) = 8.318 mm^{-1}, F(000) = 3728; $T_{max/min}$ = 0.992/0.774; 95777 reflections were collected (2.797° ≤ θ ≤ 72.116°, index ranges: –28 ≤ h ≤ 28, –38 ≤ k ≤ 39, –12 ≤ l ≤ 12), 7540 of which were unique, R_{int} = 0.0804, $R_σ$ = 0.0364; completeness to $θ_{max}$ 99.8 %. The refinement of 493 parameters with no restraints converged to R_1 = 0.0560 and wR_2 = 0.1500 for 6369 reflections with $I > 2σ(I)$ and R_1 = 0.0655 and wR_2 = 0.1564 for all data with S = 1.111 and residual electron density, $ρ_{max/min}$ = 2.346 and –1.158 e Å^{-3}. The crystals were grown by slow evaporation of a diethyl ether solution at –30°C.

Detailed information about crystal structure determination can be accessed via supplementary cif files. The crystallographic data for the investigated compounds have been deposited in the Cambridge Crystallographic Data Centre as supplementary publication numbers CCDC 2082472 (**1**-B(Ar^F)$_4$), 2082473 (**1**-OAc), 2082474 (**2**), 2082475 (**2** (solvate)), 2082476 (**3**), 2082477 (**4**), 2082478 (**5**), and 2082479 (**6**). These data can be obtained free of charge via https://www.ccdc.cam.ac.uk/structures/.

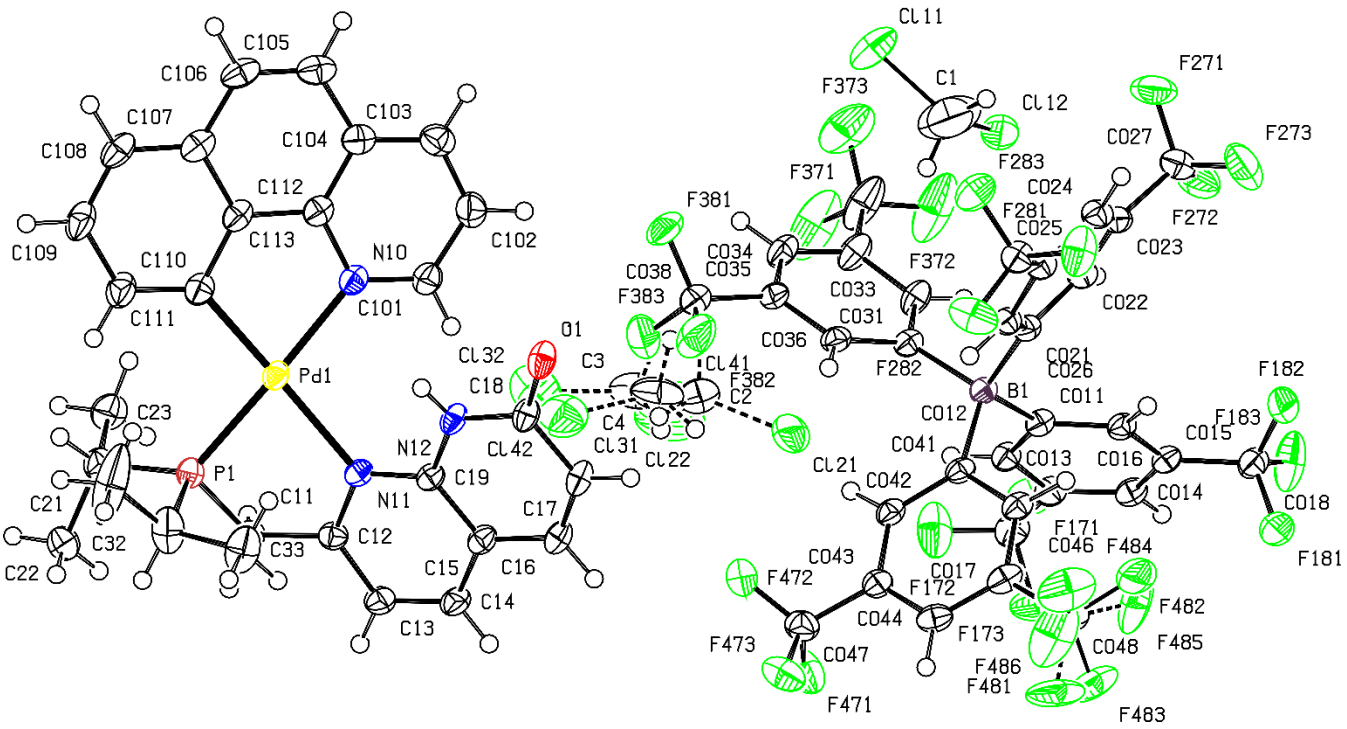

Figure S82. ORTEP at 50 % probability anisotropic displacement ellipsoids of non-hydrogen atoms for compound **1**-B(Ar^{F})$_4$ according to SC-XRD. Selected interatomic distances [Å]: Pd1–P1 2.2317(6), Pd1–N11 2.1959(19), Pd1–N10 2.122(2), Pd1–C111 2.002(2), N12–H12 0.82(4). The minor disorder component is shown by dashed lines.

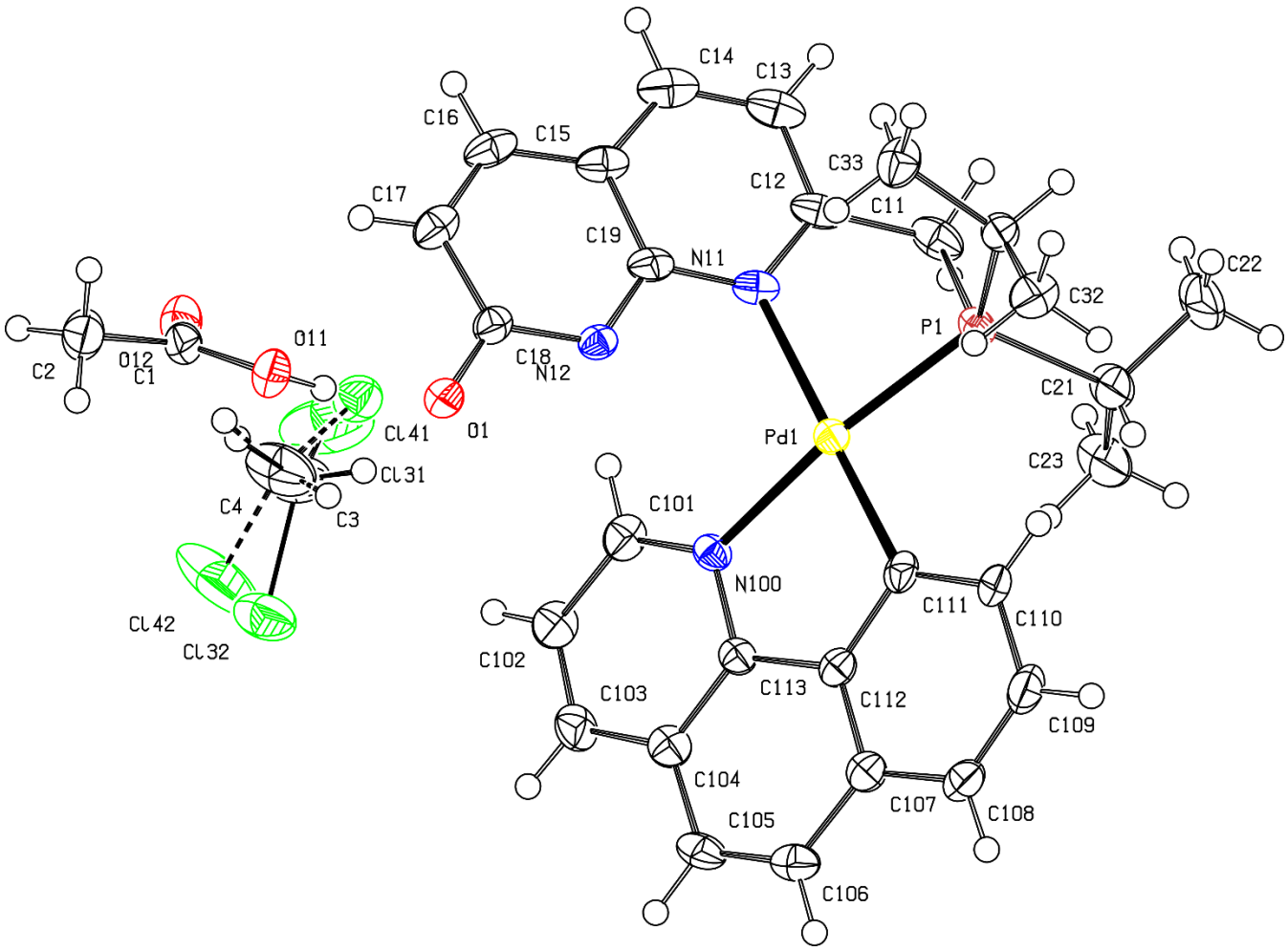

Figure S83. ORTEP at 50 % probability anisotropic displacement ellipsoids of non-hydrogen atoms for compound **1**-OAc according to SC-XRD data. Selected interatomic distances [Å] and degrees [°]: Pd1–P1 2.2314(13), Pd1–N11 2.136(4), Pd1–N100 2.127(4), Pd1–C111 2.003(5), O11–H11 0.85(15), O1···H11 1.64(15), O1···O11 2.467(5), O11–H11···O1 164(15). The minor disorder component is shown by dashed lines.

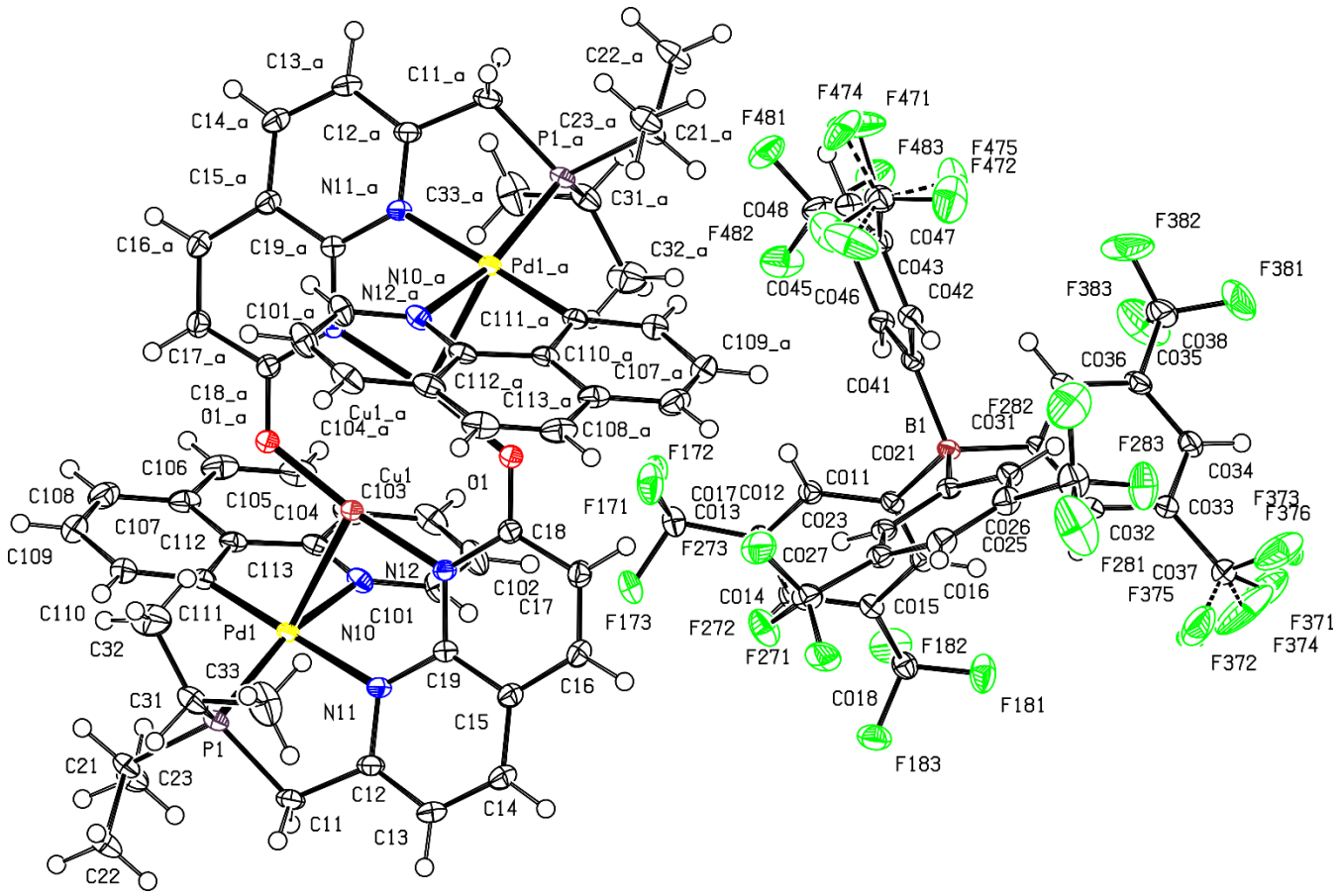

Figure S84. ORTEP at 50 % probability anisotropic displacement ellipsoids of non-hydrogen atoms for compound **2** according to SC-XRD data. Selected interatomic distances [Å]: Pd1–Cu1 2.71892(19), Cu1–Cu1^{a} 2.5239(3), Pd1–P1 2.2423(4), Pd1–N11 2.1538(12), Pd1–N10 2.1251(12), Pd1–C111 1.9999(14), Cu1–O1^{a} 1.8544(10), Cu1–N12 1.8967(11). Symmetry operation code is (1–*x*, 1–*y*, 1–*z*). The minor disorder component is shown by dashed lines.

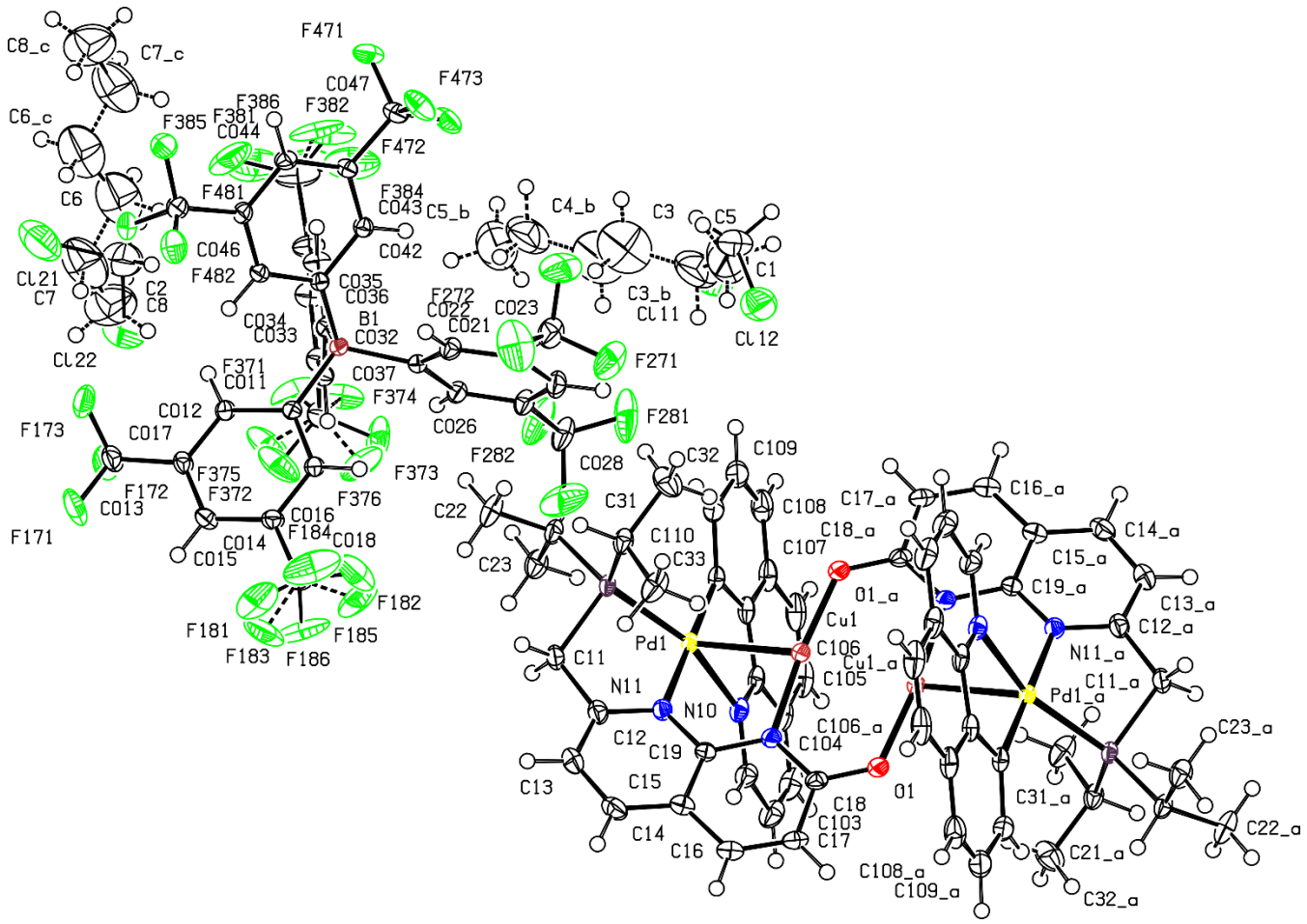

Figure S85. ORTEP at 50 % probability anisotropic displacement ellipsoids of non-hydrogen atoms for compound **2** (solvate) according to SC-XRD data. Selected interatomic distances [Å]: Pd1–Cu1 2.7171(2), Cu1–Cu1^{a} 2.5331(4), Pd1–P1 2.2350(4), Pd1–N11 2.1432(15), Pd1–N10 2.1271(14), Pd1–C111 1.9969(18), Cu1–O1^{a} 1.8537(13), Cu1–N12 1.8945(14). Symmetry operation code is (1–*x*, –*y*, 2–*z*). The minor disorder component is shown by dashed lines.

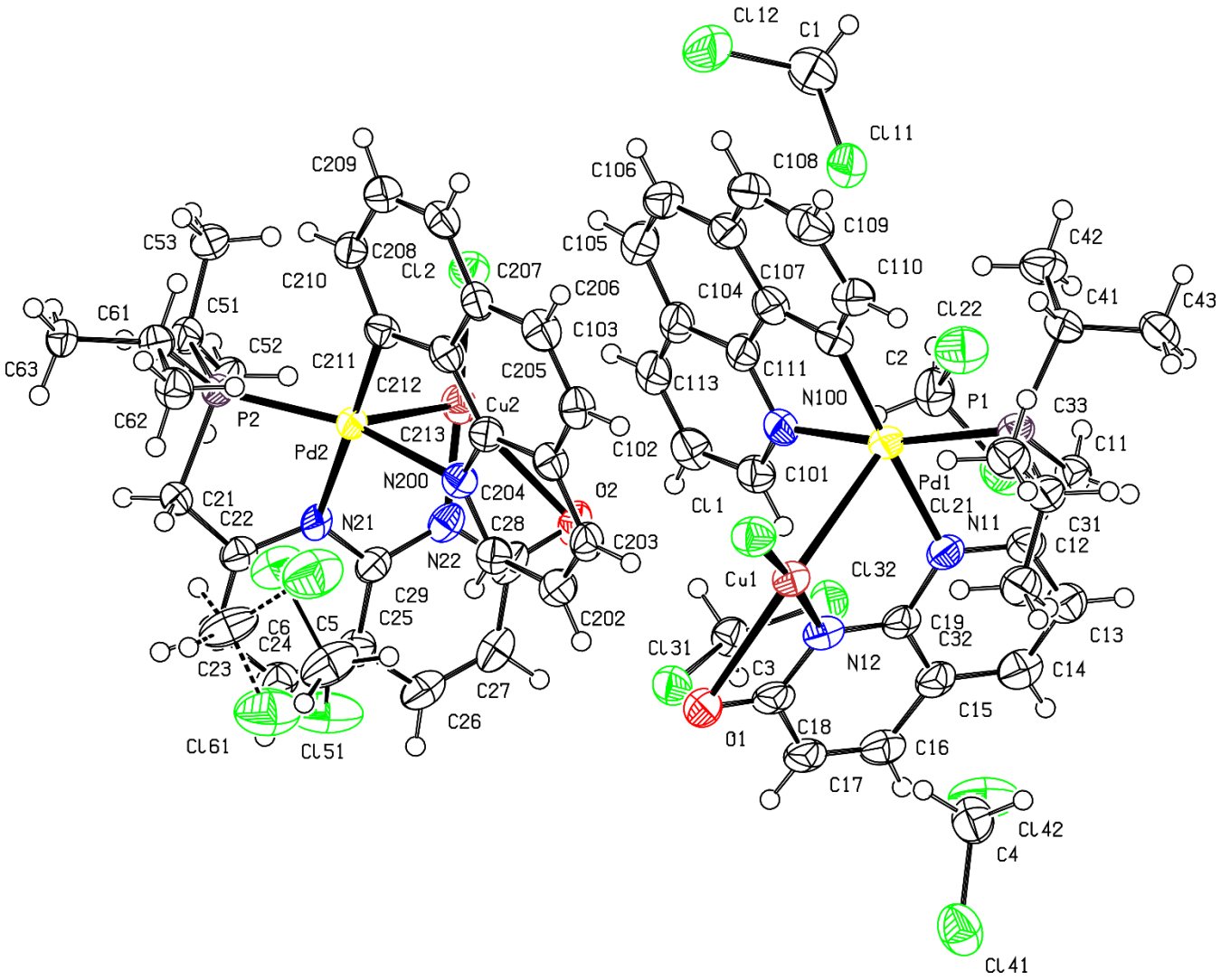

Figure S86. ORTEP at 50 % probability anisotropic displacement ellipsoids of non-hydrogen atoms for compound **3** according to SC-XRD data. Selected interatomic distances [Å]: Pd1–Cu1 2.8182(13), Pd1–P1 2.230(2), Pd1–N11 2.156(6), Pd1–N100 2.152(7), Pd1–C111 2.015(9), Cu1–Cl1 2.125(2), Cu1–N12 1.904(7), Pd2–Cu2 2.7809(12), Pd2–P2 2.2276(18), Pd2–N21 2.143(6), Pd2–N200 2.146(6), Pd2–C211 2.012(7), Cu2–Cl2 2.136(2), Cu2–N22 1.904(7). The minor disorder component is shown by dashed lines.

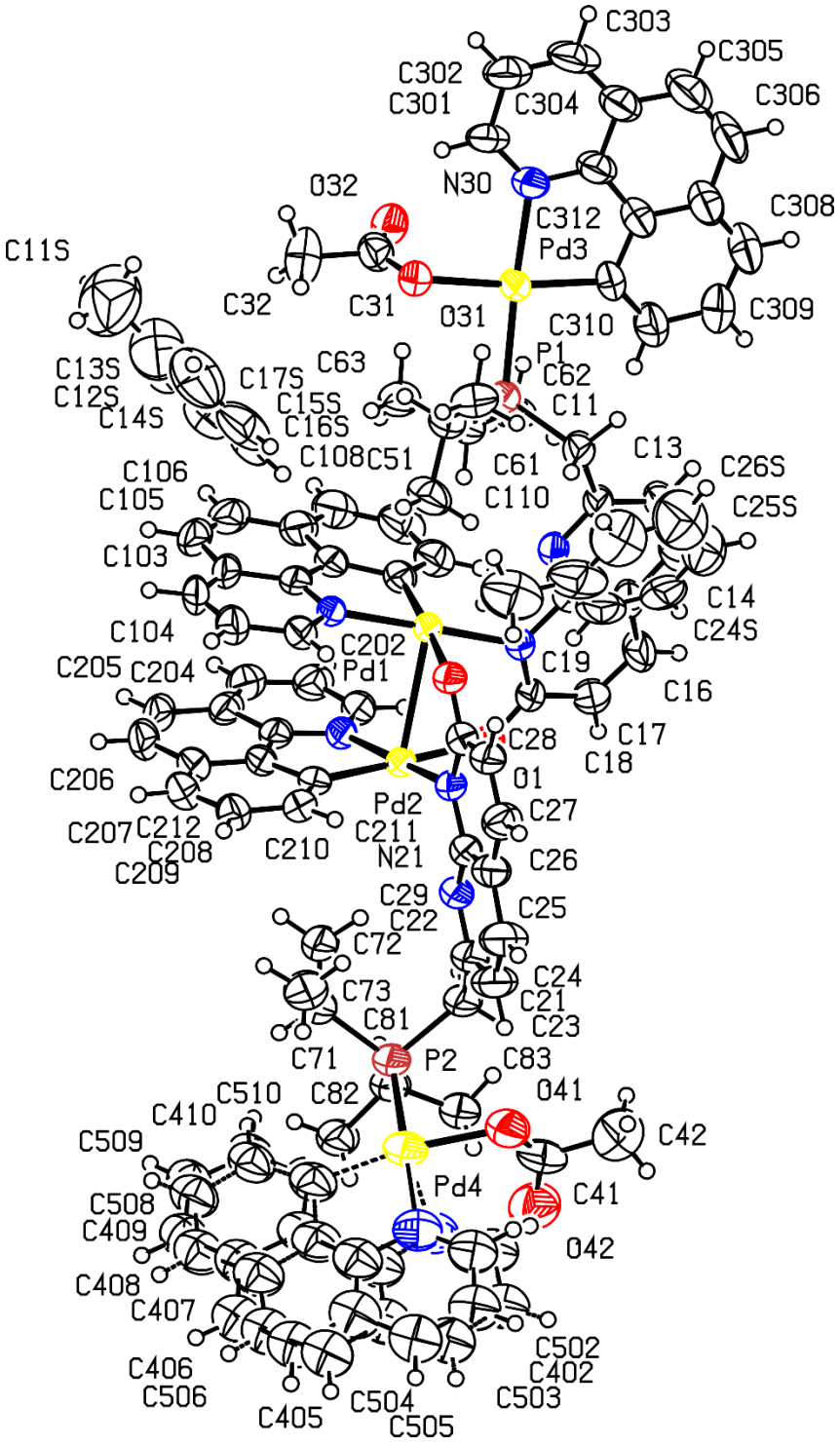

Figure S87. ORTEP at 50 % probability anisotropic displacement ellipsoids of non-hydrogen atoms for compound **4** according to SC-XRD data. Selected interatomic distances [Å]: Pd1–Pd2 2.8433(6), Pd1–N12 2.050(5), Pd1–O2 2.140(4), Pd1–N10 2.050(5), Pd1–C111 1.983(7), Pd2–N22 2.050(5), Pd2–O1 2.144(4), Pd2–N20 2.042(5), Pd2–C211 1.983(7), Pd3–P1 2.2638(17), Pd3–O31 2.115(4), Pd3–N30 2.117(5), Pd3–C311 2.015(6), Pd4–P2 2.284(2), Pd4–O41 2.105(6), Pd4–N40 2.124(7), Pd4–N50 2.121(9), Pd4–C411 2.039(8), Pd4–C511 2.025(9). The minor disorder component is shown by dashed lines.

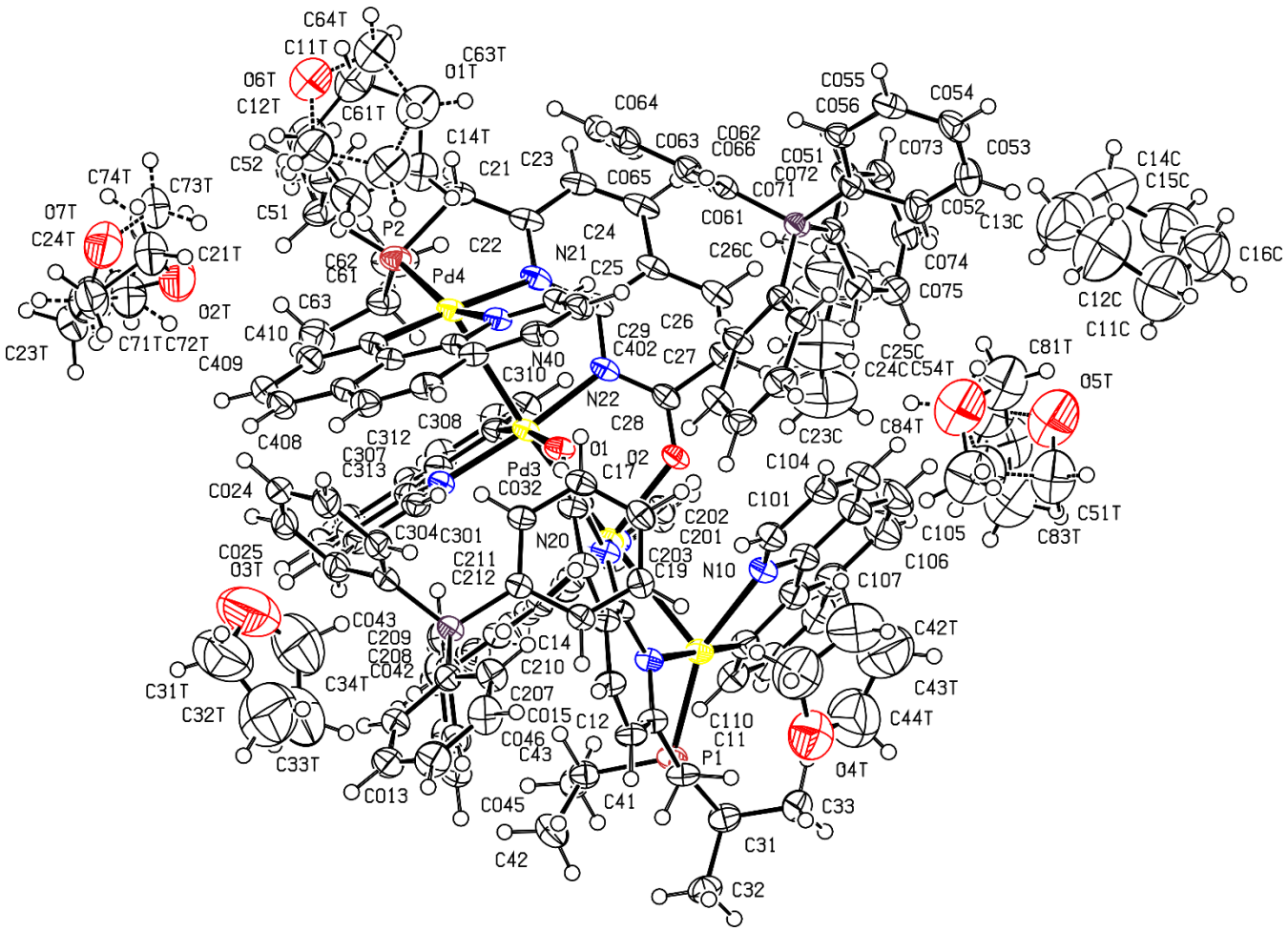

Figure S88. ORTEP at 50 % probability anisotropic displacement ellipsoids of non-hydrogen atoms for compound **5** according to SC-XRD data. Selected interatomic distances [Å]: Pd1–Pd2 2.8939(3), Pd2–Pd3 2.8187(3), Pd3–Pd4 2.8956(3), Pd1–P1 2.2287(9), Pd1–N11 2.181(3), Pd1–N10 2.144(3), Pd1–C111 1.998(3), Pd2–N12 2.055(3), Pd2–O2 2.145(2), Pd2–N20 2.045(3), Pd2–C211 1.975(3), Pd3–N22 2.056(3), Pd3–O1 2.141(2), Pd3–N30 2.048(3), Pd3–C311 1.985(3), Pd4–P2 2.2348(9), Pd4–N21 2.183(3), Pd4–N40 2.143(3), Pd4–C411 2.003(3). The minor disorder component is shown by dashed lines.

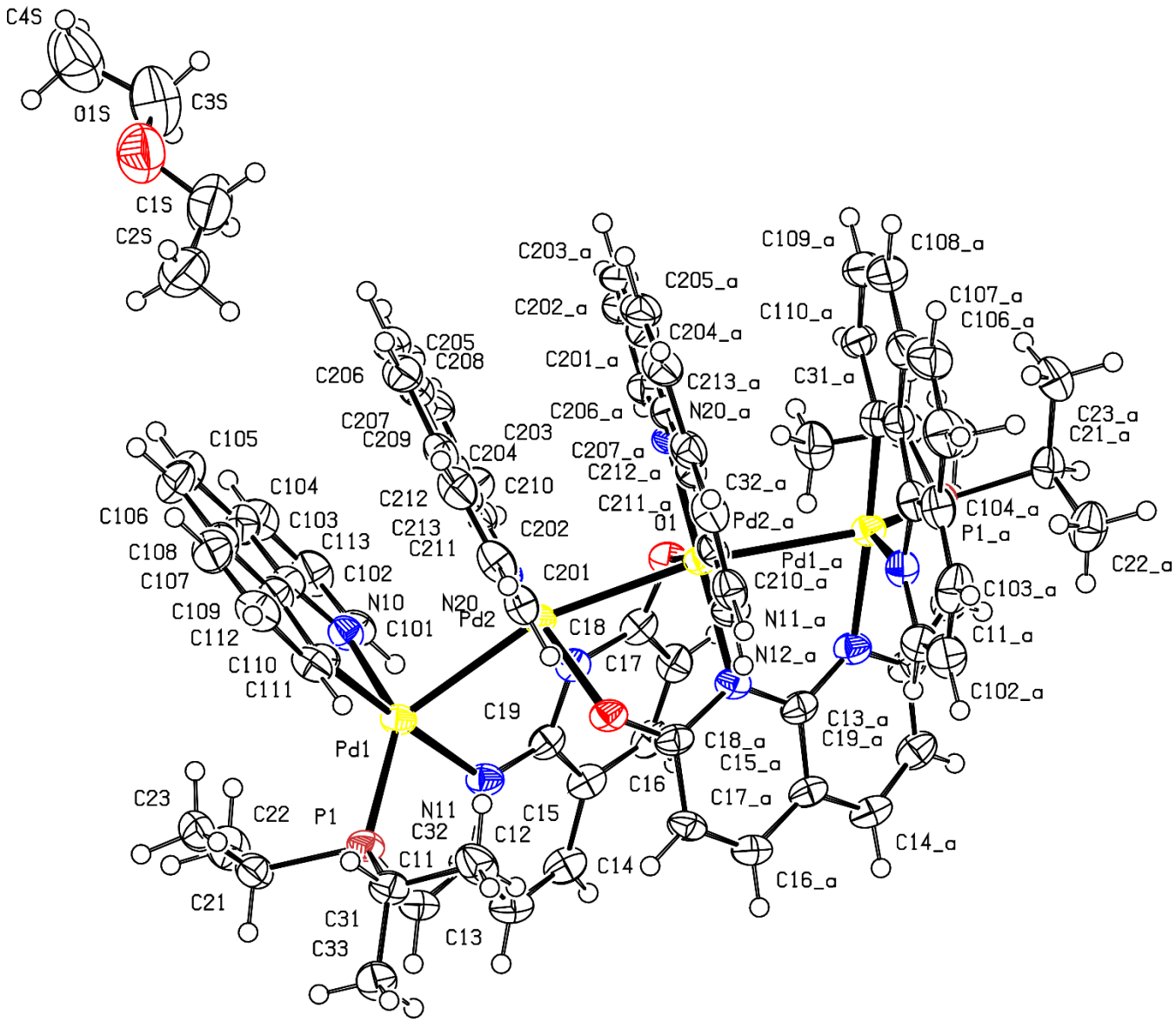

Figure S89. ORTEP at 50 % probability anisotropic displacement ellipsoids of non-hydrogen atoms for compound **6** according to SC-XRD data. Selected interatomic distances [Å]: Pd1–Pd2 2.8045(6), Pd2–Pd2^{a} 2.7754(8), Pd1–P1 2.2173(15), Pd1–N10 2.198(5), Pd1–N11 2.107(5), Pd1–C211 1.983(6), Pd2–N20 2.032(5), Pd2–O1^{a} 2.147(4), Pd2–N12 2.064(5), Pd2–C311 1.993(6), C11–C12 1.393(9). Symmetry operation code is (x, ½–y, ½–z).

III. Computational Section

All calculations were performed using density functional theory (DFT) as implemented in the Gaussian 16 suite of programs.[17] Ground-state optimizations were performed using the ωb97xd functional.[18] The metal centres (Cu, Pd) were described by the SDD basis sets[19] while the remaining atoms were described by the 6-31++G(d,p)[20-23] basis set.[24] Frequency analyses were carried out at the same level to ensure absence of imaginary frequencies. Natural Bond Orbital calculations were performed using the NBO 6.0 program [25] and the NBO orbitals were visualized using ChemCraft.[26]

NBO Analysis for complex 2:

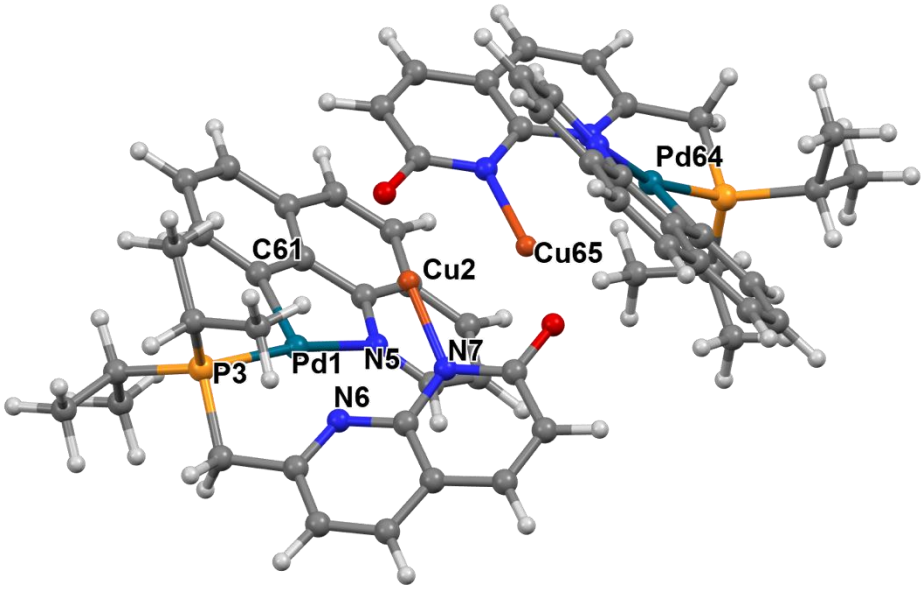

Complex **2** exhibits interactions between Cu-Pd, Cu-Cu and Pd-Cu pairs. The Cu-Pd interactions correspond to two sets of moderate donations: (1) donation of electron density ($E^{(2)}$ = 14.29 kcal/mol) from the σ(Pd-C^{Aryl}) orbital to an empty Cu-centered *s*-type orbital, and (2) donation of electron density ($E^{(2)}$ = 8.41 kcal/mol) from the σ(Pd-P) orbital into an empty Cu-centered *s*-type orbital. A donation of electrons ($E^{(2)}$ = 7.89 kcal/mol) from a Cu-centered *d*-orbital into the σ*(Pd-P) orbital was also found. Two direct Pd(*d*)-Cu(*s*) interactions ($E^{(2)}$ = 6.06, 2.63 kcal/mol) were also found. The Cu(*d*) orbital was found to back-donate ($E^{(2)}$ = 4.49 kcal/mol) into the σ*(Pd-C^{Aryl}) orbital. Similar interactions also exist at the other terminus. Interestingly, the proximal Cu-Cu pairs also demonstrate moderate ($E^{(2)}$ = 12.30, 12.12 kcal/mol) donation of electrons from Cu-centered *d*-orbitals to Cu-centered *s*-type orbitals.

Table S4. Key interactions in complex **2**.

Donor			Acceptor			$E^{(2)}$
#	Orbital	Orbitals (NAO%)	#	Orbital	Orbitals (NAO%)	kcal mol^{-1}
122	BD(1)Pd1-C61	**Pd:** s(40.03%) p(0.21%) d (59.76%) **C:** s(25.61%) p (74.38%) d (0.01%)	277	LV(1)Cu2	s(90.63%) p(0.17%) d(9.20%)	14.29
121	BD(1)Pd1- P3	**Pd:** s(56.73%) p (0.45%) d (42.82%) **P:** s(30.16%) p(69.63%) d (0.20%)	277	LV(1)Cu2	s(90.63%) p (0.17%) d(9.20%)	8.41
99	LP(5)Cu2	s(8.12%) p(0.02%) d(91.86%)	279	BD*(1)Pd1-P3	**Pd:** s(56.73%) p(0.45%) d(42.82%) **P:** s(30.16%) p(69.63%) d(0.20%)	7.89
91	LP(1)Pd1	s(1.75%) p(0.01%) d (98.24%)	277	LV(1)Cu2	s(90.63%) p(0.17%) d(9.20%)	6.06
99	LP(5)Cu2	s(8.12%) p(0.02%) d(91.86%)	280	BD*(1)Pd1-C61	**Pd:** s(40.03%) p(0.21%) d(59.76%) **C:** s(25.61%) p(74.38%) d(0.01%)	4.49
93	LP(3)Pd1	s(0.61%) p(0.01%) d(99.38%)	277	LV(1)Cu2	s(90.63%) p(0.17%) d(9.20%)	2.63
114	LP(5)Cu65	s(8.10%) p(0.01%) d(91.88%)	277	LV(1)Cu2	s(90.63%) p(0.17%) d(9.20%)	12.30
99	LP(5)Cu2	s(8.12%) p(0.02%) d(91.86%)	278	LV(1)Cu65	s(90.69%) p(0.09%) d(9.23%)	12.12

Selected NBO orbitals for complex **2**:

91 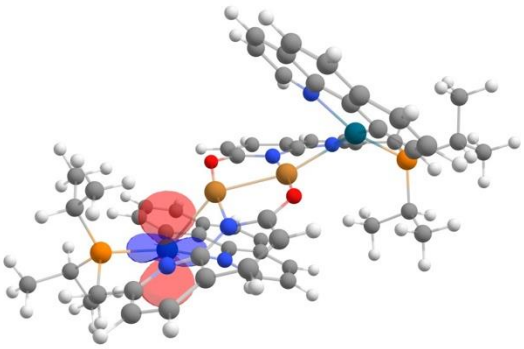

122 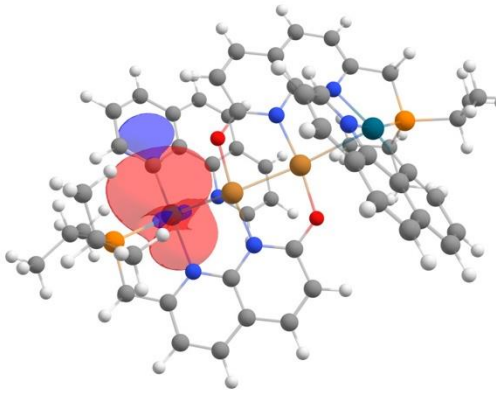

93

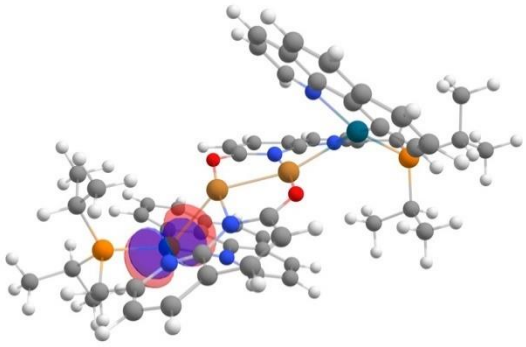

277

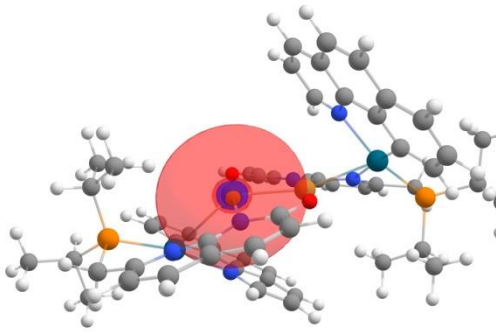

99

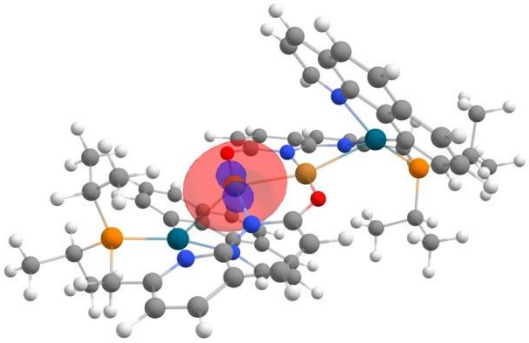

278

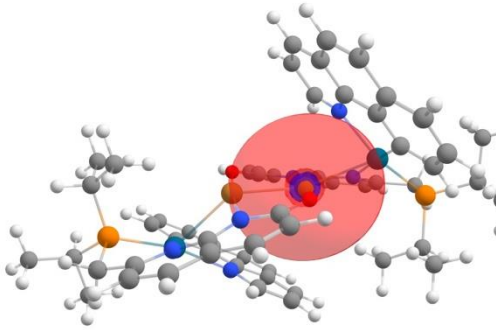

114

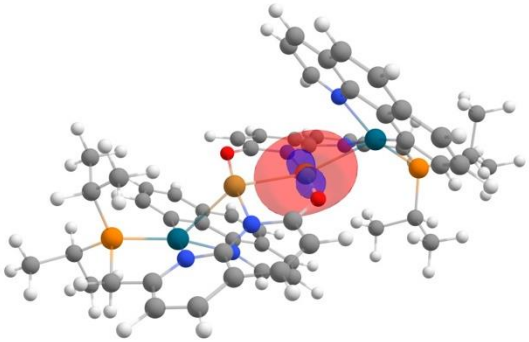

279

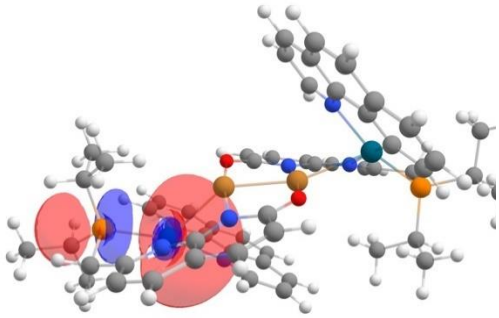

121

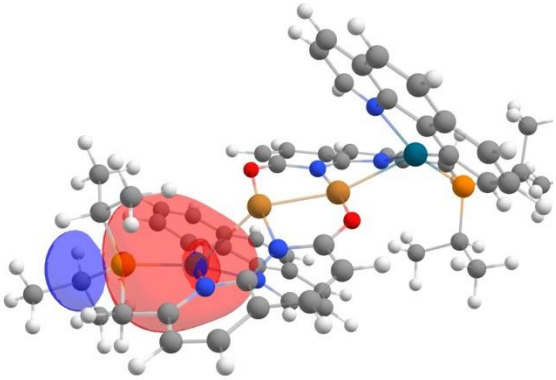

280

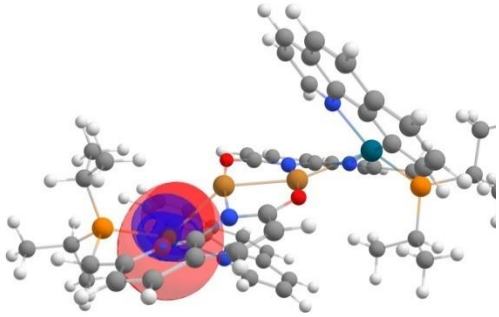

NBO Analysis for complex 3:

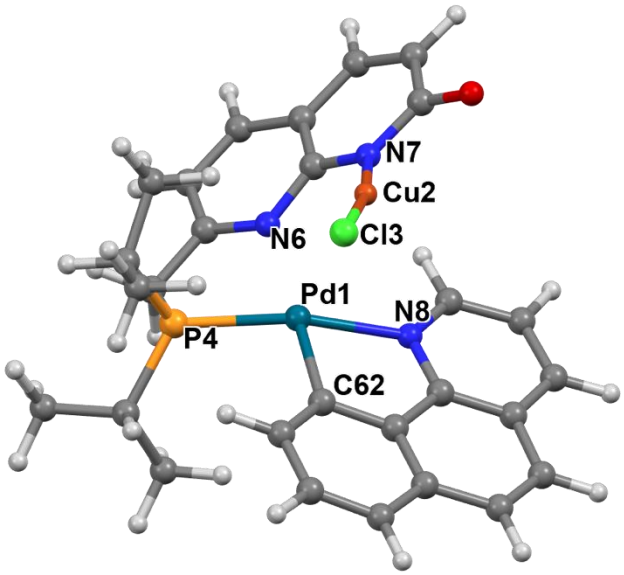

Complex **3** exhibits a moderate donation ($E^{(2)}$ = 6.37 kcal/mol) of electrons of the Cu(d_{xy}) lone-pair orbital to the σ*(Pd-P) orbital. This σ*(Pd-P) orbital is comprised of 75% Pd(*sd*-hybrid) and 25% P(sp^2-hybrid) orbitals. A weaker ($E^{(2)}$ = 3.16 kcal/mol) back-donation from the σ(Pd-P) into the Cu(*s* orbital) was also found. Consistent with these interactions, the Pd-P bond length is slightly elongated (r_{Pd-P} = 2.261 Å) Additionally, a modest ($E^{(2)}$ = 6.07 kcal/mol) donation from the σ(Pd-C^{Aryl}) orbital into the Cu(*s*) orbital was also found, with a corresponding weak ($E^{(2)}$ = 3.12 kcal/mol) back-donation from the Cu(d_{xy}) lone-pair into the σ*(Pd-C^{Aryl}) orbital. The σ(Pd-C^{Aryl}) is comprised of 39% Pd(*sd*-hybrid) and 57% C(sp^2-hybrid). Two much weaker donations ($E^{(2)}$ = 2.52 and 1.96 kcal/mol) from Pd *d*-orbitals to Cu(*s*-orbital) were also found.

Table S5. Key interactions in complex **3**.

Donor			Acceptor			$E^{(2)}$
#	Orbital	Orbitals (NAO%)	#	Orbital	Orbitals (NAO%)	kcal mol^{-1}
59	LP(5)Cu2	s(6.92%) p (0.03%) d(93.05%)	149	BD*(1)Pd1- P4	**Pd:** s(57.90%) p(0.50%) d(41.60%) **P:** s(31.93%) p(67.91%) d(0.17%)	6.37
71	BD(1)Pd1-C62	**Pd:** s(39.22%) p(0.23%) d(60.55%) **C:** s(25.93%) p(74.05%) d(0.01%)	148	LV(1)Cu2	s(91.74%) p(0.30%) d(7.95%)	6.07
70	BD(1)Pd1-P4	**Pd:** s(57.90%) p(0.50%) d(41.60%) **P:** s(31.93%) p(67.91%) d(0.17%)	148	LV (1)Cu2	s(91.74%) p(0.30%) d(7.95%)	3.16
59	LP(5)Cu2	s(6.92%) p(0.03%) d(93.05%)	150	BD*(1)Pd 1-C62	**Pd:** s(39.22%) p(0.23%) d(60.55%) **C:** s(25.93%) p(74.05%) d(0.01%)	3.12

51	LP(1)Pd1	s(1.39%) p(0.01%) d(98.59%)	148	LV (1)Cu2	s(91.74%) p(0.30%) d(7.95%)	2.52
53	LP(3)Pd1	s(0.60%) p(0.00%) d(99.40%)	148	LV (1)Cu2	s(91.74%) p(0.30%) d(7.95%)	1.96

Selected NBO orbitals for complex **3**:

51

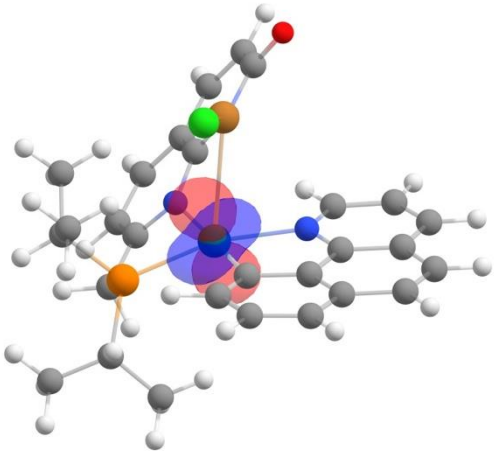

71

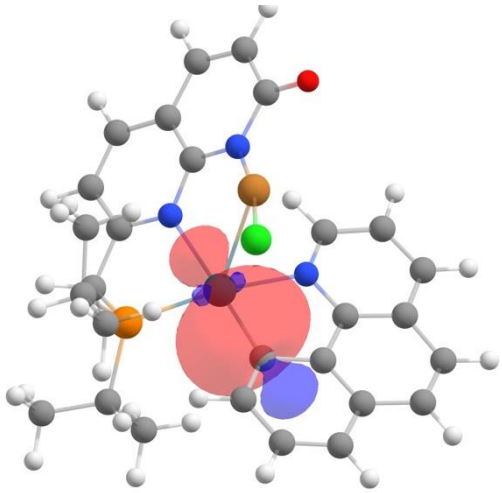

53

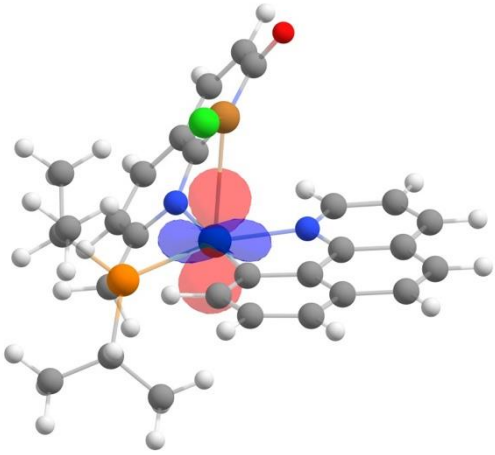

148

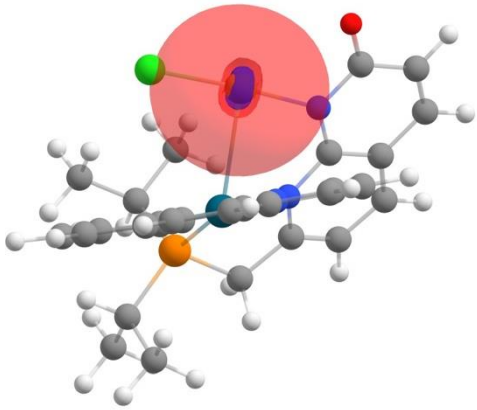

59

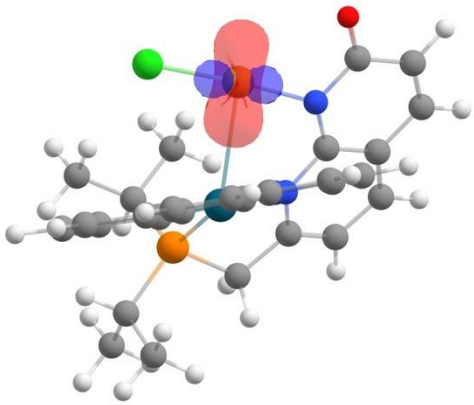

149

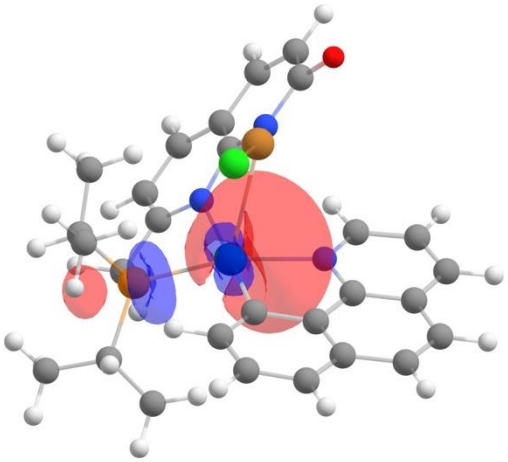

70

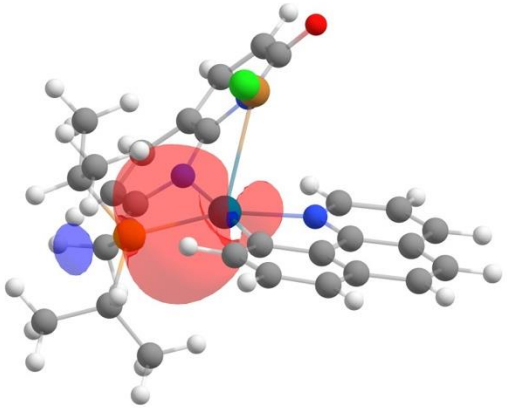

150

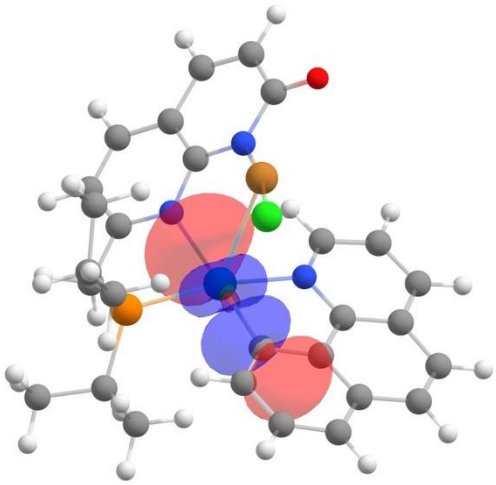

Comparison of diagnostic bond lengths (Å) in structures of complexes 2 and 3 calculated by DFT and obtained from X-ray diffraction:

Complex **2**:

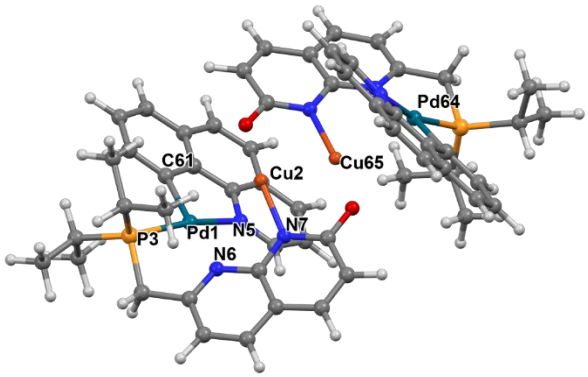

	Calculated Structure	X-ray Structure
Pd1-Cu2	2.757	2.719
Cu2-Cu65	2.518	2.524
Cu2-O67	1.879	1.855
Cu2-N7	1.917	1.897
Pd1-P3	2.274	2.242
Pd1-N6	2.236	2.154
Pd1-N5	2.156	2.125
Pd1-C61	2.004	2.000

Complex **3**:

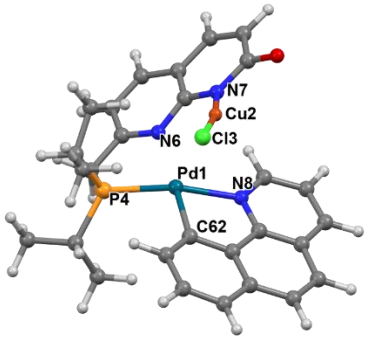

	Calculated Structure	X-ray Structure
Pd1-Cu2	2.832	2.818
Pd1-N8	2.156	2.151
Pd1-P4	2.261	2.231
Pd1-N6	2.207	2.157
Cu2-Cl3	2.124	2.124
Cu2-N7	1.923	1.904

Cartesian coordinates

Complex **2**:

Pd	-3.77231000	0.14051300	-0.55174800
Cu	-1.34550700	-0.64137900	0.49950400
P	-5.73581300	-0.71312000	0.21466100
O	1.02357700	-1.84714400	-0.79766300
N	-2.18500100	1.07974100	-1.66985100
N	-3.55798900	-1.99750500	-1.17087700
N	-1.25815600	-2.00602600	-0.84526600
C	-5.98927600	-1.98993300	-1.10197500
H	-6.71719900	-2.74628700	-0.79147400
H	-6.41452600	-1.47475300	-1.97155500
C	-4.68868800	-2.64770000	-1.48179600
C	-4.68257800	-3.89869500	-2.10949000
H	-5.61997300	-4.38629100	-2.35017900
C	-3.47153700	-4.47883400	-2.42813200
H	-3.43440700	-5.43149000	-2.94845900
C	-2.27939700	-3.84963300	-2.04832400
C	-0.97348200	-4.38438000	-2.30066200
H	-0.88304700	-5.32606800	-2.83409800
C	0.12420200	-3.70927100	-1.88928900
H	1.13311500	-4.06012900	-2.07030800
C	-0.02108600	-2.47414800	-1.15263900
C	-2.36417600	-2.62060200	-1.35720300
C	-7.28856500	0.29348800	0.16661400
H	-7.24208900	0.93247700	1.05491100
C	-8.55332100	-0.57040100	0.26630700
H	-8.67835200	-1.20694000	-0.61541400
H	-9.42915900	0.08239400	0.31876500
H	-8.56686000	-1.20368900	1.15741700
C	-7.31425200	1.19976200	-1.06988800
H	-6.43819300	1.85082500	-1.11512500
H	-8.20724900	1.83028300	-1.03746500
H	-7.36331100	0.61931200	-1.99760800
C	-5.70650400	-1.61846100	1.82709800
H	-6.67775300	-2.12130300	1.91292800
C	-5.54686100	-0.62829800	2.98751700
H	-4.60198700	-0.08007100	2.90707200
H	-5.53928900	-1.17664000	3.93380700
H	-6.36740200	0.09341500	3.04037200
C	-4.60168300	-2.68085600	1.86245200
H	-4.73331500	-3.45378800	1.10007400
H	-4.61241000	-3.17668000	2.83734500
H	-3.61402400	-2.22646500	1.72581500
C	-1.41177900	0.58061000	-2.62774200
H	-1.57468100	-0.45725500	-2.89185500
C	-0.42086700	1.33656600	-3.26295800
H	0.18192600	0.88043500	-4.03949800
C	-0.23482100	2.65082200	-2.88250500
H	0.52781400	3.26203900	-3.35639100

C	-1.05216300	3.20995800	-1.88543000
C	-0.95751300	4.57267400	-1.43725400
H	-0.20484100	5.21681200	-1.88190800
C	-1.80889700	5.04842200	-0.49284900
H	-1.73860800	6.08285400	-0.16838300
C	-2.82615800	4.21650900	0.09687000
C	-3.70108900	4.68545800	1.09732600
H	-3.63579200	5.71615000	1.43296600
C	-4.63269100	3.82699400	1.64104700
H	-5.30238300	4.18061500	2.41914700
C	-4.74411400	2.49228200	1.19700800
H	-5.49320700	1.87045600	1.67002000
C	-3.92601300	1.99240800	0.19902400
C	-2.94612600	2.87618500	-0.32703100
C	-2.03851800	2.38402500	-1.31472200
Pd	3.81557000	0.00901200	0.42121800
Cu	1.09921400	-0.18795800	0.10200300
P	5.18730700	1.04630800	-1.06518900
O	-1.19160500	0.78141200	1.71755800
N	2.94662300	-0.89685100	2.16021600
N	3.09370800	2.10596700	0.63756800
N	0.90143900	1.46062900	1.07738500
C	5.31318900	2.67507400	-0.19044700
H	5.65958100	3.46649100	-0.86315800
H	6.07884300	2.56199100	0.58643200
C	4.00430700	3.07051800	0.44565400
C	3.76700900	4.40195900	0.80745600
H	4.53117900	5.15199000	0.63995100
C	2.56828700	4.72264100	1.41161300
H	2.37450900	5.73553700	1.75279800
C	1.58263500	3.74024400	1.56788200
C	0.30747100	3.97481600	2.17610600
H	0.08075800	4.96300800	2.56548800
C	-0.59047700	2.96871900	2.26589500
H	-1.56781900	3.09204400	2.71682200
C	-0.29865700	1.68389100	1.67384400
C	1.85640400	2.43718000	1.09497200
C	6.94239800	0.49057000	-1.25145900
H	6.89391200	-0.38004500	-1.91454900
C	7.83232900	1.55088600	-1.91336300
H	7.93898700	2.43972200	-1.28312500
H	8.83430300	1.13773200	-2.05945200
H	7.46368100	1.86243500	-2.89451200
C	7.51062500	0.02468800	0.09440000
H	6.90347500	-0.76778800	0.53828300
H	8.52185300	-0.36375200	-0.05556300
H	7.58519300	0.84873600	0.81235100
C	4.54516800	1.42920300	-2.75636000
H	5.26229000	2.12616600	-3.20735700
C	4.47430100	0.15636900	-3.60825400
H	3.78719900	-0.57241300	-3.16488300

H	4.10572200	0.40704100	-4.60742000
H	5.45113700	-0.31881300	-3.73624500
C	3.17458200	2.10988000	-2.68834300
H	3.20166600	3.06856300	-2.16159600
H	2.82373200	2.30229800	-3.70754300
H	2.44048200	1.46678000	-2.19047100
C	2.38641800	-0.32576400	3.22162700
H	2.32077300	0.75604600	3.21475000
C	1.88753200	-1.06893900	4.29581100
H	1.44114200	-0.55515800	5.13882000
C	1.96924200	-2.44760500	4.25317000
H	1.57757000	-3.04924200	5.06833700
C	2.58022900	-3.07551100	3.15267600
C	2.73624100	-4.49832400	3.01617500
H	2.35163100	-5.14302200	3.80032700
C	3.36197200	-5.02379600	1.93134600
H	3.47756000	-6.09981400	1.83940300
C	3.90463500	-4.18693900	0.89104400
C	4.57500200	-4.70924300	-0.23475100
H	4.69504100	-5.78323400	-0.34038500
C	5.08258900	-3.84943700	-1.18484000
H	5.60159100	-4.24893400	-2.05098100
C	4.95205700	-2.45032700	-1.04987100
H	5.37105500	-1.83031700	-1.83253400
C	4.30712300	-1.89219100	0.03864600
C	3.77338800	-2.78789900	1.00269100
C	3.08198000	-2.24982800	2.13035700

Complex **3**:

Pd	-0.27512900	0.36154200	-0.31794500
Cu	0.90338900	-1.10799200	1.79731200
Cl	-0.51630100	-0.39010000	3.20545700
P	0.03043100	2.60188600	-0.29346600
O	2.65844000	-3.43111400	1.61251800
N	1.90012500	0.47552100	-0.67336400
N	2.31297000	-1.45777800	0.53547100
N	-0.68563200	-1.64832900	-0.98160800
C	1.41813200	2.70500500	-1.51679600
H	0.96718200	2.69324800	-2.51575600
H	1.97229100	3.64504900	-1.42181600
C	2.35717500	1.53285900	-1.36287300
C	3.64256300	1.57492700	-1.89786800
H	3.97471500	2.44720300	-2.44885200
C	4.46586000	0.46957800	-1.72420500
H	5.45905100	0.44838100	-2.16535700
C	4.04056700	-0.60447500	-0.95104100
C	4.83831400	-1.77185100	-0.67957000
H	5.81627800	-1.85736200	-1.14682200
C	4.36770200	-2.73164500	0.14046400

H	4.93123300	-3.62882900	0.36968300
C	3.06885600	-2.58964100	0.81632900
C	2.74972800	-0.54268600	-0.35134600
C	0.65583500	3.38952000	1.25905000
H	0.93255500	4.41843700	0.99349600
C	1.89916100	2.66753900	1.79230400
H	1.66372700	1.63186100	2.05610100
H	2.24187200	3.17319200	2.70050700
H	2.72680200	2.66916100	1.07645200
C	-0.45195800	3.40923400	2.32003100
H	-1.33259000	3.97470700	1.99646900
H	-0.07358400	3.88696000	3.22916600
H	-0.75225600	2.38840500	2.58240200
C	-1.25448400	3.74568400	-0.98706300
H	-2.02700300	3.79955600	-0.21274300
C	-1.89783900	3.14871900	-2.24370700
H	-1.18309000	3.08327500	-3.07176300
H	-2.72027000	3.79148200	-2.57357600
H	-2.29712100	2.14988900	-2.05341500
C	-0.72779500	5.16327800	-1.24054900
H	-0.32911800	5.63079400	-0.33611600
H	-1.54384500	5.79576200	-1.60456800
H	0.05556400	5.17006700	-2.00627200
C	0.13447600	-2.55289400	-1.49828400
H	1.17750200	-2.27310800	-1.57679700
C	-0.30255300	-3.81982400	-1.90361300
H	0.41396500	-4.52501700	-2.30769300
C	-1.63453700	-4.14873800	-1.75561100
H	-1.99881200	-5.13056200	-2.04504900
C	-2.52698200	-3.20405100	-1.21876100
C	-3.92977300	-3.44366900	-1.01397400
H	-4.33835400	-4.41062900	-1.29255600
C	-4.72351500	-2.48607500	-0.46912000
H	-5.77927100	-2.68333800	-0.30447000
C	-4.20250300	-1.19888200	-0.08557000
C	-4.99830300	-0.20387600	0.51569600
H	-6.05263200	-0.39283100	0.69592200
C	-4.42097900	0.99032700	0.89409400
H	-5.02398800	1.74769800	1.38695800
C	-3.05529500	1.24831000	0.66287900
H	-2.65212300	2.18982600	1.01596700
C	-2.24019800	0.31660500	0.04267200
C	-2.83568600	-0.92445300	-0.30291600
C	-2.00432600	-1.94982500	-0.85240500

QTAIM analysis

Geometry optimizations were carried out in the gas phase without symmetry restrictions as described above using the ωb97xd functional;[18] the metal centers (Cu, Pd) were described by the SDD basis sets[19] while the remaining atoms were described by the 6-31++G(d,p)[20-23] basis set.[24]. The quantum-topological analysis of the calculated electron density of the "gas-phase" structures was performed within the quantum topological theory of atoms in molecules by means of the *AIMAll* package (v 19.10.12).[27] According to Quantum Theory of Atoms in Molecules (QTAIM),[28-29] the bonding between two atoms is indicated by the presence of a bond critical point, bcp (in other words, a (3,-1) critical point of $\rho(\boldsymbol{r})$) along a bond path connecting two neighbouring atoms. The character of the bonding can be characterized by local indicators at the bcp and by the electron delocalization indices (DIs, an average number of electrons shared between pair of atoms) related to the degree of covalence and bond multiplicity.[30] Negative and positive values of the Laplacian at the bcp, $\nabla^2\rho_b$, are characteristics of "shared" and "closed-shell" interactions, respectively.[30-31] The value of ρ at bcp, ρ_b, is characteristic of a bond strength.[32] Metal-metal and metal-ligand interactions are typically characterized by positive values of $\nabla^2\rho_b$ and low ρ_b.[30, 33-35] Other characteristics are H_b (total energy density, $G_b + V_b$), G_b (kinetic energy density), V_b (potential energy density) at bcp and the relative ratio of the latter two, $|V_b|/G_b$. The covalent bonds are characterized by $|V_b|/G_b > 2$, the intermediate or transit region is characterized by $1 < |V_b|/G_b < 2$.[30, 36-38] Metal-metal interactions typically feature negative values for V_b and H_b (with H_b value close to zero), and $G_b \cong |V_b|$.[30-31, 34-35]

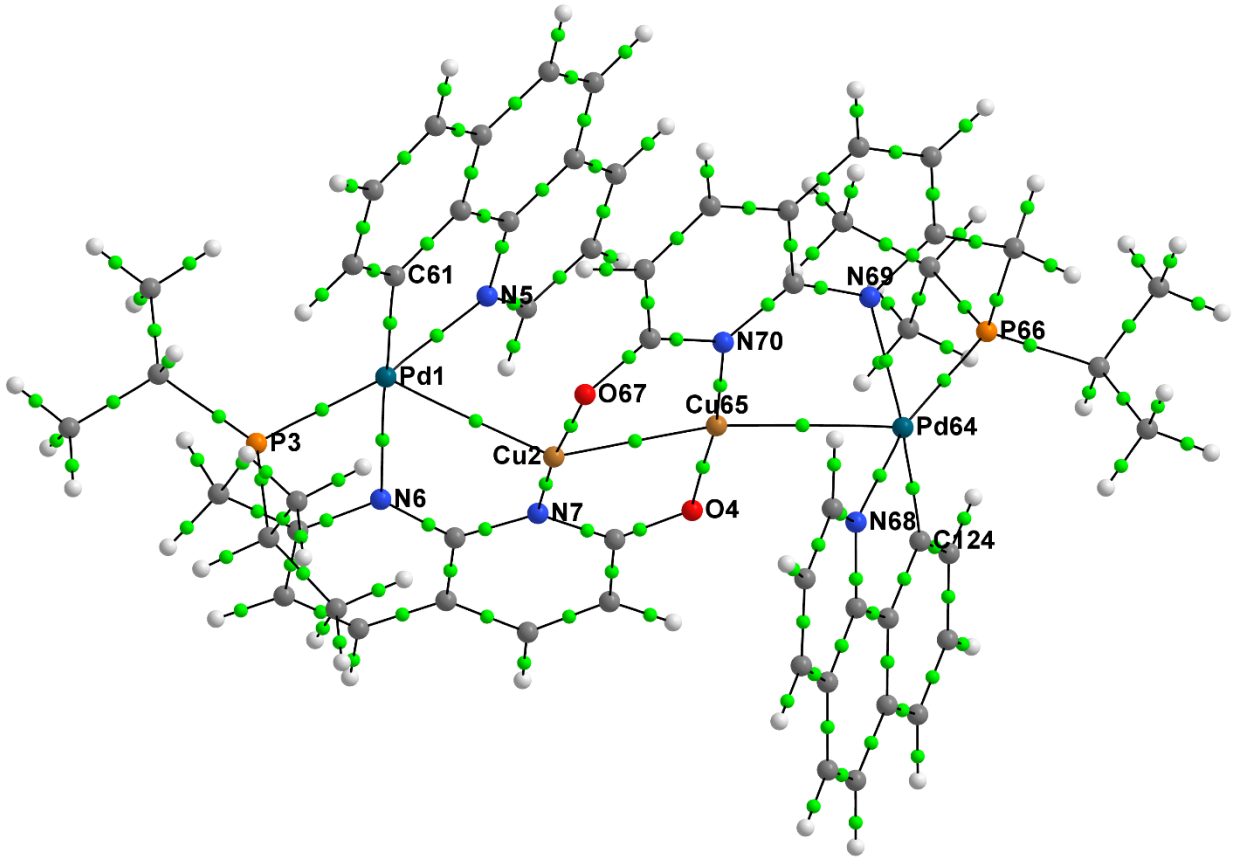

Figure S90. Molecular graph for "gas-phase" DFT-optimized ion $\mathbf{2}^{2+}$. Bond critical points (3, –1) with a threshold of $\nabla\rho_b > 0.025$ a.u. and corresponding bond paths are shown with green dots and black lines, respectively.

Table S6. Quantum-topological parameters [in a.u.] at the bond critical points and delocalization index $DI(A|B)$ involving metal atoms for "gas-phase" ion $\mathbf{2}^{2+}$.

Bonding atoms	ρ_b [a]	$\nabla^2\rho_b$ [b]	λ_1 [c]	λ_2 [c]	λ_3 [c]	ε [d]	V_b [e]	G_b [f]	H_b [g]	$DI(A\|B)$ [h]
Pd1⋯Cu2	0.028676	0.056645	–0.020785	–0.020058	0.097488	0.036235	–0.028305	0.021233	–0.007072	0.215365
Pd1⋯P3	0.106079	0.113526	–0.098551	–0.097588	0.309664	0.009868	–0.113734	0.071031	–0.042703	0.8784
Cu2⋯Cu65	0.035247	0.050311	–0.026342	–0.026029	0.102682	0.012004	–0.036905	0.024742	–0.012163	0.255108
Pd1⋯N5	0.079556	0.372857	–0.084032	–0.078346	0.535234	0.072579	–0.111833	0.102477	–0.009356	0.531658
Pd1⋯N6	0.065392	0.309296	–0.059293	–0.054477	0.423065	0.088398	–0.086866	0.082067	–0.004799	0.466361
Cu2⋯N7	0.100888	0.543033	–0.144241	–0.138836	0.82611	0.038933	–0.166261	0.15101	–0.015251	0.592214
Pd1⋯C61	0.135539	0.146593	–0.171429	–0.163807	0.481829	0.046535	–0.157763	0.097139	–0.060624	0.96673
Cu2⋯O67	0.096085	0.667325	–0.147396	–0.144034	0.958755	0.023336	–0.172674	0.169753	–0.002921	0.539357
O4⋯Cu65	0.093776	0.652286	–0.141867	–0.139712	0.933866	0.015423	–0.166389	0.16473	–0.001659	0.53336
Pd64⋯C124	0.136546	0.139985	–0.174021	–0.165984	0.47999	0.04842	–0.158305	0.096585	–0.06172	0.97184
Cu65⋯N70	0.099269	0.533674	–0.141258	–0.13594	0.810872	0.039115	–0.16197	0.147694	–0.014276	0.584151
Pd64⋯Cu65	0.029413	0.059044	–0.02153	–0.020649	0.101223	0.042678	–0.029284	0.022022	–0.007262	0.222456
Pd64⋯P66	0.105814	0.119194	–0.097986	–0.096729	0.313908	0.012994	–0.114649	0.072197	–0.042452	0.875805
Pd64⋯N68	0.082199	0.381381	–0.087984	–0.082082	0.551447	0.071904	–0.116313	0.105779	–0.010534	0.546451
Pd64⋯N69	0.06637	0.317513	–0.060538	–0.055287	0.433338	0.094971	–0.089304	0.084312	–0.004992	0.468486

[a]Electron density; [b]Laplacian of electron density; [c]Eigenvalues of the Hessian matrix of $\rho(\boldsymbol{r})$ at the bcp; [d]Bond ellipticity; [e]Potential energy density; [f]Kinetic energy density; [g]Total energy density; [h]Delocalization index. All values are given for the corresponding bcps.

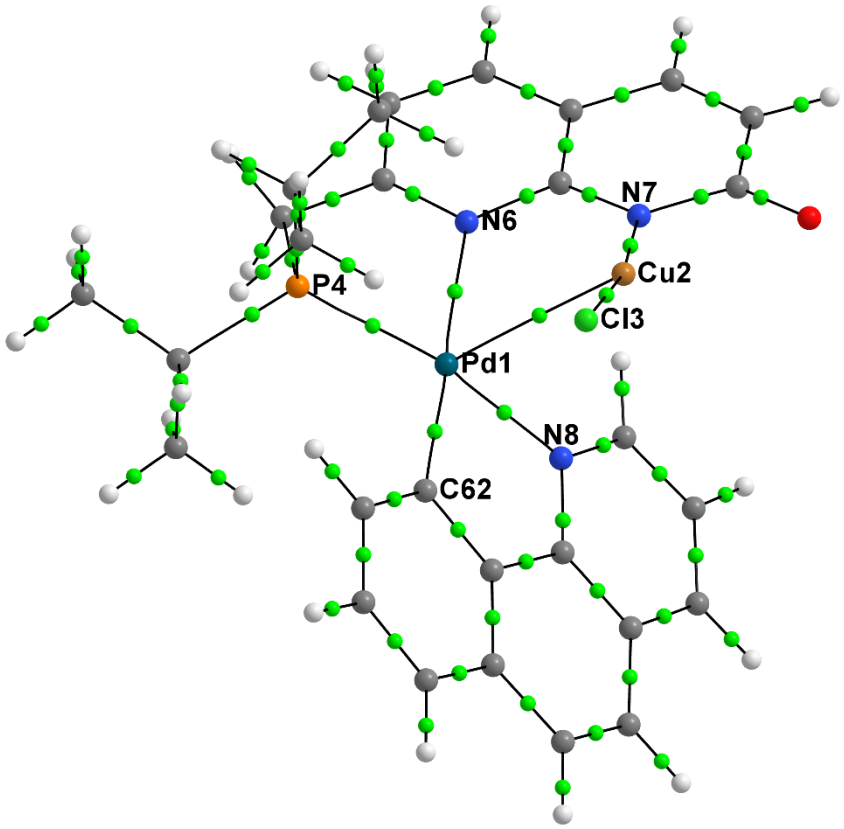

Figure S91. Molecular graph for "gas-phase" DFT-optimized complex **3**. Bond critical points (3, –1) with a threshold of $\nabla\rho_b > 0.025$ a.u. and corresponding bond paths are shown with green dots and black lines, respectively.

Table S7. Quantum-topological parameters [in a.u.] at the bond critical points and delocalization index $DI(A|B)$ involving metal atoms for "gas-phase" complex **3**.

Bonding atoms	ρ_b[a]	$\nabla^2\rho_b$[b]	λ_1[c]	λ_2[c]	λ_3[c]	ε[d]	V_b[e]	G_b[f]	H_b[g]	$DI(A\|B)$[h]
Pd1···Cu2	0.025451	0.047559	–0.017545	–0.016759	0.081863	0.04695	–0.024049	0.017969	–0.00608	0.194284
Cu2···Cl3	0.090762	0.35755	–0.105173	–0.10503	0.567753	0.001368	–0.123289	0.106338	–0.01695	0.825678
Pd1···P4	0.106843	0.130209	–0.098734	–0.096543	0.325486	0.022694	–0.118835	0.075665	–0.04317	0.888667
Pd1···N6	0.069652	0.332878	–0.064133	–0.058457	0.455468	0.097108	–0.095117	0.089133	–0.00598	0.486342
Cu2···N7	0.09802	0.543069	–0.139951	–0.133254	0.816275	0.050261	–0.162102	0.148935	–0.01317	0.58628
Pd1···N8	0.079616	0.374625	–0.085557	–0.079628	0.539809	0.074461	–0.112149	0.102857	–0.00929	0.536177
Pd1···C62	0.137107	0.153782	–0.172859	–0.165657	0.492297	0.043476	–0.161824	0.100062	–0.06176	0.964513

[a]Electron density; [b]Laplacian of electron density; [c]Eigenvalues of the Hessian matrix of $\rho(\boldsymbol{r})$ at the bcp; [d]Bond ellipticity; [e]Potential energy density; [f]Kinetic energy density; [g]Total energy density; [h]Delocalization index. All values are given for the corresponding bcps.

IV. References

1. O. Rivada-Wheelaghan, S. L. Aristizábal, J. López-Serrano, R. R. Fayzullin and J. R. Khusnutdinova, *Angew. Chem. Int. Ed.*, 2017, **56**, 16267-16271.
2. D. C. Powers, D. Benitez, E. Tkatchouk, W. A. Goddard and T. Ritter, *J. Am. Chem. Soc.*, 2010, **132**, 14092-14103.
3. M. Gallardo-Villagrán, O. Rivada-Wheelaghan, S. M. W. Rahaman, R. R. Fayzullin and J. R. Khusnutdinova, *Dalton Trans.*, 2020, **49**, 12756-12766.
4. K. Jouvin, J. Heimburger and G. Evano, *Chem. Sci.*, 2012, **3**, 756-760.
5. P. W. Seavill, K. B. Holt and J. D. Wilden, *RSC Adv.*, 2019, **9**, 29300-29304.
6. D. Gallego, A. Brück, E. Irran, F. Meier, M. Kaupp, M. Driess and J. F. Hartwig, *J. Am. Chem. Soc.*, 2013, **135**, 15617-15626.
7. J. Comas-Barceló, R. S. Foster, B. Fiser, E. Gomez-Bengoa and J. P. A. Harrity, *Chem. Eur. J.*, 2015, **21**, 3257-3263.
8. P. W. Seavill, K. B. Holt and J. D. Wilden, *Green Chem.*, 2018, **20**, 5474-5478.
9. Q. Liang, K. Sheng, A. Salmon, V. Y. Zhou and D. Song, *ACS Catal.*, 2019, **9**, 810-818.
10. Q. Xu, R. Shen, Y. Ono, R. Nagahata, S. Shimada, M. Goto and L.-B. Han, *Chem. Commun.*, 2011, **47**, 2333-2335.
11. A. R. Dick, K. L. Hull and M. S. Sanford, *J. Am. Chem. Soc.*, 2004, **126**, 2300-2301.
12. G. Sheldrick, *Acta Crystallogr., Sect. A*, 2015, **71**, 3-8.
13. G. Sheldrick, *Acta Crystallogr., Sect. C*, 2015, **71**, 3-8.
14. L. J. Farrugia, *J. Appl. Crystallogr.*, 2012, **45**, 849-854.
15. S. Parsons, H. D. Flack and T. Wagner, *Acta Crystallogr., Sect. B*, 2013, **69**, 249-259.
16. A. Spek, *Acta Crystallogr., Sect. C*, 2015, **71**, 9-18.
17. Gaussian 16, Revision B.01, M. J. Frisch, G. W. Trucks, H. B. Schlegel, G. E. Scuseria, M. A. Robb, J. R. Cheeseman, G. Scalmani, V. Barone, G. A. Petersson, H. Nakatsuji, X. Li, M. Caricato, A. V. Marenich, J. Bloino, B. G. Janesko, R. Gomperts, B. Mennucci, H. P. Hratchian, J. V. Ortiz, A. F. Izmaylov, J. L. Sonnenberg, D. Williams-Young, F. Ding, F. Lipparini, F. Egidi, J. Goings, B. Peng, A. Petrone, T. Henderson, D. Ranasinghe, V. G. Zakrzewski, J. Gao, N. Rega, G. Zheng, W. Liang, M. Hada, M. Ehara, K. Toyota, R. Fukuda, J. Hasegawa, M. Ishida, T. Nakajima, Y. Honda, O. Kitao, H. Nakai, T. Vreven, K. Throssell, J. A. Montgomery, Jr., J. E. Peralta, F. Ogliaro, M. J. Bearpark, J. J. Heyd, E. N. Brothers, K. N. Kudin, V. N. Staroverov, T. A. Keith, R. Kobayashi, J. Normand, K. Raghavachari, A. P. Rendell, J. C. Burant, S. S. Iyengar, J. Tomasi, M. Cossi, J. M. Millam, M. Klene, C. Adamo, R. Cammi, J. W. Ochterski, R. L. Martin, K. Morokuma, O. Farkas, J. B. Foresman, and D. J. Fox, Gaussian, Inc., Wallingford CT, 2016.
18. J.-D. Chai and M. Head-Gordon, *PCCP*, 2008, **10**, 6615-6620.
19. D. Andrae, U. Haeussermann, M. Dolg, H. Stoll and H. Preuss, *Theor. Chim. Acta*, 1990, **77**, 123-141.
20. P. C. Hariharan and J. A. Pople, *Mol. Phys.*, 1974, **27**, 209-214.
21. P. C. Hariharan and J. A. Pople, *Theor. Chim. Acta*, 1973, **28**, 213-222.
22. W. J. Hehre, R. Ditchfield and J. A. Pople, *J. Chem. Phys.*, 1972, **56**, 2257-2261.
23. M. M. Francl, W. J. Pietro, W. J. Hehre, J. S. Binkley, M. S. Gordon, D. J. DeFrees and J. A. Pople, *J. Chem. Phys.*, 1982, **77**, 3654-3665.
24. S. Deolka, O. Rivada, S. L. Aristizábal, R. R. Fayzullin, S. Pal, K. Nozaki, E. Khaskin and J. R. Khusnutdinova, *Chem. Sci.*, 2020, **11**, 5494-5502.
25. NBO 6.0. E. D. Glendening, J. K. Badenhoop, A. E. Reed, J. E. Carpenter, J. A. Bohmann, C. M. Morales, C. R. Landis, F. Weinhold (Theoretical Chemistry Institute, University of Wisconsin, Madison, WI, 2013); http://nbo6.chem.wisc.edu/.

26. Chemcraft - graphical software for visualization of quantum chemistry computations. https://www.chemcraftprog.com.
27. AIMAll (Version 19.10.12), Todd A. Keith, TK Gristmill Software, Overland Park KS, USA, 2019 (aim.tkgristmill.com).
28. R. F. W. Bader, *Chem. Rev.*, 1991, **91**, 893-928.
29. R. F. W. Bader, *Atoms in Molecules: A Quantum Theory*, Clarendon Press, 1994.
30. C. Lepetit, P. Fau, K. Fajerwerg, M. L. Kahn and B. Silvi, *Coord. Chem. Rev.*, 2017, **345**, 150-181.
31. R. Bianchi, G. Gervasio and D. Marabello, *Inorg. Chem.*, 2000, **39**, 2360-2366.
32. P. R. Varadwaj, A. Varadwaj and H. M. Marques, *J. Phys. Chem. A*, 2011, **115**, 5592-5601.
33. P. R. Varadwaj, I. Cukrowski and H. M. Marques, *J. Phys. Chem. A*, 2008, **112**, 10657-10666.
34. P. Macchi, D. M. Proserpio and A. Sironi, *J. Am. Chem. Soc.*, 1998, **120**, 13429-13435.
35. G. Gervasio, R. Bianchi and D. Marabello, *Chem. Phys. Lett.*, 2004, **387**, 481-484.
36. E. Espinosa, I. Alkorta, J. Elguero and E. Molins, *J. Chem. Phys.*, 2002, **117**, 5529-5542.
37. D. Cremer and E. Kraka, *Croat. Chem. Acta*, 1985, **57**, 1259-1281.
38. R. F. W. Bader and H. Essen, *J. Chem. Phys.*, 1984, **80**, 1943-1960.